

Wavelets and Multirate Filter Banks – Theory, Structure, Design, and Applications

by

Ying-Jui Chen

M.S.E.E., National Taiwan University (1996)
B.S.E.E., National Taiwan University (1994)

Submitted to the Department of Civil and Environmental Engineering
in partial fulfillment of the requirements for the degree of

Doctor of Philosophy in Computational Engineering

at the

MASSACHUSETTS INSTITUTE OF TECHNOLOGY

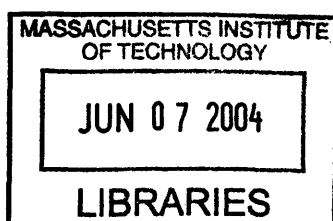
June 2004

© Massachusetts Institute of Technology 2004. All rights reserved.

Author
Department of Civil and Environmental Engineering
May 6, 2004

Certified by
Kevin S. Amaratunga
Associate Professor of Civil and Environmental Engineering
Thesis Supervisor

Accepted by
Heidi Nepf
Chairman, Department Committee on Graduate Students



BARKER

Wavelets and Multirate Filter Banks – Theory, Structure, Design, and Applications

by

Ying-Jui Chen

Submitted to the Department of Civil and Environmental Engineering
on May 6, 2004, in partial fulfillment of the
requirements for the degree of
Doctor of Philosophy in Computational Engineering

Abstract

Wavelets and filter banks have revolutionized signal processing with their ability to process data at multiple temporal and spatial resolutions. Fundamentally, continuous-time wavelets are governed by discrete-time filter banks with properties such as perfect reconstruction, linear phase and regularity. In this thesis, we study multi-channel filter bank factorization and parameterization strategies, which facilitate designs with specified properties that are *enforced by* the actual *factorization structure*. For M -channel filter banks ($M \geq 2$), we develop a complete factorization, *M-channel lifting factorization*, using simple ladder-like structures as predictions between channels to provide robust and efficient implementation; *perfect reconstruction* is structurally enforced, even under finite precision arithmetic and quantization of lifting coefficients. With lifting, optimal low-complexity integer wavelet transforms can thus be designed using a simple and fast algorithm that incorporates prescribed limits on hardware operations for power-constrained environments.

As filter bank *regularity* is important for a variety of reasons, an aspect of particular interest is the *structural imposition of regularity* onto factorizations based on the dyadic form $\mathbf{u}\mathbf{v}^\dagger$. We derive the corresponding *structural conditions* for regularity, for which M -channel lifting factorization provides an essential parameterization. As a result, we are able to design filter banks that are exactly regular and amenable to fast implementations with perfect reconstruction, regardless of the choice of free parameters and possible finite precision effects. Further constraining $\mathbf{u} = \mathbf{v}$ ensures regular orthogonal filter banks, whereas a special dyadic form is developed that guarantees linear phase. We achieve superior coding gains within 0.1% of the optimum, and benchmarks conducted on image compression applications show clear improvements in perceptual and objective performance.

We also consider the problem of completing an M -channel filter bank, given only its scaling filter. M -channel lifting factorization can efficiently complete such *biorthogonal* filter banks. On the other hand, an improved scheme for completing *paraunitary* filter banks is made possible by a novel order-one factorization which allows greater design flexibility, resulting in improved frequency selectivity and energy compaction over existing state of the art methods. In a dual setting, the technique can be applied to transmultiplexer design to achieve higher-rate data transmissions.

Thesis Supervisor: Kevin S. Amaratunga
Title: Associate Professor of Civil and Environmental Engineering

Acknowledgments

I have been feeling fortunate and privileged to be able to study at MIT. It's been challenging, rewarding and fun!

As with anything else, people have always been the best part. I take this opportunity to express my heartfelt appreciation and gratitude to my advisor, Prof. Amaratunga. Not only have his patience, guidance, and support made this thesis possible, but his admirable insights and enthusiasm also have a profound influence on me. He is one of the most knowledgeable advisors one can ever find.

I'm grateful to my thesis committee members, Prof. John Williams and Prof. Ruaidhri O'Connor, who have patiently sat through committee meetings to understand my work and provide many valuable feedbacks and comments. A special thank-you goes to Prof. O'Connor for the valuable discussions and his advice on writing and presentation.

I would also like to acknowledge with appreciation the long-distance collaborations with Prof. Soontorn Oraintara of UTA on structurally regular filter banks and Prof. Truong Nguyen of UCSD and Prof. Trac Tran of JHU on integer transforms. I'm very grateful to Prof. Nguyen, who has helped me a lot in various ways since I came to the States. A generous help from Dr. Steffen Trautmann is also acknowledged for his enthusiastic (and prompt!) assistance on UICODER, which is a very convenient tool for transform-based image compression.

Other professors have also been a great help and source of encouragement: Gilbert Strang, Richard Melrose and James Walker (University of Wisconsin-Eau Claire). Prof. Walker has read my thesis carefully and provided many feedbacks, which is very much appreciated.

I would like to thank all the friends who have accompanied and supported me during my stay in Boston. Their friendship is the most valuable gift Boston has to offer.

The beautiful minds at the Intelligent Engineering Systems Laboratory are more than wonderful: Abel, Anamika, Andy, Bharath, Ching-Huei, George, Hai, Jingsong, Julio, Mazen, Sakda, Scott, Sivaram, Stefan, Sudarshan, etc., etc. Interactions with them have been the most enjoyable part and a privilege. Special thanks go to Stefan, Bharath, and

Sudarshan for their constant help and valuable feedbacks on my presentation. Finally, our administrative assistant, Joanie, has been a great help in many aspects.

The most special gratitude goes to my parents whose unconditional love has brought me up the person I am today. My heartfelt gratitude goes to my sister, Dino, and my uncle for their undivided love and constant support. My mother-in-law has provided the most needed help and support during my PhD study, especially during my PhD qualifier period when my daughter was just born. Finally, my deepest gratitude goes to my wife Hui-Wen and my daughter Megan. They have given me the much needed comfort and inspiration during my entire PhD program. To them, this thesis is dedicated with appreciation.

Contents

1	Introduction	23
1.1	Wavelets — Mathematical Microscope	23
1.2	Filter Bank Perspective	25
1.2.1	Subband Decomposition with M -channel Filter Banks	25
1.3	Applications	26
1.4	Objectives and Concentration	28
1.4.1	Structure-Oriented Design Approach	28
1.4.2	Lifting Structures and Multiplierless Approximations	28
1.4.3	Filter Bank Completion	29
1.5	Thesis Outline	30
2	Review	33
2.1	Filter Banks	34
2.1.1	Maximally-Decimated Uniform Filter Banks	35
2.1.2	Polyphase Representation	38
2.1.3	Lifting Scheme	41
2.1.4	Categories of Filter Banks	42
2.1.5	Performance Criteria	43
2.2	Order and McMillan Degree of PRFBs	45
2.3	Wavelets and Multiresolution Analysis	47
2.3.1	Dilation and Wavelet Equations	49

2.3.2	Wavelet Series Expansion	49
2.3.3	Fast Wavelet Transform and PRFB	50
2.3.4	Cascade Algorithm and the Inner Product Formula	52
2.4	Regularity, Vanishing Moments, and Smoothness	57
2.4.1	DC Leakage	61
2.4.2	Sobolev Exponent As Smoothness Measure	62
2.5	Matrix Parameterizations	63
2.5.1	Orthogonal or Unitary Matrices	63
2.5.2	Biorthogonal Matrices	68
2.6	Dyadic-Based Structures	69
2.6.1	Paraunitary Case	70
2.6.2	Biorthogonal Case	74
3	<i>M</i>-Channel Lifting Factorization	75
3.1	Introduction	76
3.2	Preliminaries	79
3.2.1	Elementary Matrix Operations	79
3.2.2	<i>M</i> -Channel Lifting Structure	79
3.2.3	Euclidean Algorithm and <i>M</i> -Channel Lifting	81
3.3	<i>M</i> -Channel Lifting Factorization of Perfect Reconstruction Filter Banks	81
3.3.1	Prior Results For Two-Channel Lifting	81
3.3.2	Monic Euclidean Algorithm For Arbitrary <i>M</i>	82
3.3.3	Size Reduction Via Monic Euclidean Algorithm	82
3.3.4	<i>M</i> -Channel Lifting Factorization Via Size Reductions	83
3.3.5	Relaxation of Monic Determinant	84
3.3.6	Reversible Multiplierless <i>M</i> -Band Wavelet Transforms	85
3.3.7	PRFBs with Prescribed Admissible $H_0(z)$	85
3.4	Lifting Factorization and Design Examples	88
3.4.1	Degree-One Paraunitary Building Block	89

3.4.2	Householder Matrix	92
3.4.3	Degree-One Biorthogonal Building Block	93
3.4.4	Degree-One Unimodular Building Block	93
3.4.5	Discrete Cosine Transform and Cosine-Modulated Filter Bank	96
3.4.6	PRFB With Prescribed Admissible $H_0(z)$ – A B-Spline Example	98
3.5	Conclusions	100
3.A	Proof of Lemma 3.1	101
3.B	Proof of Theorem 3.1	103
3.C	Proof of Lemma 3.2	104
3.D	Proof of Theorem 3.2	105
4	Paraunitary Filter Banks With Structural Regularity	107
4.1	Introduction	107
4.2	Dyadic-based Factorizations with Structural Regularity	110
4.2.1	One-Regular PUFBs	110
4.2.2	Two-Regular PUFBs	112
4.3	Regular Linear-Phase PUFBs Revisited	119
4.3.1	LPPUFB in Standard Order-One Form (2.53)	120
4.3.2	Some Observations	121
4.3.3	Specialization of Two-Regular Condition (4.7)	122
4.4	Regular M -channel Lifting Structures	124
4.4.1	Degree-One Paraunitary Building Block $\mathbf{V}_m(z)$	124
4.4.2	Order-One Paraunitary Building Block $\mathbf{W}_m(z)$	126
4.4.3	Householder Matrix \mathbf{H}	127
4.4.4	Properties of Lifting Structures	128
4.4.5	One-Regular Lifting Structure	131
4.4.6	Two-Regular Lifting Structures	132
4.5	Design Examples of Regular PUFBs	133
4.5.1	One-Regular PUFB	135

4.5.2	Two-Regular PUFB	136
4.6	Application to Lossy Image Compression	138
4.7	Concluding Remarks	140
5	A Class of Structurally Regular Biorthogonal Filter Banks	145
5.1	Introduction	146
5.2	A Class of Regular Biorthogonal Filter Banks	148
5.2.1	(1, 1)-Regular BOFBs	149
5.2.2	(1, 2)-Regular BOFBs	151
5.2.3	(2, 1)-Regular BOFBs	153
5.3	Linear-Phase Biorthogonal Filter Banks Revisited	155
5.3.1	BOLP in Standard Dyadic Form (5.1)	156
5.3.2	LP-Propagating Standard Dyadic Structure	157
5.3.3	Degrees of Freedom	158
5.4	Regular Linear-Phase Biorthogonal Filter Banks	159
5.5	Examples of Regular Biorthogonal Filter Banks	160
5.5.1	Example 1: (1, 1)-Regular, 8×16 BOFB	160
5.5.2	Example 2: (1, 2)-Regular, 8×16 BOFB	162
5.5.3	Example 3: (1, 2)-Regular, 4×8 BOFB	162
5.5.4	Example 4: (1, 1)-Regular, 8×24 BOFB	162
5.5.5	Example 5: (1, 2)-Regular, 8×24 BOFB	162
5.5.6	Example 6: (1, 2)-Regular, 8×32 BOFB	162
5.6	Application to Data Compression	167
5.6.1	Performance Summary	169
5.7	Conclusion	171
6	Paraunitary Filter Bank Completion	179
6.1	Introduction	179
6.2	Prior Arts on PUFB Completion	182

6.2.1	PUFB Admissibility	182
6.2.2	Degree-One Factorization of $M \times 1$ Lossless FIR Systems	182
6.2.3	Degree-One Completion of PUFBs	182
6.3	Improved Technique For Completing General Paraunitary Filter Banks . . .	184
6.3.1	Order-One Factorization of $M \times 1$ Lossless FIR Systems	184
6.3.2	Order-One Completion of PUFBs	187
6.4	Completing Linear-Phase Paraunitary Filter Banks	189
6.5	Completion Examples	193
6.5.1	General PUFBs	193
6.5.2	Linear-Phase PUFBs	193
6.6	Completion As Filter Bank Design Technique	194
6.6.1	PUFB Design Based On Order-One Completion	194
6.6.2	Examples of Completion-Based Design	195
6.7	Concluding Remarks	196
7	Low-Power Integer Tranforms via Multiplierless Approximation with Adder Constraint	203
7.1	Introduction	203
7.2	Minimum-Adder Multiplications	204
7.2.1	Integers	204
7.2.2	Binary Fractions	206
7.3	Adder-Constrained Multiplierless Approximation Algorithm	207
7.3.1	Finding the n -ABA	207
7.3.2	Quasi-Coordinate Descent	208
7.3.3	Adaptation to Lifting Structures	209
7.4	Design Examples	210
7.4.1	IntDCT	210
7.4.2	BinDCT	211
7.5	Conclusions	212

8 Conclusion and Future Work	215
8.1 Summary	215
8.2 Future Directions	217

List of Figures

1-1	M -channel uniform filter bank.	25
1-2	M -band wavelet. (a) tree structure of lowpass-iterated filter bank, (b) frequency partitioning for $M = 2$ after four levels of iteration, (c) frequency partitioning for $M = 4$ after two levels of iteration.	27
2-1	M -channel maximally-decimated uniform filter bank with perfect reconstruction, where $\hat{x}[n] = cx[n - \ell]$ for some $c \neq 0$ and integer ℓ which is the system delay. $H_i(z)$ and $F_i(z)$ denote the analysis and synthesis filters, respectively, $i = 0, 1, \dots, M - 1$.	36
2-2	Equivalent polyphase representation of the M -channel maximally-decimated uniform filter bank shown in Figure 2-1(a).	39
2-3	The Noble Identities.	40
2-4	The more efficient polyphase representation with the Noble Identities applied.	40
2-5	Sweldens' two-channel lifting scheme [39].	42
2-6	Optimal coding gains versus the number of channels M .	45
2-7	Filter bank interpretation of the fast wavelet transform (FWT).	52
2-8	Cascade algorithm for $M = 3$. (a) $h[n] = \frac{1}{27}[1, 3, 6, 7, 6, 3, 1]$ having triple zeros at the aliasing frequencies $z_m = e^{j2\pi m/3}$, $m = 1, 2$. The cascade algorithm converges to a 3-band quadratic B-spline with $s_{max} = 2.50$. (b) $h[n] = [1, -3, 6, -7, 6, -3, 1]$ having no zeros at the aliasing frequencies. The cascade algorithm fails to converge in L^2 . $s_{max} = -3.00$.	58

3-8 A 4-channel lifting factorization of the normalized 4-point Type-II DCT using 9 simple liftings, 6 of which are dyadic numbers. In the figure, $\alpha = \csc(\pi/8)(\cos(\pi/8) - \sqrt{2}/2)$, $\beta = \sqrt{2}\sin(\pi/8)$, and $\gamma = \csc(\pi/8)(1/2\cos(\pi/8) - \sqrt{2}/2)$. Their magnitudes are all less than unity, providing a good dynamic range performance.	97
3-9 An 8-channel lifting factorization of $\sqrt{2}\mathbf{C}_8$ using 29 simple liftings, 13 of which are floating point numbers. The determinant of the polyphase matrix is 2^4 . In the figure, the block of 4-point DCT-II is exactly as shown in Figure 3-8.	98
3-10 Design example of a PRFB with a prescribed admissible scaling filter $H_0(z)$ which comes from the three-channel “linear-hat” B-spline. $H_i(z)$ are chosen to have equal length, and the lifting steps, $A_k(z)$, shown in Figure 3-4 have been chosen so that the synthesis scaling filter $F_0(z)$ has first-order regularity. The coding gain is 5.9259dB.	100
4-1 Geometry for imposing two degrees of regularity, the case where the distance between S_k and S'_k , $\ \mathbf{g}_k\ $, is large enough such that $S_k \not\subseteq S'_k$. In this case, $\bar{\varphi}_k$ is the maximum angle of deviation that a feasible β^k can make with \mathbf{g}_k , and is given by $\bar{\varphi}_k = \cos^{-1} \left(\ \mathbf{g}_k\ + \frac{1-(N-k)^2}{4\ \mathbf{g}_k\ } \right)$	118
4-2 The M -channel lifting factorization of $\mathbf{V}(z)$, drawn for $M = 5$ and $r = 2$	125
4-3 A parallel implementation of the order-one PU building block $\mathbf{W}_m(z) = \mathbf{I} - \mathbf{w}_m\mathbf{w}_m^\dagger + z^{-1}\mathbf{w}_m\mathbf{w}_m^\dagger$ of degree γ_m [see (2.57)], $1 \leq \gamma_m \leq M$	127
4-4 The M -channel lifting factorization of Householder matrix \mathbf{H} , drawn for $M = 5$ and $r = 2$	128
4-5 Analysis filters and their frequency magnitude responses of the 4-channel PUFB in Table 4.1 with $s = +1$. (a) frequency response and basis functions, (b) zeros of $H_0(z)$, (c) the corresponding wavelet basis with at least one vanishing moment; $s_{max} = .915$	137

4-6	Analysis filters and their frequency magnitude responses of the one-regular 8×24 PUFB with $s = +1$. (a) frequency response and basis functions, (b) zeros of $H_0(z)$, (c) the corresponding wavelet basis with one vanishing moment; $s_{max} = .989$.	138
4-7	Analysis filters and their frequency magnitude responses of the two-regular 8×24 PUFB with $s = +1$. (a) frequency response and basis functions, (b) zeros of $H_0(z)$, (c) the corresponding wavelet basis with two vanishing moments; $s_{max} = 1.30$.	139
4-8	The two-regular 8×32 LPPUFB. $s_{max} = 1.3378$.	140
4-9	The two-regular 8×40 LPPUFB. $s_{max} = 1.5803$.	141
4-10	PSNR versus compression ratio for the 512×512 8-bit grayscale test images <i>Barbara</i> , <i>Goldhill</i> , and <i>Lena</i> . A JPEG-like block-based lossy compression scheme is used with the transforms.	142
4-11	Compression results at 32:1 for visual comparison. The original image and a zoomed-in patch are shown in the first column. The reconstructed images and their zoomed-in patches using one- and two-regular 8×24 PUFBs are shown in the second and the third columns, respectively. Notably, the current design PUv1 produces a much smoother reconstruction than LPv1.	144
5-1	Structure for parameterizing \mathbf{E}_0 satisfying $K_a \geq 1$ (5.5a).	151
5-2	Lattice structure for biorthogonal LP lapped transform.	156
5-3	(1,1)-regular 8×16 BOFB: impulse and frequency responses, along with zero plots of $H_0(z)$ and $F_0(z)$, and the wavelet bases.	161
5-4	(1,2)-regular 8×16 BOFB: impulse and frequency responses, along with zero plots of $H_0(z)$ and $F_0(z)$, and the wavelet bases.	163
5-5	(1,2)-regular 4×8 BOFB: impulse and frequency responses, along with zero plots of $H_0(z)$ and $F_0(z)$, and the wavelet bases.	164
5-6	(1,1)-regular 8×24 BOFB: impulse and frequency responses, along with zero plots of $H_0(z)$ and $F_0(z)$, and the wavelet bases.	165

5-7	(1,2)-regular 8×24 BOFB: impulse and frequency responses, along with zero plots of $H_0(z)$ and $F_0(z)$, and the wavelet bases.	166
5-8	(1,2)-regular 8×32 BOFB: impulse and frequency responses, along with zero plots of $H_0(z)$ and $F_0(z)$, and the wavelet bases.	168
5-9	Transform-based image coder. Examples of the transform stage include DWT, DCT, M -channel PRFB, etc. Common encoding algorithms include wavelet difference reduction (e.g. [148]), JPEG, and embedded zerotree coder (e.g. [104]).	
	169	
5-10	Enlarged portions of original <i>Barbara</i> , <i>Lena</i> , <i>Goldhill</i> (Left column), and three fingerprints <i>fp1</i> , <i>fp2</i> , and <i>fp3</i> (Right column).	172
5-11	Enlarged portions of <i>Barbara</i> at 32:1 compression using Daubechies 9/7 wavelet, 8×8 DCT, 8×24 PUv1 and PUv2, 8×16 and 8×24 BOFBv12.	173
5-12	Enlarged portions of <i>Lena</i> at 64:1 compression using Daubechies 9/7 wavelet, 8×8 DCT, 8×24 PUv1 and PUv2, 8×16 and 8×24 BOFBv12.	174
5-13	Enlarged portions of <i>Goldhill</i> at 32:1 compression using Daubechies 9/7 wavelet, 8×8 DCT, 8×24 PUv1 and PUv2, 8×16 and 8×24 BOFBv12.	175
5-14	Fingerprint compression performance.	177
6-1	M -channel perfect reconstruction filter bank.	180
6-2	Completions of general PUFBs: (a) Coding gain 9.17dB, stopband energy 1.16. (b) Coding gain 9.32dB, stopband energy 0.14.	194
6-3	Order-one completion of general 8×40 PUFB.	195
6-4	Example of PUFB design based on order-one completion	198
6-5	Three design approaches to 4×32 PUFBs with McMillan degree 14, along with one which is based on degree-one completion and renders only degree 7. Design objective is to minimize stopband energy C_{stop} . In the figures, C_{att} and CG denote stopband attenuation and coding gain, respectively.	199

6-6	Comparison of the proposed completion-based approach, the CMFB and the direct approach for designing 8×48 PUFBs, where the design objective is to minimize stopband energy.	200
6-7	One-regular 4×32 PUFB design based on completion.	201
6-8	One-regular 8×48 PUFB design based on completion.	201
7-1	The lifting structure, used exclusively in the design examples of the proposed algorithm, consists of several one-wing butterflies with multipliers λ . The adder \oplus will effectively vanish if the corresponding λ_i or λ_j is zero.	210
7-2	The IntDCT parameterized by p_i and u_j . \mathbf{H}_w is the Walsh-Hadamard transform and \mathbf{B} is bit-reversal. $N_0 = 24$ is the number of the adders that remain when all the p_i and u_j are set to zero. Actually, these are the adders internal to \mathbf{H}_w	211
7-3	The BinDCT parameterized by p_i and u_j . $N_0 = 18$ is the number of the adders that remain when all the p_i and u_j are set to zero.	212

List of Tables

3.1	Several adder-constrained reversible multiplierless approximations of the normalized 4-point DCT	96
3.2	Prototype filter $p_0[n]$ for the 3-channel CMFB.	99
4.1	The design variables for the 4×8 PUFBs with the minimum degree. The resulting FB is structurally one-regular as a result of the predetermined σ_1^0 , σ_2^0 and σ_3^0 . The coding gains are 8.1079 and 8.1075dB, respectively.	136
4.2	Objective Properties of the PUFBs Used in Block-based Lossy Image Compression Experiments: G =coding gain, C_{stop} =stopband energy, s_{\max} =Sobolev smoothness. LPvn= n -Regular PULP in [92]; PUv1 and PUv2 are presented in Sec. 4.5.1 and Sec. 4.5.2, respectively.	142
4.3	Objective compression performance—PSNR in dB based on chosen transforms. LPvn are the n -Regular PULP in [92]; PUv1 and PUv2 are designed in Sec. 4.5.1 and Sec. 4.5.2.	143
5.1	Objective properties of the regular perfect reconstruction filter banks used in transform-based image coding experiments: G =coding gain, C_{stop} =stopband energy, s_{\max} =Sobolev smoothness. LPvn= n -Regular PULP in [92]; PUv1 and PUv2 are presented in Sec. 4.5.1 and Sec. 4.5.2, respectively. BOvn _a n _s 's are the corresponding eight-channel designs presented in the previous section. For coding gain with $M = 8$, $G_{\text{KLT}} = 8.85$ dB, $G_{\text{brick-wall}} = 9.69$ dB.	170

5.2	Objective coding performance using the various transforms with two levels of decomposition in the lowpass band.	171
5.3	Objective coding performance using the various transforms with two levels of decomposition in the lowpass band.	176
7.1	Proposed multiplierless approximations of the DCT based on the IntDCT structure, with various adder constraints. C1 has better MSE performance than was previously published at the same adder constraint. C2 – C8 are our new designs.	214
7.2	Proposed multiplierless approximations of the DCT based on the BinDCT structure, with various adder constraints. The MSE performance (C2 – C8) is better than that previously published at the same adder constraints, except for C1.	214

Chapter 1

Introduction

To See The Wood And The Trees

1.1 Wavelets — Mathematical Microscope

Wavelet transforms have emerged as a powerful tool for signal processing and mathematical analysis over the past two decades [3, 19, 38, 72, 80, 108, 113, 129, 139, 144]. *Wavelets* are functions that oscillate as a short wave, hence the name. Due to their *compact support*¹, they can study and characterize efficiently the *local* behavior of a function, and consequently are referred to as a “mathematical microscope.” With wavelet transforms, functions or signals are dissected according to the scale of the features present, and each component is studied with a resolution matched to its scale. A compact representation is obtained.

The earliest wavelet basis was constructed by Haar back in 1910. It is the simplest example of orthonormal wavelets, consisting of up and down box functions which compute local differences and averages of signals. Since then, the field of wavelets was further developed independently in such disciplines as pure mathematics, physics, and engineering. Many of these ideas merged in the 80’s due to the French school [56, 81–83], and the name

¹This is to be contrasted with the conventional Fourier approach which uses infinite-support sinusoidal functions for analysis. Though perfect in frequency resolution, the Fourier transform provides no information on time localization at all. This is remedied by the compact support of the wavelet basis.

wavelet was coined. A major advance in the field was the introduction of the *multiresolution analysis* (MRA) framework by Meyer and Mallat [70, 71], which has connected wavelet theory with discrete-time filter banks originally developed for subband coding of speech [35, 36, 47], leading to the *discrete wavelet transform* (DWT). In other words, wavelets and the MRA framework are governed by a set of discrete-time filters (Chapter 2). Such one-to-one correspondence enables one to study and design wavelets purely in the digital domain. Furthermore, the filter bank representation leads to the *fast wavelet transform* (FWT).

Daubechies' well known work on compactly supported wavelets [34, 37, 38] has been the foundation of a great amount of research in the field. In her design, a particular family of compactly supported wavelets was constructed which possesses a certain flatness property in the corresponding filters. These *Daubechies wavelets* have been employed in many applications ever since, and particularly in the FBI fingerprint compression specification [48] and in the latest image compression standard, JPEG2000 [60, 116]. One can arrive at the conclusion that the signal/image processing community has been revolutionized by the development of wavelet theory.

Extensions of conventional wavelet constructions have been made from two-band wavelets to M -band wavelets [59, 105, 129, 155], and even from scalar to vector wavelets [109]. More recently, Sweldens proposed in 1996 a new framework, dubbed *lifting*, for a spatial-domain² based construction of wavelets [114], which includes the conventional wavelets as a special case and allows for fast implementation, memory efficiency, and reversibility [39]. In particular, integer-to-integer (wavelet) transforms have become possible based on this idea [2, 20, 29, 55, 91, 99, 152, 154].

²In particular, wavelets over bounded intervals and complex, unstructured geometries can be constructed using lifting. Such wavelets, which are not translatation and dilation invariant (and hence cannot be constructed from classical Fourier domain approaches) were dubbed “the second generation wavelets” [115]. Recent research efforts have been geared toward designing second generation wavelets that facilitate local refinement and incremental solution to the governing equations (usually in the form of a PDE or a boundary integral equation) of a physical problem [4, 5, 7, 21, 112].

1.2 Filter Bank Perspective

Perfect reconstruction filter banks were initially developed in the 1980's [35, 127, 137] independently of wavelet theory. They have become an immensely popular signal processing tool. The conventional discrete Fourier transform (DFT), and the discrete cosine transform (DCT) used in JPEG and MPEG, are two examples of multi-channel filter banks. Figure 1-1 depicts a typical M -channel uniform filter bank.

The theories of wavelets and filter banks were unified within the framework of Meyer and Mallat's MRA [70, 71]. As we will see in Chapter 2, a given MRA corresponds to a perfect reconstruction filter bank, but the converse is not always true, unless the filter bank satisfies an extra property which is referred to as "zeros at π " for the conventional two-channel filter banks. This important property is the *regularity* of the filter bank whose significance will be reviewed in Section 2.4. One concentration of this thesis is to study the structural theory

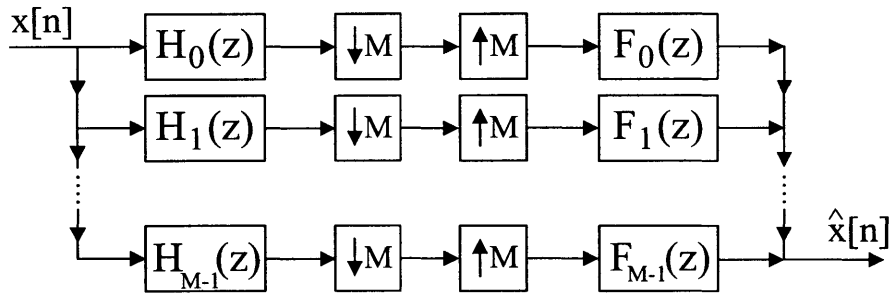


Figure 1-1: M -channel uniform filter bank.

and design of regular perfect reconstruction filter banks.

1.2.1 Subband Decomposition with M -channel Filter Banks

From the analysis viewpoint, wavelets and filter banks are a tool for *subband decomposition* of signals, their use being justified by the uneven distribution of signal energy in the frequency domain [3]. The goal is to obtain an efficient representation of signals by way of *energy compaction*.

Conventional wavelets are two-band, corresponding to two-channel perfect reconstruction filter banks (Chapter 2) which divide the frequency spectrum into lowpass and highpass bands. They can be iterated in either of the two channels to achieve dyadic frequency decompositions with desired characteristics. One can also design an intrinsic M -band filter bank to achieve a finer subband partitioning and better frequency resolution, as opposed to iterating two-band systems resulting in severe penalty on the system delay. Of course an M -band system can be iterated in any channel as is done for $M = 2$. Figure 1-2 illustrates the structure where the lowpass band is iterated *ad infinitum*, along with decomposition of frequency spectrum. This is an M -band wavelet decomposition. Compared to $M = 2$, the basis functions are more compactly supported than the full dyadic wavelet packet counterpart; subband energy compaction is improved over the conventional two-channel case [3]. It can be shown that, as M increases, the wavelet coefficients decay faster and we obtain a more compact representation (see Section 2.4 or [108]). Furthermore, the increased degrees of freedom allow for optimal designs of the M -channel filter banks, by designing them so as to adapt to signals of a particular nature and tailoring them for the given applications (see, e.g., [45] for optimized and improved seismic data compression, and [122] for natural image compression); orthogonality and symmetry of (real-valued) wavelet basis can coexist for $M > 2$ which is not possible for the two-channel case [108] except for the trivial Haar wavelet.

Examples of existing M -channel filter banks include the DFT [90], the DCT [100], lapped orthogonal transform (LOT) [74], generalized LOT (GenLOT) [41], BiOrthogonal LOT (BOLT) [132], generalized BOLT (GLBT) [119], lapped unimodular transform (LUT) [63, 98], etc.

1.3 Applications

Together, wavelets and filter banks have found applications in a wide variety of engineering fields: feature detection [24, 33, 64, 73, 151] and classification [23], audio processing [42, 75, 76], image compression [48, 60, 77, 116, 143, 146–148, 153], video compression such as MPEG4 and

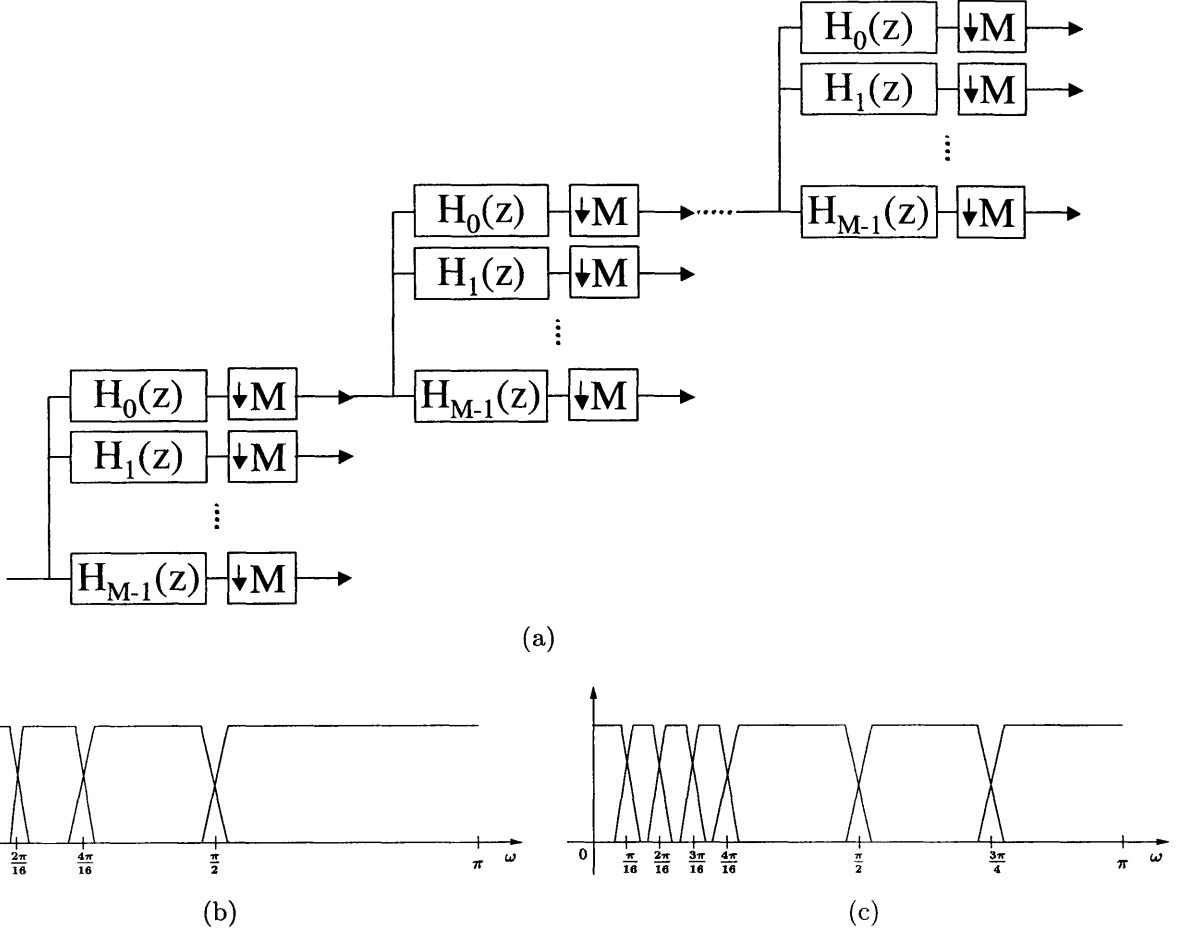


Figure 1-2: M -band wavelet. (a) tree structure of lowpass-iterated filter bank, (b) frequency partitioning for $M = 2$ after four levels of iteration, (c) frequency partitioning for $M = 4$ after two levels of iteration.

H.26x [78, 84, 152], seismic data compression [45, 46, 141], biomedical applications (such as ECG [43] and fMRI [67]), signal denoising [12, 44, 142, 145, 151], smooth signal interpolation, data fusion [65], digital communications [32, 108, 129, 131, 150] (e.g. transmultiplexers used in xDSL), analog-to-digital conversion [10, 126, 135, 136], fault localization in CMOS circuits [17], transmission line protection [96], signal reconstruction [16], regularization for feature selection [62], solutions of large-scale partial differential equations arising from computer simulations [4, 5, 8, 14, 15], etc.

In all cases, it is important to be able to design a filter bank which matches or adapts

well to the nature of a given signal and application.

1.4 Objectives and Concentration

In this thesis, we will focus on the factorization strategies for the polyphase matrix characterizing filter banks, motivated by the desire to build filter banks that achieve specified design criteria (such as perfect reconstruction, orthogonality, phase linearity and regularity) through the actual factorization structure, which offers a robust and efficient approach to implementation and design.

1.4.1 Structure-Oriented Design Approach

M -channel perfect reconstruction filter banks can be designed and implemented using factorizations of their polyphase matrices. This *structure-oriented* approach robustly enforces the most important property—perfect reconstruction, and also exposes the remaining degrees of freedom for optimal design. An aspect of particular interest is the structural imposition of regularity onto factorizations based on the dyadic form $\mathbf{u}\mathbf{v}^\dagger$ with $\mathbf{v}^\dagger\mathbf{u} = 1$. Filter bank regularity is important for a variety of reasons, as it determines the accuracy of wavelet approximations, the compactness of wavelet representations and the smoothness of the wavelet basis, and it ensures no DC leakage in the subbands. Due to the approach taken, the resulting filter banks are exactly regular regardless of the choice of free parameters, and they have a higher approximation power and better energy compaction with no DC leakage, and provide a smoother reconstruction given a bit budget. Both orthogonal and biorthogonal filter banks with structural regularity will be considered, and a special dyadic form will be derived that guarantees linear phase.

1.4.2 Lifting Structures and Multiplierless Approximations

But when it comes to finite-precision implementations, perfect reconstruction may not always be available; it all depends on how a particular implementation takes place. Further

specialized structures are needed. For this purpose, Sweldens' conventional two-channel *lifting scheme* has been found to be effective, always guaranteeing perfect reconstruction. An important by-product is reversible integer-to-integer transforms, including integer wavelet transforms for lossless coding. Moreover, lifting-based implementations of two-channel filter banks are memory-efficient and asymptotically faster than the already-efficient direct polyphase implementation.

As a natural extension of Sweldens' factorization, we develop an intrinsic and systematic M -channel lifting factorization, which extends the lifting benefits to arbitrary M -channel perfect reconstruction filter banks, $M \geq 2$. The proposed structures take advantage of simple inter-channel prediction steps to provide robust and efficient implementation. As a result, perfect reconstruction is structurally enforced, even under finite precision arithmetic and quantization of lifting coefficients. This leads to an approach (to be described below) for designing low-complexity reversible integer-to-integer wavelet transforms, with prescribed limits on hardware operations for use in power-constrained environments.

Although the lifting factorization allows for multiplierless implementations, it does not guarantee the efficiency of a particular multiplierless approximation given fixed implementation resources, e.g., the number of adders. Of course, one could use trial and error until a satisfactory multiplierless approximation is obtained, but this soon becomes intractable even though there are just a few multipliers to approximate. Even if one could find a solution with satisfactory performance (or accuracy), the implementation cost may not be efficient. To address this practical issue, we propose an optimization algorithm for finding the optimal multiplierless approximation subject to an adder budget. The method is simple yet fast and effective, guaranteed to converge in a finite number of steps. During the design process, one increases the adder budget until the desired accuracy is achieved, and the design is guaranteed to be efficient. Reversibility is not lost since the lifting factorization is used.

1.4.3 Filter Bank Completion

Motivated by earlier work on filter bank design, we also study the problem of *filter bank completion* given partial information about the filter bank. In particular, suppose we have

designed part of the filter bank. The proposed completion algorithm will identify the causal relations between the remaining free parameters, so as to enable design and parameterization. In this way, one has the option to design a filter bank by *sequentially* designing the individual filters, where each of the subproblems becomes easier to solve. Moreover, the proposed completion algorithm is no longer constrained as its conventional counterpart — given the filter length, the conventional approach is confined within a restricted set of filter banks having only some fixed, minimal degrees of freedom for parameterization and design, resulting in filter banks with moderate performance; on the other hand, we show how more design freedom can be incorporated into the completed filter bank (given the same length constraint) using the proposed completion algorithm, thus allowing for improved frequency selectivity and energy compaction property.

1.5 Thesis Outline

In **Chapter 2**, we provide a brief review on fundamentals of wavelets and filter banks, along with required background theory. Topics covered include wavelets and multiresolution analysis, fast wavelet transforms, basics of perfect reconstruction filter banks, regularity, degree-one and order-one dyadic-based building blocks, and matrix parameterization techniques which are essential to the discussions of this thesis.

Chapter 3 develops the lifting scheme for arbitrary M -channel perfect reconstruction filter banks, $M \geq 2$. We begin with the Euclidean algorithm which finds the gcd of M Laurent polynomials, and show how repeated applications of the algorithm reduce the size of the polyphase matrix, resulting in M -channel lifting factorization. We also propose a specialized version of the Euclidean algorithm, dubbed *Monic Euclidean algorithm*, which ensures that the gcd's leading coefficient is always unity. As a result, the corresponding (monic) M -channel lifting factorization has a special property of unity diagonal scaling, which is very desirable for finite-precision implementations. On top of this, multiplierless or integer transforms are readily obtained without sacrificing the reversibility of the system. Though formulated under a general setting, the proposed M -channel lifting factorization is

specialized to paraunitary, unimodular, and a class of biorthogonal building blocks, as well as block transforms such as the DCT. They are all *minimum* structures in the McMillan sense, and enable a lifting-based filter bank parameterization, implementation, and design. They can better initialize the design process as suggested by numerical experiments. Using the proposed Monic Euclidean algorithm, the completion of perfect reconstruction filter banks given some of the filters can be studied. The construction of multi-channel B-spline filter banks is given as an example, which can potentially benefit numerical solutions of large-scale PDE's.

Chapter 4 studies the design of *regular* paraunitary filter banks (PUFB) where the regularity conditions are *structurally* enforced through the factorization structure, which offers a fast, efficient, and robust design tool. Consequently, the filter banks are guaranteed to be *exactly* paraunitary and regular, regardless of the free parameters in the lattice structures. Both *order-one* and *degree-one* paraunitary building blocks are considered, enabling the design of regular PUFBs with and without filter length constraint. The minimum length requirement is derived. Linear phase specialization of the theory is made. Interestingly, during the course of theory development, it was found that M -channel lifting factorization (**Chapter 3**) possesses a physical interpretation in this context, and thus can conveniently parameterize the problem. Conditions for, and important properties of, the regular lifting structures are derived, along with their geometric interpretations. The resulting regular PUFBs are shown to provide smoother reconstructions and outperform existing designs in terms of transform-based image coding.

We then extend the study of structural regularity to a class of biorthogonal filter banks in **Chapter 5**. The lattice considered can be regarded as a biorthogonal extension of that used for PUFBs in **Chapter 4**. This biorthogonal extension enables more degrees of design freedom, and in particular the analysis and synthesis banks are allowed to be significantly different (e.g., having different lengths and/or degrees of regularity), which can be properly exploited to match a given class of signals or applications. For example, one can optimize the analysis bank for coding gain to improve energy compaction, and the synthesis bank for

basis smoothness. We show how the structural conditions for regularity are derived, and the designs are evaluated using image coding to demonstrate how regularity improves the perceptual quality of compressed images.

Chapter 6 deals with the problem of completing a PUFB given its scaling filter $H_0(z)$. This is motivated by **Chapter 3** where M -channel lifting is shown to facilitate completion of a *biorthogonal* filter bank. However, as lifting steps are biorthogonal in nature, a PUFB-specialized method is needed. On the other hand, this chapter is also motivated by earlier work of Vaidyanathan *et al.* on PUFB design techniques [134]. We propose a novel *order-one* factorization which relaxes the constraint on McMillan degree inherent in the construction of [134]. In addition, the completion of linear-phase PUFBs has thus become possible. Furthermore, the proposed order-one completion facilitates PUFB design by providing superior results. Examples are given to illustrate the effectiveness of the proposed theory.

In **Chapter 7**, we consider the problem of approximating a given filter bank using only integer arithmetic, i.e., bit shifts and adds. Particularly, we want to minimize the approximation error subject to some adder budget. Namely, the most accurate *multiplierless approximation* is desired for a given number of adders — the more adders at our disposal, the more accurate the multiplierless approximation can be. A simple yet effective quasi-coordinate descent algorithm is proposed for finding the optimal adder allocation. Consequently, a desired accuracy level is achieved using the fewest adders possible. Furthermore, to enforce reversibility, the algorithm is built on top of the lifting factorization. By systematically finding the optimal adder allocation given an adder budget, this algorithm avoids trial-and-error multiplierless approximations, and it complements M -channel lifting factorization developed in **Chapter 3**.

Finally, in **Chapter 8** we summarize our main contributions and point out some future research directions.

Chapter 2

Review

In this chapter, we will review some background materials important for the thesis, including perfect reconstruction filter banks (PRFBs) and the corresponding wavelets and multiresolution analysis (MRA) of the space of finite-energy functions. The significance of regularity of filter banks and smoothness of the wavelet basis will be explained, followed by parameterization of matrices and important building blocks for PRFBs.

The unit impulse is denoted by $\delta[n]$ or δ_n . The output $y[n]$ of a linear time-invariant (LTI) system is its impulse response $h[n]$ convolved with the input $x[n]$, with $y[n] = (h * x)[n] = \sum_m h[n - m] x[m] = \sum_m h[m] x[n - m]$. A filter $h[n]$ is said to be *causal* if $h[n] = 0, \forall n < 0$. A filter $h[n]$ is *lossless* if it is *stable* and *allpass*. If $h[n]$ is of finite duration, the LTI filter is said to be *finite-impulse-response* or FIR, as opposed to the *infinite-impulse-response* or IIR filters for which $h[n]$ has an infinite support in time. FIR filters are unconditionally stable and can be efficiently implemented, and thus are preferred to their IIR counterparts [90].

Boldfaced characters will denote matrices and column vectors. $\mathbf{0}_M$ and $\mathbf{1}_M$ are the M -vectors of all zeros and all ones, respectively. The identity and reverse identity matrices are denoted by \mathbf{I} and \mathbf{J} . We use $\text{diag}(A, B, \dots, C)$ to denote a (block) diagonal matrix composed of A, B, \dots, C along the diagonal. Subscripts will be used if the dimension is not clear from the context. Complex conjugation is denoted by superscript $*$. The superscripts T and \dagger denote matrix transposition and conjugate transposition, respectively. The determinant

and rank of a matrix \mathbf{A} are denoted by $\det(\mathbf{A})$ and $\rho(\mathbf{A})$, respectively. Such notations as $\mathbf{E}(z)$ denote a matrix polynomial whose use is necessary in the context of PRFBs. The tilde notation $\tilde{\mathbf{E}}(z)$ is defined to be the transposition of $\mathbf{E}(z^{-1})$ followed by conjugation of coefficients (with z untouched). The M -dimensional Euclidean space is represented by \mathbb{R}^M , with $\mathbf{e}_0, \mathbf{e}_1, \dots, \mathbf{e}_{M-1}$ forming its standard basis. The symbols $\mathbb{Z}, \mathbb{N}, \mathbb{R}$, and \mathbb{C} denote the set of integers, natural numbers, real numbers, and complex numbers, respectively.

2.1 Filter Banks

A filter bank (FB), as the name suggests, consists of a bank of filters, each of which can be low-pass, band-pass, or high-pass, covering a different portion of the frequency spectrum. When operating on a common input signal $x[n]$, these filters jointly decompose the input into several *subband signals*, which are subject to further processing such as feature analysis or compression. As this is equivalent to analyzing the frequency content of the input, the corresponding filter bank is referred to as an *analysis bank*. Given the fact that input signals of interest have an uneven distribution of energy in frequency, their subband decomposition will result in an alternative characterization that is more compact [3].

It is usually required that a subband decomposition be *invertible*, because we want to be able to reconstruct or synthesize the input signal from its subband representation. In this case, no information loss should be introduced by the analysis bank, and there exist another set of filters referred to as the *synthesis filters* which operate on the subband signals to synthesize the input signal at the output of the filter bank.

Definition 2.1 (Perfect Reconstruction). A filter bank is said to have perfect reconstruction if the output, $\hat{x}[n]$, of the synthesis bank is a delayed (and possibly scaled) version of the input, $x[n]$, i.e.,

$$\hat{x}[n] = c \cdot x[n - \ell]$$

for some $c \neq 0$ and some integer ℓ . Such a filter bank is referred to as a perfect reconstruction filter bank or PRFB [108, 129]. Without loss of generality, one can assume $c = 1$.

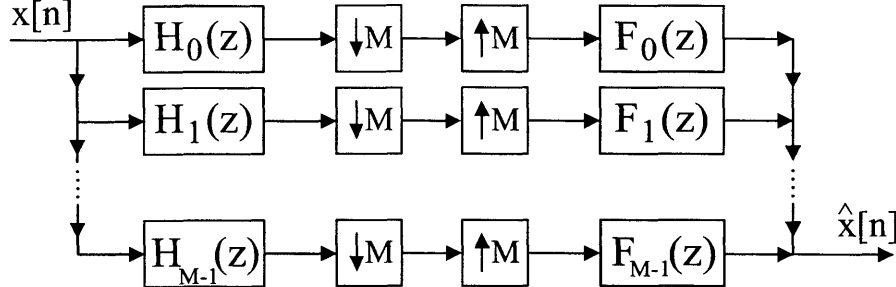
In performing the subband decomposition, a PRFB can introduce redundancy to the subband signals, in which case the overall sampling rate is increased and the subband representation is said to be *overcomplete*. Some examples of overcomplete or *oversampled* PRFBs can be found in [49, 51, 69]. In this thesis, we will focus only on the class of PRFBs which preserve the overall sampling rate, i.e. which do not introduce redundancy nor information loss. Such PRFBs are called the *maximally-decimated* or *critically-sampled* filter banks. They depend additionally on the rate change operators (downsamplers and upsamplers) to preserve the overall sampling rate. In particular, we are interested in the maximally-decimated *uniform* filter banks where all the downsamplers have the same downsampling factor equal to the number of channels, M , as shown in Figure 2-1(a). In what follows, the term PRFB will refer exclusively to the maximally-decimated uniform filter banks.

2.1.1 Maximally-Decimated Uniform Filter Banks

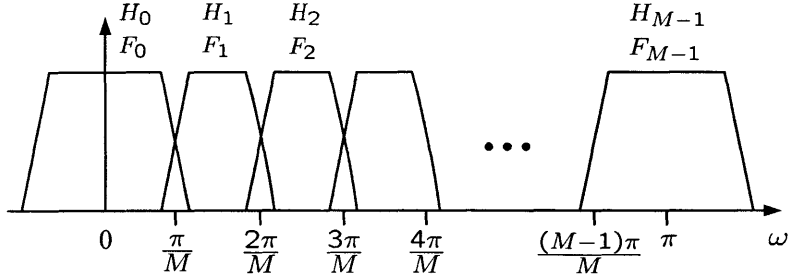
Figure 2-1(a) depicts an M -channel maximally-decimated uniform filter bank [87, 113, 129] with analysis and synthesis filters $H_i(z)$ and $F_i(z)$, respectively, for $i = 0, 1, \dots, M - 1$. The sampling rate of each subband is $\frac{1}{M}$ of that of input $x[n]$, and therefore the overall sampling rate of the subbands is equal to that of $x[n]$, resulting in a non-redundant representation — it is maximally decimated or critically sampled because any further decimation of the subband signals will result in information loss and render perfect reconstruction impossible.

To satisfy PR, we first need to understand the possible sources of error in the filter bank. As downsamplers are involved in the system, aliasing [90, 108] will in general be observed at the output $\hat{x}[n]$. In particular, one can show that the output $\hat{x}[n]$ in Figure 2-1(a) is related to the input $x[n]$ as follows:

$$\hat{X}(z) = \underbrace{\frac{1}{M} \left(\sum_{i=0}^{M-1} F_i(z) H_i(z) \right) X(z)}_{\text{amplitude distortion}} + \underbrace{\sum_{k=1}^{M-1} \frac{1}{M} \left(\sum_{i=0}^M F_i(z) H_i(zW^k) \right) X(zW^k)}_{\text{aliasing components}} \triangleq T_0(z) \quad (2.1)$$



(a) M -channel maximally-decimated uniform filter bank



(b) Frequency spectrum partitioning

Figure 2-1: M -channel maximally-decimated uniform filter bank with perfect reconstruction, where $\hat{x}[n] = c x[n - \ell]$ for some $c \neq 0$ and integer ℓ which is the system delay. $H_i(z)$ and $F_i(z)$ denote the analysis and synthesis filters, respectively, $i = 0, 1, \dots, M - 1$.

where $W \triangleq e^{-j2\pi/M}$. Note that there are two sources of error in (2.1): *amplitude distortion* due to imperfect $T_0(z)$ and *aliasing* as a result of non-vanishing $T_k(z)$, $1 \leq k \leq M - 1$. To avoid amplitude distortion, we require that $T_0(z) = z^{-\ell}$, which is called the *distortion free condition* and requires $T_0(z)$ be simply a delay. In this case, the reconstructed signal $\hat{X}(z)$ is a superposition of $X(z)$ and a linear combination of the aliasing components $X(zW^k)$. It is clear that we also need to set $T_k(z) = 0$ for $1 \leq k \leq M - 1$ to eliminate the aliasing components. This is called the *alias cancellation condition*. The objective of filter bank design is to find a set of PR filters $H_i(z)$ and $F_i(z)$ such that both conditions hold.

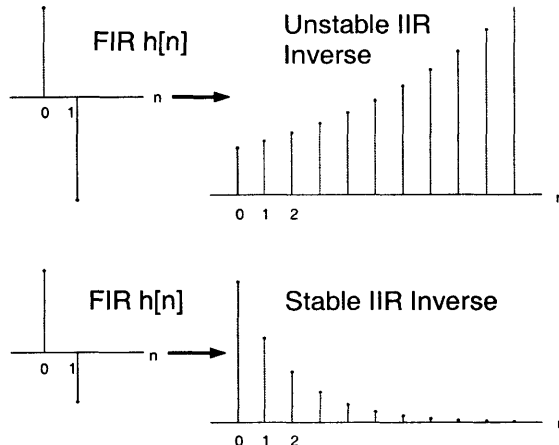
The PR conditions implied from (2.1) can be written in the following matrix form

$$\begin{aligned} \begin{bmatrix} T_0(z) & T_1(z) & \dots & T_{M-1}(z) \end{bmatrix} &= \frac{1}{M} \begin{bmatrix} F_0(z) & F_1(z) & \dots & F_{M-1}(z) \end{bmatrix} \mathbf{H}_m(z) \\ &= z^{-\ell} \begin{bmatrix} 1 & 0 & \dots & 0 \end{bmatrix} \end{aligned} \quad (2.2)$$

where $\mathbf{H}_m(z)$ is the *analysis modulation matrix* defined as

$$\mathbf{H}_m(z) = \begin{bmatrix} H_0(z) & H_0(zW) & \dots & H_0(zW^{M-1}) \\ H_1(z) & H_1(zW) & \dots & H_1(zW^{M-1}) \\ \vdots & \vdots & \ddots & \vdots \\ H_{M-1}(z) & H_{M-1}(zW) & \dots & H_{M-1}(zW^{M-1}) \end{bmatrix}. \quad (2.3)$$

From (2.2), it is clear that an FIR analysis bank has an FIR synthesis bank that gives PR if and only if $\det\{\mathbf{H}_m(z)\}$ = nonzero monomial in z . Note that it is impossible for an FIR *single filter* (as opposed to filter *bank*) to have an FIR inverse¹ — the inverse is at least IIR, let alone stability [90], as illustrated below.



The synthesis modulation matrix $\mathbf{F}_m(z)$ can be similarly defined as follows

$$\mathbf{F}_m(z) = \begin{bmatrix} F_0(z) & F_1(z) & \dots & F_{M-1}(z) \\ F_0(zW) & F_1(zW) & \dots & F_{M-1}(zW) \\ \vdots & \vdots & \ddots & \vdots \\ F_0(zW^{M-1}) & F_1(zW^{M-1}) & \dots & F_{M-1}(zW^{M-1}) \end{bmatrix}. \quad (2.4)$$

Note the *transpose convention* between $\mathbf{H}_m(z)$ and $\mathbf{F}_m(z)$. Then, substituting zW^n for z in

¹Except for a simple delay z^{-k} , which is just trivial.

(2.2) followed by rearranging results in

$$\mathbf{F}_m(z)\mathbf{H}_m(z) = Mz^{-\ell} \begin{bmatrix} 1 & & & \\ & W^{-\ell} & & \\ & & \ddots & \\ & & & W^{-\ell(M-1)} \end{bmatrix} \quad (2.5)$$

for a PRFB.

In the time domain, one can show that the above PR conditions are equivalent to the following *M-shift biorthogonality* between filters $h_i[-n]$ and $f_k[n + \ell]$:

$$\sum_n h_i[-n] f_k[n + Mp + \ell] = \delta[p] \delta[i - k] \quad (2.6)$$

which implies that each *product filter* $P_i(z) \triangleq F_i(z)H_i(z)$ is an *Mth-band filter* [86, 88, 95, 108, 149], satisfying

$$p_i[Mn + \ell] = \delta[n].$$

2.1.2 Polyphase Representation

An analysis filter $H_i(z) = \sum_n h_i[n]z^{-n}$ can be *uniquely* decomposed into M phases $E_{ij}(z)$, $j = 0, \dots, M - 1$, as follows:

$$H_i(z) = \sum_{j=0}^{M-1} z^{-j} E_{ij}(z^M), \quad E_{ij}(z) = \sum_n h_i[Mn + j] z^{-n}, \quad (\text{Type-I polyphase})$$

$i = 0, 1, \dots, M - 1$. This is the Type-I polyphase representation of filter $H_i(z)$. $E_{ij}(z)$ is called the j th phase of filter $H_i(z)$. Extending this idea to the entire analysis bank, we obtain the Type-I polyphase matrix $\mathbf{E}(z)$ of the analysis bank given by

$$\left[\mathbf{E}(z) \right]_{ij} = E_{ij}(z), \quad i, j = 0, 1, \dots, M - 1.$$

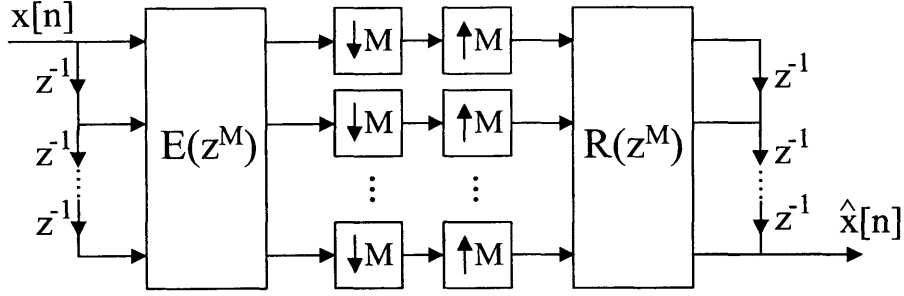


Figure 2-2: Equivalent polyphase representation of the M -channel maximally-decimated uniform filter bank shown in Figure 2-1(a).

It follows that the analysis filters $H_i(z)$ are related to $\mathbf{E}(z)$ via

$$\begin{bmatrix} H_0(z) \\ H_1(z) \\ \vdots \\ H_{M-1}(z) \end{bmatrix} = \mathbf{E}(z^M) \begin{bmatrix} 1 \\ z^{-1} \\ \vdots \\ z^{-(M-1)} \end{bmatrix}. \quad (2.7)$$

Similarly, the Type-II polyphase matrix $\mathbf{R}(z)$ of the synthesis bank is defined to be

$$[\mathbf{R}(z)]_{ji} = R_{ji}(z) = \sum_n f_i[Mn + M - j - 1] z^{-n} \quad (\text{Type-II polyphase})$$

so that

$$F_i(z) = \sum_{j=0}^{M-1} z^{-(M-1-j)} R_{ji}(z^M),$$

and that the synthesis bank can be expressed in terms of $\mathbf{R}(z)$ as

$$\begin{bmatrix} F_0(z) & F_1(z) & \dots & F_{M-1}(z) \end{bmatrix} = \begin{bmatrix} z^{-(M-1)} & z^{-(M-2)} & \dots & z^{-1} & 1 \end{bmatrix} \mathbf{R}(z^M). \quad (2.8)$$

$R_{ji}(z)$ is referred to as the j th (Type-II) phase of filter $F_i(z)$. Both (2.7) and (2.8) provide an equivalent matrix characterization of the filter bank, as depicted in Figure 2-2. It can be further simplified by switching the matrix filters $\mathbf{E}(z^M)$ and $\mathbf{R}(z^M)$ with the downsamplers and upsamplers, respectively. The validity is furnished by the Noble Identities [108, 113]

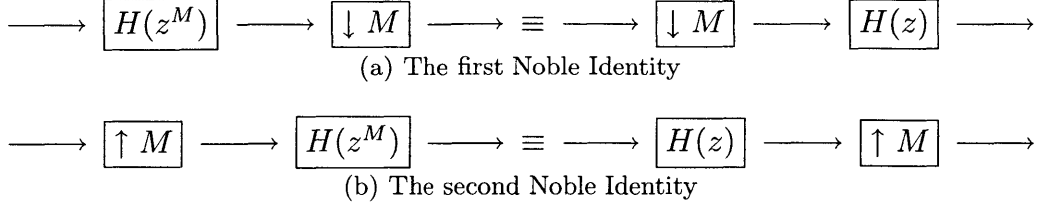


Figure 2-3: The Noble Identities.

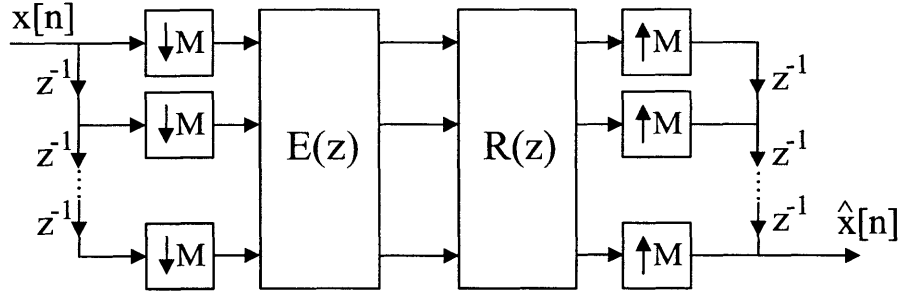


Figure 2-4: The more efficient polyphase representation with the Noble Identities applied.

illustrated in Figure 2-3. Figure 2-4 shows the resulting simplified polyphase representation. The main difference between Figures 2-2 and 2-4 is a more efficient rate of operation — the filtering in Figure 2-4 is done at $\frac{1}{M}$ of the input rate, while in Figure 2-2 the filters within $E(z^M)$ operate at the input rate with only $\frac{1}{M}$ of the computed results kept.

In summary, the analysis bank is equivalent to a multi-input multi-output (MIMO) linear system represented by $E(z)$, and similarly for the synthesis bank. As the mapping between the filters and the polyphase matrices is one to one, the filter bank has PR if and only if the corresponding polyphase matrix is non-singular. In particular, we have the following necessary and sufficient condition for perfect reconstruction (PR) [129]:

Theorem 2.1 (Polyphase Representation and Perfect Reconstruction). *An M -channel maximally-decimated uniform filter bank with analysis and synthesis polyphase matrices $E(z)$ and $R(z)$, respectively, has PR if and only if*

$$R(z)E(z) = c z^{-L} \begin{bmatrix} \mathbf{0}_{(M-r) \times r} & \mathbf{I}_{M-r} \\ z^{-1}\mathbf{I}_r & \mathbf{0}_{r \times (M-r)} \end{bmatrix} \quad (2.9)$$

for some integer r with $0 \leq r \leq M - 1$, some integer L , and some constant $c \neq 0$.

This is a fundamental theorem on the polyphase representation of a PRFB. In fact, the polyphase representation holds the key to *design* and *implementation* of a PRFB. If we know how to design a suitable non-singular polynomial matrix $\mathbf{E}(z)$ with good desired properties, we solve the filter bank design problem. Moreover, the special structures or building blocks used in the design process also serve as a means of efficient implementation. In this thesis, we will focus on such structure-oriented approaches to filter bank design/implementation with desired properties *structurally* imposed.

In practice, FIR PRFBs are preferred to IIR ones as the former can be efficiently implemented without the stability problem. One can show that an FIR analysis bank has a PR FIR synthesis bank if and only if $\det\{\mathbf{E}(z)\} = \text{nonzero monomial in } z$. For a PRFB satisfying (2.9), the reconstructed signal is given by

$$\widehat{x}[n] = c \cdot x[n - n_d], \quad n_d = ML + r + M - 1$$

which is a delayed and possibly scaled version of the input $x[n]$. The overall system delay is $\ell = ML + r + M - 1$ so that $T_0(z) = cz^{-\ell}$. Without loss of generality, we will assume $r = 0$ and $c = 1$ throughout this thesis.

2.1.3 Lifting Scheme

Daubechies and Sweldens demonstrate that any two-channel perfect reconstruction filter bank can be factored into lifting steps [39]:

$$\mathbf{E}(z) = \begin{bmatrix} K & 0 \\ 0 & 1/K \end{bmatrix} \prod_{i=1}^m \begin{bmatrix} 1 & s_i(z) \\ 0 & 1 \end{bmatrix} \begin{bmatrix} 1 & 0 \\ t_i(z) & 1 \end{bmatrix}$$

for some nonzero constant K and some Laurent polynomials $s_i(z)$ and $t_i(z)$, $i = 1, 2, \dots, m$. The filters $s_i(z)$ and $t_i(z)$ are referred to as the *lifting steps*. The lifting scheme provides a faster and in-place implementation, and is trivial to invert—just reverse the order of the

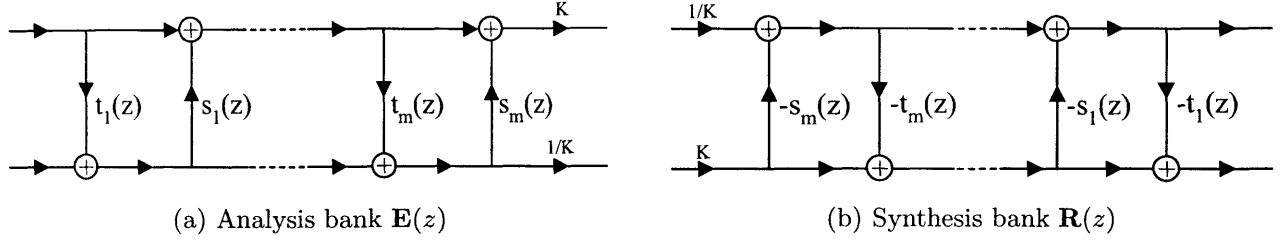


Figure 2-5: Sweldens' two-channel lifting scheme [39].

lifting steps and change signs. See Figure 2-5. The invertibility is structurally enforced by lifting. As a result, one can apply any nonlinear operations to the outputs of lifting steps without losing reversibility. Based on this principle, rational- and dyadic-coefficient perfect reconstruction filter banks are readily obtained. We will develop an M -channel version of lifting scheme in Chapter 3.

2.1.4 Categories of Filter Banks

A PRFB is either orthogonal or biorthogonal. Generally speaking, an analysis FB with a non-singular polyphase matrix $\mathbf{E}(z)$ is said to be *biorthogonal*, in which case the synthesis polyphase matrix can be chosen to be

$$\mathbf{R}(z) = z^{-\ell} \{\mathbf{E}(z)\}^{-1}, \quad \text{some integer } \ell \quad (2.10)$$

from which the synthesis filter $F_i(z)$ can be determined using (2.8). For all practical purposes, $\mathbf{E}(z)$ is usually FIR. However, FIR $\mathbf{R}(z)$ is not necessarily guaranteed by (2.10), unless the determinant of $\mathbf{E}(z)$ is a monomial $c z^{-L}$ for some $c \neq 0$ and $L \in \mathbb{Z}$.

If additionally $\mathbf{E}(z)$ is unitary on the unit circle $|z| = 1$, namely,

$$\{\mathbf{E}(e^{j\omega})\}^{-1} = \{\mathbf{E}(e^{j\omega})\}^\dagger = \underbrace{\{\mathbf{E}(e^{-j\omega})\}^T}_{\text{if real-valued FB}},$$

the FB is called *orthogonal* or *paraunitary* (PU), and the synthesis filters are just time-

reversed or flipped versions of the analysis filters. In particular, one can choose

$$\mathbf{R}(z) = \widetilde{\mathbf{E}}(z) \quad \text{or} \quad \mathbf{R}(z) = z^{-d}\widetilde{\mathbf{E}}(z), \quad \text{some } d \in \mathbb{N}$$

for a PUFB. Namely, the inverse of $\mathbf{E}(z)$ is just its conjugate transposition followed by time-reversal of the polyphase components ($z \rightarrow z^{-1}$). Along with (2.8), this accounts for the time-reversal relation between the analysis and synthesis filters. Namely, the synthesis filters can be found directly from the analysis filters by inspection (time reversal and complex conjugation) [129].

Another important subclass of PRFBs is the *unimodular* filter banks, for which not only need $\det\{\mathbf{E}(z)\}$ be a monomial, but it has no z dependency, i.e., it is a constant. The importance of unimodular filter banks lies in that they achieve the minimal system delay among all PRFBs given the number of channels, M , regardless of the filer length [98, 129]. This is a desirable property for real-time signal processing such as audio processing. Moreover, it has been established that *any* causal FIR PR $\mathbf{E}(z)$ can be factored as a product of a PU matrix and a unimodular matrix [128]. As PUFBs are known to have a complete structure [50, 52, 129], we can parameterize *all* PRFBs if we know how to completely cover the entire space of unimodular FBs.

In this thesis, we will consider exclusively causal and FIR PRFBs.

2.1.5 Performance Criteria

Several criteria can be used to evaluate the performance of a PRFB [122], including DC and mirror frequency attenuation, stopband energy, transform coding gain, etc. Among them, *stopband energy* is the most general criterion which is the L^2 norm of stopband frequency responses, defined as

$$C_{\text{stop}} = \sum_{i=0}^{M-1} \int_{\Omega_i} |H_i(e^{j\omega})|^2 d\omega \quad (2.11)$$

for the analysis filter bank, where Ω_i denotes the stopband for filter $H_i(z)$. It measures the frequency selectivity of the analysis filters. See Figure 2-1(b) for typical passbands and

stopbands of the filters. Stopband energy is similarly defined for the synthesis bank. Note that C_{stop} has a closed-form expression in terms of the autocorrelations of the $h_i[n]$'s [129]. Better frequency selectivity is achieved if stopband energy is minimized. For ideal brick-wall filter banks, stopband energy is zero, which has been shown to be necessary for optimal orthogonal [130] and biorthogonal [133] subband coders.

Similar to stopband energy is *stopband attenuation* which is the L^1 norm of stopband frequency responses:

$$C_{\text{att}} = \sum_{i=0}^{M-1} \sup_{\omega \in \Omega_i} |H_i(e^{j\omega})| \quad (2.12)$$

where Ω_i denotes the stopband for filter $H_i(z)$. By minimizing C_{att} , filters with equiripple stopband response are obtained.

Transform coding gain measures how well the signal energy is compacted in the subbands or the transform domain, and is defined as

$$G = 10 \log_{10} \frac{\sigma_x^2}{\left(\prod_{i=0}^{M-1} \sigma_{x_i}^2 \|f_i\|^2 \right)^{1/M}}, \quad (2.13)$$

where σ_x^2 and $\sigma_{x_i}^2$ refer to the variance of the input and the i th subband, respectively, and $\|f_i\|$ is the ℓ_2 -norm of synthesis filter $F_i(z)$. Maximizing G is equivalent to minimizing the mean square reconstruction error due to subband quantization [130]. To compute G , a commonly used model for natural signals is AR(1) with inter-sample correlation ρ , for which the subband variance can be computed as

$$\sigma_{x_i}^2 = \sigma_x^2 \sum_m \sum_n h_i[m] h_i[n] \rho^{|m-n|}.$$

Given a signal model such as AR(N), better coding gain can be obtained by filter banks with more channels, i.e., larger M . In fact, the *optimal* coding gain is an increasing function

of M , and has been established in [1] to be

$$G_{opt} = \frac{1}{4M^2} \left[\prod_{k=1}^M \int_{\frac{\pi(k-1)}{M}}^{\frac{\pi k}{M}} \sqrt{\frac{S_{xx}(e^{j\omega})}{\sigma_x^2}} \frac{d\omega}{2\pi} \right]^{-\frac{2}{M}} \quad (2.14)$$

where $S_{xx}(e^{j\omega})$ denotes the power spectral density (PSD) of the input signal. This optimal value is obtained by allowing ideal brick-wall filters. Therefore, FIR solutions cannot achieve this optimum, but the difference can be quite negligible as we will see in the design examples of Chapter 5. Figure 2-6 plots G_{opt} for various values of M , along with coding gain of the KLT.

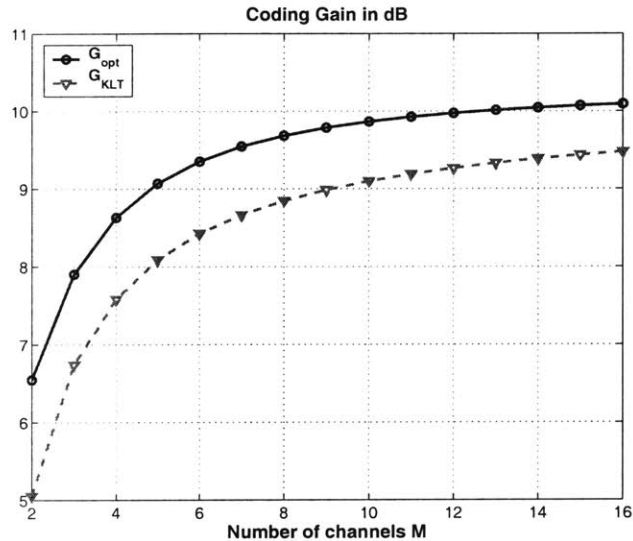


Figure 2-6: Optimal coding gains versus the number of channels M .

2.2 Order and McMillan Degree of PRFBs

Consider an $M \times M$ FIR causal polynomial matrix $\mathbf{E}(z)$. The *McMillan degree* and the *order* of $\mathbf{E}(z)$ are two distinct but important concepts. The (*McMillan*) *degree* of $\mathbf{E}(z)$ refers to the minimum number of delay elements required for its implementation. A *minimal* structure of $\mathbf{E}(z)$ is one which uses this minimum number of delay elements in it; as a contrast, the

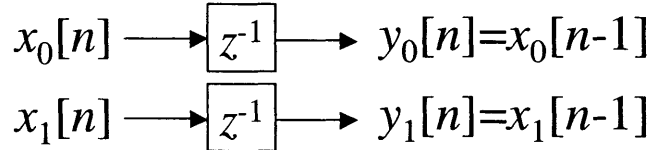
order of $\mathbf{E}(z)$ refers to the highest power of z^{-1} in (causal) $\mathbf{E}(z)$. In particular, since $\mathbf{E}(z)$ is assumed to be causal and FIR, one can always write $\mathbf{E}(z) = \mathbf{A}_0 + \mathbf{A}_1 z^{-1} + \dots + \mathbf{A}_N z^{-N}$ for some coefficient matrices \mathbf{A}_i and some integer N with $\mathbf{A}_N \neq \mathbf{0}$. We see that the highest power of z^{-1} is N , which is the order of $\mathbf{E}(z)$.

A (causal FIR) PRFB is said to have degree (or order) N if its polyphase matrix has degree (or order) N . Note that the degree can be greater than the order. In terms of the filters, for an M -channel $\mathbf{E}(z)$ of order L , the filters $H_i(z)$ will in general have lengths $M(L+1)$. However, a PUFB of length $M(L+1)$ can have degree ranging from L to ML .

For example,

$$\mathbf{E}(z) = z^{-1}\mathbf{I} = \begin{bmatrix} z^{-1} & \\ & z^{-1} \end{bmatrix}$$

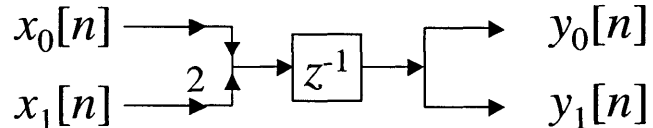
is order-one, but has degree two, because a minimum of two delay elements are needed for its implementation:



On the other hand, consider the following 2×2 system:

$$\mathbf{E}(z) = z^{-1} \begin{bmatrix} 1 & 2 \\ 1 & 2 \end{bmatrix} = \begin{bmatrix} 1 \\ 1 \end{bmatrix} z^{-1} \begin{bmatrix} 1 & 2 \end{bmatrix}$$

which has degree one because the single delay element can be shared between the two channels:



In general, the degree of $z^{-1}\mathbf{A}$ is $\rho(\mathbf{A})$, the rank of \mathbf{A} [129]. As another example,

$$\mathbf{E}(z) = \begin{bmatrix} 1 & 0 & 0 \\ z^{-1} & 1 & 0 \\ 1 & z^{-1} & 1 \end{bmatrix} = \begin{bmatrix} 1 & 0 & 0 \\ 0 & 1 & 0 \\ 1 & 0 & 1 \end{bmatrix} + z^{-1} \begin{bmatrix} 0 & 0 & 0 \\ 1 & 0 & 0 \\ 0 & 1 & 0 \end{bmatrix}$$

is order-one and degree-two.

2.3 Wavelets and Multiresolution Analysis

Strictly speaking, wavelets are for analysis of *continuous*-time functions in a multi-resolution fashion [38, 103, 108, 110, 111]. The term “multiresolution analysis” (MRA) refers to the sequences of nested subspaces of the Hilbert space $L^2(\mathbb{R})$:

$$\text{Primal} \quad \{0\} \leftarrow \dots \subset V_{-1} \subset V_0 \subset V_1 \subset \dots \longrightarrow L^2(\mathbb{R}) \quad (2.15a)$$

$$\text{Dual} \quad \{0\} \leftarrow \dots \subset \tilde{V}_{-1} \subset \tilde{V}_0 \subset \tilde{V}_1 \subset \dots \longrightarrow L^2(\mathbb{R}). \quad (2.15b)$$

These subspaces V_j and \tilde{V}_j represent coarse approximations of $L^2(\mathbb{R})$ at different resolutions indexed by j , where a larger j corresponds to an approximation subspace of higher resolution or detail. The reason for having two such sequences of nested subspaces is to allow for *biorthogonal* wavelet bases for function expansion (to be elaborated below). In the spirit of MRA, we require the spaces V_0 and \tilde{V}_0 be *shift-invariant*, i.e., they are spanned by translations of a single function, called the *scaling function*, as given by

$$V_0 = \text{span}\{\phi(t - n) : n \in \mathbb{Z}\}, \quad (2.16a)$$

$$\tilde{V}_0 = \text{span}\{\tilde{\phi}(t - n) : n \in \mathbb{Z}\}, \quad (2.16b)$$

where ϕ and $\tilde{\phi}$ are the respective scaling functions of the two spaces. The nested subspaces are then related by time scaling defined by

$$V_j = \text{span}\{\phi_n^j : n \in \mathbb{Z}\}, \quad (2.17a)$$

$$\tilde{V}_j = \text{span}\{\tilde{\phi}_n^j : n \in \mathbb{Z}\}, \quad (2.17b)$$

where $\phi_n^j(t) \triangleq M^{j/2} \phi(M^j t - n)$ and the same is for $\tilde{\phi}_n^j$. Scaling functions at the same resolution are required to be biorthogonal to each other:

$$\langle \phi_n^j, \tilde{\phi}_{n'}^j \rangle = \delta_{nn'}, \quad \forall j, n, n' \in \mathbb{Z}. \quad (2.18)$$

The complement of V_j in V_{j+1} is constructed as the union of $M - 1$ subspaces W_j^k , $k = 1, 2, \dots, M - 1$,

$$V_j + \sum_{k=1}^{M-1} W_j^k = V_{j+1} \quad (2.19a)$$

$$\tilde{V}_j + \sum_{k=1}^{M-1} \tilde{W}_j^k = \tilde{V}_{j+1}. \quad (2.19b)$$

Each W_j^k or \tilde{W}_j^k consists of detail at different frequencies. Per MRA, the W_j^k are also required to be shift-invariant, spanned by translates of $M^{j/2}\psi_k(M^j t)$ for some function $\psi_k(t)$, called the *mother wavelet*, as follows:

$$W_j^k = \text{span}\{\psi_{k,n}^j : n \in \mathbb{Z}\} \quad (2.20a)$$

where $\psi_{k,n}^j(t) \triangleq M^{j/2}\psi_k(M^j t - n)$ are the scaled and translated versions of the mother wavelet. Similarly for the dual subspaces \tilde{W}_j^k :

$$\tilde{W}_j^k = \text{span}\{\tilde{\psi}_{k,n}^j : n \in \mathbb{Z}\}. \quad (2.20b)$$

The wavelet bases $\psi_{k,n}^j$ and $\tilde{\psi}_{k',n'}^{j'}$ are also required to be biorthogonal to each other and to their dual scaling functions at coarser resolutions:

$$\left\langle \psi_{k,n}^j, \tilde{\psi}_{k',n'}^{j'} \right\rangle = \delta_{jj'} \delta_{kk'} \delta_{nn'} \quad (2.21a)$$

$$\left\langle \phi_n^j, \tilde{\psi}_{k',n'}^{j'} \right\rangle = 0, \quad \forall j' \geq j \quad (2.21b)$$

$$\left\langle \psi_{k,n}^j, \tilde{\phi}_{n'}^{j'} \right\rangle = 0, \quad \forall j \geq j'. \quad (2.21c)$$

Altogether, the W_j^k (\tilde{W}_j^k) represent the detail information needed in going from V_j to V_{j+1} (from \tilde{V}_j to \tilde{V}_{j+1}).

2.3.1 Dilation and Wavelet Equations

Due to (2.15) and (2.19), there exist some *discrete-time* filters \tilde{h}_i and f_i , $i = 1, 2, \dots, M - 1$, which relate the wavelets and scaling functions at two consecutive scales by

$$\text{Primal} \quad \overbrace{\phi(t) = \sqrt{M} \sum_n f_0[n] \phi(Mt - n)}^{\text{dilation equations}}, \quad \overbrace{\psi_i(t) = \sqrt{M} \sum_n f_i[n] \phi(Mt - n)}^{\text{wavelet equations}} \quad (2.22\text{a})$$

$$\text{Dual} \quad \tilde{\phi}(t) = \sqrt{M} \sum_n \tilde{h}_0[n] \tilde{\phi}(Mt - n), \quad \tilde{\psi}_i(t) = \sqrt{M} \sum_n \tilde{h}_i[n] \tilde{\phi}(Mt - n) \quad (2.22\text{b})$$

where the normalization is $\sum_n \tilde{h}_0[n] = \sum_n f_0[n] = \sqrt{M}$. These are the governing equations of the MRA and are referred to as the *dilation* and *wavelet* equations as noted above. In terms of the notation $\phi_n^j(t) = M^{j/2} \phi(M^j t - n)$, they can be more compactly written as

$$\begin{aligned} \phi(t) &= \sum_n f_0[n] \phi_n^1(t), & \psi_i(t) &= \sum_n f_i[n] \phi_n^1(t), \\ \tilde{\phi}(t) &= \sum_n \tilde{h}_0[n] \tilde{\phi}_n^1(t), & \tilde{\psi}_i(t) &= \sum_n \tilde{h}_i[n] \tilde{\phi}_n^1(t), \end{aligned} \quad (2.23)$$

which is also intuitive if one notes

$$\phi(t) \in V_0 \subset V_1 = \text{span}\{\phi_n^1 : n \in \mathbb{Z}\}.$$

Namely, the $f_0[n]$ are the expansion coefficients of $\phi(t)$ with respect to the basis $\{\phi_n^1\}$. Similar comments apply for the other filters.

2.3.2 Wavelet Series Expansion

Given a function $f \in L^2(\mathbb{R})$, there exist expansion coefficients $c_J[n]$ and $d_{j,k}[n]$ (and their \sim versions) such that

$$f(x) = \underbrace{\sum_n c_J[n] \phi_n^J(x)}_{f_J = (\mathcal{P}_J f)(x)} + \sum_{j=J}^{\infty} \sum_{k=1}^{M-1} \underbrace{\sum_n d_{j,k}[n] \psi_{k,n}^j(x)}_{r_j^k \in W_j^k} \quad (2.24)$$

$$= \sum_n \tilde{c}_J[n] \tilde{\phi}_n^J(x) + \sum_{j=J}^{\infty} \sum_{k=1}^{M-1} \sum_n \tilde{d}_{j,k}[n] \tilde{\psi}_{k,n}^j(x) \quad (2.25)$$

for an arbitrary initial resolution index J , which can be chosen to be 0 without loss of generality. As defined, f_J is the projection of f onto the subspace V_J . The expansion coefficients can be computed as inner products of f with the dual wavelet basis:

$$c_j[n] = \langle f, \tilde{\phi}_n^j \rangle, \quad d_{j,k}[n] = \langle f, \tilde{\psi}_{k,n}^j \rangle, \quad (2.26)$$

$$\tilde{c}_j[n] = \langle f, \phi_n^j \rangle, \quad \tilde{d}_{j,k}[n] = \langle f, \psi_{k,n}^j \rangle. \quad (2.27)$$

as a result of the biorthogonality conditions (2.18) and (2.21).

2.3.3 Fast Wavelet Transform and PRFB

The fast wavelet transform (FWT) relates efficiently the projections of $f \in L^2(\mathbb{R})$ at two consecutive resolutions, $\mathcal{P}_j f \in V_j$ and $\mathcal{P}_{j+1} f \in V_{j+1}$. Without loss of generality, let us consider $\mathcal{P}_0 f$ and $\mathcal{P}_1 f$. By definition, there exist expansion coefficients $c_0[n]$ and $c_1[n]$ such that

$$(\mathcal{P}_0 f)(t) = \sum_n c_0[n] \phi_n^0(t) = \sum_n c_0[n] \phi(t - n) \quad (2.28)$$

$$(\mathcal{P}_1 f)(t) = \sum_n c_1[n] \phi_n^1(t) = (\mathcal{P}_0 f)(t) + \sum_{k=1}^{M-1} \sum_n d_{0,k}[n] \psi_k(t - n) \quad (2.29)$$

and that $c_0[n] = \langle f, \tilde{\phi}(\cdot - n) \rangle$. However, since $V_0 \subset V_1 \subset L^2(\mathbb{R})$, we further have

$$c_0[n] = \langle \mathcal{P}_1 f, \tilde{\phi}(\cdot - n) \rangle. \quad (2.30)$$

Forward FWT

The forward FWT computes $c_j[n]$ from $c_{j+1}[n]$. Substituting (2.29) into (2.30) gives

$$\begin{aligned}
c_0[n] &= \int \sum_{n'} c_1[n'] \phi_{n'}^1(t) \sum_{\ell} \tilde{h}_0[\ell] \tilde{\phi}_{\ell}^1(t-n) dt \quad \dots \dots \text{ using (2.23)} \\
&= \sum_{n'} \sum_{\ell} c_1[n'] \tilde{h}_0[\ell] \underbrace{\left\langle \phi_{n'}^1, \tilde{\phi}_{Mn+\ell}^1 \right\rangle}_{\delta_{n', Mn+\ell}} = \sum_{\ell} c_1[Mn + \ell] \tilde{h}_0[\ell] \\
&= \sum_{\ell} c_1[Mn + \ell] h_0[-\ell] = (c_1 * h_0)(Mn)
\end{aligned} \tag{2.31a}$$

which is a convolution of $c_1[n]$ and $h_0[n]$ followed by M -fold downsampling. Similarly, the wavelet coefficients $d_{0,k}[n]$ can be computed by

$$\begin{aligned}
d_{0,k}[n] &= \left\langle \mathcal{P}_1 f, \tilde{\psi}_k(\cdot - n) \right\rangle = \sum_{\ell} c_1[Mn + \ell] \tilde{h}_k[\ell] \\
&= \sum_{\ell} c_1[Mn + \ell] h_k[-\ell] = (c_1 * h_k)(Mn)
\end{aligned} \tag{2.31b}$$

for $k = 1, 2, \dots, M-1$. Eqn. (2.31) is referred to as the *forward* FWT.

Inverse FWT

To derive the *inverse* FWT, which synthesizes $c_{j+1}[n]$ from $c_j[n]$ and $d_{j,k}[n]$, substitute (2.28) into (2.29) and use the dilation and wavelet equations (2.22) or (2.23), obtaining

$$\begin{aligned}
\sum_n c_1[n] \phi_n^1(t) &= \sum_n \sum_{\ell} \left(c_0[n] f_0[\ell] + \sum_{k=1}^{M-1} d_{0,k}[n] f_k[\ell] \right) \phi_{Mn+\ell}^1(t) \\
&= \sum_n \sum_{n'} \left(c_0[n] f_0[n' - Mn] + \sum_{k=1}^{M-1} d_{0,k}[n] f_k[n' - Mn] \right) \phi_{n'}^1(t).
\end{aligned}$$

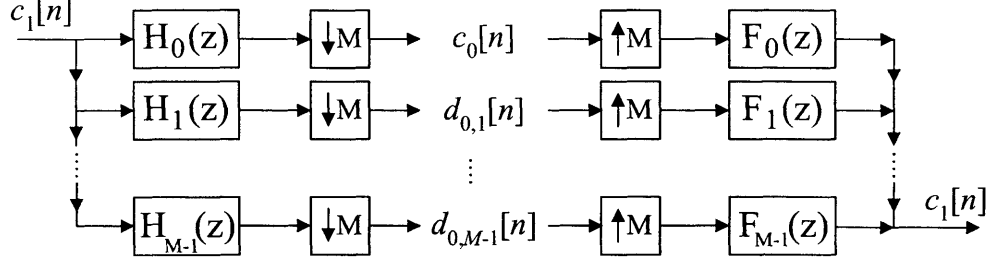


Figure 2-7: Filter bank interpretation of the fast wavelet transform (FWT).

As $\phi_n^1, n \in \mathbb{Z}$, form a basis for V_1 , it follows that

$$\begin{aligned} c_1[n] &= \sum_{n'} c_0[n'] f_0[n - Mn'] + \sum_{k=1}^{M-1} d_{0,k}[n'] f_k[n - Mn'] \\ &= \left(f_0 * (\uparrow M) c_0 \right)[n] + \sum_{k=1}^{M-1} \left(f_k * (\uparrow M) d_{0,k} \right)[n], \end{aligned} \quad (2.32)$$

which is the inverse FWT.

It is apparent from (2.31) and (2.32) that the FWT admits a filter bank interpretation as Figure 2-7 illustrates, where the analysis filters $H_i(z)$ correspond to the time-reversed filters $\tilde{h}_i[-n]$, while the synthesis filters $F_i(z)$ correspond to exactly the filters $f_i[n]$.

Note that one may as well consider the projections onto the dual subspaces \tilde{V}_j and \tilde{V}_{j+1} as we did in (2.25) and (2.27). In this case, we will still have a similar FWT algorithm for which the corresponding analysis bank consists of $f_i[-n]$ and the synthesis bank $\tilde{h}_i[n]$.

2.3.4 Cascade Algorithm and the Inner Product Formula

The solution to the dilation equation with filter h , $\sum_n h[n] = 1$,

$$\phi(t) = M \sum_{n=0}^N h[n] \phi(Mt - n), \quad \text{some } N \in \mathbb{N} \quad (2.33)$$

governs the underlying MRA. This fundamental equation can be solved by the following iterations:

$$\phi^{(i+1)}(t) = M \sum_{n=0}^N h[n] \phi^{(i)}(Mt - n), \quad i = 0, 1, 2, \dots \quad (2.34)$$

called the *cascade algorithm*. Usually $\phi^{(0)}$ = a box function over [0,1). In fact, any $\phi^{(0)}$ that satisfies $\sum_n \phi^{(0)}(t - n) \equiv 1$ can be used to initialize the cascade algorithm [108, Prob. 7.2.4].

The *existence* of a finite-energy (or L^2) solution to the dilation equation (2.33) can be examined by calculating the inner products of $\phi^{(i)}$ and its translates [108]:

$$a^{(i)}[k] \triangleq \int_{-\infty}^{\infty} \phi^{(i)}(t) \phi^{(i)}(t + k) dt, \quad -\infty < k < \infty,$$

the rationale being that if $\lim_{i \rightarrow \infty} \phi^{(i)}$ is in L^2 , the inner products converge, i.e., $\lim_{i \rightarrow \infty} a^{(i)}[k]$ exist. As $\phi^{(i)}(t)$ is compactly supported on $[0, N)$, the inner products $a^{(i)}[k] = 0$ for all $|k| \geq N$. Note that $a^{(i)}[k] = a^{(i)}[-k]$ and that $a^{(i)}[0] = \|\phi^{(i)}\|_2^2$ = energy of $\phi^{(i)}$. Across iterations, these inner products are connected by the *transition matrix* \mathbf{T} , which governs the convergence of the inner products. In summary, the cascade algorithm converges if and only if the inner products do, in which case the eigenvalues of \mathbf{T} should not exceed 1 in absolute value, with 1 being a non-repeated eigenvalue. The matrix \mathbf{T} also characterizes the smoothness of the scaling function.

Transition Matrix

Consider the vector of inner products

$$\mathbf{a}^{(i)} = \begin{pmatrix} a^{(i)}[1 - N] & \dots & a^{(i)}[0] & \dots & a^{(i)}[N - 1] \end{pmatrix}^T.$$

Due to the cascade algorithm, one expects $\mathbf{a}^{(i+1)}$ and $\mathbf{a}^{(i)}$ to be related. To see this, substitute (2.34) into the definition of $a^{(i+1)}[k]$ and obtain

$$\begin{aligned}
a^{(i+1)}[k] &= M^2 \sum_{\ell=0}^N \sum_{n=0}^N h[\ell] h[n] \int_{-\infty}^{\infty} \phi^{(i)}(Mt - \ell) \phi^{(i)}(Mt + Mk - n) dt \\
&= M \sum_{\ell=0}^N \sum_{n=0}^N h[\ell] h[n] \int_{-\infty}^{\infty} \phi^{(i)}(\tau - \ell) \phi^{(i)}(\tau + Mk - n) d\tau \\
&= M \sum_{\ell=0}^N \sum_{n=0}^N h[\ell] h[n] a^{(i)}[Mk - (n - \ell)] \\
&= M \sum_{n'=-N}^N \left(\sum_{\ell=0}^N h[\ell] h[n' + \ell] \right) a^{(i)}[Mk - n'] \\
&= M \sum_{n'=-N}^N h * h^T(n') a^{(i)}[Mk - n'] \\
&= M \sum_{m=-N+1}^{N-1} h * h^T(Mk - m) a^{(i)}[m] = M(\downarrow M)h * h^T * a^{(i)}[k]
\end{aligned} \tag{2.35}$$

for $k \in \{-N + 1, \dots, N - 1\}$. In matrix form, this is

$$\mathbf{a}^{(i+1)} = (\downarrow M)M\mathbf{H}\mathbf{H}^T\mathbf{a}^{(i)} \triangleq \mathbf{T}\mathbf{a}^{(i)}$$

or equivalently

$$\mathbf{a}^{(i)} = \mathbf{T}^i \mathbf{a}^{(0)}$$

where \mathbf{H} is the convolution matrix of filter h and \mathbf{T} is referred to as the *transition matrix*. Note that the power method $\mathbf{a}^{(i+1)} = \mathbf{T}\mathbf{a}^{(i)}$ connects the inner products due to one iteration of the cascade algorithm. The right eigenvector of \mathbf{T} w.r.t. a simple eigenvalue 1 gives the inner products of $\lim_{i \rightarrow \infty} \phi^{(i)}$ and its translates. The other eigenvalues should be less than 1 in magnitude for the power method to converge. Then, L^2 -convergence of the cascade algorithm becomes convergence of the power method.

Based on (2.35), the entries of \mathbf{T} can be computed as follows, where R_{hh} denotes the autocorrelation of h :

```

for i = -N + 1 : N - 1
    for j = -N + 1 : N - 1
        m = M * i - j;
        if (m < -N + 1) || (m > N - 1)
            Tij = 0;
        else
            Tij = M * Rhh(m);
        end
    end
end

```

We note below an efficient MATLAB implementation to construct the transition matrix corresponding to a given filter h :

```

function T = trans_matrix(h, M)
%TRANS_MATRIX Computes the M-band transition matrix
%      T = (\downarrow M) M*H*H'
%      associated with a filter h.

h = h / sum(h);  N = length(h)-1;
Rhh = conv(h, h(end:-1:1));
n = 2*N+1;        T = zeros(n,n);
[jj,ii] = meshgrid([-N:N]);
idx = M*ii-jj+N+1;
T(idx>=1 & idx<=n) = M*Rhh(idx>=1 & idx<=n);

```

Infinite Product Formula for $\Phi(\omega)$

By taking the Fourier transform of (2.34) and iterating, we obtain that of $\lim_{i \rightarrow \infty} \phi^{(i)}(t)$:

$$\Phi^{(i)}(\omega) = \Phi^{(0)}(\omega/M^i) \prod_{j=1}^i H(\omega/M^j), \quad \Phi(\omega) = \prod_{j=1}^{\infty} H(\omega/M^j) \quad (2.36)$$

where the normalization is $\int \phi^{(0)}(t) dt = 1$.

Iterated Filter Bank Approach to Scaling Function Computation

Computationally, the cascade algorithm (2.34) can be efficiently implemented using iterated filter banks. The idea is to treat discrete-time signals as samples of a continuous-time

signal. As the cascade algorithm usually begins with $\phi^{(0)}(t) =$ a box function over $[0, 1]$, the corresponding (initial) discrete-time signal $y^{(0)}[n]$ is chosen to be $\phi^{(0)}(n) = \delta[n]$, the sampling rate being 1. Now, for $\phi^{(1)}(t)$, we want to increase the sampling rate by a factor of M , resulting in $y^{(1)}[n] \triangleq \phi^{(1)}\left(\frac{n}{M}\right)$. In general, we will sample according to $y^{(i)}[n] \triangleq \phi^{(i)}\left(\frac{n}{M^i}\right)$ in order to increase the sample density. One expects that in the limit the “entire” curve of $\phi(t)$ will be captured.

By definition of the cascade formula (2.34), one has

$$y^{(1)}[n] = M \sum_k h[k] \phi^{(0)}\left(M \frac{n}{M} - k\right) = M(h * y^{(0)})[n] = Mh[n].$$

The samples of the next iteration are then

$$\begin{aligned} y^{(2)}[n] &= \phi^{(2)}\left(\frac{n}{M^2}\right) = M \sum_k h[k] \phi^{(1)}\left(M \frac{n}{M^2} - k\right) = M \sum_k h[k] y^{(1)}[n - Mk] \\ &= M \left(\{(\uparrow M)h\} * y^{(1)} \right)[n] \\ &= M^2 \left(\{(\uparrow M)h\} * h \right)[n] = M \left(\{(\uparrow M)y^{(1)}\} * h \right)[n]. \end{aligned}$$

Another iteration will reveal the general rule:

$$\begin{aligned} y^{(3)}[n] &= \phi^{(3)}\left(\frac{n}{M^3}\right) = M \sum_k h[k] \phi^{(2)}\left(\frac{n}{M^2} - k\right) = M \sum_k h[k] y^{(2)}[n - M^2k] \\ &= M \left(\{(\uparrow M)^2 h\} * y^{(2)} \right)[n] = M^3 \left(\{(\uparrow M)^2 h\} * \{(\uparrow M)h\} * h \right)[n] \\ &= \left(Mh * \underbrace{M^2 (\{(\uparrow M)^2 h\} * \{(\uparrow M)h\})}_{(\uparrow M)y^{(2)}} \right)[n] = M \left(\{(\uparrow M)y^{(2)}\} * h \right)[n]. \end{aligned}$$

After K iterations, we have

$$\begin{aligned} y^{(K)}[n] &\triangleq \phi^{(K)}\left(\frac{n}{M^K}\right) = M^K \left(\{(\uparrow M)^{K-1} h\} * \cdots * \{(\uparrow M)h\} * h \right)[n] \\ &= M \left(\{(\uparrow M)y^{(K-1)}\} * h \right)[n], \end{aligned} \tag{2.37}$$

which has the following filter bank interpretation:

$$Mh[n] \xrightarrow{y^{(1)}[n]} \boxed{\uparrow M} \longrightarrow \boxed{MH(z)} \xrightarrow{y^{(2)}[n]} \boxed{\uparrow M} \longrightarrow \boxed{MH(z)} \xrightarrow{y^{(3)}[n]} \dots \longrightarrow \phi(t)$$

Note that one can approximate the Fourier transform of $\phi^{(K)}(t)$ using the above relation:

$$\begin{aligned} \Phi^{(K)}(\omega) &\triangleq \int \phi^{(K)}(t)e^{-j\omega t}dt \approx \frac{1}{M^K} \sum_n \phi^{(K)}\left(\frac{n}{M^K}\right) e^{-j\omega n/M^K} = \frac{1}{M^K} \mathcal{F}\{y^{(K)}\}\left(\frac{\omega}{M^K}\right) \\ &= \mathcal{F}\left\{\{(\uparrow M)^{K-1}h\} * \dots * \{(\uparrow M)h\} * h\right\}\left(\frac{\omega}{M^K}\right) = \prod_{j=1}^K H\left(\frac{\omega}{M^j}\right). \end{aligned}$$

Taking the limit, we obtain

$$\Phi(\omega) = \prod_{j=1}^{\infty} H\left(\frac{\omega}{M^j}\right),$$

which is exactly the infinite product formula (2.36), suggesting the above *iterated filter bank* approach solves the dilation equation. Two examples are given in Figure 2-8.

An alternative to iterated filter banks would be to formulate the eigenvalue problem [9, 108] for the M -channel setting, in order to obtain scaling function values at integers. Then use recursion to compute the function values at n/M^K .

Once we have computed the scaling function, the wavelets $\psi_k(t) = M \sum_n h_k[n]\phi(Mt - k)$ are readily obtained using the $M - 1$ wavelet equations, or equivalently

$$Mh_k[n] \longrightarrow \boxed{\uparrow M} \longrightarrow \boxed{MH(z)} \longrightarrow \boxed{\uparrow M} \longrightarrow \boxed{MH(z)} \longrightarrow \dots \longrightarrow \psi_k(t)$$

2.4 Regularity, Vanishing Moments, and Smoothness

The degree of regularity of a filter bank refers to the number of zeros that the lowpass filter has at the M th roots of unity $e^{j2\pi m/M}$, $m = 1, \dots, M - 1$, which can be shown to be equivalent to the number of zeros that the bandpass and highpass filters possess at DC frequency.

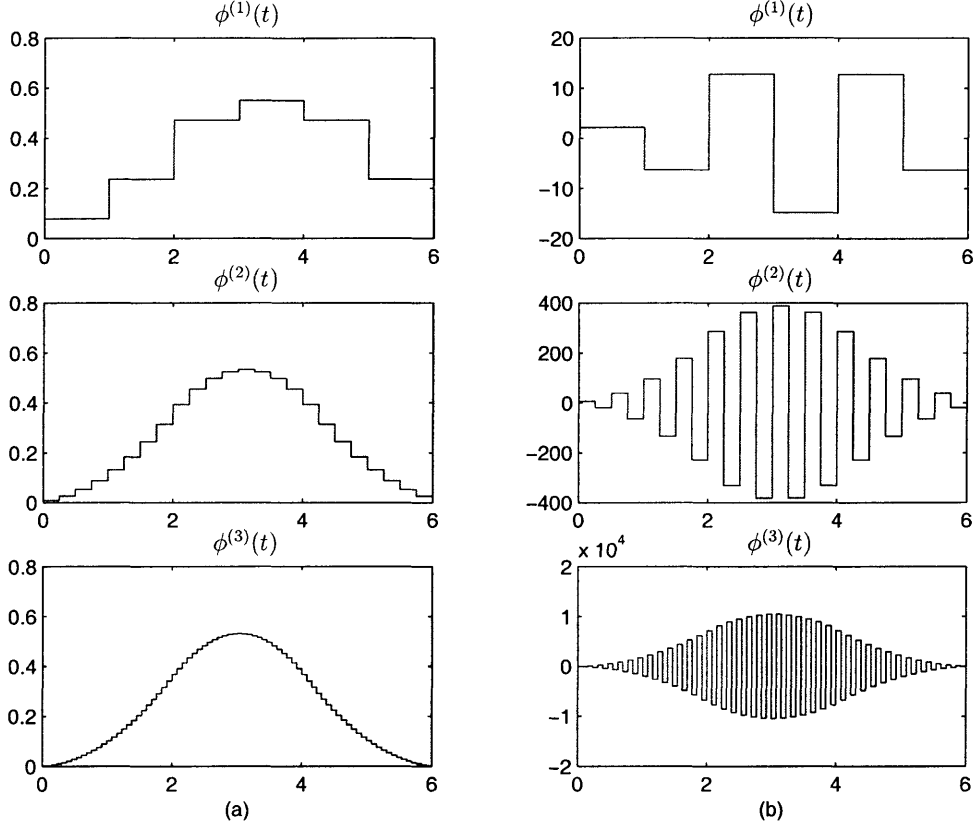


Figure 2-8: Cascade algorithm for $M = 3$. (a) $h[n] = \frac{1}{27}[1, 3, 6, 7, 6, 3, 1]$ having triple zeros at the aliasing frequencies $z_m = e^{j2\pi m/3}$, $m = 1, 2$. The cascade algorithm converges to a 3-band quadratic B-spline with $s_{max} = 2.50$. (b) $h[n] = [1, -3, 6, -7, 6, -3, 1]$ having no zeros at the aliasing frequencies. The cascade algorithm fails to converge in L^2 . $s_{max} = -3.00$.

Definition 2.2 (Regular PRFB). An M -channel PRFB with analysis and synthesis filters $H_i(z)$ and $F_i(z)$, respectively, is said to be (K_a, K_s) -regular if the lowpass filters $H_0(z)$ and $F_0(z)$ have zeros of multiplicity K_a and K_s , respectively, at the M th roots of unity $e^{j2\pi m/M}$ for $m = 1, \dots, M-1$. In general, K_a and K_s can be different, unless the PRFB is paraunitary, in which case the PUFB is said to be K -regular where $K \triangleq K_a = K_s$.

Regularity determines the number of vanishing moments of the M -band wavelets [105], which are suitable for approximating the Sobolev space as they are orthogonal to polynomials up to a certain order [105, 108]. As such, the decay of wavelet coefficients [72, 93, 108] and the accuracy of approximation [108, 124, 140] are both determined by the degree of

regularity, which is further related to the smoothness of the scaling function. One smoothness index is the Sobolev regularity, which measures the L^2 or finite-energy differentiability of the scaling function [57, 108]. One can show that the more regular the filter bank, the smoother the scaling function, and the more derivatives it has. In many applications such as image processing, numerical analysis, smooth signal interpolation, approximation, and data compression [3, 19, 67, 72, 108, 139], smoothness plays a strong role and regular filter banks are thus very desirable.

Below we summarize some important properties of regular PRFBs. For a proof, one can generalize the lines of analysis for $M = 2$ [108] to an arbitrary $M > 2$. Proof for the paraunitary case can be found in [155], for example.

Theorem 2.2. *For a (K_a, K_s) -regular M -channel PRFB with analysis and synthesis filters $H_i(z)$ and $F_i(z)$, respectively, the following statements hold:*

$$1. \left. \frac{d^\ell}{dz^\ell} H_i(z) \right|_{z=1} = 0, \text{ for } \ell = 0, 1, \dots, K_s - 1, \forall i \neq 0.$$

$$2. \left. \frac{d^\ell}{dz^\ell} F_i(z) \right|_{z=1} = 0, \text{ for } \ell = 0, 1, \dots, K_a - 1, \forall i \neq 0.$$

3. *Polynomial cancellations:*

$$\begin{aligned} \sum_n n^\ell h_i[n] &= 0, \text{ for } \ell = 0, 1, \dots, K_s - 1, \forall i \neq 0 \\ \sum_n n^\ell f_i[n] &= 0, \text{ for } \ell = 0, 1, \dots, K_a - 1, \forall i \neq 0 \end{aligned} \tag{2.38}$$

4. *Vanishing moment of wavelets:*

$$\begin{aligned} \int t^\ell \tilde{\psi}_i(t) dt &= 0, \text{ for } \ell = 0, 1, \dots, K_s - 1, \forall i \geq 1 \\ \int t^\ell \psi_i(t) dt &= 0, \text{ for } \ell = 0, 1, \dots, K_a - 1, \forall i \geq 1 \end{aligned} \tag{2.39}$$

5. *Accuracy of Approximation:* In (2.24), if f has at least K_s derivatives, the wavelet

coefficients $d_{j,k}[n]$ decay like M^{-jK_s} :

$$|d_{j,k}[n]| = \left| \int f(t) \tilde{\psi}_{k,n}^j(t) dt \right| = \mathcal{O}(M^{-jK_s}). \quad (2.40)$$

Similarly, if f has at least K_a derivatives, the wavelet coefficients $\tilde{d}_{j,k}[n]$ decay like M^{-jK_a} :

$$\left| \tilde{d}_{j,k}[n] \right| = \left| \int f(t) \psi_{k,n}^j(t) dt \right| = \mathcal{O}(M^{-jK_a}). \quad (2.41)$$

Remarks: The regularity assumption along with Statements 1 and 2 is equivalent to the following conditions on the polyphase matrices:

$$\frac{d^n}{dz^n} \left\{ \mathbf{E}(z^M) \begin{bmatrix} 1 \\ z^{-1} \\ \vdots \\ z^{-(M-1)} \end{bmatrix} \right\}_{z=1} = \begin{bmatrix} c_n \\ 0 \\ \vdots \\ 0 \end{bmatrix}, \quad \text{some } c_n \neq 0, \quad 0 \leq n \leq K_s - 1 \quad (2.42a)$$

and

$$\frac{d^m}{dz^m} \left\{ \begin{bmatrix} z^{-(M-1)} & z^{-(M-2)} & \dots & z^{-1} & 1 \end{bmatrix} \mathbf{R}(z^M) \right\}_{z=1} = \begin{bmatrix} d_m & 0 & \dots & 0 \end{bmatrix} \quad (2.42b)$$

for some $d_m \neq 0$, $0 \leq m \leq K_a - 1$. Statement 3 pertains to the capability of rejecting discrete polynomials up to a certain degree by the bandpass and highpass filters. Statement 5 shows that, for smooth functions, the rate of decay of the wavelet coefficients is dictated by the degree of regularity and equivalently by the number of vanishing moments of wavelets. For example, this asymptotic rate is $\mathcal{O}(64^j)$ for a two-regular eight-channel PUFB, and is $\mathcal{O}(16^j)$ for the four-regular two-channel Daubechies wavelet. In practice, $K \lesssim 4$ is satisfactory for the $M = 2$ case as pointed out in [89, 108]. This suggests that regularity of degree two will be sufficient in practice when the number of channels M is at least four.

2.4.1 DC Leakage

DC leakage refers to the situation where the bandpass and highpass filters do not have zero responses at DC, causing the DC component to leak out of the lowpass band ($H_0(z)$). Ideally, we want the lowpass band to contain all the DC information, as higher frequency bands are usually heavily quantized, and we don't want this to affect the DC component of the signal. By definition, a regular filter bank is free from DC leakage. Figure 2-9 shows the effect of DC leakage and thus the importance of regularity.

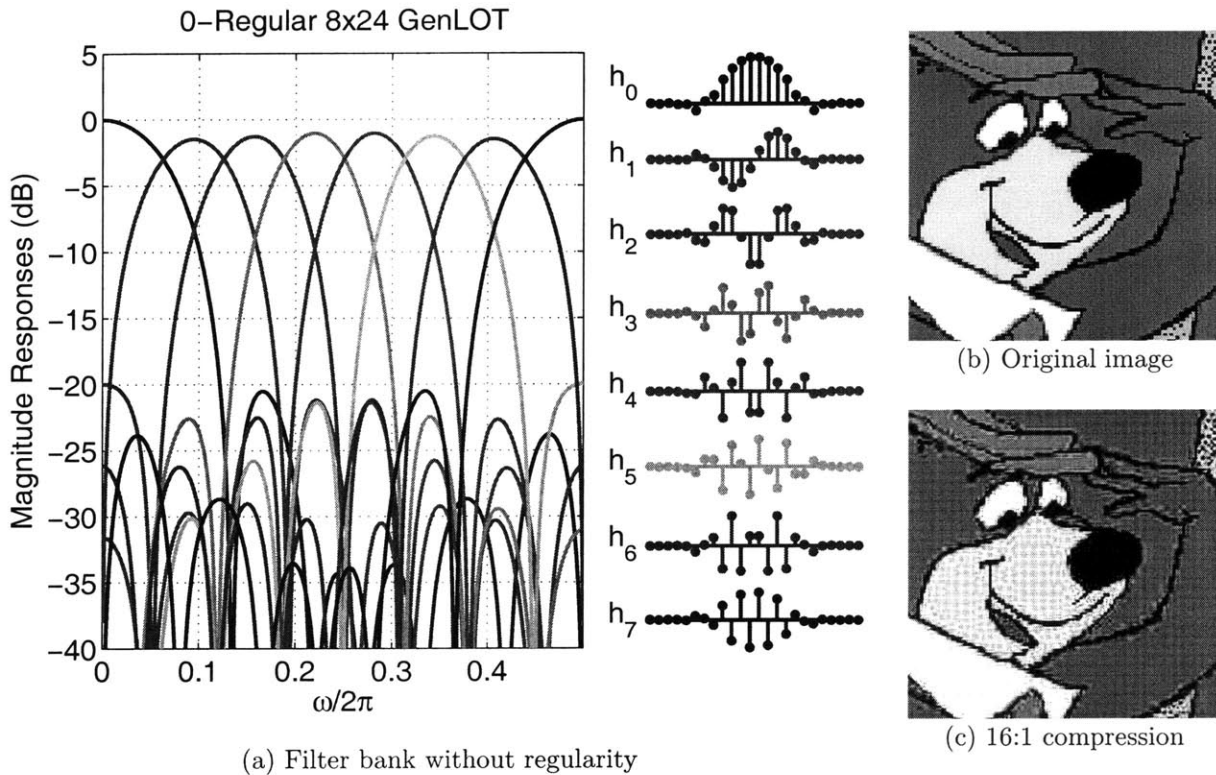


Figure 2-9: Regularity and DC leakage. The (PU) filter bank is not regular: observe that the bandpass and highpass filters do not have zero responses at DC, causing DC leakage. The compressed image exhibits the checkerboard artifact.

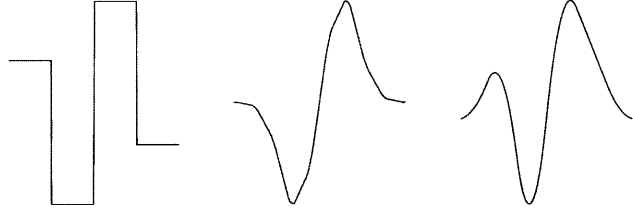


Figure 2-10: Illustration of functions with different s_{max} : from left to right, 0.50, 1.75, 2.50.

2.4.2 Sobolev Exponent As Smoothness Measure

Closely related to regularity or vanishing moments is the concept of smoothness of the M -band wavelet basis. The Sobolev exponent of a filter bank measures the L^2 differentiability of the corresponding scaling function $\phi(t)$ (and thus the wavelet functions $\psi_i(t)$), and is completely determined by the scaling filter $H_0(z)$. Assume $H_0(z)$ is K -regular. Then it can be factored as

$$H_0(z) = \left[\frac{1 + z^{-1} + \dots + z^{-(M-1)}}{M} \right]^K Q(z) \quad (2.43)$$

for some $Q(z)$. Let $Q(z)$ be normalized such that $Q(1) = 1$, and let \mathbf{Q} be the associated convolution matrix. Then the Sobolev exponent or Sobolev smoothness, s_{max} , of the scaling function $\phi(t)$ is given by [57, 108]

$$s_{max} = K - \frac{\log |\lambda_{max}(\mathbf{T}_Q)|}{2 \log M}$$

where $\lambda_{max}(\cdot)$ denotes the largest eigenvalue of its argument and $\mathbf{T}_Q \triangleq (\downarrow M) M \mathbf{Q} \mathbf{Q}^\dagger$ is the *transition matrix* associated with $Q(z)$, which captures how the cascade algorithm

$$g^{(i+1)}(t) = M \sum_n q[n] g^{(i)}(Mt - n)$$

converges in $L^2(\mathbb{R})$, or equivalently, the stability of $q[n]$ under iteration [108]. As revealed by the above relation, the smaller the spectral radius of \mathbf{T}_Q , the smoother the scaling function associated with (2.43). The maximum smoothness for K -regularity is achieved by B-splines,

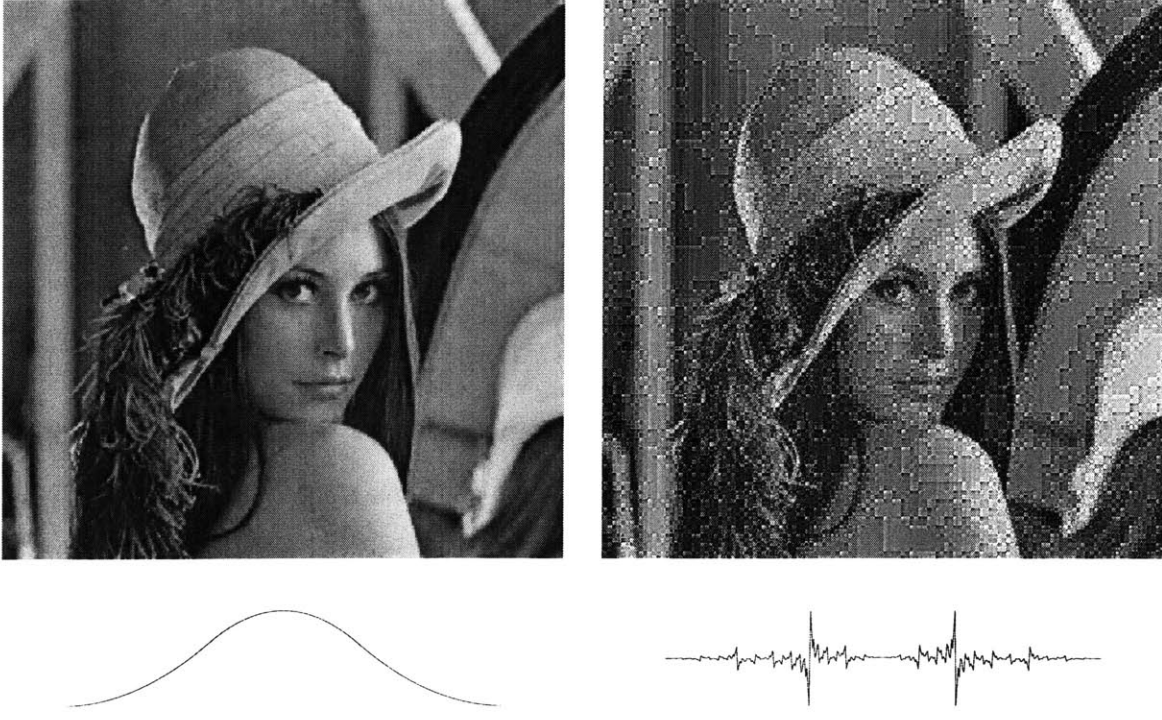


Figure 2-11: Impact of basis smoothness on visual quality. (Left) Compressed image resulting from the *smooth* synthesis basis with $s_{max} = 2.50$. (Right) Compressed image resulting from the *non-smooth* synthesis basis with $s_{max} = -0.56$. Compression ratio is 16:1 for both cases. The basis functions shown are scaling functions with the mentioned s_{max} .

for which $Q(z) \equiv 1$, $\lambda_{max}(\mathbf{T}_Q) = M$, and $s_{max} = K - 1/2$. Figure 2-10 shows some functions with different Sobolev regularity, and the impact of s_{max} on the visual quality of reconstructed images is demonstrated in Figure 2-11.

2.5 Matrix Parameterizations

We briefly summarize the various approaches to matrix parameterization which are essential to filter bank design in this thesis.

2.5.1 Orthogonal or Unitary Matrices

This class of matrices can be completely parameterized either by Givens rotation [85, 129] or by Householder transform [129].

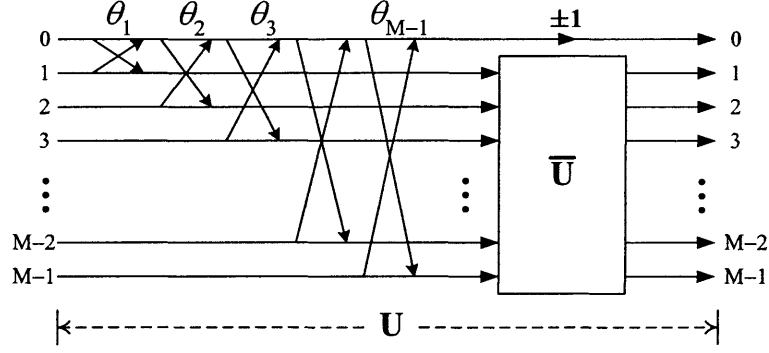


Figure 2-12: Any orthonormal matrix \mathbf{U} is decomposed into a product of Givens rotations. $\bar{\mathbf{U}}$ is also orthonormal.

Givens Rotation

Figure 2-12 demonstrates how an orthonormal matrix \mathbf{U} is decomposed into a cascade of Givens rotations of the form

$$\begin{bmatrix} \cos \theta_i & \sin \theta_i \\ -\sin \theta_i & \cos \theta_i \end{bmatrix}$$

operating on pairs of channels, along with a sign parameter and a smaller matrix $\bar{\mathbf{U}}$ which is still orthonormal. The same decomposition can be recursively applied on $\bar{\mathbf{U}}$ and so on, until we have exhausted all the dimensions. An $M \times M$ orthonormal matrix requires $\binom{M}{2}$ rotation angles and M sign parameters to parameterize.

For a unitary matrix, one has a similar parameterization, but with M rotation angles [85].

Householder Factorization of Unitary Matrices

Instead of using Givens rotations, which have determinant 1, one can use reflection. This is the idea behind the Householder transform. An M -dimensional Householder transform with parameter \mathbf{p} , $\mathbf{H}[\mathbf{p}]$, maps a given vector \mathbf{x} in \mathbb{C}^M to the mirror image \mathbf{y} with respect to a plane E with unit normal \mathbf{p} [107, 129]. By simple geometry, it can be derived that

$$\mathbf{H}[\mathbf{p}] = \mathbf{I} - 2\mathbf{p}\mathbf{p}^\dagger, \quad \|\mathbf{p}\| = 1. \quad (2.44)$$

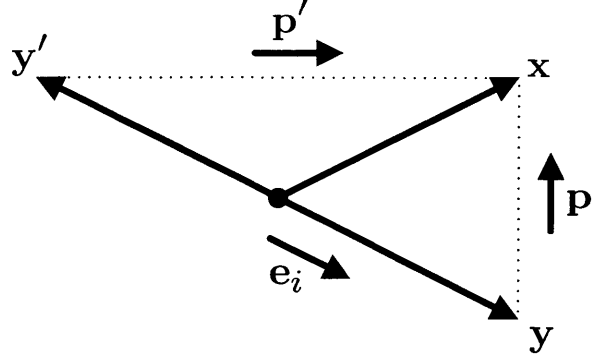


Figure 2-13: The Householder transformation which “turns” \mathbf{x} into the direction of \mathbf{e}_i in a length-preserving fashion. There are two possible outcomes \mathbf{y} (for $\hat{s} = +1$) and \mathbf{y}' (for $\hat{s} = -1$), corresponding to unit-norm \mathbf{p} and \mathbf{p}' in forming the Householder matrix, respectively.

Apparently, this is an invertible, length-preserving and thus unitary transformation. Since \mathbf{x} is also the mirror image of \mathbf{y} with respect to E , the inverse of $\mathbf{H}[\mathbf{p}]$ is simply itself:

$$(\mathbf{H}[\mathbf{p}])^{-1} = \mathbf{H}[\mathbf{p}].$$

Given a nonzero vector $\mathbf{x} = [x_0 \ x_1 \ \dots \ x_{M-1}]^T \in \mathbb{C}^M$ with $x_i = |x_i|e^{j\angle x_i} \triangleq |x_i|\angle x_i$ and a desired coordinate axis \mathbf{e}_i , one can choose a unit vector \mathbf{p}_i such that the transformation $\mathbf{H}[\mathbf{p}_i]\mathbf{x}$ aligns with the desired coordinate axis:

$$\mathbf{H}[\mathbf{p}_i]\mathbf{x} = \hat{s}\|\mathbf{x}\|\mathbf{e}_i\angle x_i, \quad \hat{s} = \pm 1.$$

In this case, one can show that $\mathbf{p}_i = e^{j\phi} \frac{\mathbf{x} - \hat{s}\|\mathbf{x}\|\mathbf{e}_i\angle x_i}{\|\mathbf{x} - \hat{s}\|\mathbf{x}\|\mathbf{e}_i\angle x_i\|}$ for any $\phi \in \mathbb{R}$ and a proper choice of $\hat{s} = \pm 1$ such that $\mathbf{x} - \hat{s}\|\mathbf{x}\|\mathbf{e}_i\angle x_i \neq \mathbf{0}$ [129]. Figure 2-13 provides a geometric interpretation.

A unitary matrix can be factored as a product of Householder matrices. Let \mathbf{U} be $M \times M$ unitary. There exists a Householder transformation $\mathbf{H}[\mathbf{p}_0]$ which aligns the 0th column of \mathbf{U} with \mathbf{e}_0 , namely,

$$\mathbf{H}[\mathbf{p}_0] \mathbf{U} = \left[\begin{array}{c|c} e^{j\theta_0} & \mathbf{0}^T \\ \hline \mathbf{0} & \bar{\mathbf{U}} \end{array} \right]$$

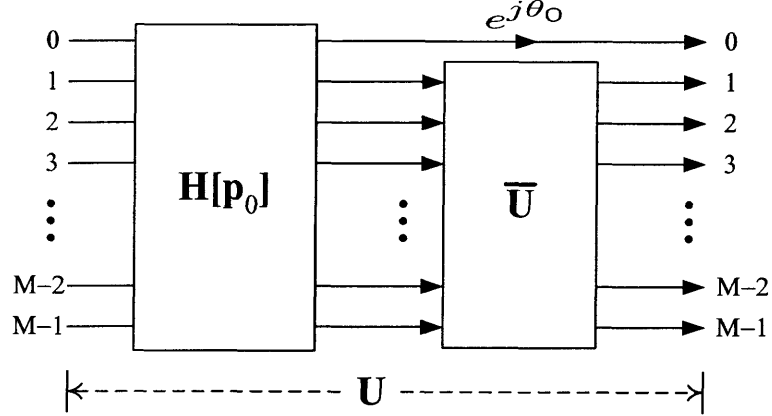


Figure 2-14: Any unitary matrix \mathbf{U} is decomposed into a product of Householder matrices. $\bar{\mathbf{U}}$ is also unitary.

for some unit-norm vector \mathbf{p}_0 and some square unitary matrix $\bar{\mathbf{U}}$. Such a process can be repeated on $\bar{\mathbf{U}}$ and so on to arrive at

$$\mathbf{H}[\mathbf{p}_{M-2}] \mathbf{H}[\mathbf{p}_{M-3}] \dots \mathbf{H}[\mathbf{p}_0] \mathbf{U} = \mathbf{D} \quad (2.45)$$

where $\mathbf{D} = \text{diag}(e^{j\theta_0}, \dots, e^{j\theta_{M-1}})$ is diagonal containing the phase parameters, $\theta_m \in \mathbb{R}$. If \mathbf{U} is real-valued, the θ_m are chosen to be either 0 or π . Inverting (2.45), we obtain the Householder factorization of \mathbf{U} :

$$\mathbf{U} = \mathbf{H}[\mathbf{p}_0] \dots \mathbf{H}[\mathbf{p}_{M-2}] \mathbf{D}. \quad (2.46)$$

Note that the vectors \mathbf{p}_m take the following form,

$$\left[\begin{array}{c|c|c|c} | & | & & | \\ \mathbf{p}_0 & \mathbf{p}_1 & \dots & \mathbf{p}_{M-2} \\ | & | & & | \end{array} \right] = \left[\begin{array}{ccccc} \times & 0 & 0 & \dots & 0 \\ \times & \times & 0 & \dots & 0 \\ \vdots & \vdots & \ddots & \vdots & \vdots \\ \times & \times & \times & \dots & 0 \\ \times & \times & \times & \dots & \times \\ \times & \times & \times & \dots & \times \end{array} \right] \quad (2.47)$$

where \times denotes possibly nonzero values.

A Special Householder Matrix $\mathbf{R}[\cdot]$

The following special Householder matrix will be found useful and convenient for the structural imposition of regularity (biorthogonal case) in Chapter 5 and for the PUFB completion in Chapter 6.

Definition 2.3 (Householder Matrix). Given a vector $\mathbf{x} = \begin{bmatrix} x_0 & x_1 & \dots & x_{M-1} \end{bmatrix}^T \in \mathbb{C}^M$ where $x_0 = |\mathbf{x}| e^{j\theta_0}$, let $\mathbf{R}[\mathbf{x}]$ be the Householder matrix that reflects \mathbf{x} in a length-preserving fashion and aligns it with \mathbf{e}_0 , i.e.,

$$\mathbf{R}[\mathbf{x}] \mathbf{x} = e^{j\theta_0} \|\mathbf{x}\| \mathbf{e}_0 \quad \text{or} \quad \mathbf{x} = e^{j\theta_0} \|\mathbf{x}\| \mathbf{R}[\mathbf{x}] \mathbf{e}_0.$$

See Figure 2-15. If $\mathbf{u} \triangleq \mathbf{x}/\|\mathbf{x}\| - e^{j\theta_0} \mathbf{e}_0 \neq \mathbf{0}$, one can show that

$$\mathbf{R}[\mathbf{x}] = \mathbf{I} - 2 \frac{\mathbf{u} \mathbf{u}^\dagger}{\|\mathbf{u}\|^2}; \quad (2.48a)$$

otherwise, simply define

$$\mathbf{R}[\alpha \mathbf{e}_0] = \mathbf{I}, \quad \alpha \in \mathbb{C} \quad (2.48b)$$

in this degenerate case.

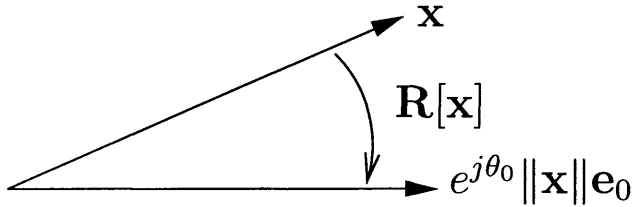


Figure 2-15: Illustration of Householder matrix $\mathbf{R}[\mathbf{x}]$.

Remark: In practice, the degenerate case (2.48b) need be identified and handled appropriately; otherwise numerical instability may occur. Below is a MATLAB function showing how one may compute $\mathbf{R}[\mathbf{x}]$, where the threshold of 10^{-10} can be adjusted as seen fit.

```

function R=house(x)
% R=HOUSE(x)
%
% R*x=||x|| * e0

M=length(x); I=eye(M); e0=I(:,1);
u=x(:)/norm(x)-e0*exp(j*angle(x(1)));

if norm(u)<1e-10 % Very IMPORTANT!!!
    R=I; return;
end

R=I-2*u*u'/(u'*u);
% END of HOUSE.M -----

```

2.5.2 Biorthogonal Matrices

The use of SVD to parameterize a non-singular matrix was proposed in [119], where an invertible matrix \mathbf{A} is decomposed into

$$\mathbf{A} = \mathbf{U}\Lambda\mathbf{V}$$

with \mathbf{U} , \mathbf{V} unitary and Λ diagonal containing the positive *singular values*:

$$\Lambda = \begin{bmatrix} \lambda_0 & & & \\ & \lambda_1 & & \\ & & \ddots & \\ & & & \lambda_{M-1} \end{bmatrix}.$$

See Figure 2-16. The unitary \mathbf{U} , \mathbf{V} can in turn be further parameterized using either Givens rotations or the Householder transform. In practice, the sign parameters (or phase parameters if complex case) of \mathbf{U} and \mathbf{V} can be absorbed by Λ — no longer are the λ_m positively constrained as the original SVD formulation would require; they can even be complex-valued.

Another approach to non-singular matrix parameterization is based the QR factorization

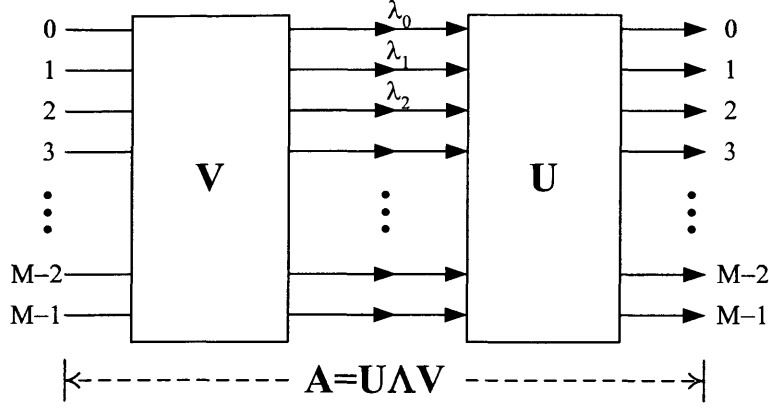


Figure 2-16: SVD-based parameterization of an invertible matrix \mathbf{A} .

where an invertible matrix \mathbf{A} can be written as

$$\mathbf{A} = \mathbf{Q}\mathbf{R}$$

where \mathbf{Q} is unitary and

$$\mathbf{R} = \begin{bmatrix} r_{00} & r_{01} & \dots & r_{0,M-1} \\ & r_{11} & \dots & r_{1,M-1} \\ & \ddots & & \vdots \\ & & & r_{M-1,M-1} \end{bmatrix}$$

upper triangular with positive diagonal elements. See Figure 2-17. In practice, the sign constraint on the diagonal of \mathbf{R} can be relaxed as described above for the SVD-based approach.

2.6 Dyadic-Based Structures

The philosophy of filter bank design is to start with a trivial PRFB — the *lazy* filter bank [108] which does no filtering at all but has perfect reconstruction, and then work one's way toward nontrivial, longer filters. This is often achieved by cascading *building blocks* of some sort to increase the degree and/or order of the PRFB in a modular way. In particular, these

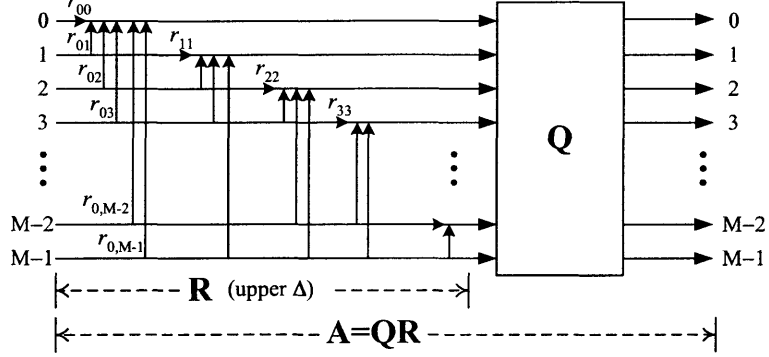


Figure 2-17: QR-based parameterization of an invertible matrix \mathbf{A} .

building blocks take the following general form:

$$\mathcal{W}_m(z) = \mathbf{I} - \mathcal{U}_m \mathcal{V}_m^\dagger + z^{-1} \mathcal{U}_m \mathcal{V}_m^\dagger \quad (2.49)$$

where \mathcal{U}_m and \mathcal{V}_m are $M \times \gamma_m$ parameter matrices with $1 \leq \gamma_m \leq M$. They are referred to as the *dyadic-based structures* [52, 129, 132, 134].

2.6.1 Paraunitary Case

In (2.49), if we assume $\mathcal{U}_m = \mathcal{V}_m$ having orthonormal columns, the resulting building block becomes paraunitary. Depending on the value of γ_m , we have a degree-one PU building block ($\gamma_m = 1$) or a general order-one PU building block. Both provide a complete factorization of a PUFB with or without length constraint, referred to as the order-one factorization [50, 52] and the degree-one factorization [52, 129], respectively.

Lemma 2.1 (Degree-one Paraunitary Building Block [129]). *The dyadic-based structure with parameter vector \mathbf{v}_m*

$$\mathbf{V}_m(z) = \mathbf{I} - \mathbf{v}_m \mathbf{v}_m^\dagger + z^{-1} \mathbf{v}_m \mathbf{v}_m^\dagger, \quad \|\mathbf{v}_m\| = 1 \quad (2.50)$$

is the degree-one paraunitary building block: any degree- N paraunitary polyphase matrix $\mathbf{E}(z)$

can be factored as

$$\mathbf{E}(z) = \mathbf{V}_N(z) \mathbf{V}_{N-1}(z) \dots \mathbf{V}_1(z) \mathbf{E}_0 \quad (\text{degree-one factorization}) \quad (2.51)$$

where \mathbf{E}_0 is unitary: $\mathbf{E}_0^\dagger \mathbf{E}_0 = \mathbf{I}$. This structure is referred to as the *degree-one factorization* and is complete for any given degree N .

Remark: This structure covers a larger class than the GenLOT [41] as the linear phase constraint is not assumed by (2.51). Each $\mathbf{V}_m(z)$ increases the filter length by M upon cascaded, and therefore is of *order* one. However, it is not the most general building block of order one. In fact, an $M \times M$ PU building block of order one can have *degree* up to M .

Generalizing the above degree-constrained structure $\mathbf{V}_m(z)$, Gao *et al.* have recently proposed a complete and minimal factorization given the *order* of the PUFB [52]. They also proposed an efficient parameterization using fewer free parameters than before, without affecting the completeness of the factorization, which has been further improved in [50].

Lemma 2.2 (Order-One Paraunitary Building Block [52]). *The dyadic-based structure with parameter matrix \mathbf{w}_m*

$$\mathbf{W}_m(z) = \mathbf{I} - \mathbf{w}_m \mathbf{w}_m^\dagger + z^{-1} \mathbf{w}_m \mathbf{w}_m^\dagger, \quad \mathbf{w}_m^\dagger \mathbf{w}_m = \mathbf{I}_{\gamma_m} \quad (2.52)$$

is the order-one paraunitary building block for some integer γ_m with $1 \leq \gamma_m \leq M$. Any order- L paraunitary polyphase matrix $\mathbf{E}(z)$ can be factored as

$$\mathbf{E}(z) = \mathbf{W}_L(z) \mathbf{W}_{L-1}(z) \dots \mathbf{W}_1(z) \mathbf{E}_0 \quad (\text{order-one factorization}) \quad (2.53)$$

*for some $M \times M$ unitary \mathbf{E}_0 and some integers $\gamma_1, \dots, \gamma_L$. This structure is referred to as the *order-one factorization* of $\mathbf{E}(z)$. It is complete for any given order L , and the integers γ_m can be monotonically ordered*

$$1 \leq \gamma_L \leq \gamma_{L-1} \leq \dots \leq \gamma_1 \leq M \quad (2.54)$$

or

$$1 \leq \gamma_1 \leq \gamma_2 \leq \dots \leq \gamma_L \leq M \quad (2.55)$$

without affecting the completeness of the structure.

Remarks: In (2.52), the parameter matrix \mathbf{w}_m consists of γ_m orthonormal columns,

$$\mathbf{w}_m = \begin{bmatrix} | & | & & | \\ \mathbf{w}_{m,1} & \mathbf{w}_{m,2} & \dots & \mathbf{w}_{m,\gamma_m} \\ | & | & & | \end{bmatrix}, \quad (2.56)$$

with $\mathbf{w}_{m,n}^\dagger \mathbf{w}_{m,\ell} = \delta_{n\ell}$. Since the $M \times \gamma_m$ matrix \mathbf{w}_m is unitary, we have $\rho(\mathbf{w}_m) = \rho(\mathbf{w}_m \mathbf{w}_m^\dagger) = \gamma_m$, and the degree of $\mathbf{W}_m(z)$ is thus γ_m [129]. In fact, $\mathbf{W}_m(z)$ in (2.52) can be decomposed into a cascade of γ_m degree-one PU building blocks:

$$\mathbf{W}_m(z) = \mathbf{V}_{m,\gamma_m}(z) \dots \mathbf{V}_{m,1}(z) \quad (2.57)$$

where for each $i = 1, \dots, \gamma_m$, $\mathbf{V}_{m,i}(z)$ is the degree-one PU building block (2.50) with parameter vector $\mathbf{w}_{m,i}$ coming from (2.56); on the other hand, given an orthonormal basis $\{\mathbf{w}_{m,i} \in \mathbb{C}^M \mid \text{some } i\}$ of any non-zero subspace of \mathbb{C}^M and the corresponding degree-one PU building blocks $\mathbf{V}_{m,i}(z)$, the product (2.57) is always of order one. In view of $\mathbf{W}_m(z)$, $\mathbf{V}_m(z)$ is the minimum-degree order-one building block. In practice, order-one factorization is preferred as one cares more about the filter length than the McMillan degree of the PUFB. It is also necessary because when the order or filter length is specified, it allows for more design flexibility than the *degree-one* factorization.

Order-One vs. Degree-One Factorizations

In practice, order-one factorization is preferred as one cares more about the filter length² than the McMillan degree of the PUFB. It is also necessary because with the order (L) or

²Recall that the polyphase matrix $\mathbf{E}(z)$ of a causal M -channel PUFB with filter length $M(L + 1)$ is of order L .

filter length specified, it allows for more design flexibility than the *degree-one* factorization, as demonstrated in Figure 2-18 where $L = 2$. In particular, one adjusts γ_m to obtain a

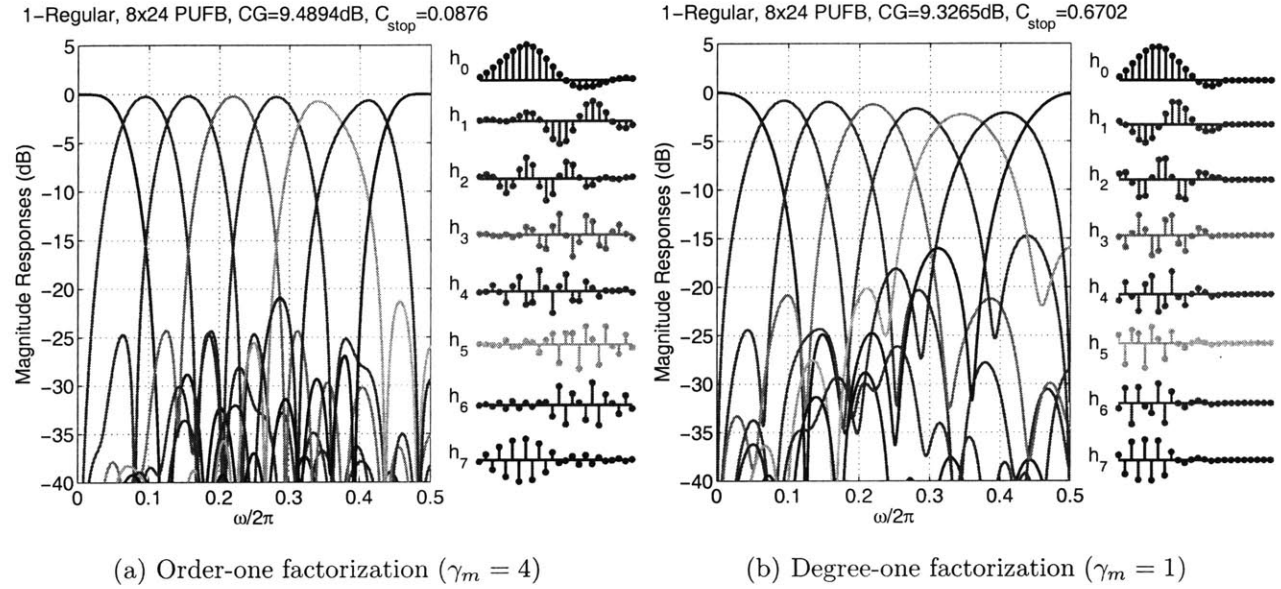


Figure 2-18: Comparison of order-one and degree-one factorizations in regular PUFB design. Both are one-regular eight-channel with length 24. Order-one factorization allows for more degrees of freedom to optimize filter bank performance. (a) is the one-regular 8×24 PUFB discussed in Section 4.5.1 of the thesis.

different number of design variables, where $\gamma_m \geq 1$ denotes the rank of parameter matrix \mathbf{w}_m as in the order-one PU building block

$$\mathbf{W}_m(z) = \mathbf{I} - \mathbf{w}_m \mathbf{w}_m^\dagger + z^{-1} \mathbf{w}_m \mathbf{w}_m^\dagger, \quad \mathbf{w}_m^\dagger \mathbf{w}_m = \mathbf{I}_{\gamma_m}$$

for $m = 1, 2, \dots, L$. In this perspective, the *degree-one* factorization is a special case where all γ_m are equal to unity, permitting only the fewest degrees of freedom for the given order L . The resulting design is restricted and usually exhibits a nearly minimum- or maximum-phase pattern, where the filters energy is highly unbalanced, concentrating towards either end of the filters regardless of filter length (Figure 2-18(b)). This should be compared to linear-phase PUFBs or GenLOTs [41], which assume an *order-one* form in their factorizations. Specifically, one can show that (nontrivial) linear phase is only possible with order-one

factorization [6].

2.6.2 Biorthogonal Case

Any biorthogonal filter bank can be written as a cascade of paraunitary and unimodular systems [128, 132]. However, the problem of completely parameterizing the space of unimodular matrices remains unsolved, in the sense that there do not exist any finite-degree building blocks which arbitrary-order unimodular filter banks can be factorized into³ [98, 128, 132]. Therefore, it is still unclear how to have a complete structure for the most general biorthogonal filter banks.

However, we can still pick a structure *a priori* and consider the corresponding class of BOFBs. In this thesis, we will consider the class of causal FIR BOFBs spanned by the following structure

$$\mathbf{E}(z) = \mathbf{W}_L(z) \dots \mathbf{W}_1(z) \mathbf{E}_0 \quad (2.58)$$

which has an FIR inverse, where \mathbf{E}_0 is non-singular and each $\mathbf{W}_m(z)$ is the first-order biorthogonal building block given by

$$\mathbf{W}_m(z) = \mathbf{I} - \mathcal{U}_m \mathcal{V}_m^\dagger + z^{-1} \mathcal{U}_m \mathcal{V}_m^\dagger \quad (2.59)$$

where the $M \times \gamma_m$ parameter matrices \mathcal{U}_m and \mathcal{V}_m satisfy certain biorthogonality conditions (See Eqn. (5.3)). This can be viewed as a generalization of the paraunitary order-one factorization given in [52] where $\mathcal{U}_m = \mathcal{V}_m$, and has been used for factoring the BOLT [132]. More details are found in Chapter 5.

³Except that order-one unimodular matrices, also known as the *lapped unimodular transform* or LUT, can always be factored as a product of degree-one unimodular building blocks [98]. Such a structure is complete.

Chapter 3

M-Channel Lifting Factorization

An intrinsic M -channel lifting factorization of perfect reconstruction filter banks (PRFBs) is presented as an extension of Sweldens' conventional two-channel lifting scheme. Given a polyphase matrix $\mathbf{E}(z)$ of an FIR M -channel PRFB with $\det(\mathbf{E}(z)) = z^{-K}$, $K \in \mathbb{Z}$, a systematic M -channel lifting factorization is derived based on the Monic Euclidean algorithm. The M -channel lifting structure provides an efficient factorization and implementation; examples include optimizing the factorization for the number of lifting steps, delay elements, and dyadic coefficients. Specialization to paraunitary building blocks enables the design of paraunitary filter banks based on lifting. We show how to achieve reversible, possibly multiplierless, implementations under finite precision, through the unit diagonal scaling property of the Monic Euclidean algorithm. Furthermore, filter bank regularity of a desired order can be imposed on the lifting structure; in fact, as will be shown in the next chapter, M -channel lifting factorization bears a physical interpretation in designing regular paraunitary filter banks. Finally, PRFBs with a prescribed admissible scaling filter are conveniently parameterized.

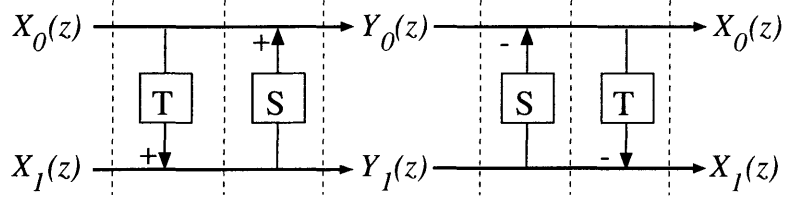


Figure 3-1: Two lifting steps with lifting multipliers \mathbf{T} and \mathbf{S} which can be any time-invariant, even nonlinear, systems. The first lifting step filters input $X_0(z)$ with \mathbf{T} and adds the result to $X_1(z)$, the sum being the output $Y_1(z)$. The second lifting step then applies \mathbf{S} to $Y_1(z)$ and adds the result to $X_0(z)$ to give $Y_0(z)$. To invert, just subtract what was added in the reverse order.

3.1 Introduction

The lifting scheme, also known as the ladder structure [18], has been used in both factorization [39] and design [27, 114] of filter banks (FBs). It features reversible and in-place computation [39], and it leads to fast implementations of the discrete wavelet transform. Notably, the JPEG2000 standard [60, 116] uses the two-channel lifting scheme to implement two-band wavelet transforms. The lifting scheme consists of a series of so-called “lifting steps,” each of which is a one-wing butterfly that adds a certain multiple of or a filtered version of one channel to another. As a result, lifting steps can be easily inverted by subtracting whatever was added in the forward transform. Figure 3-1 shows two lifting steps and their inverses. It is this special structure of the one-wing butterfly that gives the lifting scheme its power and flexibility. For example, one can design (nonlinear) wavelet-like transforms that map integers to integers [20, 30]; or one can design dyadic- and/or rational-coefficient filter banks that possess perfect reconstruction (PR) [22, 66, 120, 154].

Many practical applications in digital communications make use of M -channel filter banks. For example, cosine-modulated filter banks [129] are frequently used in xDSL technology. Furthermore, greater design flexibility is allowed in the M -channel setting ($M > 2$), such as the coexistence of orthogonality and linear phase. Because of the desirable properties that the lifting scheme provides, it is natural to extend the two-channel result to an M -channel setting, $M > 2$. By *M -channel lifting factorization*, we mean the factorization of

an M -channel polyphase matrix $\mathbf{E}(z)$ with determinant z^{-K} into $M \times M$ triangular matrices with only ± 1 on their diagonals, and possibly some permutations. Such triangular matrices are called (M -channel) *liftings* or *lifting steps*, or *shears* if the diagonals consist of only 1's.

For the class of PRFBs with a constant polyphase matrix having determinant 1, an interesting, but rather restricted, form of M -channel lifting known as the *ULU* decomposition has been proposed [117]. The focus there was to express a matrix with unit determinant as a product of lower and upper shears, with a canonical form for the lower shear. The *ULU* decomposition is obtained by solving a few systems of linear equations. However, the number of non-trivial lifting multipliers in the two upper shears tends to grow very quickly as the matrix size increases, since special structure of the matrix, such as symmetry, is not fully exploited. Although one can perform row/column permutations to the matrix followed by *ULU*, the reduction in the number of non-trivial lifting multipliers is marginal, and it becomes asymptotically infeasible to enumerate all row/column permutations as the matrix size increases: an 8×8 matrix can be permuted in $(8!)^2 = 1,625,702,400$ ways!

In this chapter, we aim to factor an arbitrary M -channel PRFB into lifting steps (and thereby provide a construction in which all matrix factors have diagonal entries of unity) by using only Type-3 elementary matrices. Permutations can also be used wherever necessary, with the possibility of having -1 's on the diagonals. We will refer to this condition later as a *unit diagonal scaling*, which in fact includes scaling factors of the form $\pm z^{-m}$, $m \in \mathbb{Z}$. This will permit a reversible implementation of the PRFB under finite precision. The implementation can be rendered multiplierless if the lifting multipliers are re-optimized to be dyadic numbers, $k/2^n$, $k, n \in \mathbb{Z}$. Consequently, the lifting structure lends itself to reversible integer transforms.

As in [39], the proposed M -channel lifting factorization will assume a PRFB $\mathbf{E}(z)$ with $\det(\mathbf{E}(z)) = z^{-K}$ (although some relaxation of this constraint is possible, as discussed in Section 3.3.5). Furthermore, the M -channel lifting factorization is not unique, a direct consequence of the non-uniqueness of Laurent polynomial division. As a result, it is desirable to come up with the “best” lifting factorization. Fortunately, for $M = 2$, it is a relatively

simple task to enumerate all possible lifting factorizations into a tree-like data structure [79], as there is no ambiguity in choosing a divisor among the $M - 1 = 1$ polyphase components when performing the Euclidean algorithm.

For $M > 2$, the approach provided in this chapter serves as general guidance, as it becomes intractable to enumerate all possible lifting factorizations. Several variations of the basic algorithm can be applied to derive a good factorization, depending on the particular PRFB given. For example, the location of the pivot used in size reduction (Section 3.3.3) can be anywhere seen fit. One can also perform some sort of locally optimal quotient selection rule during the process of long division. Furthermore, exploiting the particular structure, if present, in the PRFB can lead to more efficient results. These will be further discussed in Section 3.4.

Though formulated under a general setting, the proposed algorithm is specialized to paraunitary, unimodular, and a class of biorthogonal building blocks, as well as block transforms such as the DCT. Also considered are the imposition of desirable properties such as structural regularity, and the reduction of complexity through the minimization of delay elements and floating-point multiplications. The interesting problem of designing a PRFB given an admissible lowpass (scaling) filter will be discussed within the context of the proposed Monic Euclidean algorithm and the M -channel lifting factorization.

The remainder of the chapter is organized as follows. Section 3.2 provides preliminaries on the lifting structure and the Euclidean algorithm. In Section 3.3, the proposed M -channel lifting factorization is presented, based on the so-called Monic Euclidean algorithm, which always generates a monic gcd. PRFB design with a prescribed admissible scaling filter is also discussed within this context. All the proofs encountered in the above two sections are given in the Appendices, and they are constructive. In Section 3.4, several PRFBs are examined in the context of M -channel liftings, demonstrating the versatility of the proposed algorithm. Finally, Section 3.5 concludes this chapter.

3.2 Preliminaries

3.2.1 Elementary Matrix Operations

An elementary operation on a (polynomial) matrix can be any one of the following:

Type-1: Interchange two rows/columns.

Type-2: Multiply a row/column with a nonzero constant.

Type-3: Add a (polynomial) multiple of a row/column to another row/column.

In the context of the proposed M -channel lifting factorization, Type-2 operations will be excluded, because we want to avoid non-dyadic scaling factors on the diagonals. This is essential for reversibility in a finite-precision implementation. Type-3 operations will mainly be the ones of choice. In case sign negation is permitted, Type-1 can also be admitted, but we will show that the M -channel lifting can be achieved by using only Type-3 operations.

3.2.2 M -Channel Lifting Structure

Definition 3.1 (M -Channel Simple Lifting Step). *An M -channel simple lifting step, from channel j to i ($i, j = 0, 1, \dots, M - 1; i \neq j$) with multiplier $\lambda(z)$, is defined by the following matrix operator:*

$$\Gamma_{i,j}[\lambda(z)] = \mathbf{I} + \lambda(z) \mathbf{e}_i \mathbf{e}_j^T, \quad (3.1)$$

where \mathbf{I} is $M \times M$ and \mathbf{e}_i is $M \times 1$. A simple lifting is said to be FIR if the multiplier $\lambda(z)$ is FIR. \diamond

As defined, $\Gamma_{i,j}[\lambda(z)]$ is a triangular matrix with only 1's on the diagonal, implying $\det(\Gamma_{i,j}[\cdot]) = 1$. Its inverse is also a simple lifting:

$$(\Gamma_{i,j}[\lambda(z)])^{-1} = \mathbf{I} - \lambda(z) \mathbf{e}_i \mathbf{e}_j^T = \Gamma_{i,j}[-\lambda(z)]. \quad (3.2)$$

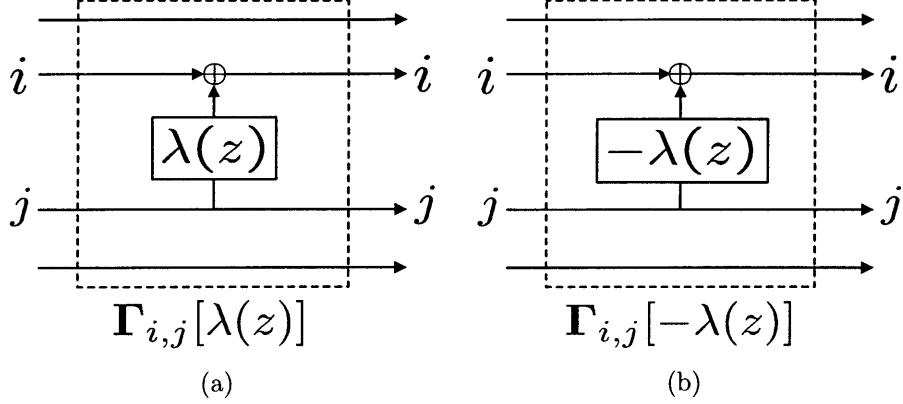


Figure 3-2: (a) an M -channel simple lifting $\Gamma_{i,j}[\lambda(z)]$ from channel j to $i \neq j$ with multiplier $\lambda(z)$, and (b) the inverse of $\Gamma_{i,j}[\lambda(z)]$.

The signal flow diagram for $\Gamma_{i,j}[\lambda(z)]$ and its inverse is shown in Figure 3-2. These are Type-3 elementary operations. Our goal will be to decompose the given $\mathbf{E}(z)$ into a product of simple liftings, through the *Monic Euclidean algorithm* (Section 3.3.2), with each factor containing only 1's on its diagonal. A possible extension is to include a combination of $\pm 2^m$, $m \in \mathbb{N} \cup \{0\}$, on the diagonal [18], in which case the extended version of the simple lifting can be expressed as

$$\widehat{\Gamma}_{i,j}[\lambda(z)] = \Gamma_{i,j}[\lambda(z)] \mathbf{D},$$

with

$$\left(\widehat{\Gamma}_{i,j}[\lambda(z)] \right)^{-1} = \mathbf{D}^{-1} \Gamma_{i,j}[-\lambda(z)], \quad (3.3)$$

where \mathbf{D} is a diagonal matrix containing the particular combination of $\pm 2^m$ on the diagonal, and \mathbf{D}^{-1} can be implemented exactly by construction, using only bit shifts and adds. We refer to this constraint on the diagonal entries as the *lifting requirement*, a consideration that is important for applications such as reversible integer transforms [20]. In particular, we will focus on the lifting requirement with ± 1 and $\pm z^{-m}$ on the diagonal, $m \in \mathbb{Z}$.

Equations (3.2) and (3.3) are key to the perfect reconstruction property imposed by the lifting structure. Note that perfect reconstruction is guaranteed by the lifting structure even when the multiplier $\lambda(z)$ is quantized, provided that the same quantized version of the multiplier, $\lambda^Q(z)$, is used in both $\Gamma_{i,j}[\lambda^Q(z)]$ and $\Gamma_{i,j}[-\lambda^Q(z)]$. Furthermore, PR is still guaranteed in nonlinear liftings where the multiplication result of $\lambda(z)$ (or of $\lambda^Q(z)$ if the multiplier is quantized) is rounded. This makes it possible to design reversible wavelet transforms that map integers to integers [20].

3.2.3 Euclidean Algorithm and M -Channel Lifting

The greatest common divisor (gcd) of $M \geq 2$ Laurent polynomials, $p_0(z), p_1(z), \dots, p_{M-1}(z)$, can be computed using the Euclidean algorithm, which relies on repeated divisions to find the gcd.

Lemma 3.1 (Euclidean Algorithm). *Given a vector $\mathbf{p}(z) = [p_0(z) \ p_1(z) \ \dots \ p_{M-1}(z)]^T$ of M Laurent polynomials, not all zero, there exist a finite number of M -channel liftings which reduce $\mathbf{p}(z)$ to an M -vector $\mathbf{r}(z)$ consisting of a (non-unique) gcd, $g(z)$, of $\mathbf{p}(z)$ along with $M-1$ zeros, i.e. $\mathbf{r}^T(z) = [0 \ \dots \ 0 \ g(z) \ 0 \ \dots \ 0]$. If desired, the M -channel liftings can be chosen so that the gcd appears in the first entry of $\mathbf{r}(z)$.*

Proof: See Appendix 3.A. ■

Note that $p_0(z), \dots, p_{M-1}(z)$ are said to be *relatively prime* if $g(z)$ is a monomial.

3.3 M -Channel Lifting Factorization of Perfect Reconstruction Filter Banks

3.3.1 Prior Results For Two-Channel Lifting

Daubechies and Sweldens [39] have detailed the lifting factorization of two-channel ($M = 2$) filter banks. In summary, any 2×2 polyphase matrix $\mathbf{E}(z)$ with $\det(\mathbf{E}(z)) = 1$ can always

be lifting-factorized as (Theorem 7, [39])

$$\mathbf{E}(z) = \begin{bmatrix} K & 0 \\ 0 & 1/K \end{bmatrix} \prod_{i=1}^m \begin{bmatrix} 1 & s_i(z) \\ 0 & 1 \end{bmatrix} \begin{bmatrix} 1 & 0 \\ t_i(z) & 1 \end{bmatrix},$$

for some nonzero constant K and some Laurent polynomials $s_i(z)$ and $t_i(z)$, $i = 1, 2, \dots, m$. Specifically, K is the gcd of the even and the odd phases of the lowpass filter, and can be made 1 by four more lifting steps [39].

3.3.2 Monic Euclidean Algorithm For Arbitrary M

We now present, for the M -channel case, the *Monic Euclidean algorithm* where the generated gcd always has unit scaling. For this we need:

Definition 3.2 (Monic Polynomials). A polynomial is said to be monic if the leading coefficient is 1. \diamond

Consider a set of Laurent polynomials $\mathbf{p}(z) = [p_0(z) \ p_1(z) \ \dots \ p_{M-1}(z)]^T$ with gcd $g(z)$. Note that the gcd is not unique—any nonzero monomial multiple of $g(z)$ will be a gcd as well. Therefore, we can always normalize the gcd to be monic. However, the gcd of $\mathbf{p}(z)$ returned by the Euclidean algorithm may not always be monic. Hence,

Theorem 3.1 (Monic Euclidean Algorithm). Let $\mathbf{p}(z)$ be defined as in Lemma 3.1. Then there exist a finite number of M -channel lifting steps, which reduce $\mathbf{p}(z)$ to an M -vector $\mathbf{r}(z)$ containing a monic gcd of $\mathbf{p}(z)$ in the first entry and $M - 1$ zeros elsewhere.

Proof: See Appendix 3.B. \blacksquare

3.3.3 Size Reduction Via Monic Euclidean Algorithm

Lemma 3.2 (Size Reduction). Let $\mathbf{E}(z)$ be an $M \times M$ FIR polyphase matrix with $\det(\mathbf{E}(z)) = z^{-K}$ for some $K \in \mathbb{Z}$ and $M \geq 2$. Then there exist two sets of FIR M -channel simple lifting

steps, $\mathbf{L}_1(z)$ and $\mathbf{V}_1(z)$, such that

$$\mathbf{E}(z) = \mathbf{L}_1(z) \begin{bmatrix} 1 & 0 & \dots & 0 \\ \hline 0 & & & \\ \vdots & & \Theta_1(z) & \\ 0 & & & \end{bmatrix} \mathbf{V}_1(z),$$

where $\Theta_1(z)$ is $(M - 1) \times (M - 1)$ FIR with

$$\det(\Theta_1(z)) = \det(\mathbf{E}(z)) = z^{-K}.$$

Proof: See Appendix 3.C. ■

3.3.4 M -Channel Lifting Factorization Via Size Reductions

Theorem 3.2 (Lifting Factorization of PRFBs). *Let $\mathbf{E}(z)$ be the polyphase matrix of an M -channel ($M \geq 2$) FIR filter bank with $\det(\mathbf{E}(z)) = z^{-K}$, $K \in \mathbb{Z}$. Then there exist two sets of FIR M -channel simple lifting steps, $\mathbf{L}(z)$ and $\mathbf{V}(z)$, and a diagonal matrix $\Lambda(z) = \text{diag}(1, 1, \dots, 1, z^{-K})$ such that*

$$\mathbf{E}(z) = \mathbf{L}(z) \Lambda(z) \mathbf{V}(z).$$

Proof: See Appendix 3.D. ■

Figure 3-3 shows the lifting factorization of $\mathbf{E}(z)$ with determinant z^{-K} . Note that this result can be extended such that z^{-K} appears anywhere on the diagonal of $\Lambda(z)$, or that $\Lambda(z)$ becomes $\text{diag}(z^{-K_0}, z^{-K_1}, \dots, z^{-K_{M-1}})$ with $K_0 + K_1 + \dots + K_{M-1} = K$, or even its row- or column-permuted version. Furthermore, the diagonal matrix $\Lambda(z)$ can be moved

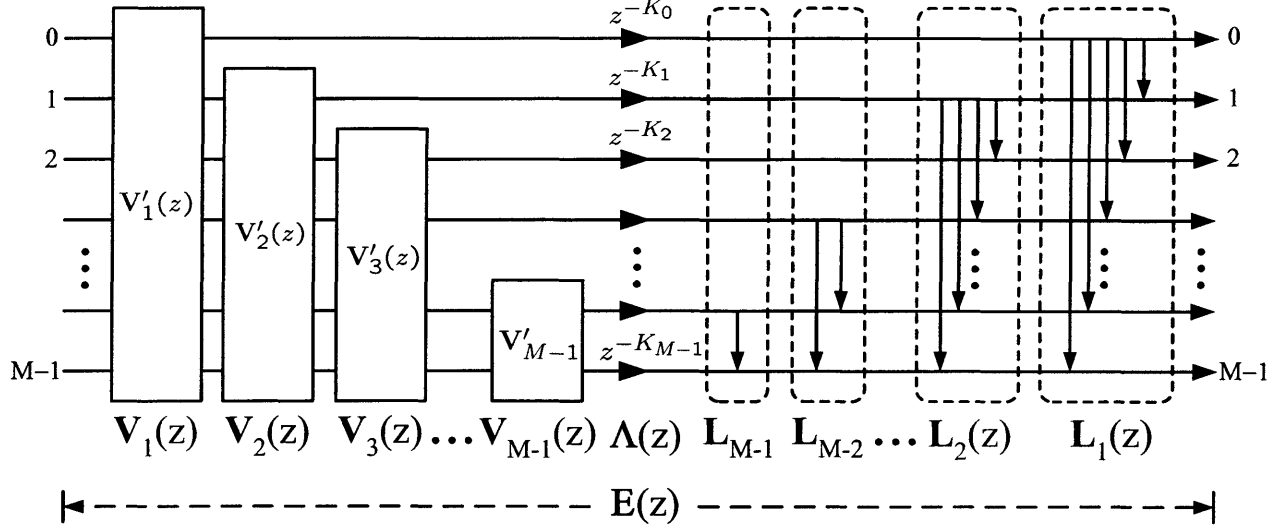


Figure 3-3: The lifting factorization structure of an FIR M -channel filter bank $\mathbf{E}(z)$ with determinant z^{-K} , with $K_0 + \dots + K_{M-1} = K$. $\mathbf{V}_i(z)$ and $\mathbf{L}_i(z)$ are all sets of FIR M -channel liftings, and $\mathbf{V}_i(z)$ correspond to applications of the Monic Euclidean algorithm, while $\mathbf{L}_i(z)$ correspond to Gaussian eliminations. See Appendix 3.D for definitions of $\mathbf{V}'_i(z)$.

towards the beginning:

$$\mathbf{E}(z) = \Lambda(z) [\Lambda^{-1}(z) \mathbf{L}(z) \Lambda(z)] \mathbf{V}(z),$$

where $[\Lambda^{-1}(z) \mathbf{L}(z) \Lambda(z)]$ is still an M -channel lifting. Similarly, $\Lambda(z)$ may be moved to the end of the expression.

3.3.5 Relaxation of Monic Determinant

The assumption $\det(\mathbf{E}(z)) = z^{-K}$ can be relaxed to include the case where $\det(\mathbf{E}(z)) = \pm 2^m z^{-K}$, $m \in \mathbb{N} \cup \{0\}$, while preserving PR. In this case, the size reduction algorithm remains the same except $\det(\Theta_1(z)) = \pm 2^m z^{-K}$; hence, z^{-K} in $\Lambda(z)$ will be replaced by $\pm 2^m z^{-K}$.

3.3.6 Reversible Multiplierless M -Band Wavelet Transforms

The lifting structure lends itself to implementation of reversible wavelet transforms [20], despite the finite word-length effect and/or rounding of intermediate multiplication results in the lifting steps. Based on this structure, one can also design multiplierless reversible wavelet transforms [22], even with a constraint on the number of hardware adders [31].

3.3.7 PRFBs with Prescribed Admissible $H_0(z)$

Recall (Appendix 3.C) that the M polyphase components of any filter $H_i(z)$ of an M -band PRFB must be relatively prime. In this sense, a filter $G(z)$ is said to be *PRFB-admissible* or simply *admissible* if its M polyphase components are relatively prime. Hence,

Theorem 3.3 (PRFB with Prescribed Admissible $H_0(z)$). *Given an admissible filter $G(z)$ with $G(1) \neq 0$, there exists a PRFB having $H_0(z) = G(z)$.*

Vetteri [138] has studied the simpler two-channel version ($M = 2$) of the problem. Here, for an arbitrary M , it turns out that the proposed M -channel lifting factorization can parameterize the problem efficiently, by appropriately confining the degrees of freedom within the remaining $M - 1$ filters while guaranteeing $H_0(z)$ as prescribed.

For example, given the fact that the B-spline, $\beta^p(t)$, of degree p satisfies the two-scale equation [125]

$$\beta^p(t) = \sum_n u_M^p[n] \beta^p(Mt - n), \quad (3.4)$$

where $M \in \mathbb{N}$ is the dilation factor, one can use $U_M^p(z^{-1})$ as an admissible $H_0(z)$ for an M -band PRFB, where $U_M^p(z)$ is the z -transform of $u_M^p[n]$. In this case, the corresponding scaling function is exactly $\beta^p(t)$, which governs the M -band multiresolution analysis (MRA) of $L^2(\mathbb{R})$.

The remaining $M - 1$ wavelets of the MRA can be designed based on the proposed M -channel lifting factorization. The procedure is as follows:

1. Apply the Monic Euclidean algorithm (Theorem 3.1) to the M polyphase components of the admissible $H_0(z)$. The result is an M -vector

$$\mathbf{r}(z) = \begin{bmatrix} \pm z^{-K_1} & 0 & \dots & 0 \end{bmatrix}^T.$$

In particular, Theorem 3.1 furnishes the existence and structure of $[\mathbf{V}_1(z)]^{-1}$, a product of finitely many M -channel lifting steps, such that

$$\underbrace{\begin{bmatrix} H_{0,0}(z) & \dots & H_{0,M-1}(z) \end{bmatrix}}_{\mathbf{p}^T(z)} [\mathbf{V}_1(z)]^{-1} = \mathbf{r}^T(z),$$

where $H_{0,k}(z)$ is the k th polyphase component of $H_0(z)$. The row vector $\mathbf{p}^T(z)$ will be the first row of the polyphase matrix $\mathbf{E}(z)$.

2. Complete the remaining rows of the polyphase matrix by augmenting $\mathbf{r}^T(z)$ with the row vectors \mathbf{e}_i^T , $i = 1, 2, \dots, M - 1$. This results in an initial PRFB, $\hat{\mathbf{E}}(z)$, where

$$\hat{\mathbf{E}}(z) = \begin{bmatrix} \mathbf{r}^T(z) \\ \hline 0 & 1 & 0 & \dots & 0 \\ \hline 0 & 0 & 1 & \dots & 0 \\ \hline \vdots & & \ddots & & \vdots \\ \hline 0 & 0 & 0 & \dots & 1 \end{bmatrix} \quad \mathbf{V}_1(z) = \begin{bmatrix} H_{0,0}(z) & H_{0,1}(z) & \dots & H_{0,M-1}(z) \\ \hline 0 & \times & \dots & \times \\ 0 & \times & \dots & \times \\ \vdots & \vdots & \ddots & \vdots \\ 0 & \times & \dots & \times \end{bmatrix}$$

with corresponding filters $H_0(z), \hat{H}_1(z), \dots, \hat{H}_{M-1}(z)$.

3. Improve the filters $\hat{H}_k(z)$, $k = 1, \dots, M - 1$, of the initial PRFB $\hat{\mathbf{E}}(z)$ via a suitable biorthogonal $(M - 1) \times (M - 1)$ sub-system $\Theta(z)$, to arrive at the final $\mathbf{E}(z)$ with corresponding filters $H_i(z)$, $i = 0, 1, \dots, M - 1$, as follows:

$$\mathbf{E}(z) = \mathbf{L}_1(z) \left[\begin{array}{c|c} 1 & \\ \hline & \Theta(z) \end{array} \right] \hat{\mathbf{E}}(z),$$

where $\mathbf{L}_1(z)$ contains the lifting steps corresponding to Gaussian elimination:

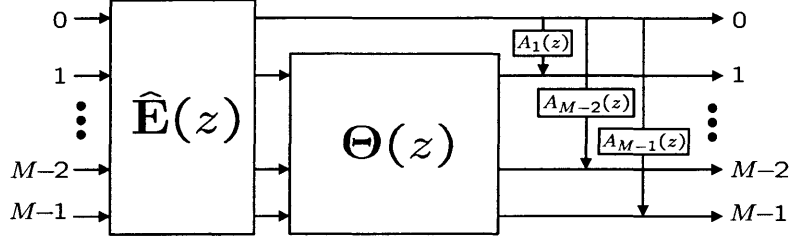


Figure 3-4: PRFB with prescribed admissible scaling filter $H_0(z)$. $\hat{\mathbf{E}}(z)$ is the initial PRFB which is subject to further improvement in terms of $\hat{H}_i(z)$, $i = 1, \dots, M - 1$, using an invertible matrix $\Theta(z)$ along with the final lifting steps $A_k(z)$, $k = 1, \dots, M - 1$.

$$\mathbf{L}_1(z) = \begin{bmatrix} 1 & 0 & 0 & \dots & 0 \\ A_1(z) & 1 & 0 & \dots & 0 \\ A_2(z) & 0 & 1 & \dots & 0 \\ \vdots & & \ddots & & \vdots \\ A_{M-1}(z) & 0 & 0 & \dots & 1 \end{bmatrix}.$$

In particular, the lifting steps $A_i(z)$ can be chosen so that $H_i(1) = 0$ for $i = 1, 2, \dots, M - 1$, and that the synthesis scaling filter $F_0(z)$ thus has regularity of at least first order. Higher-order regularity of $F_0(z)$ can be obtained by setting $\left. \frac{\partial^\ell}{\partial z^\ell} H_i(z) \right|_{z=1} = 0$, $\forall i = 1, \dots, M - 1$, and $\ell = 0, \dots, p - 1$, for some order p .

4. Assume that $H_0(z)$ corresponds to a finite-energy scaling function, i.e. that the cascade algorithm converges [108]. Then the $M - 1$ wavelets are readily obtained from the scaling function.

Figure 3-4 summarizes the above structure and provides a complete parameterization of PRFBs based on a prescribed $H_0(z)$ (cf. the general M -channel lifting structure in Figure 3-3). The above design procedure will be demonstrated in the next section by a B-spline example. The same procedure applies to other non-B-spline cases as well, provided that the prescribed $H_0(z)$ is admissible.

3.4 Lifting Factorization and Design Examples

The previous section on the construction of an M -channel lifting factorization is meant to serve as general guidance. Issues such as *dynamic range* and *Laurent degree* of the resulting lifting multipliers and the *number of simple liftings needed* have not been addressed. These issues are easier to deal with for $M = 2$: for example, the number of simple liftings is the smaller degree of the two polyphase components plus one [39]. The minimization of multiplier dynamic range can be achieved by choosing long division steps that optimize the dynamic range of the quotient. The minimization of lifting multiplier degree can be performed by carrying out partial long division instead of full long division [39]; however, this increases the number of lifting steps. Nevertheless, it is a tractable problem to enumerate all possible two-channel lifting factorizations [79].

When it comes to $M \geq 3$, the situation becomes more complicated. For example, there is usually a choice of more than one divisor from among the polyphase components to perform one step of the Euclidean algorithm. Furthermore, the size reduction can be performed in any order seen fit, instead of the order adopted in Appendix 3.D. If desired, some “pre-processing” liftings can be employed to reduce the relative degrees of the polyphase components (or to even the degree distributions), so that the Euclidean algorithm that follows will not generate quotients with large degrees. If there is structure present in $\mathbf{E}(z)$, it can in some cases be exploited either to reduce the number of simple liftings or to make the lifting multipliers dyadic numbers. As in the two-channel case, the issue of dynamic range of the lifting multipliers can be addressed by choosing the long division operation that results in the best dynamic range of the quotient. For example, one can choose as divisor a polyphase component whose smallest (absolute value) coefficient is maximized among the divisor candidates.

The general factorization guidance outlined in Appendix 3.D is employed in conjunction with the aforementioned criteria. In particular, the factorizations presented below in Section 3.4.1 and 3.4.2 (and consequently in Section 4.5) are *minimal* in the McMillan sense [129].

3.4.1 Degree-One Paraunitary Building Block

An $M \times M$ matrix

$$\mathbf{U}(z) = \mathbf{I} - \mathbf{u}\mathbf{u}^T + z^{-1}\mathbf{u}\mathbf{u}^T, \quad \|\mathbf{u}\| = 1,$$

is the most general degree-1 paraunitary building block for FIR PUFB design¹ [129]. The determinant is z^{-1} , regardless of \mathbf{u} . $\mathbf{U}(z)$ can be factorized as follows. Let

$$\mathbf{u} = \begin{bmatrix} u_0 & u_1 & \dots & u_{M-1} \end{bmatrix}^T \in \mathbb{R}^M.$$

For the size-reduction step, one can choose any non-zero u_k as divisor. To limit the dynamic range of the resulting lifting multipliers, the largest of $\{|u_0|, |u_1|, \dots, |u_{M-1}|\}$, say u_r , can be chosen as divisor. The lifting factorization begins as

$$\begin{aligned} \mathbf{U}(z) &= \begin{bmatrix} 1 & & & & \\ & \ddots & & & \\ & & 1 & & \\ & \frac{-u_0}{u_r} & \dots & \frac{-u_{r-1}}{u_r} & 1 & \frac{-u_{r+1}}{u_r} & \dots & \frac{-u_{M-1}}{u_r} \\ & & & & 1 & & & \\ & & & & & \ddots & & \\ & & & & & & 1 & \end{bmatrix} \\ &= \underbrace{\begin{bmatrix} 1 & (z^{-1} - 1)u_0u_r & & & & & \\ & \vdots & & & & & \\ & 1 & (z^{-1} - 1)u_{r-1}u_r & & & & \\ & \frac{-u_0}{u_r} & \dots & \frac{-u_{r-1}}{u_r} & 1 + (z^{-1} - 1)u_r^2 & \frac{-u_{r+1}}{u_r} & \dots & \frac{-u_{M-1}}{u_r} \\ & & & & (z^{-1} - 1)u_{r+1}u_r & 1 & & \\ & & & & & \vdots & \ddots & \\ & & & & (z^{-1} - 1)u_{M-1}u_r & & & 1 \end{bmatrix}}_{\mathbf{U}_1(z)} \quad (3.5) \end{aligned}$$

to null the first row of $\mathbf{U}(z)$ except the first and the r th entries of the row. The reason for choosing $r = \arg \max_{k=0, \dots, M-1} \{|u_k|\}$ should become clear now. Observe that, in (3.5), $\mathbf{U}_1(z)$ has a structure whereby multiple entries in the r th column can be nulled at a time:

¹Replace \mathbf{u}^T by \mathbf{u}^\dagger if designing complex-valued filter banks.

$$\mathbf{U}_1(z) \begin{bmatrix} 1 & -(z^{-1} - 1)u_0u_r \\ \ddots & \vdots \\ 1 & -(z^{-1} - 1)u_{r-1}u_r \\ & 1 \\ -(z^{-1} - 1)u_{r+1}u_r & 1 \\ \vdots & \ddots \\ -(z^{-1} - 1)u_{M-1}u_r & 1 \end{bmatrix} = \begin{bmatrix} 1 & & & & & & \\ & \ddots & & & & & \\ & & 1 & & & & \\ & & \frac{-u_0}{u_r} & \dots & \frac{-u_{r-1}}{u_r} & z^{-1} & \frac{-u_{r+1}}{u_r} \dots \frac{-u_{M-1}}{u_r} \\ & & & & & 1 & \\ & & & & & & \ddots \\ & & & & & & 1 \end{bmatrix} \quad (3.6)$$

where the fact that $\|\mathbf{u}\| = 1$ has been used. Then, the lifting factorization of $\mathbf{U}(z)$ reads

$$\mathbf{U}(z) = \begin{bmatrix} 1 & & & & & & \\ & \ddots & & & & & \\ & & 1 & & & & \\ -\alpha_0 & \dots & -\alpha_{r-1} & 1 & -\alpha_{r+1} & \dots & -\alpha_{M-1} \\ & & & & 1 & & \\ & & & & & \ddots & \\ & & & & & & 1 \end{bmatrix} \begin{bmatrix} 1 & \beta_0 & & & & & \\ & \ddots & \vdots & & & & \\ & 1 & \beta_{r-1} & & & & \\ & & 1 & & & & \\ & & \beta_{r+1} & 1 & & & \\ & & & \vdots & & \ddots & \\ & & & & \beta_{M-1} & & 1 \end{bmatrix} \\ \cdot \begin{bmatrix} 1 & -\beta_0 & & & & & \\ & \ddots & \vdots & & & & \\ & 1 & -\beta_{r-1} & & & & \\ & & z^{-1} & & & & \\ & & -\beta_{r+1} & 1 & & & \\ & & & \vdots & & & \\ & & & & \ddots & & \\ & & & & & 1 & \end{bmatrix} \begin{bmatrix} 1 & & & & & & \\ & \ddots & & & & & \\ & & 1 & & & & \\ \alpha_0 & \dots & \alpha_{r-1} & 1 & \alpha_{r+1} & \dots & \alpha_{M-1} \\ & & & & 1 & & \\ & & & & & \ddots & \\ & & & & & & 1 \end{bmatrix}, \quad (3.7)$$

where $\alpha_i = u_i/u_r$ and $\beta_i = u_iu_r$. An alternative factorization can be obtained by transposing (3.7), since $\mathbf{U}(z)$ is symmetric. Both (3.7) and its transposed version require only 1 delay element to implement, and thus are *minimal* in the McMillan sense. Figures 3-5(a) and (a') show both minimal lifting factorizations of $\mathbf{U}(z)$ for $M = 5$ and $r = 2$, and Figures 3-5(b) and (b') show those of $\mathbf{U}^{-1}(z)$. Observe that the lifting factorizations have unit diagonal scaling throughout, which permits a reversible, possibly multiplierless, implementation of $\mathbf{U}(z)$. In case dynamic range is not an issue, one can choose other values of r with $u_r \neq 0$

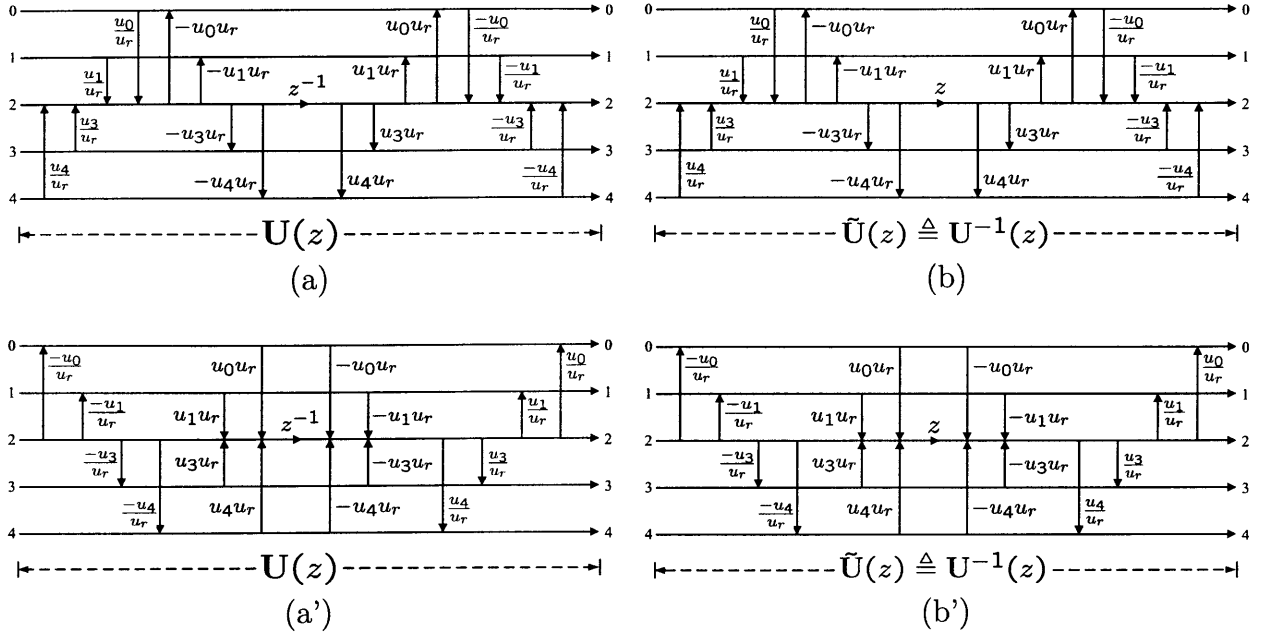


Figure 3-5: (a) and (a'): lifting factorizations of degree-1 paraunitary building block $\mathbf{U}(z)$ drawn for $M = 5$ and $r = 2$. Both structures are minimal in terms of the number of delay elements (the McMillan degree) and the independent lifting multipliers. (b) and (b'): lifting factorizations of $\mathbf{U}^{-1}(z)$, obtained by reversing the order of the lifting steps in (a) and (a') and flipping the signs.

and come up with similar factorizations.

From the synthesis perspective, (3.7) shows that $\mathbf{U}(z)$ can be parameterized by $(M - 1)$ independent lifting multipliers:

$$\alpha_i = u_i/u_r, \quad i = 0, 1, \dots, r-1, r+1, \dots, M-1.$$

Each $u_i u_r$ in the middle sections of (3.7) can be expressed in terms of the α_i :

$$u_i u_r = \alpha_i u_r^2 = \frac{\alpha_i}{1 + \sum_{k=0, k \neq r}^{M-1} \alpha_k^2} \triangleq \beta_i,$$

where the second equality is a direct consequence of $\|\mathbf{u}\| = 1$. Note that the definition of β_i in terms of α_k ensures paraunitarity. This parameterization of $\mathbf{U}(z)$ using the lifting multipliers α_i is also minimal in the sense that only $M - 1$ independent parameters are needed.

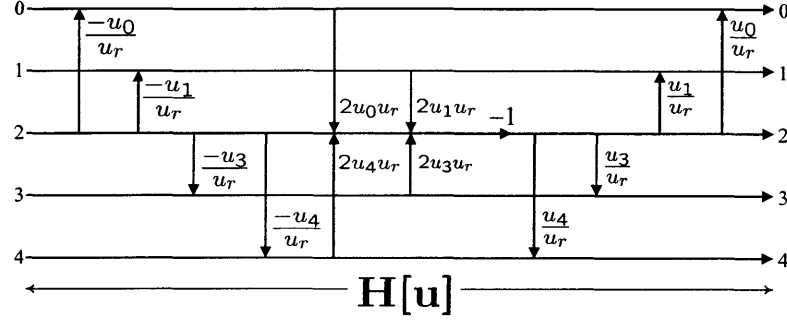


Figure 3-6: The lifting factorization of the Householder matrix $\mathbf{H}[\mathbf{u}]$, $\|\mathbf{u}\| = 1$, drawn for $M = 5$ and $r = 2$. Again, the diagonal scaling is unity throughout and the structure is suitable for reversible integer implementations of $\mathbf{H}[\mathbf{u}]$.

3.4.2 Householder Matrix

An $M \times M$ Householder matrix

$$\mathbf{H}[\mathbf{u}] = \mathbf{I} - 2\mathbf{u}\mathbf{u}^T, \quad \|\mathbf{u}\| = 1,$$

reflects a vector in \mathbb{R}^M with respect to a plane having \mathbf{u} as normal. $\mathbf{H}[\mathbf{u}]$ is related to $\mathbf{U}(z)$ by letting $z = -1$. One of its lifting factorizations is given in (3.8),

$$\mathbf{H}[\mathbf{u}] = \begin{bmatrix} 1 & \frac{u_0}{u_r} & & & \\ \ddots & \vdots & & & \\ & 1 & \frac{u_{r-1}}{u_r} & & \\ & & 1 & \frac{u_{r+1}}{u_r} & 1 \\ & & & \vdots & \ddots \\ & & & \frac{u_{M-1}}{u_r} & 1 \end{bmatrix} \begin{bmatrix} 1 & & & & \\ & \ddots & & & \\ & & 1 & -2u_0u_r & \\ & & & \vdots & \\ & & & & 1 \end{bmatrix}^T \begin{bmatrix} 1 & & & & \\ \ddots & & & & \\ & 1 & \frac{-u_0}{u_r} & & \\ & & \vdots & & \\ & & & 1 & \frac{-u_{r-1}}{u_r} \\ & & & & 1 \\ & & & & \frac{-u_{r+1}}{u_r} & 1 \\ & & & & \vdots & \ddots \\ & & & & \frac{-u_{M-1}}{u_r} & 1 \end{bmatrix} \quad (3.8)$$

which is based on the transposed version of (3.7). This lifting structure is shown in Figure 3-6.

3.4.3 Degree-One Biorthogonal Building Block

A useful class of biorthogonal filter banks (BOFBs), including BOLT [132], can be constructed by cascading the following degree-one BO building block [27, 28, 132]:

$$\mathbf{G}(z) = \mathbf{I} - \mathbf{u}\mathbf{v}^\dagger + z^{-1}\mathbf{u}\mathbf{v}^\dagger, \quad \mathbf{v}^\dagger\mathbf{u} = 1.$$

This can be viewed as a generalization of the degree-one PU building block $\mathbf{U}(z)$ discussed above. $\mathbf{G}(z)$ assumes the following lifting factorization [27]:

$$\mathbf{G}(z) = \begin{bmatrix} 1 & & & & \\ & \ddots & & & \\ & & 1 & & \\ -\alpha_0 & \dots & -\alpha_{r-1} & 1 & -\alpha_{r+1} \dots -\alpha_{M-1} \\ & & & 1 & \\ & & & & \ddots \\ & & & & 1 \end{bmatrix} \begin{bmatrix} 1 & & & & \\ & \ddots & & & \\ & & 1 & \lambda_0 & \\ & & & \vdots & \\ & & & 1 & \lambda_{r-1} \\ & & & & 1 \\ & & & & \lambda_{r+1} & 1 \\ & & & & & \vdots \\ & & & & & \ddots \\ & & & & & \lambda_{M-1} & 1 \end{bmatrix} \cdot \begin{bmatrix} 1 & -\lambda_0 & & & \\ & \vdots & & & \\ & 1 & -\lambda_{r-1} & & \\ & & z^{-1} & & \\ & & -\lambda_{r+1} & 1 & \\ & & & \vdots & \\ & & & & 1 \end{bmatrix} \begin{bmatrix} 1 & & & & \\ & \ddots & & & \\ & & 1 & & \\ \alpha_0 & \dots & \alpha_{r-1} & 1 & \alpha_{r+1} \dots \alpha_{M-1} \\ & & & 1 & \\ & & & & \ddots \\ & & & & 1 \end{bmatrix} \quad (3.9)$$

where $\alpha_i = v_i^*/v_r^*$ and $\lambda_i = u_i v_r^*$ for some $r \in \{0, 1, \dots, M-1\}$ with $v_r \neq 0$. The structure of (3.9) is similar to that of $\mathbf{U}(z)$ as shown in Figure 3-5. Both α_i and λ_i in (3.9) are design variables. The condition $\mathbf{v}^\dagger\mathbf{u} = 1$ is structurally imposed by the lifting factorization.

3.4.4 Degree-One Unimodular Building Block

Unimodular filter banks are a special class of FIR PRFBs, where the polyphase matrix $\mathbf{E}(z)$ is unimodular, i.e. $\det\{\mathbf{E}(z)\} = c$ for some $c \neq 0$. They achieve the minimum system delay of $M-1$ samples given the number of channels M , regardless of the filter length. Some

important properties of unimodular FBs are summarized in [63]. In particular, the special class, the *lapped unimodular transforms* (LUT), can be constructed using the following two types of degree-one unimodular building blocks [63]:

Type-I Unimodular Building Block of Degree One

An $M \times M$ matrix of the form

$$\hat{\mathbf{D}}(z) = \mathbf{I} - \hat{\mathbf{u}}\hat{\mathbf{v}}^\dagger + \hat{\mathbf{u}}\hat{\mathbf{v}}^\dagger z^{-1}, \quad \hat{\mathbf{v}}^\dagger \hat{\mathbf{u}} = 0$$

is the degree-one unimodular building block of Type I, whose inverse is given by $\hat{\mathbf{D}}^{-1}(z) = \mathbf{I} + \hat{\mathbf{u}}\hat{\mathbf{v}}^\dagger - \hat{\mathbf{u}}\hat{\mathbf{v}}^\dagger z^{-1}$. Using a similar technique as in Section 3.4.1, one arrives at the M -channel lifting factorization of $\hat{\mathbf{D}}(z)$:

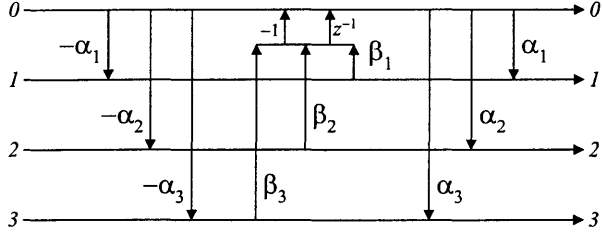
$$\hat{\mathbf{D}}(z) = \begin{bmatrix} 1 & & \alpha_0 & & \\ & \ddots & \vdots & & \\ & & 1 & \alpha_{r-1} & \\ & & & 1 & \\ & & & & 1 \\ & & & & \alpha_{r+1} & 1 \\ & & & & \vdots & \ddots \\ & & & & \alpha_{M-1} & 1 \end{bmatrix} \begin{bmatrix} 1 & & (z^{-1}-1)\beta_0 & & \\ & \ddots & \vdots & & \\ & & 1 & (z^{-1}-1)\beta_{r-1} & \\ & & & 1 & \\ & & & & (z^{-1}-1)\beta_{r+1} & 1 \\ & & & & \vdots & \ddots \\ & & & & (z^{-1}-1)\beta_{M-1} & 1 \end{bmatrix}^T \cdot \begin{bmatrix} 1 & & -\alpha_0 & & \\ & \ddots & \vdots & & \\ & & 1 & -\alpha_{r-1} & \\ & & & 1 & \\ & & & & -\alpha_{r+1} & 1 \\ & & & & \vdots & \ddots \\ & & & & -\alpha_{M-1} & 1 \end{bmatrix} \quad (3.10)$$

where $\alpha_i = u_i^*/u_r^*$ and $\beta_i = u_r^*v_i^*$ for any $r \in \{0, 1, \dots, M-1\}$ with $u_r \neq 0$.

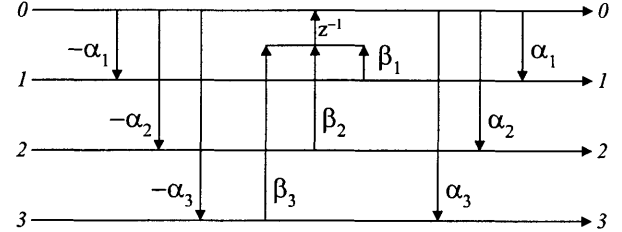
Type-II Unimodular Building Block of Degree One

An $M \times M$ matrix of the form

$$\mathbf{D}(z) = \mathbf{I} + \mathbf{u}\mathbf{v}^\dagger z^{-1}, \quad \mathbf{v}^\dagger \mathbf{u} = 0$$



(a) Type I



(b) Type II

Figure 3-7: Lifting factorizations of (a) Type-I degree-one unimodular building block $\hat{\mathbf{D}}(z)$ and (b) Type-II degree-one unimodular building block $\mathbf{D}(z)$. Both structures are drawn for $M = 4$ and $r = 0$ [63].

is the degree-one unimodular building block of Type II, whose inverse is given by $\mathbf{D}^{-1}(z) = \mathbf{D}(-z) = \mathbf{I} - \mathbf{u}\mathbf{v}^\dagger z^{-1}$. Using a similar technique as in Section 3.4.1, one arrives at the M -channel lifting factorization of $\mathbf{D}(z)$:

$$\mathbf{D}(z) = \begin{bmatrix} 1 & & \alpha_0 & & \\ & \ddots & \vdots & & \\ & & 1 & \alpha_{r-1} & \\ & & & 1 & \\ & & & & \alpha_{r+1} & 1 \\ & & & & \vdots & \ddots \\ & & & & & 1 \end{bmatrix} \begin{bmatrix} 1 & & & & \\ & \ddots & & & \\ & & 1 & & \\ & & & \beta_0 z^{-1} & \dots & \beta_{r-1} z^{-1} & 1 & \beta_{r+1} z^{-1} & \dots & \beta_{M-1} z^{-1} \\ & & & & & & 1 & & & \\ & & & & & & & \ddots & & \\ & & & & & & & & & 1 \end{bmatrix} \begin{bmatrix} 1 & & -\alpha_0 & & \\ & \ddots & \vdots & & \\ & & 1 & -\alpha_{r-1} & \\ & & & 1 & \\ & & & & \alpha_{r+1} & 1 \\ & & & & \vdots & \ddots \\ & & & & & 1 \end{bmatrix} \quad (3.11)$$

where $\alpha_i = u_i^*/u_r^*$ and $\beta_i = u_r^* v_i^*$ for any $r \in \{0, 1, \dots, M-1\}$ with $u_r \neq 0$.

Both lifting structures are depicted in Figure 3-7 for $M = 4$ and $r = 0$. Designs of the LUT based on (3.10) and (3.11) can be found in [63].

	floating-pt	C1	C2	C3	C4	C5	C6	C7
γ	0.566454497	1/2	1/2	9/16	9/16	9/16	145/256	145/256
β	0.541196100	17/32	69/128	69/128	69/128	277/512	277/512	4433/8192
α	-0.640652284	-5/8	-5/8	-5/8	-41/64	-41/64	-41/64	-41/64
MSE	0	3.1e-5	2.0e-5	1.3e-5	3.4e-7	1.1e-7	2.2e-9	3.2e-10
CG	7.5701	7.5640	7.5665	7.5690	7.5699	7.5701	7.5701	7.5701
Adds	-	14	15	16	17	18	19	20
Shifts	-	8	9	10	11	12	13	14

Table 3.1: Several adder-constrained reversible multiplierless approximations of the normalized 4-point DCT.

3.4.5 Discrete Cosine Transform and Cosine-Modulated Filter Bank

The discrete cosine transform (DCT) [100] is perhaps the most popular block transform. It is orthogonal and normalized: $\mathbf{C}_M^T \mathbf{C}_M = \mathbf{I}$, where \mathbf{C}_M is the M -point DCT kernel. Here, we present lifting factorizations of the DCT which are different from the conventional Givens rotation-based approaches. In particular, the presented factorizations have unit diagonal scaling throughout, which benefits applications requiring reversible transforms.

DCT with $M = 4$

By exploiting the symmetry structure in \mathbf{C}_4 and maximizing the occurrence of dyadic quotients (± 1 and $\pm 1/2$ in this example) in the course of the Monic Euclidean algorithm, one can arrive at the 4-channel lifting factorization shown in Figure 3-8. This implementation is normalized, and it requires 9 lifting steps, only 3 of which are floating-point multiplications. In contrast, the best ULU factorization [117] of an appropriately permuted \mathbf{C}_4 requires 13 lifting steps, 12 of which are floating-point multiplications.

The structure in Figure 3-8 lends itself very well to a reversible multiplierless approximation [31] of \mathbf{C}_4 , as only 3 floating-point multipliers need be approximated. Several reversible multiplierless approximations are given in Table 3.1 to demonstrate the idea. The configurations with 17 adders or more (C4, ..., C7) provide good approximations of the 4-point DCT.

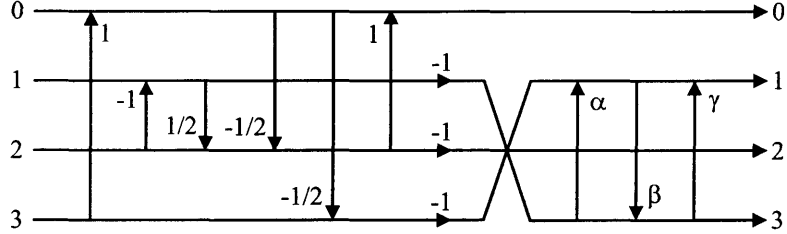


Figure 3-8: A 4-channel lifting factorization of the normalized 4-point Type-II DCT using 9 simple liftings, 6 of which are dyadic numbers. In the figure, $\alpha = \csc(\pi/8)(\cos(\pi/8) - \sqrt{2}/2)$, $\beta = \sqrt{2} \sin(\pi/8)$, and $\gamma = \csc(\pi/8)(1/2 \cos(\pi/8) - \sqrt{2}/2)$. Their magnitudes are all less than unity, providing a good dynamic range performance.

DCT with $M = 8$

Figure 3-9 shows the proposed 8-channel lifting factorization of $\sqrt{2}\mathbf{C}_8$. Again, this is reversible due to the proposed M -channel lifting structure. It requires 29 simple liftings, 13 of which are floating-point numbers. In Figure 3-9, the lifting multipliers are $\lambda_1 = 0.534511$, $\lambda_2 = -0.831470$, $\lambda_3 = -0.303347$, $\lambda_4 = 0.555570$, $\lambda_5 = -0.465489$, $\lambda_6 = 0.696653$, $\lambda_7 = -0.707107$, $\lambda_8 = -0.707107$, $\lambda_9 = 0.707107$, $\lambda_{10} = 0.707107$. In contrast to [68], our structure achieves a reversible implementation, at a cost of two extra floating-point multiplications. As a comparison, the best *ULU* requires 55 floating-point multiplications.

The above DCT examples demonstrate the M -channel lifting factorizations of a given constant (order 0) polyphase matrix. Below we consider an order-3 polyphase matrix and its lifting factorization, using a 3-channel cosine-modulated filter bank with genus 4.

Cosine-Modulated Filter Bank (CMFB)

Table 3.2 lists the prototype filter $p_0[n]$ of a 3-channel CMFB with 12 taps for each filter. It can be verified that $\det(\mathbf{E}(z)) = -z^{-4}$. We give below one possible 3-channel factorization

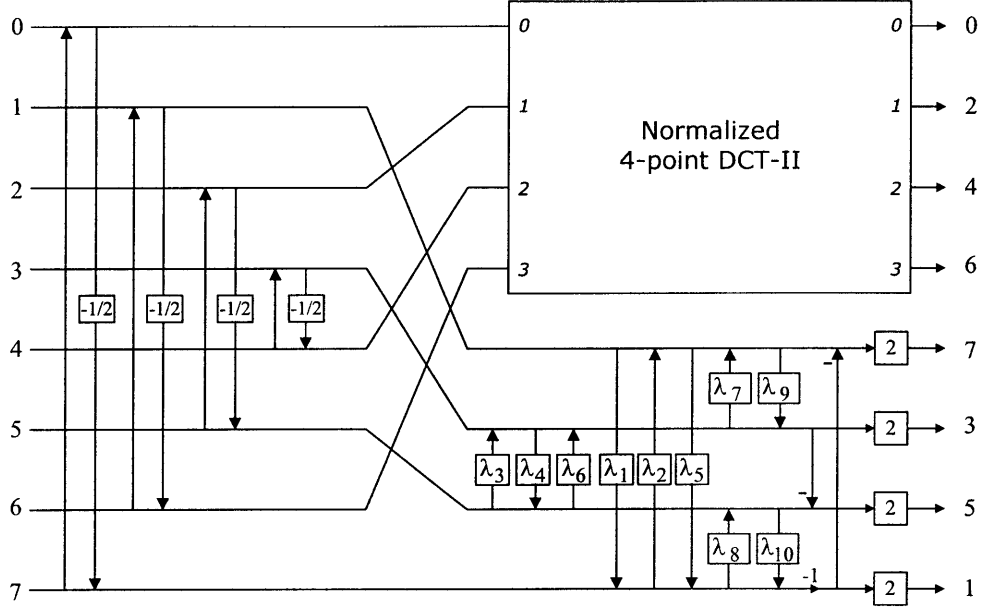


Figure 3-9: An 8-channel lifting factorization of $\sqrt{2}\mathbf{C}_8$ using 29 simple liftings, 13 of which are floating point numbers. The determinant of the polyphase matrix is 2^4 . In the figure, the block of 4-point DCT-II is exactly as shown in Figure 3-8.

with low order lifting steps:

$$\begin{aligned} \mathbf{E}(z) = & \Gamma_{1,0} [0.73206] \Gamma_{0,1} [-0.57735] \Gamma_{2,1} [0.57735] \Gamma_{1,0} [0.73206] \Gamma_{0,2} [-1] \Gamma_{1,0} [-0.57735] \\ & \Gamma_{2,0} [-0.11738 z + 0.71132 - 0.64871 z^{-1}] \text{diag} \left(\begin{bmatrix} z^{-1} & -z^{-1} & z^{-2} \end{bmatrix} \right) \\ & \Gamma_{0,2} [1.54152] \Gamma_{2,0} [-0.24699 - 0.18727 z^{-2}] \Gamma_{0,2} [-0.50361]. \quad (3.12) \end{aligned}$$

3.4.6 PRFB With Prescribed Admissible $H_0(z)$ – A B-Spline Example

As described in Section 3.3.7, given an admissible filter $G(z)$ with $G(1) \neq 0$, there exists a PRFB having $H_0(z) = G(z)$. To illustrate the process of designing such PRFBs, let us take for example the B-spline with $M = 3$ and $p = 1$. This is the “linear-hat” function in the

n	$p_0[n]$
0,11	-0.1028004872325624
1,10	0
2,9	0.2041290690989870
3,8	0.4378825255433416
4,7	0.7071067811865476
5,6	0.8694954150524967

Table 3.2: Prototype filter $p_0[n]$ for the 3-channel CMFB.

3-channel setting. The initial PRFB obtained from the filter $u_M^p[-n]$ is

$$\hat{\mathbf{E}}(z) = \begin{bmatrix} 1 & (z+2)/3 & (2z+1)/3 \\ 0 & 1 & 0 \\ 0 & 0 & 1 \end{bmatrix},$$

for which the band-pass and high-pass filters have no frequency selectivity. This is improved by using a suitable biorthogonal sub-system $\Theta(z)$ to increase their length (see Figure 3-4). There is no unique way to choose $\Theta(z)$, although one possibility is to generalize the PU building blocks in Sections 3.4.1 and 3.4.2 to $\mathbf{V}_m(z) = \mathbf{I} - \mathbf{u}_m \mathbf{v}_m^T + z^{-1} \mathbf{u}_m \mathbf{v}_m^T$ and $\mathbf{V}_m(-1) = \mathbf{I} - 2\mathbf{u}_m \mathbf{v}_m^T$, with $\mathbf{u}_m^T \mathbf{v}_m = 1$ [132]. The results are degree-1 and degree-0 biorthogonal building blocks², and $\Theta(z) = \prod_m \mathbf{V}_m(z) \prod_{m'} \mathbf{V}_{m'}(-1)$ in this case. Once the structure of $\Theta(z)$ is in place, one can design the PRFB subject to suitable criteria, for example, stopband attenuation and the transform coding gain [129]. Figure 3-10 shows a design which has equal-length analysis filters $H_i(z)$, with a coding gain of 5.93dB. Note that $H_0(z)$ is as prescribed, and that the analysis scaling function $\phi(t)$ is indeed the linear-hat B-spline. For this example, the lifting steps, $A_k(z)$, shown in Figure 3-4 are chosen so that the synthesis scaling filter $F_0(z)$ has first-order regularity—a necessary condition for the synthesis scaling function to exist in $L^2(\mathbb{R})$ [108].

²Other biorthogonal building blocks exist. For example, see [98].

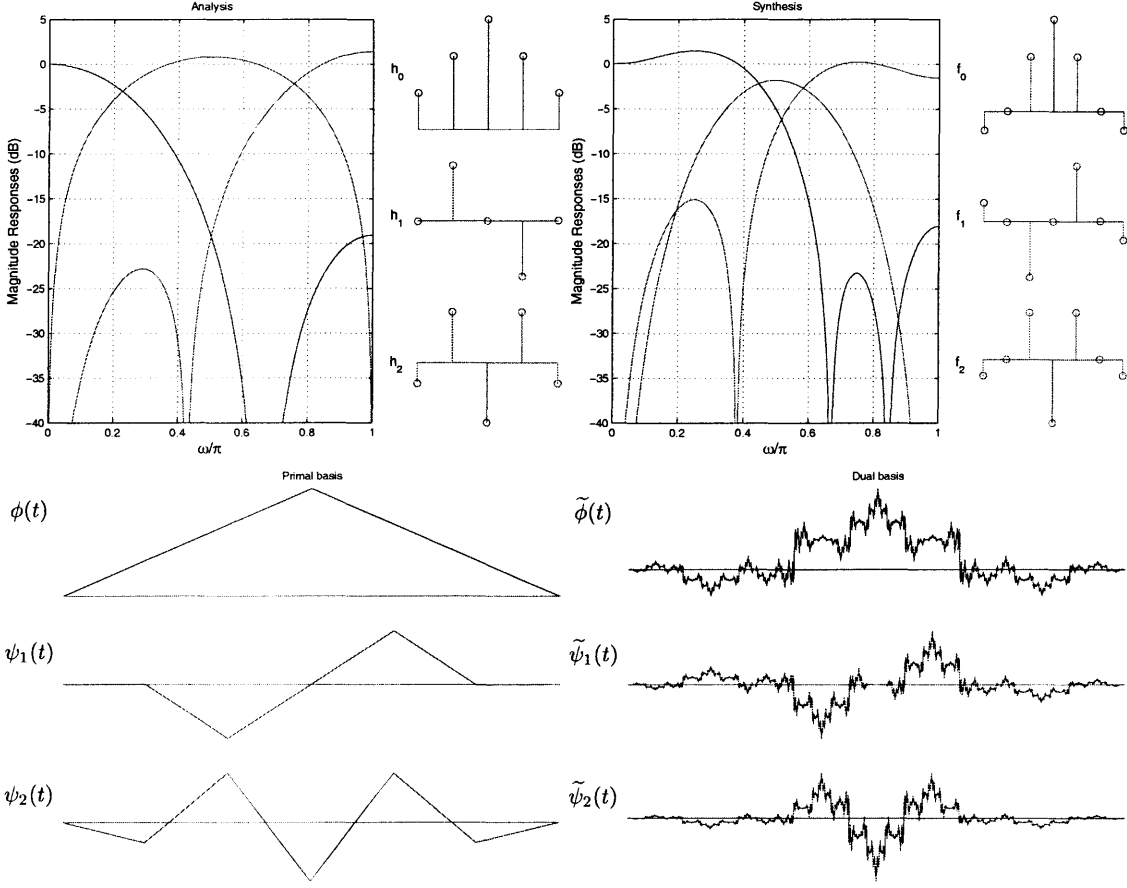


Figure 3-10: Design example of a PRFB with a prescribed admissible scaling filter $H_0(z)$ which comes from the three-channel “linear-hat” B-spline. $H_i(z)$ are chosen to have equal length, and the lifting steps, $A_k(z)$, shown in Figure 3-4 have been chosen so that the synthesis scaling filter $F_0(z)$ has first-order regularity. The coding gain is 5.9259dB.

3.5 Conclusions

We have presented a systematic M -channel lifting factorization of a perfect reconstruction filter bank $\mathbf{E}(z)$ with $\det(\mathbf{E}(z)) = z^{-K}$, $K \in \mathbb{Z}$, based on the Monic Euclidean algorithm. The proposed M -channel lifting factorization is suitable for reversible, possibly multiplierless [31], implementations of given filter banks and their corresponding M -band wavelet transforms, even under finite precision and/or nonlinear liftings. We consider how to optimize the M -channel lifting structure for the number of lifting steps, delay elements, and dyadic coefficients, and also for the dynamic range. PRFBs with a prescribed admissible scaling

filter $H_0(z)$ can be naturally parameterized by a lifting structure that appropriately confines the degrees of freedom within the remaining $M - 1$ filters. Specializing the M -channel lifting factorization to paraunitary, biorthogonal, and unimodular building blocks enables a lifting-based FB design [27, 63]. Finally, we note that regularity can be conveniently imposed on the lifting structure. Design examples have been given to demonstrate the versatility of the proposed method.

Appendices

3.A Proof of Lemma 3.1

Since $p_i(z)$ are not all zero, we can choose from $\mathbf{p}(z) = \begin{bmatrix} p_0(z) & p_1(z) & \dots & p_{M-1}(z) \end{bmatrix}^T$ the one with the minimum finite Laurent degree, say, $p_{\ell_1}(z)$. The finiteness is needed to exclude zero polynomials from being selected. Then, divide each of the $p_i(z)$ by $p_{\ell_1}(z)$, for $i \in \{0, 1, \dots, M-1\} \setminus \{\ell_1\}$. Denoting the corresponding quotients and remainders by $q_i(z)$ and $r_i(z)$, respectively, we have $p_i(z) - q_i(z)p_{\ell_1}(z) = r_i(z)$ with $\deg(r_i(z)) < \deg(p_{\ell_1}(z))$ for all $i \in \{0, 1, \dots, M-1\} \setminus \{\ell_1\}$. This can be cast into matrix-vector form:

$$\begin{aligned} \mathbf{p}^T(z) & \underbrace{\begin{bmatrix} 1 & \dots & 0 & 0 & 0 & \dots & 0 \\ \vdots & \ddots & & & & & \vdots \\ 0 & & 1 & 0 & 0 & \dots & 0 \\ -q_0(z) & \dots & -q_{\ell_1-1}(z) & 1 & -q_{\ell_1+1}(z) & \dots & -q_{M-1}(z) \\ 0 & \dots & 0 & 0 & 1 & & 0 \\ \vdots & & & & & \ddots & \vdots \\ 0 & \dots & 0 & 0 & 0 & \dots & 1 \end{bmatrix}}_{\mathbf{Q}_{\ell_1}(z)} \\ &= \underbrace{\begin{bmatrix} r_0(z) & \dots & r_{\ell_1-1}(z) & p_{\ell_1}(z) & r_{\ell_1+1}(z) & \dots & r_{M-1}(z) \end{bmatrix}}_{\mathbf{r}_1^T(z)}, \end{aligned}$$

or

$$\mathbf{p}^T(z) \mathbf{Q}_{\ell_1}(z) = \mathbf{r}_1^T(z).$$

Note that $\mathbf{Q}_{\ell_1}(z)$ is actually a cascade of at most $M - 1$ simple lifting steps:

$$\mathbf{Q}_{\ell_1}(z) = \prod_{j=0, j \neq \ell_1}^{M-1} \Gamma_{\ell_1, j}[-q_j(z)].$$

Thus its inverse is straightforward:

$$[\mathbf{Q}_{\ell_1}(z)]^{-1} = \prod_{j=0, j \neq \ell_1}^{M-1} \Gamma_{\ell_1, j}[q_j(z)], \quad (\text{A.1})$$

which is also FIR.

We can apply the same procedure to $\mathbf{r}_1(z)$ to obtain

$$\begin{aligned} \mathbf{r}_1^T(z) \mathbf{Q}_{\ell_2}(z) &= \mathbf{r}_2^T(z) \\ \mathbf{r}_2^T(z) \mathbf{Q}_{\ell_3}(z) &= \mathbf{r}_3^T(z) \\ &\vdots \end{aligned}$$

and so on. This procedure is guaranteed to converge, because in going from $\mathbf{r}_i(z)$ to $\mathbf{r}_{i+1}(z)$, the maximum Laurent degree strictly decreases:

$$\text{MAXDEG}^{(i)} - 1 \geq \text{MINDEG}^{(i)} = \text{MAXDEG}^{(i+1)},$$

where $i \geq 1$ and $\text{MAXDEG}^{(i)}/\text{MINDEG}^{(i)}$ is the maximum/minimum finite Laurent degree of the elements of $\mathbf{r}_i(z)$. Therefore, there exists some finite integer N such that $\mathbf{r}_N(z)$, which is the M -vector $\mathbf{r}(z)$ in the Lemma, contains only one non-zero polynomial $g(z)$ —the gcd of $\mathbf{p}(z)$. $\mathbf{p}(z)$ is thus related to $\mathbf{r}_N(z)$ by

$$\mathbf{p}^T(z) \prod_{i=1}^N \mathbf{Q}_{\ell_i}(z) = \mathbf{r}_N^T(z) = \left[\begin{array}{cccccc} 0 & \dots & 0 & g(z) & 0 & \dots & 0 \end{array} \right].$$

In case the gcd $g(z)$ appears in the ℓ_N th entry of $\mathbf{r}_N(z)$, for some $1 \leq \ell_N \leq M - 1$, it can be brought to the first entry by either a permutation, if so desired, or two more *simple liftings*

$$\Gamma_{\ell_N,0}[1] \quad \text{and} \quad \Gamma_{0,\ell_N}[-1].$$

In the latter case, it is easy to show that

$$\mathbf{r}_N^T(z) \Gamma_{\ell_N,0}[1] \Gamma_{0,\ell_N}[-1] = \begin{bmatrix} g(z) & 0 & \dots & 0 \end{bmatrix}.$$

■

3.B Proof of Theorem 3.1

Suppose that the gcd $g(z)$ of $\mathbf{p}(z)$ is found by the Euclidean algorithm after N repeated divisions, for some integer N . Therefore, there exist some FIR M -channel liftings, $\mathbf{Q}_i(z)$, $i = 1, 2, \dots, N$, such that

$$\mathbf{p}^T(z) \prod_{i=1}^N \mathbf{Q}_i(z) = \begin{bmatrix} g(z) & 0 & \dots & 0 \end{bmatrix}. \quad (\text{A.2})$$

If $g(z)$ is monic, then a monic gcd has been found; otherwise, there exists a scalar $\alpha \neq 0, 1$ such that

$$g_0(z) \triangleq g(z)/\alpha$$

is a monic gcd of $\mathbf{p}(z)$.

The following post-processing on (A.2) guarantees both a monic gcd and the lifting requirement as defined in Section 3.2.2:

$$\mathbf{Q}_{N+1}(z) = \mathbf{I} + \alpha^{-1} z^{-n} \mathbf{e}_0 \mathbf{e}_j^T, \quad (\text{A.3})$$

$$\mathbf{Q}_{N+2}(z) = \mathbf{I} + (1 - \alpha z^n) \mathbf{e}_j \mathbf{e}_0^T, \quad (\text{A.4})$$

$$\mathbf{Q}_{N+3}(z) = \mathbf{I} - \mathbf{e}_0 \mathbf{e}_j^T, \quad (\text{A.5})$$

for any $n \in \mathbb{Z}$ and any fixed $j \in \{1, \dots, M-1\}$. This results in

$$\mathbf{P}^T(z) \prod_{i=1}^{N+3} \mathbf{Q}_i(z) = \begin{bmatrix} g_0(z) z^{-n} & 0 & \dots & 0 & 0 & 0 & \dots & 0 \end{bmatrix}.$$

■

3.C Proof of Lemma 3.2

Since $\det(\mathbf{E}(z))$ is a (monic) monomial, the entries in each row (column) of $\mathbf{E}(z)$ are relatively prime; otherwise, any polynomial common factor of them will also divide $\det(\mathbf{E}(z))$, contradicting the assumption that $\det(\mathbf{E}(z))$ is a monomial.

Then, a monic *monomial* gcd of the first row of $\mathbf{E}(z)$ can be found using the Monic Euclidean algorithm, and furthermore the gcd can be chosen to be a constant, i.e. $1 = z^0$, by an appropriate choice of n in Appendix 3.B. Thus, there exist a set of FIR M -channel liftings $\mathbf{Q}_1(z), \mathbf{Q}_2(z), \dots, \mathbf{Q}_N(z)$, such that

$$\mathbf{E}(z) \underbrace{\prod_{i=1}^N \mathbf{Q}_i(z)}_{[\mathbf{V}_1(z)]^{-1}} = \begin{bmatrix} 1 & 0 & 0 & \dots & 0 \\ \mu_1(z) & \times & \times & \dots & \times \\ \mu_2(z) & \times & \times & \dots & \times \\ \vdots & & & \ddots & \vdots \\ \mu_{M-1}(z) & \times & \times & \dots & \times \end{bmatrix}, \quad (\text{A.6})$$

where \times denotes possibly nonzero entries, and all the $\mu_i(z)$ are FIR, since the left-hand side of (A.6) is FIR. Now, using the gcd 1 as the pivot to perform Gaussian eliminations, we can null all the $\mu_i(z)$ using only FIR liftings. This amounts to pre-multiplying (A.6) by

$$[\mathbf{L}_1(z)]^{-1} = \prod_{\ell=1}^{M-1} \Gamma_{\ell,0}[-\mu_\ell(z)],$$

which is FIR and lower-triangular by construction. Therefore,

$$[\mathbf{L}_1(z)]^{-1} \mathbf{E}(z) [\mathbf{V}_1(z)]^{-1} = \begin{bmatrix} 1 & \mathbf{0}^T \\ \mathbf{0} & \Theta_1(z) \end{bmatrix} \quad (\text{A.7})$$

for some FIR $\Theta_1(z)$. The fact that both $\mathbf{L}_1(z)$ and $\mathbf{V}_1(z)$ are FIR is a direct consequence of (A.1). Now, since M -channel liftings are determinant-preserving, we have

$$\det(\mathbf{E}(z)) = \det\left(\begin{bmatrix} 1 & \mathbf{0}^T \\ \mathbf{0} & \Theta_1(z) \end{bmatrix}\right) = \det(\Theta_1(z)).$$

■

3.D Proof of Theorem 3.2

Since $\Theta_1(z)$ in Lemma 3.2 is FIR with $\det(\Theta_1(z)) = z^{-K}$, one can again apply Lemma 3.2 to $\Theta_1(z)$ to obtain two FIR $(M - 1)$ -channel liftings $\mathbf{L}'_2(z)$ and $\mathbf{V}'_2(z)$. Upon being augmented to

$$\mathbf{L}_2(z) = \begin{bmatrix} 1 & \mathbf{0}^T \\ \mathbf{0} & \mathbf{L}'_2(z) \end{bmatrix} \quad \text{and} \quad \mathbf{V}_2(z) = \begin{bmatrix} 1 & \mathbf{0}^T \\ \mathbf{0} & \mathbf{V}'_2(z) \end{bmatrix},$$

these factors map (A.7) to

$$\left(\prod_{i=2}^1 [\mathbf{L}_i(z)]^{-1} \right) \mathbf{E}(z) \prod_{i=1}^2 [\mathbf{V}_i(z)]^{-1} = \left[\begin{array}{cc|c} 1 & 0 & \\ 0 & 1 & \\ \hline & & \Theta_2(z) \end{array} \right]$$

with $\Theta_2(z)$ being $(M - 2) \times (M - 2)$ FIR, and $\det(\Theta_2(z)) = \det(\Theta_1(z)) = z^{-K}$. Repeating this procedure recursively on $\Theta_i(z)$ with the augmentations

$$\mathbf{L}_{i+1}(z) = \begin{bmatrix} \mathbf{I}_i & \mathbf{0}^T \\ \mathbf{0} & \mathbf{L}'_{i+1}(z) \end{bmatrix} \quad \text{and} \quad \mathbf{V}_{i+1}(z) = \begin{bmatrix} \mathbf{I}_i & \mathbf{0}^T \\ \mathbf{0} & \mathbf{V}'_{i+1}(z) \end{bmatrix},$$

will eventually lead to a scalar $\Theta_{M-1}(z) = z^{-K}$:

$$\left(\prod_{i=M-1}^1 [\mathbf{L}_i(z)]^{-1} \right) \mathbf{E}(z) \left(\prod_{i=1}^{M-1} [\mathbf{V}_i(z)]^{-1} \right) = \underbrace{\begin{bmatrix} \mathbf{I} & \\ & z^{-K} \end{bmatrix}}_{\Lambda(z)}.$$

Setting $\mathbf{L}(z) = \prod_{i=1}^{M-1} \mathbf{L}_i(z)$ and $\mathbf{V}(z) = \prod_{i=M-1}^1 \mathbf{V}_i(z)$, we arrive at

$$\mathbf{E}(z) = \mathbf{L}(z) \boldsymbol{\Lambda}(z) \mathbf{V}(z),$$

with $\mathbf{L}(z)$ and $\mathbf{V}(z)$ being FIR M -channel liftings. ■

Chapter 4

Paraunitary Filter Banks With Structural Regularity

Paraunitary filter banks (PUFBs) can be designed and implemented using either degree-one or order-one dyadic-based factorizations. This chapter discusses how regularity of a desired degree is *structurally* imposed on such factorizations for any number of channels $M \geq 2$, without necessarily constraining the phase responses. The regular linear-phase PUFBs become a special case under the proposed framework. We show that the regularity conditions are conveniently expressed in terms of M -channel lifting structures, which allow for fast, reversible, and possibly multiplierless implementations, in addition to improved design efficiency as suggested by numerical experience. M -band orthonormal wavelets with structural vanishing moments are obtained by iterating the resulting regular PUFBs on the lowpass channel. Design examples are presented and evaluated using a transform-based image coder, and they are found to outperform previously reported designs.

4.1 Introduction

Recall that an M -channel filter bank with polyphase matrix $\mathbf{E}(z)$ is said to be paraunitary (PU) if $\tilde{\mathbf{E}}(z)\mathbf{E}(z) = \mathbf{I}$, where the \sim operation stands for conjugate transpose (\dagger) and time-

reversal ($z \rightarrow z^{-1}$). Namely, $\mathbf{E}(z)$ is unitary on the unit circle $|z| = 1$. If $\mathbf{E}(z)$ is both PU and FIR, it is automatically lossless, and the synthesis filters can be found directly from the analysis filters by inspection (in fact, by time reversal and complex conjugation) [129].

Any PUFB $\mathbf{E}(z)$ of degree N always assumes the degree-one factorization as in (2.51), which is repeated here for ease of reference:

$$\mathbf{E}(z) = \prod_{m=N}^1 \mathbf{V}_m(z) \mathbf{E}_0.$$

Each dyadic-based building block $\mathbf{V}_m(z)$ can be implemented using only one delay element [129]. In [134], the use of dyadic-based structure for filter bank design was studied and was shown to outperform the Givens rotation-based parameterization. Generalizing the above degree-constrained structure, Gao *et al.* have recently proposed a factorization given the order of the PUFB [52]. Definitions of the order and McMillan degree of PUFBs can be found in Section 2.2.

Regularity of PRFBs is very desirable as explained in Section 2.4. In [58, 59, 105], a closed-form expression for K -regular scaling filter $H_0(z)$ was derived, and a technique for constructing a family of PUFBs or $\mathbf{E}(z)$ from $H_0(z)$ was proposed by further assuming a given unitary matrix \mathbf{E}_0 , which was chosen in an *ad-hoc* fashion — the issue of how to choose \mathbf{E}_0 was not fully addressed. Consequently, the resulting PUFB may not be optimal given certain design criteria, and faces the same problem of being (McMillan) degree-constrained as pointed out in [134].

For the class of M -channel linear-phase PUFBs (a.k.a. GenLOT [41]) with M even, the imposition of up to two degrees of regularity on the lattice structure was discussed in [92]. The regularity conditions were expressed in terms of the Givens rotation angles of the lattice components. On the other hand, for the most general class of M -channel regular PUFBs without the linear-phase constraint, the imposition of structural regularity has not been reported, except when $M = 2$ for which regularity of degree one is guaranteed if all the rotation angles of the lattice structure sum up to $\pi/4$ [108]. We aim to solve this problem in its most general form by considering a higher degree of regularity and an arbitrary number of

channels $M \geq 2$ without necessarily constraining the phase responses. The resulting design outperforms and spans a larger class than the regular GenLOT [92]. Preliminary results can be found in [27].

In the following, we will focus on *structurally* imposing regularity on the *degree-one* (2.51) and *order-one* (2.53) dyadic-based factorizations of the PUFBs, with important properties and conditions derived and geometric interpretations given. In this way, regularity is always guaranteed by the structure and does not appear as a side constraint during optimization. The special class of linear-phase PUFBs is revisited within the proposed framework, and the corresponding regularity conditions are shown to simplify in this case. All the regularity conditions on the dyadic-based structures are shown to be conveniently expressed in terms of the M -channel lifting factorization proposed in Chapter 3 (Section 4.4), which allows for efficient and reversible implementations of the filter bank, and results in faster convergence than the Givens rotation-based parameterization in the design process. Regular lifting structures are proposed. Finally, based on the derived regularity conditions, design examples are presented (Section 4.5) and evaluated in a transform-based image coder (Section 4.6) — the resulting regular PUFBs outperform existing ones in terms of both subjective and objective measures. Concluding remarks are found in Section 4.7.

The following notations will be used. The i th column of an m -indexed matrix \mathbf{w}_m is denoted as $\mathbf{w}_{m,i}$, with $\mathbf{w}_m = [\dots \mathbf{w}_{m,i} \dots]$. When references are made to the i th element of an M -vector \mathbf{v}_m , we use v_i^m , or equivalently, $\mathbf{v}_m = [v_0^m \ v_1^m \ \dots \ v_{M-1}^m]^T$. An $m \times n$ constant matrix \mathbf{A} is said to be unitary if $\mathbf{A}^\dagger \mathbf{A} = \mathbf{I}_n$.

4.2 Dyadic-based Factorizations with Structural Regularity

4.2.1 One-Regular PUFBs

We begin our discussion with the construction of one-regular PUFBs. The following Lemmas will help establish the one-regular results for both the degree-one and order-one factorizations (2.51) and (2.53).

Lemma 4.1. *In the Householder factorization of a unitary matrix \mathbf{U} as in (2.46), the 0th column of \mathbf{U} is completely determined by the unit-norm \mathbf{p}_0 and the entry $e^{j\theta_0}$ of \mathbf{D} .*

Proof: Consider the special form (2.47) the \mathbf{p}_i take on. ■

Lemma 4.2. *A degree-0 (and thus order-0) M -channel PUFB with Type-I analysis polyphase matrix $\mathbf{E}(z) = \mathbf{E}_0$ is one-regular if and only if the 0th row of \mathbf{E}_0 has identical elements. In particular, these elements are equal to $\frac{1}{\sqrt{M}}e^{j\phi}$ (equal magnitudes and equal phases), for arbitrary $\phi \in \mathbb{R}$.*

Proof: Consider (2.43) with $Q(z) = \sqrt{M}e^{j\phi}$ and $K = 0$. ■

Lemma 4.2 is equivalent to the Type-II synthesis polyphase matrix, \mathbf{E}_0^\dagger , having identical elements ($= \frac{1}{\sqrt{M}}e^{-j\phi}$) of its 0th column.

Lemma 4.3. *A degree-0 (and thus order-0) M -channel PUFB with Type-I analysis polyphase matrix $\mathbf{E}(z) = \mathbf{E}_0$ is one-regular if and only if the Householder factorization of \mathbf{E}_0^\dagger*

$$\mathbf{E}_0^\dagger = \mathbf{H}[\mathbf{p}_0] \dots \mathbf{H}[\mathbf{p}_{M-2}] \mathbf{D}^\dagger \quad (4.1)$$

where $\mathbf{D} = \text{diag}(e^{j\theta_0}, \dots, e^{j\theta_{M-1}})$, is such that $\mathbf{p}_0 = \begin{bmatrix} p_0^0 & p_1^0 & \dots & p_{M-1}^0 \end{bmatrix}^T$ with

$$p_0^0 = \sqrt{\frac{\sqrt{M} - s}{2\sqrt{M}}} e^{j\eta}, \quad (4.2)$$

$$p_i^0 = \frac{-s e^{j\eta}}{\sqrt{2(M - s\sqrt{M})}}, \quad i = 1, 2, \dots, M-1 \quad (4.3)$$

where s can be either 1 or -1 , and η is any real number. In this case, we have

$$\mathbf{E}_0 \mathbf{1}_M = \begin{bmatrix} c_0 & 0 & \dots & 0 \end{bmatrix}^T \quad (4.4)$$

where

$$c_0 = s\sqrt{M}e^{j\theta_0}. \quad (4.5)$$

Proof: By Lemma 4.2, \mathbf{E}_0 is one-regular if and only if each element of the 0th row equals $\frac{1}{\sqrt{M}}e^{j\phi}$. By Lemma 4.1, the 0th row of \mathbf{E}_0 in (4.1) is $e^{j\theta_0} \begin{bmatrix} 1 - 2|p_0^0|^2 & -2p_0^0 p_1^{0*} & \dots & -2p_0^0 p_{M-1}^{0*} \end{bmatrix}$. This gives $e^{j\theta_0}(1 - 2|p_0^0|^2) = \frac{1}{\sqrt{M}}e^{j\phi}$ or $1 - 2|p_0^0|^2 = \frac{1}{\sqrt{M}}e^{j(\phi - \theta_0)} \triangleq \frac{s}{\sqrt{M}}$ for some sign parameter $s = \pm 1$, as $1 - 2|p_0^0|^2 \in \mathbb{R}$. One can then obtain $|p_0^0|^2 = \frac{\sqrt{M}-s}{2\sqrt{M}}$ and $|p_i^0|^2 = \frac{1}{2(M-s\sqrt{M})}$, $i = 1, 2, \dots, M-1$, and hence (4.2) and (4.3). Now, since the PUFB is one-regular, (2.42a) implies (4.4), which in turn implies $|c_0| = \|\mathbf{1}_M\| = \sqrt{M}$ as \mathbf{E}_0 is unitary. In fact, $c_0 = M \cdot \frac{1}{\sqrt{M}}e^{j\phi} = \sqrt{M}e^{j\phi} = s\sqrt{M}e^{j\theta_0}$. ■

Theorem 4.1. A degree- N PUFB (2.51) is one-regular if and only if \mathbf{E}_0 is one-regular as in Lemma 4.3.

Proof: Since $\mathbf{E}(1) = \mathbf{V}_N(1) \dots \mathbf{V}_1(1) \mathbf{E}_0 = \mathbf{E}_0$,

$$\mathbf{E}(1) \mathbf{1}_M = \mathbf{E}_0 \mathbf{1}_M = \begin{bmatrix} c_0 & 0 & \dots & 0 \end{bmatrix}^T.$$

■

Using (2.53) and (2.57), one can establish the following one-regular result for the order-one factorization.

Corollary 4.1. An order- L PUFB (2.53) is one-regular if and only if \mathbf{E}_0 is one-regular as in Lemma 4.3.

Remarks: This also establishes that regularity of degree one is completely determined by the unitary matrix \mathbf{E}_0 in (2.51) and (2.53), irrespective of the filter length and the McMillan

degree. Furthermore, the Householder matrix $\mathbf{H}[\mathbf{p}_0]$ in (4.1) is the only controlling factor for one degree of regularity. An order- L PUFB can have degree ranging from L to ML .

4.2.2 Two-Regular PUFBs

Having developed the conditions for one-regularity, we are now ready to derive the two-regularity conditions on the dyadic-based structures.

Two-Regular Dyadic-based Structures With or Without Length Constraint

Theorem 4.2 (Two-Regular Dyadic-based Structure). *A degree- N PUFB (2.51) is two-regular if and only if*

1. \mathbf{E}_0 is one-regular as in Lemma 4.3, and
2. the unit-norm parameter vectors \mathbf{v}_m of $\mathbf{V}_m(z)$ as in (2.50) are such that

$$sM^{3/2} \sum_{m=1}^N v_0^{m*} \check{\mathbf{v}}_m = -e^{-j\theta_0} \check{\mathbf{E}}_0 \mathbf{b}_M \quad (4.6)$$

$$\text{where } \mathbf{b}_M = \begin{bmatrix} 0 & 1 & \dots & M-1 \end{bmatrix}^T, \mathbf{v}_m = \begin{bmatrix} v_0^m \\ \check{\mathbf{v}}_m \end{bmatrix}, \text{ and } \mathbf{E}_0 = \begin{bmatrix} \frac{se^{j\theta_0}}{\sqrt{M}} \mathbf{1}_M^T \\ \check{\mathbf{E}}_0 \end{bmatrix}.$$

Proof: Setting $K = 2$ in (2.42a) with the degree-one factorization (2.51) for $\mathbf{E}(z)$, we have

$$\mathbf{E}_0 \mathbf{1}_M = s\sqrt{M} e^{j\theta_0} \mathbf{e}_0$$

from (4.5), and

$$-M \sum_{m=1}^N \mathbf{v}_m \mathbf{v}_m^\dagger \mathbf{E}_0 \mathbf{1}_M - \mathbf{E}_0 \mathbf{b}_M = c_1 \mathbf{e}_0$$

for some $c_1 \neq 0$. By deleting the 0th rows from both sides of the equation, we arrive at (4.6). ■

Similarly, we have the following two-regular result for the order-one factorization (2.53).

Corollary 4.2 (Two-Regularity with Length Constraint). *An order- L PUFB (2.53) is two-regular if and only if*

1. \mathbf{E}_0 is one-regular as in Lemma 4.3, and

2. the unitary parameter matrices $\mathbf{w}_m \triangleq \begin{bmatrix} \mathbf{w}_{m,1} & \mathbf{w}_{m,2} & \dots & \mathbf{w}_{m,\gamma_m} \end{bmatrix}$ of the order-one PU building blocks $\mathbf{W}_m(z)$ are such that

$$sM^{3/2} \sum_{m=1}^L \sum_{i=1}^{\gamma_m} w_0^{m,i*} \check{\mathbf{w}}_{m,i} = -e^{-j\theta_0} \check{\mathbf{E}}_0 \mathbf{b}_M \quad (4.7)$$

$$\text{where } \mathbf{w}_{m,i} = \begin{bmatrix} w_0^{m,i} \\ \hline \check{\mathbf{w}}_{m,i} \end{bmatrix}.$$

Proof: Using the order-one factorization for $\mathbf{E}(z)$ in (2.42a) with $K = 2$, one again obtains $\mathbf{E}_0 \mathbf{1}_M = s\sqrt{M} e^{j\theta_0} \mathbf{e}_0$ and

$$\begin{aligned} c_1 \mathbf{e}_0 &= -M \sum_{m=1}^L \mathbf{w}_m \mathbf{w}_m^\dagger (\mathbf{E}_0 \mathbf{1}_M) - \mathbf{E}_0 \mathbf{b}_M \\ &= -sM\sqrt{M} e^{j\theta_0} \sum_{m=1}^L \mathbf{w}_m (\mathbf{w}_m^\dagger \mathbf{e}_0) - \mathbf{E}_0 \mathbf{b}_M \\ &= -sM^{3/2} e^{j\theta_0} \sum_{m=1}^L \sum_{i=1}^{\gamma_m} w_0^{m,i*} \mathbf{w}_{m,i} - \mathbf{E}_0 \mathbf{b}_M, \end{aligned}$$

and thus (4.7). ■

Having obtained the two-regular dyadic-based structures, we now present the following two Lemmas which are useful for further analysis.

Lemma 4.4 (Norm of $v_0^{m*}\check{\mathbf{v}}_m$). *For each of the terms $v_0^{m*}\check{\mathbf{v}}_m$, the norm is upper-bounded by $1/2$:*

$$\begin{aligned}\|v_0^{m*}\check{\mathbf{v}}_m\|^2 &= |v_0^m|^2 \sum_{i=1}^{M-1} |v_i^m|^2 \\ &= |v_0^m|^2 (1 - |v_0^m|^2) \leq 1/4.\end{aligned}\tag{4.8}$$

The equality holds when $|v_0^m| = 1/\sqrt{2}$.

This norm bound will be used to prove the triangle inequality in the subsequent sections.

Lemma 4.5 (Constant Norm). *If the PUFB $\mathbf{E}(z)$ is at least one-regular, the norm of $\check{\mathbf{E}}_0 \mathbf{b}_M$, as appears in (4.6) and (4.7), will be constant, irrespective of \mathbf{E}_0 .*

Proof: Since $\check{\mathbf{E}}_0 \mathbf{b}_M$ is obtained by deleting the 0th entry of $\mathbf{E}_0 \mathbf{b}_M$, we have

$$\begin{aligned}\|\check{\mathbf{E}}_0 \mathbf{b}_M\| &= \sqrt{\|\mathbf{E}_0 \mathbf{b}_M\|^2 - \left| \frac{s}{\sqrt{M}} e^{j\theta_0} \mathbf{1}_M^T \mathbf{b}_M \right|^2} \\ &= \sqrt{\sum_{n=1}^{M-1} n^2 - \frac{1}{M} \left(\sum_{n=1}^{M-1} n \right)^2} \\ &= \sqrt{\frac{M(M^2 - 1)}{12}},\end{aligned}\tag{4.9}$$

independent of \mathbf{E}_0 . ■

Based on the above, the first result is the minimum McMillan degree required for two-regularity.

Theorem 4.3 (Minimum Degree for Two-Regulararity). *For a PUFB to be two-regular, its McMillan degree has to be at least one.*

Proof: Taking the norm of (4.6) and using (4.8) and (4.9) give

$$\sqrt{\frac{M(M^2 - 1)}{12}} = \left\| M^{3/2} \sum_{m=1}^N v_0^{m*} \check{\mathbf{v}}_m \right\| \leq M^{3/2} \frac{N}{2},\tag{4.10}$$

from which it can easily be seen that N , the degree of the PUFB, has to be at least one for the inequality to hold. ■

Note that this result is consistent with the fact that, for a two-regular PUFB, the minimum order is one, and that the filter length is thus $2M$ [105] which is a stronger requirement. One should also note that, if the linear-phase property is imposed, this minimum length is increased to $3M$ [92].

Existence of Two-Regular Solutions

Not all choices of unit-norm vectors \mathbf{v}_m satisfy (4.6) for the degree-one factorization. Similarly for the order-one case (4.7). In particular, the parameter vectors \mathbf{v}_m and $\mathbf{w}_{m,i}$ have to satisfy the triangle inequalities imposed by (4.6) and (4.7), respectively. Take (4.6) for example. Dividing it by $sM^{3/2}$ and moving the first k terms of the summation to the other side of the equation, we have the following inequalities

$$\left\| \frac{se^{-j\theta_0}}{M^{3/2}} \check{\mathbf{E}}_0 \mathbf{b}_M + \sum_{m=1}^k v_0^{m*} \check{\mathbf{v}}_m \right\| = \left\| \sum_{m=k+1}^N v_0^{m*} \check{\mathbf{v}}_m \right\| \leq \frac{N-k}{2} \quad (4.11)$$

for $k = 0, 1, \dots, N - 1$. The last inequality is obtained by appealing to triangle inequality and Lemma 4.4. The following theorem summarizes the results obtained from this idea.

Theorem 4.4 (Two-Regular Feasibility—I). *Consider a two-regular PUFB with the degree-one factorization (2.51). In the corresponding two-regular condition (4.6), suppose that $\mathcal{A}_k \triangleq \{\mathbf{v}_1, \dots, \mathbf{v}_k\}$ has been given. Then there always exist unit-norm vectors $\mathbf{v}_{k+1}, \dots, \mathbf{v}_N$ which, together with \mathbf{v}_i in \mathcal{A}_k , satisfy (4.6) regardless of the choice of \mathcal{A}_k , for any $k \in \{1, \dots, \lceil \frac{N}{2} \rceil - 1\}$, where it is understood that $\mathcal{A}_k \equiv \emptyset$ if $N \leq 2$.*

Proof: In the LHS of (4.11), we have

$$\left\| \frac{se^{-j\theta_0}}{M^{3/2}} \check{\mathbf{E}}_0 \mathbf{b}_M + \sum_{m=1}^k v_0^{m*} \check{\mathbf{v}}_m \right\| \leq \sqrt{\frac{M^2 - 1}{12M^2}} + \frac{k}{2} \leq \frac{1}{\sqrt{12}} + \frac{k}{2}$$

by triangle inequality and (4.9). We want this bound to be upper-bounded by $(N - k)/2$ as in (4.11) so that there always exist some $\mathbf{v}_{k+1}, \dots, \mathbf{v}_N$ which, together with $\mathbf{v}_1, \dots, \mathbf{v}_k$, satisfy (4.6). This results in $k \leq \frac{N}{2} - \frac{1}{\sqrt{12}}$ or $k \leq \lceil \frac{N}{2} \rceil - 1$. ■

This theorem guarantees that for the two-regular degree-one factorization, approximately half of the unit-norm vectors \mathbf{v}_m in (4.6) can be arbitrarily chosen in imposing two degrees of regularity. Suppose the vectors \mathbf{v}_m are determined in the increasing order of $m = 1, 2, \dots$. Then the condition (4.11) need be checked only for \mathbf{v}_m with $m = \lceil \frac{N}{2} \rceil, \dots, N - 1$.

The following inequality is important in establishing the order-one equivalence of Theorem 4.4.

Lemma 4.6. *In (4.7), we have*

$$\left\| \sum_{i=1}^{\gamma_m} w_0^{m,i*} \breve{\mathbf{w}}_{m,i} \right\| \leq \frac{\sqrt{\gamma_m}}{2}.$$

Proof: We will postpone the proof to Lemma 4.7 in the next section where we establish the properties and geometric interpretations of regular M -channel lifting structures. ■

We are now ready to state the order-one equivalence of Theorem 4.4.

Theorem 4.5 (Two-Regular Feasibility—II). *Consider a two-regular PUFB with the order-one factorization (2.53). In the corresponding two-regular condition (4.7), suppose that $\mathcal{B}_\ell \triangleq \{\mathbf{w}_1, \dots, \mathbf{w}_\ell\}$ has been given. Then there always exist unitary matrices $\mathbf{w}_{\ell+1}, \dots, \mathbf{w}_L$ which, together with \mathbf{w}_i in \mathcal{B}_ℓ , satisfy (4.7) regardless of the choice of \mathcal{B}_ℓ , for any $\ell \leq \lceil \frac{L}{2} \rceil - 1$, with $\mathcal{B}_\ell \equiv \emptyset$ if $L \leq 2$.*

Proof: By triangle inequality, we have

$$\left\| \frac{se^{-j\theta_0}}{M^{3/2}} \breve{\mathbf{E}}_0 \mathbf{b}_M + \sum_{m=1}^{\ell} \sum_{i=1}^{\gamma_m} w_0^{m,i*} \breve{\mathbf{w}}_{m,i} \right\| \leq \frac{1}{\sqrt{12}} + \sum_{m=1}^{\ell} \frac{\sqrt{\gamma_m}}{2}$$

and

$$\left\| \sum_{m=\ell+1}^L \sum_{i=1}^{\gamma_m} w_0^{m,i*} \breve{\mathbf{w}}_{m,i} \right\| \leq \sum_{m=\ell+1}^L \frac{\sqrt{\gamma_m}}{2}.$$

By the feasibility assumption on $\mathbf{w}_{\ell+1}, \dots, \mathbf{w}_L$, we want

$$\frac{1}{\sqrt{12}} + \sum_{m=1}^{\ell} \frac{\sqrt{\gamma_m}}{2} \leq \sum_{m=\ell+1}^L \frac{\sqrt{\gamma_m}}{2}.$$

Since the γ_m can be ordered as in (2.55), it is sufficient that

$$\frac{1}{\sqrt{12}} + \ell \frac{\sqrt{\gamma_{\ell+1}}}{2} \leq (L - \ell) \frac{\sqrt{\gamma_{\ell+1}}}{2}, \quad \text{or} \quad \ell \leq \left\lceil \frac{L}{2} \right\rceil - 1.$$

■

Remark: For the two-regular order-one factorization, approximately half of the order-one PU building blocks $\mathbf{W}_m(z)$ can be arbitrarily chosen without violating the two-regular feasibility, where (2.55) is assumed on the γ_m 's.

Procedures for Obtaining Feasible Solutions to Two-Regular PUFBs

Degree-One Factorization Case (4.6)

Since \mathbf{v}_k , $k = 1, \dots, \lceil \frac{N}{2} \rceil - 1$, can be arbitrary as Theorem 4.4 guarantees, consider $k \geq \lceil \frac{N}{2} \rceil$.

Having determined $\mathbf{v}_1, \mathbf{v}_2, \dots, \mathbf{v}_{k-1}$, we have to choose \mathbf{v}_k such that

$$v_0^{k*} \check{\mathbf{v}}_k + \sum_{m=k+1}^N v_0^{m*} \check{\mathbf{v}}_m = \mathbf{g}_k, \quad (4.12)$$

where

$$\mathbf{g}_k \triangleq - \sum_{m=1}^{k-1} v_0^{m*} \check{\mathbf{v}}_m - s M^{-3/2} e^{-j\theta_0} \check{\mathbf{E}}_0 \mathbf{b}_M$$

is known, as $\mathbf{v}_1, \mathbf{v}_2, \dots, \mathbf{v}_{k-1}$ have been chosen. Eqn. (4.12) specifies the feasibility condition on \mathbf{v}_k in terms of a triangle with two undetermined sides [the two terms on the LHS of (4.12)]. For \mathbf{v}_k to be two-regularly feasible, these two undetermined sides, together with the given side \mathbf{g}_k , must form a triangle or a closed loop.

With this geometric perspective, feasible \mathbf{v}_k can be determined as follows. To simplify

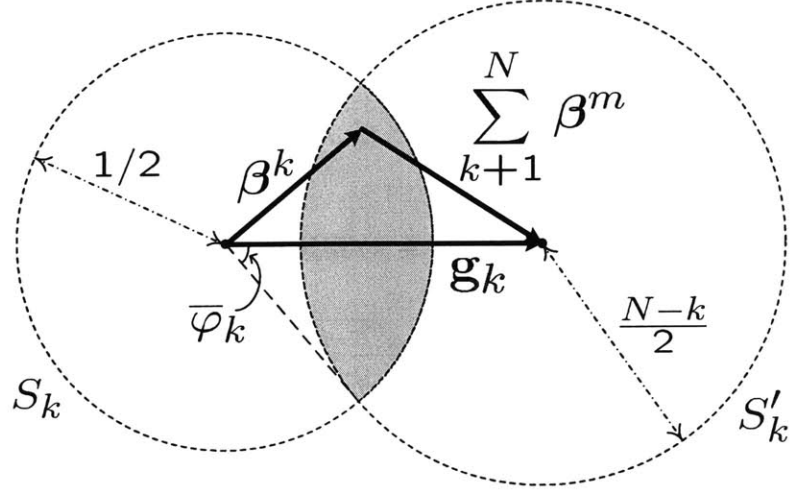


Figure 4-1: Geometry for imposing two degrees of regularity, the case where the distance between S_k and S'_k , $\|\mathbf{g}_k\|$, is large enough such that $S_k \not\subseteq S'_k$. In this case, $\bar{\varphi}_k$ is the maximum angle of deviation that a feasible β^k can make with \mathbf{g}_k , and is given by $\bar{\varphi}_k = \cos^{-1} \left(\|\mathbf{g}_k\| + \frac{1-(N-k)^2}{4\|\mathbf{g}_k\|} \right)$.

notations, define $\beta^m \triangleq v_0^{m*} \check{\mathbf{v}}_m$, and (4.12) becomes

$$\beta^k + \sum_{m=k+1}^N \beta^m = \mathbf{g}_k.$$

We will see that the β^m are vectors consisting of the lifting multipliers of the PU building blocks (Sec. 4.4). By Lemma 4.4, we have $\|\beta^m\| \leq 1/2$ for all m . Therefore, the first undetermined side or feasible β^k is contained within a hyper-sphere $S_k \subset \mathbb{R}^{M-1}$ of radius $1/2$, and the other undetermined side is contained within another hyper-sphere $S'_k \subset \mathbb{R}^{M-1}$ of radius $(N-k)/2$. Figure 4-1 depicts S_k and S'_k centered at the starting and the ending points of vector \mathbf{g}_k , respectively. Depending on the relative sizes of S_k and S'_k , two possibilities are in order: If S_k is completely contained in S'_k , β^k and thus \mathbf{v}^k can be chosen in an unconstrained fashion. This is the case if $\|\mathbf{g}_k\|$ is small enough. Otherwise, β^k has to be chosen out of the shaded area in Figure 4-1 so as to satisfy (4.12). In this case, it is clear from the geometry

that the angle of deviation, φ_k , that any feasible β^m makes with \mathbf{g}_k is upper-bounded by

$$\bar{\varphi}_k = \cos^{-1} \left(\|\mathbf{g}_k\| + \frac{1 - (N - k)^2}{4\|\mathbf{g}_k\|} \right).$$

For any feasible angle $\varphi_k \in [0, \bar{\varphi}_k]$, the length of β^k satisfies

$$\|\mathbf{g}_k\| \cos \varphi_k - \sqrt{\frac{(N - k)^2 - 4\|\mathbf{g}_k\|^2 \sin^2 \varphi_k}{4}} \leq \|\beta^k\| \leq 1/2.$$

At any rate, the intersection of the two hyper-spheres S_k and S'_k is the collection of all feasible β^k . Having chosen \mathbf{v}_k , we repeat the same procedure to find \mathbf{v}_{k+1} , and so on and so forth.

Order-One Factorization Case (4.7)

The above procedure can be extended to this case by replacing β^m with $\sum_{i=1}^{\gamma_m} \beta^{m,i}$ with the norm bound $\|\sum_{i=1}^{\gamma_m} \beta^{m,i}\| \leq \sqrt{\gamma_m}/2$ presented in Lemma 4.6. The radii of the hyper-spheres S_ℓ and S'_ℓ therefore become $\frac{\sqrt{\gamma_\ell}}{2}$ and $\frac{(L-\ell)\sqrt{\gamma_{\ell+1}}}{2}$, respectively. The intersection of S_ℓ and S'_ℓ is the set of feasible vector sums $\sum_{i=1}^{\gamma_\ell} \beta^{\ell,i}$.

4.3 Regular Linear-Phase PUFBs Revisited

As linear-phase PUFBs (LPPUFB) are a special class of PUFBs, this section aims to show how the above general theory on regular PUFBs specializes under the linear phase (LP) assumption, and as a by-product, to derive a simplified dyadic-based representation for LPPUFBs with approximately 50% reduction in the number of free parameters. The number of channels $M \geq 4$ is assumed to be even in this section.

Recall that an M -channel LPPUFB of order L can always be factored as follows [41, 121]

$$\mathbf{E}(z) = \mathbf{G}_L(z)\mathbf{G}_{L-1}(z)\dots\mathbf{G}_1(z)\mathbf{E}_0^{\text{LP}} \quad (4.13)$$

where $\mathbf{G}_m(z) = \mathbf{\Gamma}_m \mathbf{Q} \Lambda(z) \mathbf{Q}$ is the PU linear-phase building block, and $\mathbf{E}_0^{\text{LP}} = \mathbf{\Gamma}_0 \mathbf{Q} \tilde{\mathbf{I}}$, with

$$\begin{aligned}\mathbf{\Gamma}_m &= \begin{bmatrix} \mathbf{U}_m & \mathbf{0}_{M/2} \\ \mathbf{0}_{M/2} & \mathbf{V}_m \end{bmatrix}, \quad \mathbf{Q} = \frac{1}{\sqrt{2}} \begin{bmatrix} \mathbf{I}_{M/2} & \mathbf{I}_{M/2} \\ \mathbf{I}_{M/2} & -\mathbf{I}_{M/2} \end{bmatrix}, \\ \Lambda(z) &= \begin{bmatrix} \mathbf{I}_{M/2} & \mathbf{0}_{M/2} \\ \mathbf{0}_{M/2} & z^{-1} \mathbf{I}_{M/2} \end{bmatrix}, \quad \text{and} \quad \tilde{\mathbf{I}} = \begin{bmatrix} \mathbf{I}_{M/2} & \mathbf{0}_{M/2} \\ \mathbf{0}_{M/2} & \mathbf{J}_{M/2} \end{bmatrix}.\end{aligned}$$

The \mathbf{U}_m and \mathbf{V}_m are $M/2 \times M/2$ unitary. In [52], the authors show that \mathbf{U}_m for $m > 0$ can be set to \mathbf{I} without affecting the completeness of the structure in (4.13).

4.3.1 LPPUFB in Standard Order-One Form (2.53)

Obviously, each LP building block $\mathbf{G}_m(z)$ is of order one. Therefore, one can express it in terms of the order-one PU building block $\mathbf{W}_m(z)$. It can be shown that (with subscripts $M/2$ omitted for notation simplicity)

$$\begin{aligned}\mathbf{G}_L(z) &= \begin{bmatrix} \mathbf{U}_L & \mathbf{0} \\ \mathbf{0} & \mathbf{V}_L \end{bmatrix} \mathbf{Q} \Lambda(z) \mathbf{Q} \\ &= \left\{ \mathbf{I} + (z^{-1} - 1) \frac{1}{2} \begin{bmatrix} \mathbf{I} & -\mathbf{U}_L \mathbf{V}_L^T \\ -\mathbf{V}_L \mathbf{U}_L^T & \mathbf{I} \end{bmatrix} \right\} \begin{bmatrix} \mathbf{U}_L & \mathbf{0} \\ \mathbf{0} & \mathbf{V}_L \end{bmatrix} \\ &\triangleq \mathbf{W}_L(z) \begin{bmatrix} \mathbf{U}_L & \mathbf{0} \\ \mathbf{0} & \mathbf{V}_L \end{bmatrix},\end{aligned}$$

where the order-one PU building block $\mathbf{W}_L(z)$ is given by

$$\mathbf{W}_L(z) = \mathbf{I} + (z^{-1} - 1) \frac{1}{2} \begin{bmatrix} \mathbf{I} & -\mathbf{U}_L \mathbf{V}_L^T \\ -\mathbf{V}_L \mathbf{U}_L^T & \mathbf{I} \end{bmatrix}.$$

The trailing factor $\text{diag}(\mathbf{U}_L, \mathbf{V}_L)$ is absorbed by $\mathbf{G}_{L-1}(z)$ so that

$$\begin{aligned}\mathbf{G}_L(z)\mathbf{G}_{L-1}(z) &= \mathbf{W}_L(z) \begin{bmatrix} \mathbf{U}_L & \mathbf{0} \\ \mathbf{0} & \mathbf{V}_L \end{bmatrix} \mathbf{G}_{L-1}(z) \\ &= \mathbf{W}_L(z) \begin{bmatrix} \tilde{\mathbf{U}}_{L-1} & \mathbf{0} \\ \mathbf{0} & \tilde{\mathbf{V}}_{L-1} \end{bmatrix} \mathbf{Q}\Lambda(z)\mathbf{Q} \\ &= \mathbf{W}_L(z)\mathbf{W}_{L-1}(z) \begin{bmatrix} \tilde{\mathbf{U}}_{L-1} & \mathbf{0} \\ \mathbf{0} & \tilde{\mathbf{V}}_{L-1} \end{bmatrix},\end{aligned}$$

where $\tilde{\mathbf{U}}_m \triangleq \mathbf{U}_L\mathbf{U}_{L-1}\dots\mathbf{U}_m$ and $\tilde{\mathbf{V}}_m \triangleq \mathbf{V}_L\mathbf{V}_{L-1}\dots\mathbf{V}_m$ are unitary, and $\mathbf{W}_m(z)$ is given by

$$\mathbf{W}_m(z) = \mathbf{I} + (z^{-1}-1)\frac{1}{2} \begin{bmatrix} \mathbf{I} & -\tilde{\mathbf{U}}_m\tilde{\mathbf{V}}_m^T \\ -\tilde{\mathbf{V}}_m\tilde{\mathbf{U}}_m^T & \mathbf{I} \end{bmatrix}. \quad (4.14)$$

We can carry out the same procedure until arriving at

$$\mathbf{E}(z) = \mathbf{W}_L(z)\dots\mathbf{W}_1(z) \underbrace{\begin{bmatrix} \tilde{\mathbf{U}}_0 & \mathbf{0} \\ \mathbf{0} & \tilde{\mathbf{V}}_0 \end{bmatrix}}_{\mathbf{E}_0} \mathbf{Q}\tilde{\mathbf{I}}. \quad (4.15)$$

This alternative factorization (4.15) of the LPPUFB is considered to be the order-one factorization in its “standard” form (2.53).

4.3.2 Some Observations

Two observations are in order based on the standard order-one form (4.15) derived above. Firstly, for each order-one PU building block $\mathbf{W}_m(z)$ as given in (4.14), the choice of the orthogonal¹ parameter matrix \mathbf{w}_m is not unique, but one can always make the following

¹We consider real-valued filters in this section.

choice

$$\mathbf{w}_m = \frac{1}{\sqrt{2}} \begin{bmatrix} \mathbf{I} \\ -\tilde{\mathbf{V}}_m \tilde{\mathbf{U}}_m^T \end{bmatrix}. \quad (4.16)$$

We will see that this choice results in a significant simplification of the two-regular condition (4.7), and achieves a reduced number of free parameters for the LPPUFB. Secondly, the standard form (4.15) provides a new parameterization of LPPUFBs by defining

$$\begin{aligned} \hat{\mathbf{U}}_0 &= \tilde{\mathbf{U}}_0, & \hat{\mathbf{V}}_0 &= \tilde{\mathbf{V}}_0, & \text{and} \\ \hat{\mathbf{V}}_m &= \tilde{\mathbf{V}}_m \tilde{\mathbf{U}}_m^T, & m &= 1, 2, \dots, L. \end{aligned}$$

Namely, there are in total $L+2$ free parameter matrices of size $M/2 \times M/2$. This is less than $2L+2$ as in (4.13) and is the same number as the reduced-parameter structure for LPPUFBs established in [52]. Note that starting with a set of (original) parameter matrices \mathbf{U}_m and \mathbf{V}_m as in (4.13), one can always obtain a corresponding *smaller* set of matrices $\hat{\mathbf{U}}_m$ and $\hat{\mathbf{V}}_m$. Hence, the completeness of the structure is not affected by the proposed parameterization.

4.3.3 Specialization of Two-Regular Condition (4.7)

With the proposed choice of the $M \times \frac{M}{2}$ orthogonal parameter matrix \mathbf{w}_m for $\mathbf{W}_m(z)$:

$$\mathbf{w}_m = \frac{1}{\sqrt{2}} \begin{bmatrix} \mathbf{I} & -\hat{\mathbf{V}}_m^T \end{bmatrix}^T, \quad (4.17)$$

the second two-regular condition (4.7) in Corollary 4.2 simplifies significantly, resulting in

$$sM^{3/2} \sum_{m=1}^L w_{1,0}^m \check{\mathbf{w}}_1^m = -\check{\mathbf{E}}_0 \mathbf{b}_M, \quad (4.18)$$

as $w_{i,0}^m \equiv 0$ for all $i > 1$ and for all $m = 1, \dots, L$, where the phase term $e^{-j\theta_0}$ becomes ± 1 in the real case and has been absorbed into the sign parameter s . The above condition can be

further simplified as

$$\frac{sM^{3/2}}{2} \sum_{m=1}^L \hat{\mathbf{V}}_m \mathbf{e}_0 = \check{\mathbf{E}}_0 \mathbf{b}_M, \quad (4.19)$$

due to LP and (4.16), where $\check{\mathbf{E}}_0$ denotes the lower $M/2$ rows of \mathbf{E}_0 , and it is understood that $\mathbf{e}_0 \in \mathbb{R}^{M/2}$. This is a condition on the 0th columns of $\hat{\mathbf{V}}_m$'s, which is a simpler geometric condition to impose.

Proof: We will first show that the first $M/2 - 1$ equations in (4.18) are automatically satisfied due to the LP assumption. Therefore, (4.19) and (4.18) are equivalent.

In the LHS of (4.18), the first $M/2 - 1$ elements are identically zero due to (4.17). For the RHS, note that

$$\mathbf{E}_0 = \begin{bmatrix} \hat{\mathbf{U}}_0 & \mathbf{0} \\ \mathbf{0} & \hat{\mathbf{V}}_0 \end{bmatrix} \mathbf{Q}\tilde{\mathbf{I}} = \frac{1}{\sqrt{2}} \begin{bmatrix} \hat{\mathbf{U}}_0 & \hat{\mathbf{U}}_0 \mathbf{J} \\ \hat{\mathbf{V}}_0 & -\hat{\mathbf{V}}_0 \mathbf{J} \end{bmatrix}.$$

Therefore, by recognizing $\mathbf{b}_M = \left[\mathbf{b}_{\frac{M}{2}}^T \quad \mathbf{b}_{\frac{M}{2}}^T + \left(\frac{M}{2}\right) \mathbf{1}_{\frac{M}{2}}^T \right]^T$ and $\mathbf{b}_{\frac{M}{2}} + \mathbf{J}\mathbf{b}_{\frac{M}{2}} = \left(\frac{M}{2} - 1\right) \mathbf{1}_{\frac{M}{2}}$, we have

$$\begin{aligned} \mathbf{E}_0 \mathbf{b}_M &= \frac{1}{\sqrt{2}} \begin{bmatrix} \hat{\mathbf{U}}_0 & \hat{\mathbf{U}}_0 \mathbf{J} \\ \hat{\mathbf{V}}_0 & -\hat{\mathbf{V}}_0 \mathbf{J} \end{bmatrix} \begin{bmatrix} \mathbf{b}_{\frac{M}{2}} \\ \mathbf{b}_{\frac{M}{2}} + \left(\frac{M}{2}\right) \mathbf{1}_{\frac{M}{2}} \end{bmatrix} \\ &= \frac{1}{\sqrt{2}} \begin{bmatrix} \hat{\mathbf{U}}_0 \left(\mathbf{b}_{\frac{M}{2}} + \mathbf{J}\mathbf{b}_{\frac{M}{2}} + \frac{M}{2} \mathbf{1}_{\frac{M}{2}} \right) \\ \hat{\mathbf{V}}_0 \left(\mathbf{b}_{\frac{M}{2}} - \mathbf{J}\mathbf{b}_{\frac{M}{2}} - \frac{M}{2} \mathbf{1}_{\frac{M}{2}} \right) \end{bmatrix} = \begin{bmatrix} \alpha \hat{\mathbf{U}}_0 \mathbf{1}_{\frac{M}{2}} \\ \times \end{bmatrix}, \end{aligned}$$

where $\alpha = \frac{M-1}{\sqrt{2}}$. As the LPPUFB is two-regular, $\hat{\mathbf{U}}_0 \mathbf{1}_{\frac{M}{2}} = \hat{c}_0 \mathbf{e}_0$, where $\mathbf{e}_0 \in \mathbb{R}^{M/2}$ and $\hat{c}_0 = \pm \sqrt{M/2}$ [92], which establishes that the first $M/2 - 1$ elements in the RHS of (4.18) are identically zero as well. ■

In this way, we have obtained an alternative characterization of structurally regular LPPUFBs [92] using dyadic-based structures, with an equivalent but simpler geometric condition (4.19) to impose. Note that based on (4.19), many properties in [92] such as the

minimum length can also be derived, and the design procedure can be fully utilized subject to suitable modifications.

4.4 Regular M -channel Lifting Structures

Recall that the M -channel lifting factorization proposed in Chapter 3 allows for efficient, reversible, and possibly multiplierless implementations of perfect reconstruction filter banks and their corresponding M -band wavelet transforms, even under finite precision and/or nonlinear liftings [25]. In the design process, the lifting-based parameterization enjoys faster convergence than the Givens rotation-based counterpart [25, 27]. Here, we will first revisit the M -channel lifting factorizations of the PU building blocks encountered so far, including a parallel implementation of $\mathbf{W}_m(z)$ based on $\mathbf{V}_m(z)$, which will be employed to obtain the M -channel lifting factorization of $\mathbf{W}_m(z)$. Then, the properties of the associated lifting multipliers will be derived which are important to the analysis of the proposed lifting factorizations. This is followed by the imposition of structural regularity in the context of lifting factorizations, and it will become clear that the proposed M -channel lifting factorization provides a natural parameterization of the problem in question.

4.4.1 Degree-One Paraunitary Building Block $\mathbf{V}_m(z)$

Recall that the degree-one paraunitary building block

$$\mathbf{V}_m(z) = \mathbf{I} - \mathbf{v}_m \mathbf{v}_m^\dagger + z^{-1} \mathbf{v}_m \mathbf{v}_m^\dagger$$

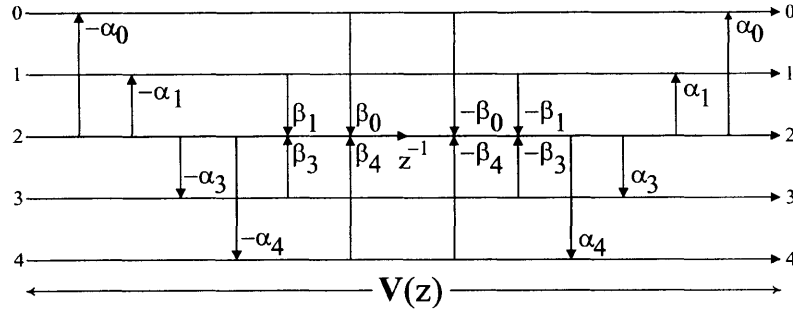


Figure 4-2: The M -channel lifting factorization of $\mathbf{V}(z)$, drawn for $M = 5$ and $r = 2$.

where $\mathbf{v}_m = [v_0^m \ v_1^m \ \dots \ v_{M-1}^m]^T$ is a unit-norm vector, can be lifting-factorized as

$$\mathbf{V}_m(z) = \begin{bmatrix} 1 & \alpha_0^m & & & & \\ \ddots & \vdots & & & & \\ & 1 & \alpha_{r-1}^m & & & \\ & & 1 & & & \\ & & \alpha_{r+1}^m & 1 & & \\ & & \vdots & \ddots & & \\ & & \alpha_{M-1}^m & & 1 & \end{bmatrix} \begin{bmatrix} 1 & & & & & & \\ & \ddots & & & & & \\ & & 1 & & & & \\ & & -\beta_0^m & \dots & -\beta_{r-1}^m & z^{-1} & -\beta_{r+1}^m \dots -\beta_{M-1}^m \\ & & & & & & 1 \\ & & & & & & \ddots \\ & & & & & & & 1 \end{bmatrix} \begin{bmatrix} 1 & & & & & & \\ & \ddots & & & & & \\ & & 1 & -\alpha_0^m & & & \\ & & & \vdots & & & \\ & & & 1 & -\alpha_{r-1}^m & & \\ & & & & 1 & & \\ & & & & -\alpha_{r+1}^m & 1 & \\ & & & & & \vdots & \ddots \\ & & & & & & & 1 \end{bmatrix} \quad (4.20)$$

where the *lifting multipliers* $\alpha_i^m \triangleq v_i^{m*}/v_r^{m*}$ and $\beta_i^m \triangleq v_i^m v_r^{m*}$ for some $r \in \{0, 1, \dots, M-1\}$ with $v_r^m \neq 0$. As we can see, the factorization is not unique unless the choice of r is. Figure 4-2 shows one lifting factorization of $\mathbf{V}_m(z)$ for $M = 5$, The factorization requires $4(M-1)$

lifting steps and only one delay element to implement, and thus is minimal in the McMillan sense. It is also minimal because exactly $2(M - 1)$ design variables (or $M - 1$ for the real case) are needed. The β_i^m are related to α_i^m according to

$$\beta_i^m = \frac{\alpha_i^{m*}}{1 + \sum_{i=0, i \neq r}^{M-1} |\alpha_i^m|^2} \quad (4.21)$$

to ensure paraunitarity. Reversible, possibly integer, implementation of $\mathbf{V}_m(z)$ is readily available under the lifting structure, as in [22, 31, 66, 91].

4.4.2 Order-One Paraunitary Building Block $\mathbf{W}_m(z)$

Although the order-one building block $\mathbf{W}_m(z)$ is related to and can be implemented by *cascading* the degree-one PU building blocks as in (2.57), we note another implementation of $\mathbf{W}_m(z)$ which consists of degree-one PU building blocks *in parallel*: as a consequence of the unitary parameter matrix \mathbf{w}_m of $\mathbf{W}_m(z)$, we have from (2.52) and (2.56) that

$$\begin{aligned} \mathbf{W}_m(z) &= \mathbf{I} + (z^{-1} - 1) \sum_{i=1}^{\gamma_m} \mathbf{w}_{m,i} \mathbf{w}_{m,i}^\dagger \\ &= -(\gamma_m - 1) \mathbf{I} + \underbrace{\sum_{i=1}^{\gamma_m} \mathbf{I} + (z^{-1} - 1) \mathbf{w}_{m,i} \mathbf{w}_{m,i}^\dagger}_{\triangleq \mathbf{V}_{m,i}(z)}. \end{aligned} \quad (4.22)$$

This parallel form (4.22) reveals the degree- γ_m nature of $\mathbf{W}_m(z)$ —a minimum of γ_m degree-one PU building blocks $\mathbf{V}_{m,i}(z)$ are needed to implement it, and (4.22) is thus minimal. Figure 4-3 depicts this parallel structure. As a result of (4.22), the M -channel lifting factorization of $\mathbf{W}_m(z)$ can be readily obtained by applying (4.20) and the corresponding lifting structure in Figure 4-2.

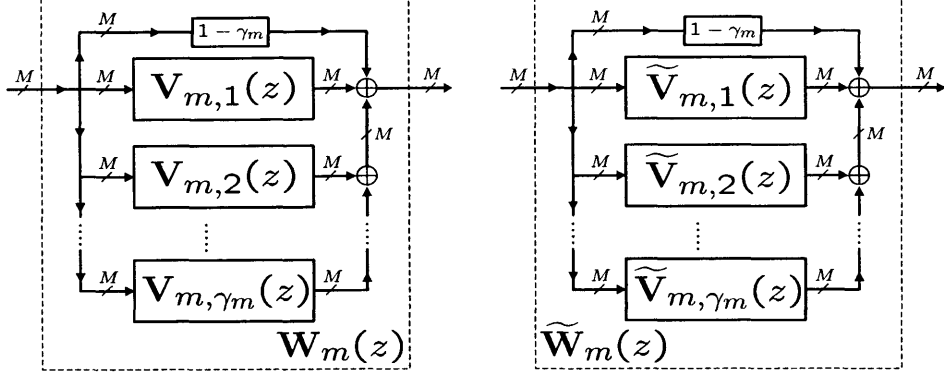


Figure 4-3: A parallel implementation of the order-one PU building block $\mathbf{W}_m(z) = \mathbf{I} - \mathbf{w}_m \mathbf{w}_m^\dagger + z^{-1} \mathbf{w}_m \mathbf{w}_m^\dagger$ of degree γ_m [see (2.57)], $1 \leq \gamma_m \leq M$.

4.4.3 Householder Matrix \mathbf{H}

Recall that the Householder matrix \mathbf{H} with parameter $\mathbf{p}_m = [p_0^m \ p_1^m \ \dots \ p_{M-1}^m]^T$ can be lifting-factorized as follows:

$$\mathbf{H}[\mathbf{p}_m] = \begin{bmatrix} 1 & \sigma_0^m & & & & \\ & \ddots & \vdots & & & \\ & 1 & \sigma_{r-1}^m & & & \\ & & 1 & & & \\ & & \sigma_{r+1}^m & 1 & & \\ & & & \ddots & & \\ & & & & & 1 \end{bmatrix} \begin{bmatrix} 1 & & & & & & \\ & \ddots & & & & & \\ & & 1 & & & & \\ & & -2\rho_0^m & \dots & -2\rho_{r-1}^m & -1 & -2\rho_{r+1}^m & \dots & -2\rho_{M-1}^m \\ & & & & & & 1 & & \\ & & & & & & & \ddots & \\ & & & & & & & & 1 \end{bmatrix} \cdot \begin{bmatrix} 1 & -\sigma_0^m & & & & & \\ & \ddots & \vdots & & & & \\ & 1 & -\sigma_{r-1}^m & & & & \\ & & 1 & & & & \\ & & -\sigma_{r+1}^m & 1 & & & \\ & & & \ddots & & & \\ & & & & & & 1 \end{bmatrix} \quad (4.23)$$

where the lifting multipliers $\sigma_i^m = p_i^{m*}/p_r^{m*}$ and $\rho_i^m = p_i^m p_r^{m*}$ for some $r \in \{0, 1, \dots, M-1\}$ with $p_r^m \neq 0$. Again, σ_i^m and ρ_i^m satisfy (4.21), with the substitutions $\alpha_i^m = \sigma_i^m$ and $\beta_i^m = \rho_i^m$, as \mathbf{H} is unitary. An example 5-channel lifting factorization of \mathbf{H} is given in Figure 4-4.

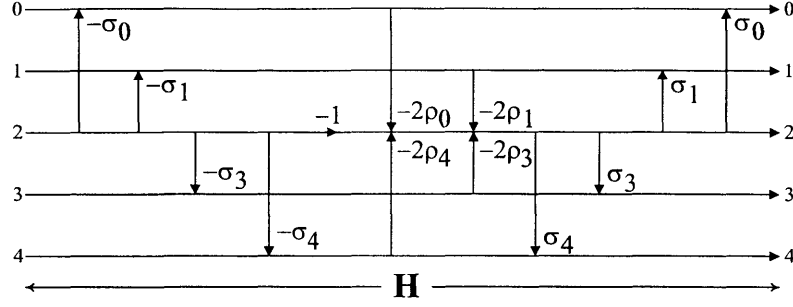


Figure 4-4: The M -channel lifting factorization of Householder matrix \mathbf{H} , drawn for $M = 5$ and $r = 2$.

4.4.4 Properties of Lifting Structures

For notation simplicity, we will consider the lifting factorizations (4.20) with $r = 0$ for the degree-one PU building block $\mathbf{V}_m(z)$, and (4.23) with $r = m$ for the Householder matrix $\mathbf{H}[\mathbf{p}_m]$. Extension to other values of r is straightforward. Necessary and sufficient conditions of regularity on the lifting multipliers of the order-one factorization (2.53) will also be derived.

Mapping Between Lifting Multipliers

For $\mathbf{V}_m(z)$, consider the vectors consisting of the lifting multipliers α_i^m and β_i^m :

$$\boldsymbol{\alpha}^m \triangleq \left[\alpha_1^m \ \alpha_2^m \ \dots \ \alpha_{M-1}^m \right]^T \quad \text{and} \quad (4.24)$$

$$\boldsymbol{\beta}^m \triangleq \left[\beta_1^m \ \beta_2^m \ \dots \ \beta_{M-1}^m \right]^T. \quad (4.25)$$

It turns out that the vector $v_0^{m*} \check{\mathbf{v}}_m$ in (4.6) is exactly $\boldsymbol{\beta}^m$ defined above. One can show that $\boldsymbol{\alpha}^m$ and $\boldsymbol{\beta}^m$ are related by

$$\boldsymbol{\beta}^m = \frac{\boldsymbol{\alpha}^{m*}}{1 + \|\boldsymbol{\alpha}^m\|^2} \quad \text{or} \quad (4.26)$$

$$\boldsymbol{\alpha}^m = |v_0^m|^{-2} \boldsymbol{\beta}^{m*}, \quad (4.27)$$

with

$$|v_0^m|^2 = \frac{1}{2} \left(1 \pm \sqrt{1 - 4\|\beta^m\|^2} \right) \quad \text{or} \quad (4.28)$$

$$= (1 + \|\alpha^m\|^2)^{-1} \quad (4.29)$$

as a result of paraunitarity. As we have seen in (4.8) of Lemma 4.4, β^m is a bounded vector:

$$\|\beta^m\| \leq 1/2.$$

On the other hand, α^m is unconstrained:

$$\|\alpha^m\|^2 = \frac{1}{|v_0^m|^2} \sum_{i=1}^{M-1} |v_i^m|^2 = \frac{1}{|v_0^m|^2} - 1 \geq 0.$$

As for the order-one building block $\mathbf{W}_m(z)$ with $\rho(\mathbf{w}_m) = \gamma_m \geq 1$, one can similarly define lifting multipliers $\alpha^{m,i}$ and $\beta^{m,i}$ for $i = 1, \dots, \gamma_m$, and they satisfy the aforementioned properties in addition to some others (see Sec. 4.4.4 below). Furthermore, the vector $w_0^{m,i*} \tilde{\mathbf{w}}_{m,i}$ in (4.7) is exactly $\beta^{m,i}$.

For the Householder matrix $\mathbf{H}[\mathbf{p}_m]$, the same comments apply with α^m , β^m , and v_0^m replaced by σ^m , ρ^m , and p_m^m , respectively, with

$$\sigma^m \triangleq \begin{bmatrix} \sigma_m^m & \sigma_{m+1}^m & \dots & \sigma_{M-1}^m \end{bmatrix}^T \quad \text{and} \quad (4.30)$$

$$\rho^m \triangleq \begin{bmatrix} \rho_m^m & \rho_{m+1}^m & \dots & \rho_{M-1}^m \end{bmatrix}^T. \quad (4.31)$$

Uniqueness Issue

Given $\mathbf{V}_m(z)$, its unit-norm parameter vector \mathbf{v}_m is unique modulo a phase: for any $\phi \in \mathbb{R}$, both \mathbf{v}_m and $e^{j\phi}\mathbf{v}_m$ correspond to the same $\mathbf{V}_m(z)$; on the other hand, the proposed lifting multipliers α^m and β^m are strictly unique given $\mathbf{V}_m(z)$. Similar comments apply to the case of the (degree-0) Householder matrix $\mathbf{H}[\mathbf{p}_m]$.

Conditions for Order-One Lifting Structure

Recall that the rank- γ_m parameter matrix \mathbf{w}_m of the order-one PU building block $\mathbf{W}_m(z)$ is unitary. This imposes some conditions on the M -channel lifting factorization derived from the parallel form (4.22). Let $\mathbf{w}_{m,i}$ be the i th column of \mathbf{w}_m . One can write

$$(\mathbf{w}_0^{m,i})^* \mathbf{w}_{m,i} = \begin{bmatrix} |w_0^{m,i}|^2 \\ \boldsymbol{\beta}^{m,i} \end{bmatrix} \quad (4.32)$$

based on the definition (4.25). Now, the unitary property of \mathbf{w}_m implies that

$$(\boldsymbol{\beta}^{m,i})^\dagger \boldsymbol{\beta}^{m,j} = -|w_0^{m,i} w_0^{m,j}|^2 \leq 0 \quad (4.33)$$

for all $1 \leq i \neq j \leq \gamma_m$. Conversely, if $(\boldsymbol{\beta}^{m,i})^\dagger \boldsymbol{\beta}^{m,j} < 0$ or equivalently $(\boldsymbol{\alpha}^{m,i})^\dagger \boldsymbol{\alpha}^{m,j} = -1$, one has $\mathbf{w}_{m,i}^\dagger \mathbf{w}_{m,j} = 0$. To ensure unitary parameter matrix \mathbf{w}_m , this order-one condition need be imposed on the lifting parameterizations of $\mathbf{W}_m(z)$ derived from either (4.22) or (2.57); mutual orthogonality translated into the lifting domain becomes an “obtuse-angle” condition on the corresponding lifting vectors $\boldsymbol{\beta}^{m,i}$ (and $\boldsymbol{\alpha}^{m,i}$).

The following lemma summarizes a fundamental inequality for the order-one lifting factorization.

Lemma 4.7. *Given an M -channel order-one PU building block $\mathbf{W}_m(z)$ with $\rho(\mathbf{w}_m) = \gamma_m$, the associated γ_m lifting vectors $\{\boldsymbol{\beta}^{m,i} \in \mathbb{C}^{M-1} \mid i=1, \dots, \gamma_m\}$ satisfy*

$$\left\| \sum_{i=1}^{\gamma_m} \boldsymbol{\beta}^{m,i} \right\| \leq \frac{\sqrt{\gamma_m}}{2}. \quad (4.34)$$

Proof: This can be shown by induction on γ_m . For $\gamma_m = 1$, the statement is true since $\|\boldsymbol{\beta}^{m,1}\| \leq \sqrt{1}/2$. Assume it is also true for $\gamma_m = n \geq 1$, i.e.,

$$\left\| \sum_{i=1}^n \boldsymbol{\beta}^{m,i} \right\| \leq \frac{\sqrt{n}}{2}.$$

Now, for $\gamma_m = n + 1$, we have

$$\begin{aligned}
\left\| \sum_{i=1}^{n+1} \beta^{m,i} \right\|^2 &= \left\| \beta^{m,n+1} + \sum_{i=1}^n \beta^{m,i} \right\|^2 \\
&= \|\beta^{m,n+1}\|^2 + \left\| \sum_{i=1}^n \beta^{m,i} \right\|^2 + 2 \cdot \Re \left[(\beta^{m,n+1})^\dagger \sum_{i=1}^n \beta^{m,i} \right] \\
&\leq \frac{1}{4} + \frac{n}{4} + 2 \cdot \left((\beta^{m,n+1})^\dagger \sum_{i=1}^n \beta^{m,i} \right) \leq \frac{n+1}{4}
\end{aligned} \tag{4.35}$$

due to the “obtuse-angle” condition (4.33) on the $n + 1$ lifting vectors. ■

Remark: As the order-one PU building block imposes the “obtuse-angle” condition on the lifting vectors $\beta^{m,i}$, the norm of their sum has a tighter upper bound ($\sqrt{\gamma_m}/2$) than the usual triangle inequality ($\gamma_m/2$).

4.4.5 One-Regular Lifting Structure

Suppose we parameterize the matrix \mathbf{E}_0 by Householder matrices as in (4.1):

$$\mathbf{E}_0 = \mathbf{D} \mathbf{H}[\mathbf{p}_{M-2}] \dots \mathbf{H}[\mathbf{p}_0].$$

where the \mathbf{p}_m are unit-norm vectors and have the form (2.47). Then Lemma 4.3 furnishes one degree of regularity of the PUFB by setting $p_0^0 = \sqrt{\frac{\sqrt{M}-s}{2\sqrt{M}}} e^{j\eta}$ and $p_i^0 = \frac{-se^{j\eta}}{\sqrt{2(M-s\sqrt{M})}}$, where s can be either 1 or -1 . Translating this into the lifting parameterization of $\mathbf{H}[\mathbf{p}_0]$ results in the following one-regular lifting structure.

Theorem 4.6 (One-Regular Lifting Structure). *Consider a PUFB in either the degree-one factorization (2.51) or the order-one factorization (2.53), with the unitary matrix \mathbf{E}_0 parameterized as in (4.1). For $i = 1, 2, \dots, M - 1$, let σ_i^0 and ρ_i^0 be the lifting multipliers of $\mathbf{H}[\mathbf{p}_0]$ as shown in (4.23) for $r = 0$. Then the PUFB is one-regular if and only if the lifting*

multipliers are such that

$$\sigma_i^0 = (1 - s\sqrt{M})^{-1} \quad (4.36)$$

$$\rho_i^0 = -s(2\sqrt{M})^{-1} \quad (4.37)$$

for $i = 1, 2, \dots, M - 1$.

Proof: This is straightforward given Lemma 4.3 and the definitions of σ_i^0 and ρ_i^0 in Sec. 4.4.3. ■

This theorem shows that no matter how the lifting multipliers in $\mathbf{V}_m(z)$, $\mathbf{W}_m(z)$, and $\mathbf{H}[\mathbf{p}_{m'}]$, $m' > 0$, are quantized, the PUFB remains one-regular as long as (4.36) and (4.37) are satisfied.

4.4.6 Two-Regular Lifting Structures

Recalling the definition of the lifting multipliers $\beta_i^m = v_i^m v_r^{m*}$ with $r = 0$, we see that the M -channel lifting factorization is a natural way of parameterizing the problem of imposing (at least) two degrees of regularity: In terms of the vectors $\boldsymbol{\beta}^m$ defined in (4.25), the second condition for two-regularity (4.6) in Theorem 4.2 is conveniently written as

$$\sum_{m=1}^N \boldsymbol{\beta}^m = -sM^{-3/2}e^{-j\theta_0} \check{\mathbf{E}}_0 \mathbf{b}_M \quad (4.38)$$

for the degree-one factorization, and the condition (4.7) in Corollary 4.2 becomes

$$\sum_{m=1}^L \sum_{i=1}^{\gamma_m} \boldsymbol{\beta}^{m,i} = -sM^{-3/2}e^{-j\theta_0} \check{\mathbf{E}}_0 \mathbf{b}_M \quad (4.39)$$

for the order-one factorization. The corresponding geometric conditions (Theorems 4.4 and 4.5) are simply

1. $\boldsymbol{\beta}^1, \boldsymbol{\beta}^2, \dots, \boldsymbol{\beta}^{\lceil N/2 \rceil - 1}$ can be arbitrarily chosen without violating the closed-loop condition for two-regularity (4.38) associated with degree-one factorization.

2. $\beta^{1,i}$, $\beta^{2,i}$, up to $\beta^{\lceil L/2 \rceil - 1, i}$ can be arbitrarily chosen without violating the closed-loop condition for two-regularity (4.39) associated with order-one factorization.

Obviously, the proposed M -channel lifting factorization has a physical interpretation in this regularity context. We summarize the results for two-regular lifting structures with the following theorem.

Theorem 4.7 (Two-Regular Lifting Structures). *Consider a PUFB as in (2.53) or (2.51). Let the unitary matrix E_0 be parameterized by the one-regular lifting structure as in Theorem 4.6. Then, the PUFB is two-regular with or without length constraint if and only if the lifting multipliers satisfy (4.39) or (4.38), respectively.*

Proof: This is again straightforward given Theorem 4.2 and Corollary 4.2. ■

4.5 Design Examples of Regular PUFBs

In this section, we implement the proposed theory of regular PUFBs. Based on the regular structures, the resulting filter banks are *structurally* guaranteed to be paraunitary (hence perfect reconstruction) and regular, regardless of the choice of free parameters in the structures. These free parameters or degrees of freedom can be chosen to be the lifting multipliers α_i^m and σ_i^m (alternatively, β_i^m and ρ_i^m). Numerical experience suggests that such a choice leads to faster convergence than the Givens rotation-based parameterization. Once a particular parameterization of the regular structures is chosen, optimal regular PUFBs are then obtained by unconstrained optimization [13] for design criteria such as *stopband energy*

$$C_{\text{stop}} = \sum_{i=0}^{M-1} \int_{\Omega_i} |H_i(e^{j\omega})|^2 d\omega$$

and *coding gain*

$$G = 10 \log_{10} \frac{\sigma_x^2}{\left(\prod_{i=0}^{M-1} \sigma_{x_i}^2 \|f_i\|^2 \right)^{1/M}},$$

although many other design criteria are also possible [122]. For stopband energy C_{stop} , Ω_i represents the stopband of filter $H_i(z)$, while for coding gain G , an AR(1) process with unit variance $\sigma_x^2 = 1$ and correlation coefficient of 0.95 is assumed; $\sigma_{x_i}^2$ represents the signal variance of the i th subband, and $\|f_i\|$ is the ℓ_2 -norm of synthesis filter $F_i(z)$. Our goal is to minimize C_{stop} and to maximize G . Together, C_{stop} and G form the objective function to be minimized:

$$C_\lambda(\mathbf{u}) = (1 - \lambda)C_{\text{stop}}(\mathbf{u}) + \lambda(-G(\mathbf{u})), \quad 0 \leq \lambda \leq 1,$$

where \mathbf{u} denotes the free parameters (α_i^m and σ_i^m) of the structures.

As with any practical filter design problems, $C_\lambda(\mathbf{u})$ is in general a nonlinear function of \mathbf{u} , which implies that the choice of initial \mathbf{u} can be crucial. Fortunately, with \mathbf{u} being the lifting multipliers, an initial guess around zero often leads to a good solution, as evidenced by numerical experience. This can be further combined with the observation that, for small $\lambda \approx 0$, the minimizer of $C_\lambda(\mathbf{u})$ is rather insensitive to the choice of initial \mathbf{u} . One possibility to exploit this property is to formulate the design of regular PUFBs as a sequence of optimization problems, starting with small λ :

For $k = 1, 2, \dots$, let $\{\lambda^k\}$ be a strictly monotonically (slowly) increasing sequence upper bounded by 1 with $\lambda_1 \approx 0$, and form a corresponding sequence of optimization problems

$$P_k : \min_{\mathbf{u}} C_{\lambda^k}(\mathbf{u}).$$

For each k , let $\mathbf{u}^k \triangleq \arg \min_{\mathbf{u}} C_{\lambda^k}(\mathbf{u})$ be the solution to problem P_k . Note that \mathbf{u}^k can serve as a good initializer for P_{k+1} , as $\{\lambda^k\}$ is slowly increased. Hence, starting with $\mathbf{u}^0 \approx \mathbf{0}$ and $\lambda^1 \approx 0$, one can initialize P_{k+1} with \mathbf{u}^k to obtain \mathbf{u}^{k+1} and so forth, until a good balance between stopband energy and coding gain is achieved. This has been found effective in the following design examples.

4.5.1 One-Regular PUFB

4×8 PUFB—Minimum Degree Case

This example is a real-valued one-regular four-channel PUFB of degree-one, with length-eight filters. The polyphase matrix $\mathbf{E}(z) = \mathbf{V}_1(z)\mathbf{E}_0$ is parameterized using the lifting structure as follows:

$$\mathbf{E}(z) = \begin{bmatrix} 1 & & & \\ \alpha_1^1 & 1 & & \\ \alpha_2^1 & & 1 & \\ \alpha_3^1 & & & 1 \end{bmatrix} \begin{bmatrix} z^{-1} & -\beta_1^1 & -\beta_2^1 & -\beta_3^1 \\ & 1 & & \\ & & 1 & \\ & & & 1 \end{bmatrix} \begin{bmatrix} 1 & \beta_1^1 & \beta_2^1 & \beta_3^1 \\ & 1 & & \\ & & 1 & \\ & & & 1 \end{bmatrix} \begin{bmatrix} 1 & & & \\ -\alpha_1^1 & 1 & & \\ -\alpha_2^1 & & 1 & \\ -\alpha_3^1 & & & 1 \end{bmatrix} \\ \cdot \left(\begin{bmatrix} 1 & & & \\ \sigma_1^0 & 1 & & \\ \sigma_2^0 & & 1 & \\ \sigma_3^0 & & & 1 \end{bmatrix} \begin{bmatrix} -1 & -2\rho_1^0 & -2\rho_2^0 & -2\rho_3^0 \\ & 1 & & \\ & & 1 & \\ & & & 1 \end{bmatrix} \begin{bmatrix} 1 & & & \\ -\sigma_1^0 & 1 & & \\ -\sigma_2^0 & & 1 & \\ -\sigma_3^0 & & & 1 \end{bmatrix} \right. \\ \cdot \begin{bmatrix} 1 & & & \\ & 1 & & \\ \sigma_2^1 & 1 & & \\ \sigma_3^1 & & 1 & \end{bmatrix} \begin{bmatrix} 1 & & & \\ & -1 & -2\rho_2^1 & -2\rho_3^1 \\ & & 1 & \\ & & & 1 \end{bmatrix} \begin{bmatrix} 1 & & & \\ & 1 & & \\ -\sigma_2^1 & 1 & & \\ -\sigma_3^1 & & 1 & \end{bmatrix} \\ \left. \cdot \begin{bmatrix} 1 & & & \\ & 1 & & \\ & & 1 & \\ & & & \sigma_3^2 & 1 \end{bmatrix} \begin{bmatrix} 1 & & & \\ & 1 & & \\ & & -1 & -2\rho_3^2 \\ & & & 1 \end{bmatrix} \begin{bmatrix} 1 & & & \\ & 1 & & \\ & & 1 & \\ & & & -\sigma_3^2 & -1 \end{bmatrix} \right)^T. \quad (4.40)$$

To impose regularity of degree one, σ_1^0 , σ_2^0 , and σ_3^0 are chosen according to the two possibilities ($s = \pm 1$) presented in Theorem 4.6. Table 4.1 consists of the resulting lifting multipliers α_i^m and σ_i^m , where the algorithm proposed in Chapter 7 has been employed to generate these binary numbers [31]. The frequency response of the PUFB is shown in Figure 4-5 for $s = +1$ with coding gain 8.1079dB and $C_{\text{stop}} = 0.3971$. The Sobolev smoothness is .9146. As a comparison, the coding gains of 4-pt DCT and 4-channel LOT [74] are 7.5701 and 7.9259dB, respectively.

$s = +1$					
σ_1^0	-1	σ_2^1	337/2048	α_1^1	-161/512
σ_2^0	-1	σ_3^1	7/64	α_2^1	15/128
σ_3^0	-1	σ_3^2	489/512	α_3^1	11/256
$s = -1$					
σ_1^0	1/3	σ_2^1	-43/64	α_1^1	161/512
σ_2^0	1/3	σ_3^1	-101/128	α_2^1	15/128
σ_3^0	1/3	σ_3^2	7/128	α_3^1	-11/256

Table 4.1: The design variables for the 4×8 PUFBs with the minimum degree. The resulting FB is structurally one-regular as a result of the predetermined σ_1^0 , σ_2^0 and σ_3^0 . The coding gains are 8.1079 and 8.1075dB, respectively.

8×24 PUFB

In this example, a one-regular eight-channel PUFB ($M = 8$) with order two ($L = 2$) is designed; i.e., two order-one PU building blocks $\mathbf{W}_m(z)$ are involved [see Eqn. (2.53)]. The ranks of the parameter matrices \mathbf{w}_m of $\mathbf{W}_m(z)$ are chosen to be $\rho(\mathbf{w}_1) = \rho(\mathbf{w}_2) = M/2 = 4$. Such a choice is necessary for a fair comparison with linear-phase PUFBs (to be compared in Sec. 4.6), and also ensures the symmetric delay property [101]. The sign parameter $s = +1$ is used. Figure 4-6 shows the resulting design with coding gain 9.4894dB and stopband energy 0.0876. The one-regular property is confirmed by Figure 4-6(b) which shows that there is at least one zero at the aliasing frequencies of $H_0(e^{j\omega})$, $\omega_k = \frac{2\pi k}{8}$ ($k = 1, \dots, 7$). The corresponding wavelet basis functions are depicted in Figure 4-6(c), with Sobolev smoothness .9889.

4.5.2 Two-Regular PUFB

Figure 4-7 shows the design of a two-regular 8×24 PUFB with two order-one PU building blocks $\mathbf{W}_m(z)$ involved [see Eqn. (2.53)]. Again, the ranks of the parameter matrices of $\mathbf{W}_m(z)$ are chosen to be $\rho(\mathbf{w}_1) = \rho(\mathbf{w}_2) = 4$ for the same reasons stated above, with the sign parameter $s = +1$ used. The frequency magnitude responses of the resulting filters are

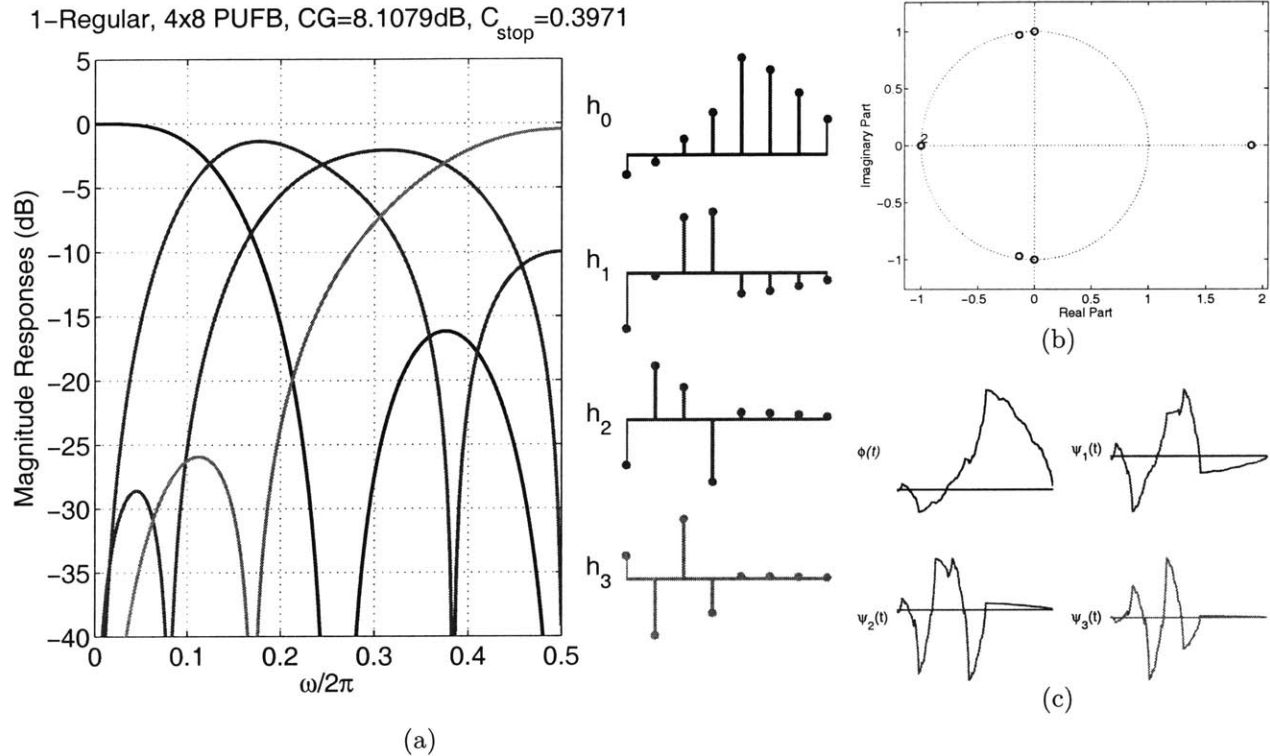


Figure 4-5: Analysis filters and their frequency magnitude responses of the 4-channel PUFB in Table 4.1 with $s = +1$. (a) frequency response and basis functions, (b) zeros of $H_0(z)$, (c) the corresponding wavelet basis with at least one vanishing moment; $s_{max} = .915$.

shown in Figure 4-7(a). The zeros of $H_0(z)$ are plotted in Figure 4-7(b), and we observe that $H_0(e^{j\omega})$ has double zeros at each aliasing frequency, confirming the PUFB is two-regular. The coding gain of this PUFB is 9.4349dB, and the stopband energy is 0.0780. The corresponding wavelet basis functions are depicted in Figure 4-7(c), with Sobolev smoothness 1.2964.

Linear-Phase PUFBs

The proposed characterization of LPPUFB using dyadic-based structures is used here to design regular LPPUFBs. The first example is a two-regular 8×32 LPPUFB. The coding gain is 9.45dB with stopband energy 0.1580. The result is shown in Figure 4-8. As a comparison, the two-regular 8×32 LPPUFB in [92] has coding gain 9.28dB and stopband energy 0.3468.

As another example, we consider the design of an 8×40 LPPUFB with two degrees of

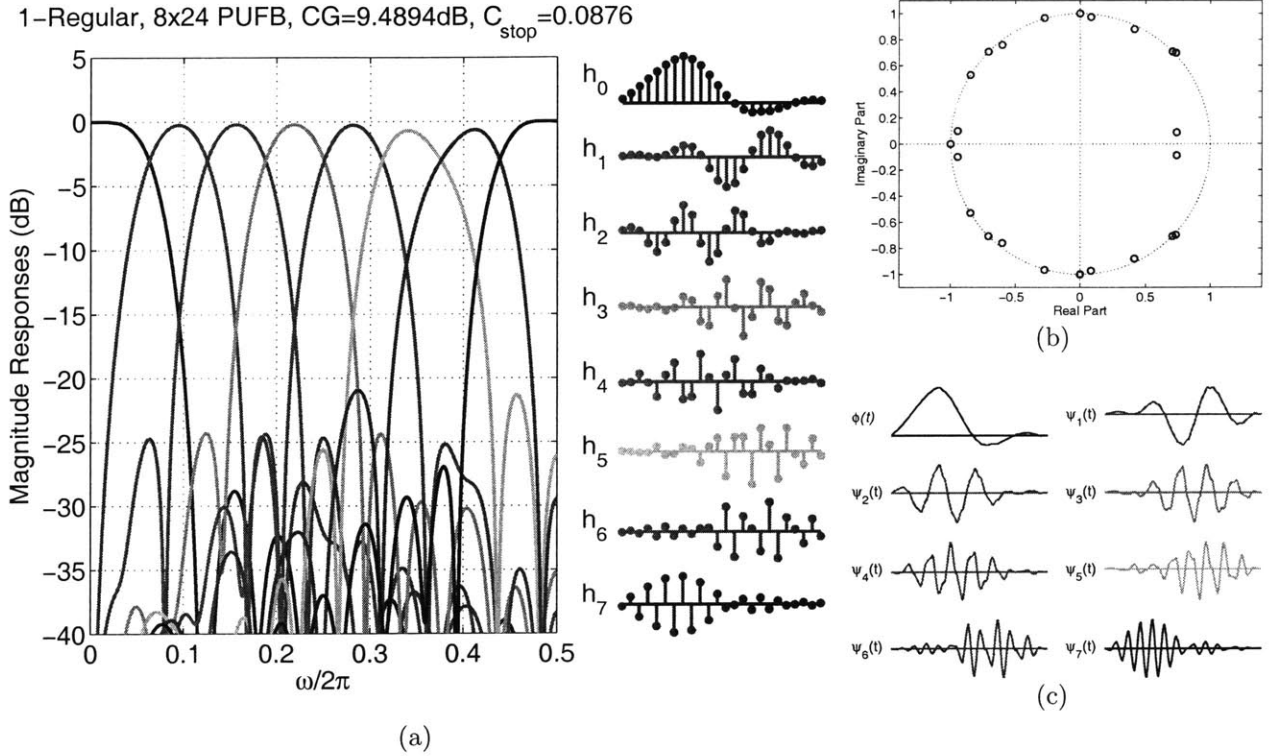


Figure 4-6: Analysis filters and their frequency magnitude responses of the one-regular 8×24 PUFB with $s = +1$. (a) frequency response and basis functions, (b) zeros of $H_0(z)$, (c) the corresponding wavelet basis with one vanishing moment; $s_{max} = .989$.

regularity. The coding gain is 9.50dB with stopband energy 0.0750. The result is shown in Figure 4-9. As a comparison, a two-regular 8×40 LPPUFB based on [92] has coding gain 9.43dB and stopband energy 0.1480.

In both designs, the two-regular property can be confirmed by the multiplicity of zeros of the resulting filters $H_0(z)$, located at the aliasing frequencies $\omega_m = \frac{2\pi m}{M}$, $m = 1, 2, \dots, M-1$.

4.6 Application to Lossy Image Compression

In this section, the above design examples are evaluated in a transform-based coder. In particular, the case of image compression is considered. Similarly to the JPEG image compression standard [97], each input image is block-transformed using the designed M -channel regular filter banks. Each block of transform coefficients is then quantized, zigzag

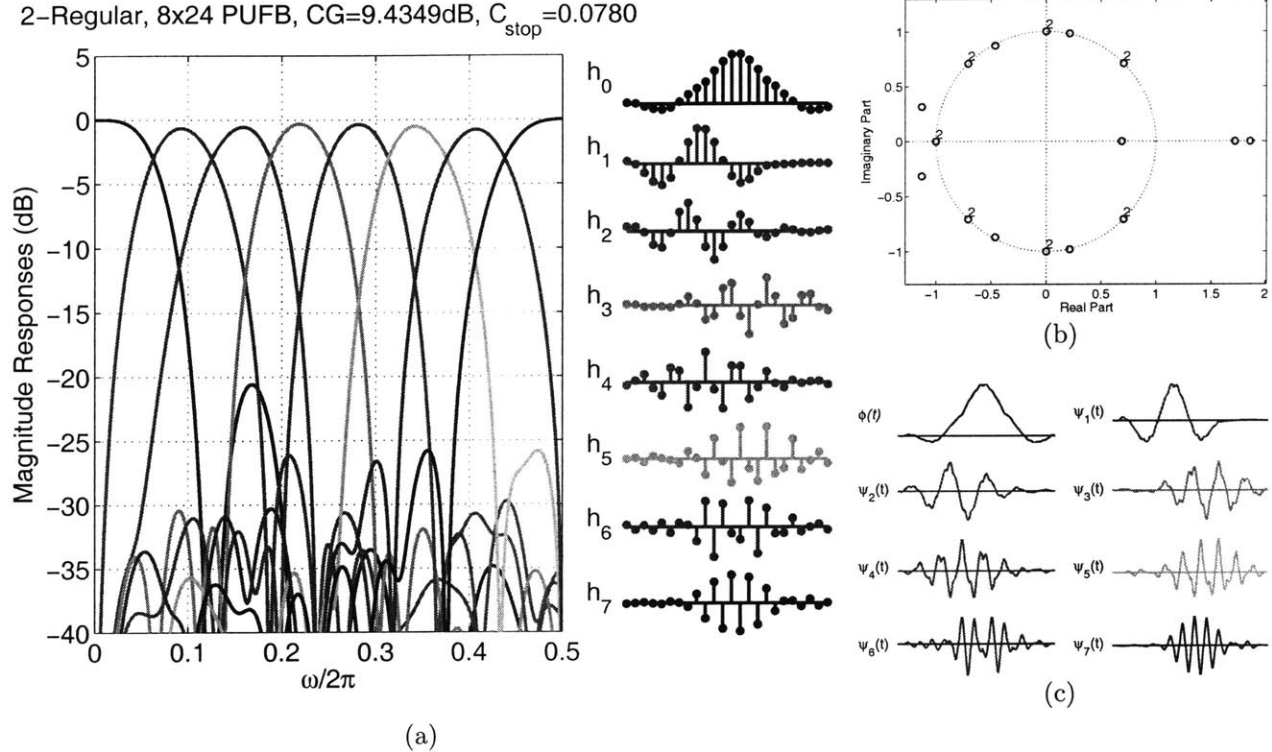


Figure 4-7: Analysis filters and their frequency magnitude responses of the two-regular 8×24 PUFB with $s = +1$. (a) frequency response and basis functions, (b) zeros of $H_0(z)$, (c) the corresponding wavelet basis with two vanishing moments; $s_{\max} = 1.30$.

scanned (runlength coding), and Huffman coded. For this purpose, we use the convenient UICODER [123] with the following transforms:

- 8×8 DCT [100]
- 8×16 LOT [74]
- 8×24 regular PULPs (LPv1, LPv2) [92]
- 8×24 regular PUFBs (PUv1, PUv2) of Sections 4.5.1 and 4.5.2

Their properties are summarized in Table 4.2. Note that the proposed PUFB designs are the most general with PULP (GenLOT) as a special case, and thus achieve the highest objective performance in terms of coding gain and stopband energy among the transforms considered.

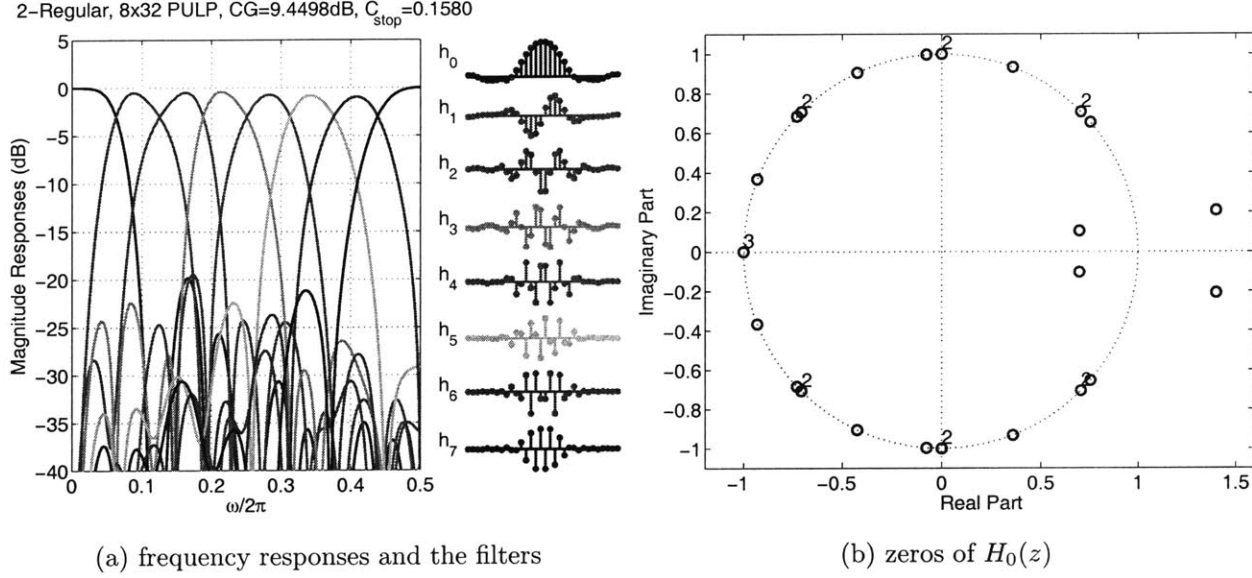


Figure 4-8: The two-regular 8×32 LPPUFB. $s_{max}=1.3378$.

The following test images are used in the compression experiments: they are the standard 512×512 8-bit grayscale *Barbara*, *Goldhill*, and *Lena* [61]. Figure 4-10 shows the rate-distortion curves at various compression ratios, with the PSNRs of the reconstructed images given in Table 4.3 for the six transforms considered. As the current designs (PUv1 and PUv2) are the most general PUFBs, they almost always result in higher PSNRs than their linear-phase counterparts (LPv1 and LPv2) [92], with an exception for the image *Goldhill* at 8:1 compression using the one-regular PUFBs. Figure 4-11 provides a comparison of the visual quality of the various reconstructed *Barbara* images. It is noticeable that the compressed images obtained by using PUv1 and PUv2 have fewer aliasing artifacts in the texture regions and that PUv1 and PUv2 result in smoother approximation (less blocky) in the smooth regions than those obtained by using LPv1 and LPv2, respectively.

4.7 Concluding Remarks

We have presented the theory, design, and structures of the most general PUFBs with up to two degrees of regularity, for any number of channels $M \geq 2$. The phase responses of the filters are not necessarily constrained. Both dyadic-based and M -channel lifting

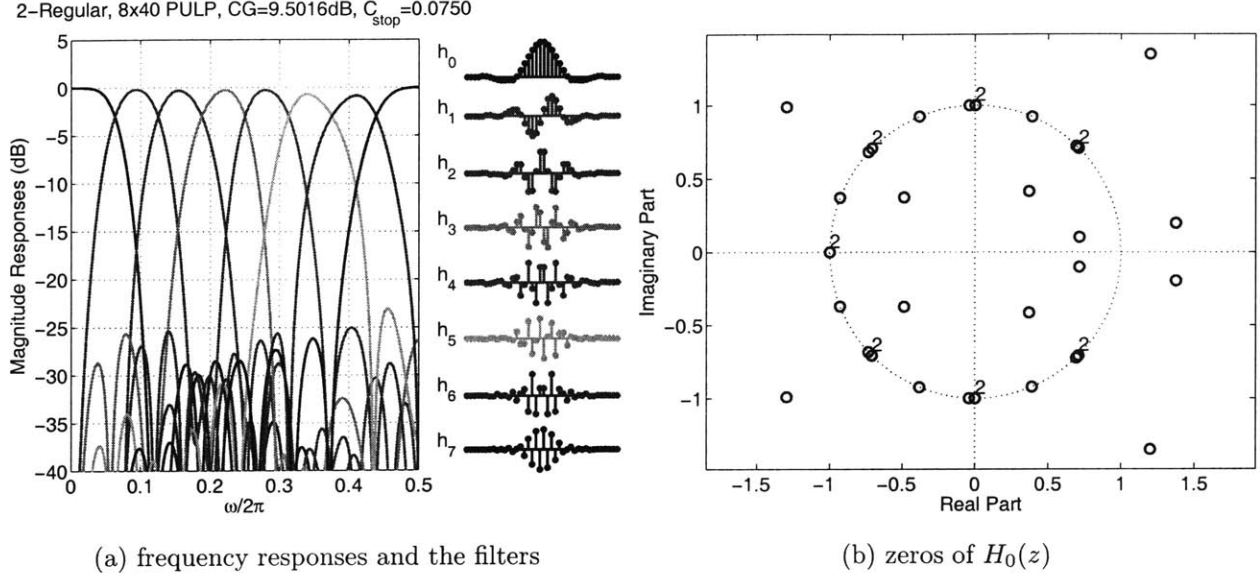


Figure 4-9: The two-regular 8×40 LPPUFB. $s_{max} = 1.5803$.

structures are considered and the corresponding regular structures are proposed, whereby the M -channel lifting factorization provides a natural and convenient parameterization of the problem of imposing regularity, as well as improved design efficiency. The resulting PUFBs are guaranteed to be regular as the regularity conditions are *structurally* imposed, and thus regular PUFBs that are optimal with respect to prescribed design criteria can be found by unconstrained optimization. Depending on whether order-one or degree-one structures are used, regular PUFBs with or without length constraint are readily obtained. Design examples have been presented and evaluated using a transform-based image coder, and they are found to outperform previously published PUFBs in the literature.

Table 4.2: Objective Properties of the PUFBs Used in Block-based Lossy Image Compression Experiments: G =coding gain, C_{stop} =stopband energy, s_{\max} =Sobolev smoothness. LPvn=n-Regular PULP in [92]; PUv1 and PUv2 are presented in Sec. 4.5.1 and Sec. 4.5.2, respectively.

	8×8	8×16	8×24	8×24	8×24	8×24
	DCT	LOT	LPv1	LPv2	PUv1	PUv2
Reg. K	1	1	1	2	1	2
G (dB)	8.83	9.22	9.36	9.33	9.49	9.43
C_{stop}	3.09	.211	.133	.374	.088	.078
s_{\max}	.500	.709	.866	1.33	.989	1.30

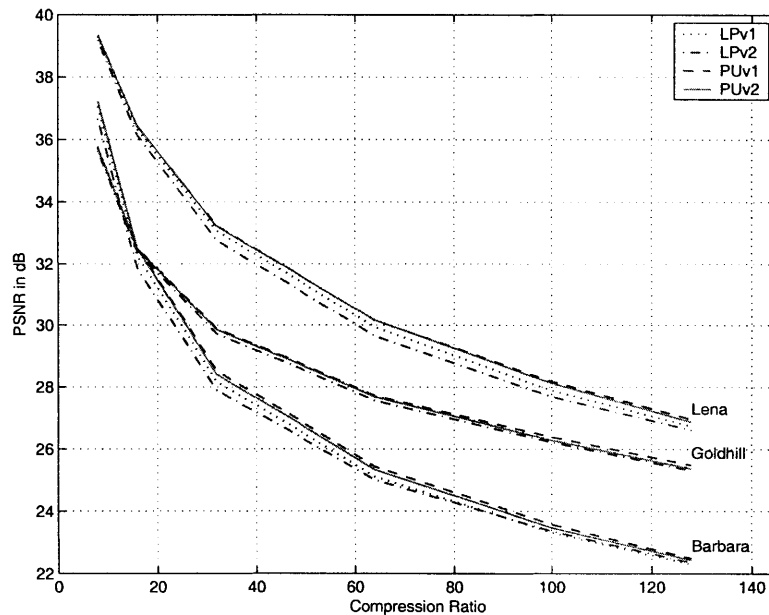


Figure 4-10: PSNR versus compression ratio for the 512×512 8-bit grayscale test images *Barbara*, *Goldhill*, and *Lena*. A JPEG-like block-based lossy compression scheme is used with the transforms.

Table 4.3: Objective compression performance—PSNR in dB based on chosen transforms. LPvn are the n -Regular PULP in [92]; PUv1 and PUv2 are designed in Sec. 4.5.1 and Sec. 4.5.2.

Barbara		PSNR(dB)					
Comp. ratio		8×8	8×16	8×24	8×24	8×24	8×24
		DCT	LOT	LPv1	LPv2	PUv1	PUv2
8:1		35.38	36.49	37.05	36.66	37.22	37.22
16:1		30.24	31.83	32.23	31.81	32.50	32.48
32:1		26.42	27.86	28.18	27.90	28.53	28.41
64:1		23.77	24.88	25.11	25.00	25.43	25.33
100:1		22.37	23.02	23.32	23.36	23.57	23.47
128:1		21.60	22.03	22.29	22.35	22.49	22.43
Lena		PSNR(dB)					
Comp. ratio		8×8	8×16	8×24	8×24	8×24	8×24
		DCT	LOT	LPv1	LPv2	PUv1	PUv2
8:1		38.83	38.96	39.29	39.18	39.34	39.33
16:1		35.51	35.79	36.31	36.12	36.41	36.42
32:1		32.08	32.66	33.07	32.76	33.24	33.22
64:1		28.91	29.60	29.94	29.65	30.16	30.16
100:1		26.83	27.62	27.88	27.68	28.18	28.12
128:1		25.60	26.35	26.74	26.62	26.97	26.88
Goldhill		PSNR(dB)					
Comp. ratio		8×8	8×16	8×24	8×24	8×24	8×24
		DCT	LOT	LPv1	LPv2	PUv1	PUv2
8:1		35.29	35.63	35.77	35.64	35.72	35.74
16:1		31.97	32.36	32.49	32.37	32.49	32.46
32:1		29.31	29.76	29.87	29.72	29.90	29.86
64:1		27.12	27.56	27.70	27.56	27.72	27.68
100:1		25.68	26.18	26.29	26.21	26.38	26.28
128:1		24.82	25.24	25.38	25.31	25.49	25.37

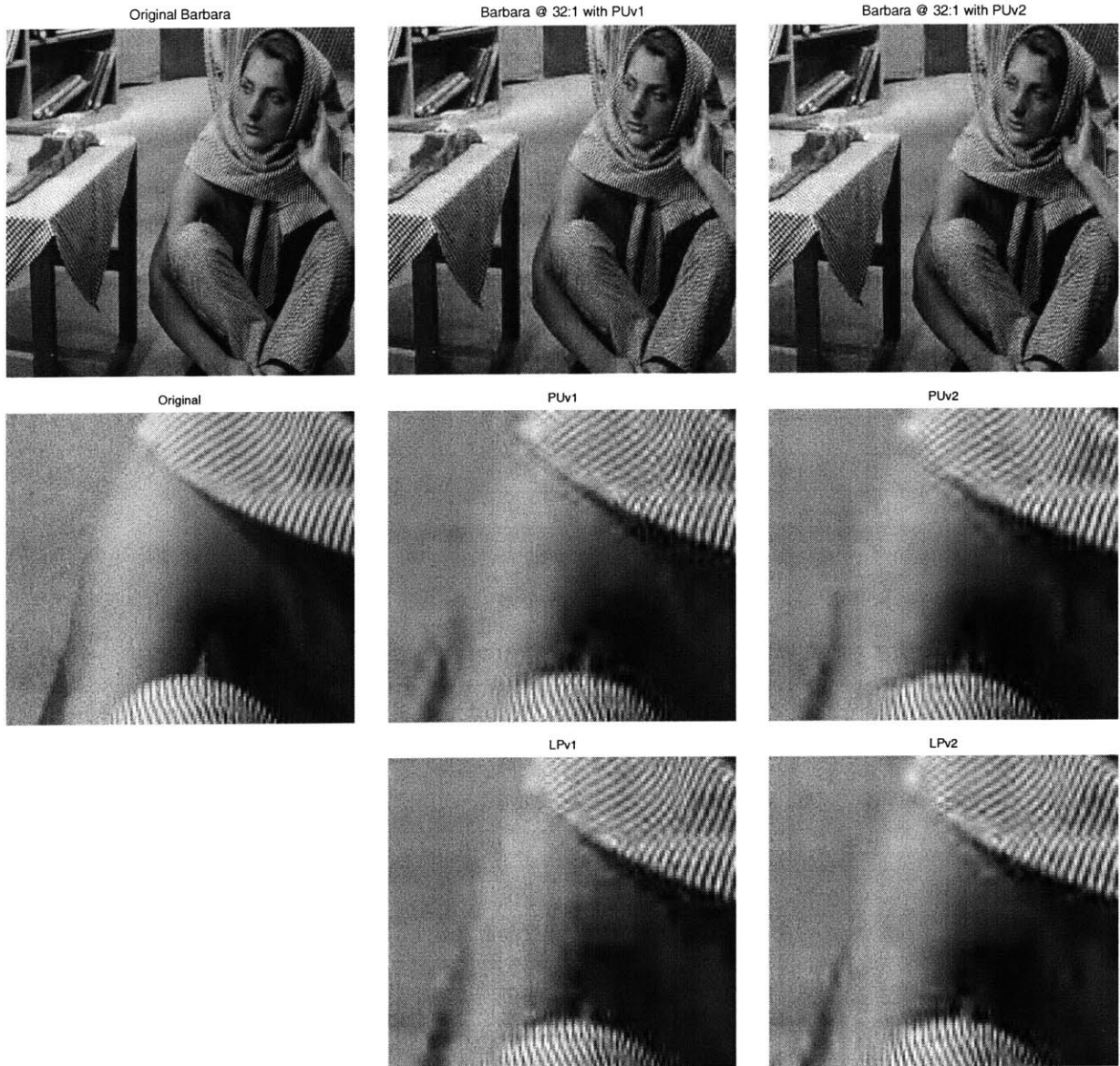


Figure 4-11: Compression results at 32:1 for visual comparison. The original image and a zoomed-in patch are shown in the first column. The reconstructed images and their zoomed-in patches using one- and two-regular 8×24 PUFBs are shown in the second and the third columns, respectively. Notably, the current design PUv1 produces a much smoother reconstruction than LPv1.

Chapter 5

A Class of Structurally Regular Biorthogonal Filter Banks

As is with paraunitary filter banks, dyadic-based structures can be used to parameterize and implement a certain class of useful and important biorthogonal filter banks (BOFBs). Extending the regularity imposition on PUFBs, we consider its biorthogonal equivalence in this chapter. We first revisit a *minimal* structure of BOFBs using order-one dyadic-based building blocks, by which BOFBs with length constraint can be designed. A special non-singular matrix parameterization is proposed which *structurally* guarantees at least two degrees of regularity, where the Householder transform is found to play an important role. As with the paraunitary case, we also specialize the framework of general biorthogonal filter banks with regularity to the case where the filters are symmetric or linear-phase (LP), resulting in dyadic-based *generalized lapped biorthogonal transform* or GLBT, for which a *simplified* parameterization is naturally obtained in fewer parameters. With the proposed theory, regular BOFBs are designed and evaluated in a transform-based image codec, and they are found to provide better objective performance and improve perceptual quality of the decompressed images, with reduced blocking artifacts and better preserved texture details.

5.1 Introduction

Recently, M -channel filter banks have found several applications in signal processing [3, 19, 72, 108, 139]. Biorthogonal filter banks (BOFBs), in particular, have been employed as a transform coder in image compression applications where their coding performances have shown to be a significant improvement over other traditional transforms [93, 119]. In addition to its frequency selectivity and coding gain, an optimized BOFB for the purpose of image coding usually has two other properties imposed: (i) linear phase (symmetry and anti-symmetry of the filters' impulse responses) and (ii) regularity. In [119], a modular structure for parameterizing BOFBs with linear phase is presented, in which linear phase and perfect reconstruction (PR) properties are structurally imposed. It is a modified version of that proposed for paraunitary filter banks (PUFBs) [41]. In [93], the structure is further extended in order to additionally impose regularity on the transform.

Regularity is fundamental to the filter bank theory and is closely related to the smoothness of the corresponding wavelet basis [108]. Recall that an M -channel filter bank is said to be (K_a, K_s) -regular if the analysis and synthesis lowpass filters $H_0(z)$ and $F_0(z)$ have a zero of multiplicity K_a and K_s , respectively, at the M th roots of unity $e^{j2\pi m/M}$ for $m = 1, \dots, M-1$. This is equivalent to the conditions (2.42a) and (2.42b) on the polyphase matrices, stating that the multiplicity of zeros at DC of the analysis (synthesis) bandpass/highpass filters is equal to that of the synthesis (analysis) lowpass filter [93, 155]. Regular filter banks are desirable in many applications such as smooth signal interpolation and data compression [3, 19, 72, 108, 139].

In this chapter, we consider the class of causal FIR M -channel biorthogonal filter banks of order L spanned by (2.58),

$$\mathbf{E}(z) = \mathbf{W}_L(z) \dots \mathbf{W}_1(z) \mathbf{E}_0, \quad \mathbf{E}_0 \text{ non-singular} \quad (5.1)$$

which have an FIR inverse. Each $\mathbf{W}_m(z)$ is the first-order biorthogonal (dyadic-based)

building block given by (2.59):

$$\mathbf{W}_m(z) = \mathbf{I} - \mathcal{U}_m \mathcal{V}_m^\dagger + z^{-1} \mathcal{U}_m \mathcal{V}_m^\dagger \quad (5.2)$$

where the $M \times \gamma_m$ parameter matrices \mathcal{U}_m and \mathcal{V}_m satisfy

$$\mathcal{V}_m^\dagger \mathcal{U}_m = \begin{bmatrix} 1 & \times & \times & \dots & \times \\ 0 & 1 & \times & \dots & \times \\ 0 & 0 & 1 & \dots & \times \\ \vdots & \vdots & \vdots & \ddots & \vdots \\ 0 & 0 & 0 & \dots & 1 \end{bmatrix}_{\gamma_m \times \gamma_m} \triangleq \Delta_m \quad (5.3)$$

for some integer $1 \leq \gamma_m \leq M$, where \times indicates possibly nonzero elements. This is a generalization of the paraunitary order-one factorization given in [52] where $\mathcal{U}_m = \mathcal{V}_m$, and has been used for factoring the BOLT [132].

Remarks:

1. Since $\rho(\mathcal{V}_m^\dagger \mathcal{U}_m) = \gamma_m$, the McMillan degree of $\mathbf{W}_m(z)$ as in (5.2) is γ_m .
2. The construction in (5.1) completely spans all causal FIR BOFBs having FIR inverses, up to a factor unimodular in z^{-1} [132]. The spanned analysis filters have filter lengths no greater than $M(L + 1)$, and the McMillan degree of $\mathbf{E}(z)$ ranges from L to ML where L is the order of the FB.
3. A causal Type-II synthesis polyphase matrix $\mathbf{R}(z)$ can be

$$\mathbf{R}(z) = z^{-L} \mathbf{E}_0^{-1} \mathbf{W}_1^{-1}(z) \dots \mathbf{W}_L^{-1}(z). \quad (5.4)$$

As a result of the possibly nonzero off-diagonal elements in (5.3), the synthesis bank can have filter lengths different from $M(L + 1)$. In fact, the lengths of the synthesis filters are bounded by $M(\mu + 1)$ from above, where $\mu = \sum_{m=1}^L \gamma_m$ is the McMillan

degree of $\mathbf{E}(z)$. The choice $\Delta_m = \mathbf{I}_{\gamma_m}$ results in equal filter lengths for the analysis and synthesis banks.

5.2 A Class of Regular Biorthogonal Filter Banks

As in the paraunitary case, we will show how we can *structurally* impose regularity onto the standard dyadic form (5.1) for a class of biorthogonal filter banks. However, unlike the paraunitary case, the analysis and synthesis banks are no longer constrained to be time-reversal of each other. They can be significantly different, e.g., having different numbers of zeros at the aliasing frequencies. Therefore, we will use an ordered pair (K_a, K_s) to denote the degree of regularity of a BOFB.

Consider a (K_a, K_s) -regular BOFB with both $K_a \geq 1$ and $K_s \geq 1$. It is necessary that (Section 2.4)

$$\mathbf{R}^T(z^M)\mathbf{J}\mathbf{e}_M(z)|_{z=1} = \mathbf{E}_0^{-T}\mathbf{1}_M = d_0\mathbf{e}_0 \quad (K_a \geq 1) \quad (5.5a)$$

and

$$\mathbf{E}(z^M)\mathbf{e}_M(z)|_{z=1} = \mathbf{E}_0\mathbf{1}_M = c_0\mathbf{e}_0 \quad (K_s \geq 1) \quad (5.5b)$$

where $\mathbf{e}_M(z) = [1 \ z^{-1} \ \dots \ z^{-(M-1)}]^T$ is the delay chain. These conditions imply some constraints on the 0th rows of \mathbf{E}_0 and \mathbf{E}_0^{-T} , as follows:

Lemma 5.1. *The conditions $\mathbf{E}_0^{-T}\mathbf{1}_M = d_0\mathbf{e}_0$ and $\mathbf{E}_0\mathbf{1}_M = c_0\mathbf{e}_0$ corresponding to $K_a \geq 1$ and $K_s \geq 1$, respectively, imply that the 0th rows of \mathbf{E}_0 and \mathbf{E}_0^{-T} consist of identical entries, respectively.*

Degrees of Regularity	Necessary Condition on \mathbf{E}_0
$K_a \geq 1$	0th row of \mathbf{E}_0 has identical entries
$K_s \geq 1$	0th row of \mathbf{E}_0^{-T} has identical entries

Proof: Suppose $\mathbf{E}_0 \mathbf{1}_M = c_0 \mathbf{e}_0$. As $\mathbf{E}_0 \mathbf{E}_0^{-1} = \mathbf{I}$, it must be true that the 0th column of \mathbf{E}_0^{-1} be equal to $(1/c_0)\mathbf{1}_M$, which establishes that the 0th row of \mathbf{E}_0^{-T} consists of identical entries $1/c_0$. The other condition can be similarly shown and is omitted. ■

Corollary 5.1. *If $K_a \geq 1$ and $K_s \geq 1$, the constants c_0 and d_0 are related by*

$$1/c_0 = d_0/M \quad \text{or} \quad c_0 d_0 = M. \quad (5.6)$$

Next, we will discuss how to parameterize $(1, 1)$ -, $(1, 2)$ -, and $(2, 1)$ -regular BOFBs based on the aforementioned properties of \mathbf{E}_0 .

5.2.1 $(1, 1)$ -Regular BOFBs

As pointed out above, the 0th rows of \mathbf{E}_0 and \mathbf{E}_0^{-T} must have identical entries if $K_a, K_s \geq 1$. Since the 0th row of \mathbf{E}_0 is $(c_0/M)\mathbf{1}^T$, post-multiplying \mathbf{E}_0 by the Householder matrix $\mathbf{R}[\mathbf{1}_M]$ as defined in Definition 2.3 results in

$$\mathbf{E}_0 \mathbf{R}[\mathbf{1}_M] = \begin{bmatrix} \frac{c_0}{\sqrt{M}} & 0 & \dots & 0 \\ \times & \times & \dots & \times \\ \vdots & \vdots & \ddots & \vdots \\ \times & \times & \dots & \times \end{bmatrix} \triangleq \underbrace{\begin{bmatrix} 1 & & & \\ \ell_1 & 1 & & \\ \vdots & & \ddots & \\ \ell_{M-1} & & & 1 \end{bmatrix}}_{\mathbf{L}} \underbrace{\begin{bmatrix} \frac{c_0}{\sqrt{M}} & 0 & \dots & 0 \\ 0 & & & \\ \vdots & & \bar{\mathbf{E}}_0 & \\ 0 & & & \end{bmatrix}}_{\mathbf{D}} \quad (5.7)$$

for some (lifting) multipliers ℓ_i and some non-singular matrix $\bar{\mathbf{E}}_0$ of dimension $(M - 1) \times (M - 1)$. Note that the 0th column of the product $\mathbf{E}_0 \mathbf{R}[\mathbf{1}_M]$ is in general not parallel to \mathbf{e}_0 as \mathbf{E}_0 is not necessarily orthogonal.

Using the above decomposition, any non-singular \mathbf{E}_0 with identical entries ($= c_0/M$) in the 0th row assumes the following structure

$$\mathbf{E}_0 = \mathbf{L} \mathbf{D} \mathbf{R}[\mathbf{1}_M] \quad (5.8)$$

which is shown in Figure 5-1. It is straightforward to show that the condition (5.5a) on \mathbf{E}_0^{-T}

is automatically satisfied, even though we have started from constraining the 0th row of \mathbf{E}_0 . In particular,

$$d_0 \mathbf{e}_0 = \mathbf{E}_0^{-T} \mathbf{1}_M = \mathbf{L}^{-T} \mathbf{D}^{-T} \mathbf{R}[\mathbf{1}_M] \mathbf{1}_M = \mathbf{L}^{-T} \mathbf{D}^{-T} \|\mathbf{1}_M\| \mathbf{e}_0 = \sqrt{M} \mathbf{L}^{-T} \mathbf{D}^{-T} \mathbf{e}_0 \quad (5.9)$$

where we have used the property of $\mathbf{R}[\mathbf{1}_M]$ (Definition 2.3) for simplification. Plugging in the definitions of \mathbf{L} and \mathbf{D} gives

$$\sqrt{M} \mathbf{L}^{-T} \mathbf{D}^{-T} \mathbf{e}_0 = \frac{M}{c_0} \mathbf{e}_0,$$

implying that

$$c_0 d_0 = M \quad (5.10)$$

which has also been established in Corollary 5.1.

It remains to ensure $\mathbf{E}_0 \mathbf{1}_M = c_0 \mathbf{e}_0$ as in (5.5b):

$$c_0 \mathbf{e}_0 = \mathbf{E}_0 \mathbf{1}_M = \mathbf{L} \mathbf{D} \mathbf{R}[\mathbf{1}_M] \mathbf{1}_M = \mathbf{L} \mathbf{D} \sqrt{M} \mathbf{e}_0 = c_0 \mathbf{L} \mathbf{e}_0 = c_0 \begin{bmatrix} 1 \\ \ell_1 \\ \vdots \\ \ell_{M-1} \end{bmatrix}.$$

Therefore, choosing $\mathbf{L} = \mathbf{I}$ on top of the structure (5.8) constitutes the necessary conditions on \mathbf{E}_0 for $K_a, K_s \geq 1$. We have thus proved the following result:

Theorem 5.1 ((1, 1)-Regular BOFB). *An M -channel BOFB as in (5.1) and (5.4) is (1, 1)-regular if and only if the non-singular matrix \mathbf{E}_0 takes the form*

$$\mathbf{E}_0 = \begin{bmatrix} \frac{c_0}{\sqrt{M}} & \mathbf{0}^T \\ \mathbf{0} & \bar{\mathbf{E}}_0 \end{bmatrix} \mathbf{R}[\mathbf{1}_M], \quad \text{some } c_0 \neq 0$$

where $\mathbf{R}[\mathbf{1}_M]$ is the Householder matrix as defined in Definition 2.3 and $\bar{\mathbf{E}}_0$ is $(M - 1) \times (M - 1)$ non-singular. The constant d_0 as in (5.5a) is such that $c_0 d_0 = M$.

Remarks: The non-singular matrix $\bar{\mathbf{E}}_0$ is not further constrained and can be parameterized

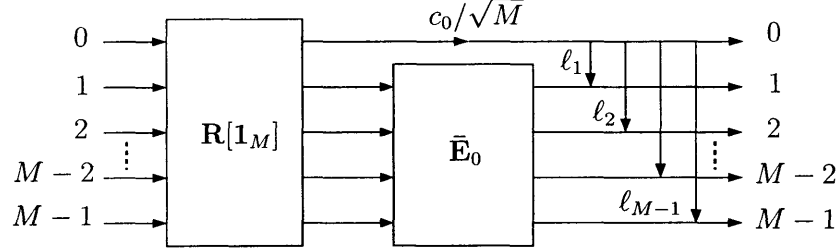


Figure 5-1: Structure for parameterizing \mathbf{E}_0 satisfying $K_a \geq 1$ (5.5a).

using the SVD- or QR-based approach as discussed in Chapter 2. An alternative approach to parameterizing such \mathbf{E}_0 was suggested in [93], which involves a certain permutation matrix (unknown *a priori*); our Householder-based approach avoids such an undetermined permutation matrix.

5.2.2 (1, 2)-Regular BOFBs

Assume the analysis and synthesis lowpass filters $H_0(z)$ and $F_0(z)$ are already one-regular as in the previous section. We now present how the second degree of regularity can be imposed on $F_0(z)$. As shown in Theorem 2.2, this is equivalent to the property that the bandpass and highpass analysis filters $H_i(z)$ have a double zero at DC ($z = 1$), $i = 1, 2, \dots, M - 1$. In terms of the analysis polyphase matrix $\mathbf{E}(z)$, this is

$$\frac{d}{dz} \mathbf{E}(z^M) \mathbf{e}_M(z) \Big|_{z=1} = \begin{bmatrix} c_1 \\ 0 \\ \vdots \\ 0 \end{bmatrix}, \quad \text{some } c_1 \neq 0$$

on top of the (1, 1)-regularity. Substituting (5.1) for $\mathbf{E}(z)$ gives

$$\begin{aligned} c_1 \mathbf{e}_0 &= \frac{d}{dz} \mathbf{E}(z^M) \Big|_{z=1} \mathbf{1}_M + \mathbf{E}(1) \frac{d}{dz} \mathbf{e}_M(z) \Big|_{z=1} \\ &= -M \sum_{m=1}^L \mathcal{U}_m \mathcal{V}_m^\dagger \mathbf{E}_0 \mathbf{1}_M - \mathbf{E}_0 \mathbf{b}_M \end{aligned}$$

where $\mathbf{b}_M = \begin{bmatrix} 0 & 1 & 2 & \dots & M-1 \end{bmatrix}^T$. The following theorem summarizes the structural conditions for $(1, 2)$ -regularity.

Theorem 5.2 ((1, 2)-Regular BOFB). *An M -channel BOFB as in (5.1) and (5.4) is $(1, 2)$ -regular if and only if it is $(1, 1)$ -regular as in Theorem 5.1 and*

$$-c_0 M \sum_{m=1}^L \mathbf{p}_m - \mathbf{E}_0 \mathbf{b}_M = c_1 \mathbf{e}_0, \quad c_1 \neq 0 \quad (5.11a)$$

where $\mathbf{p}_m = \mathcal{U}_m \mathcal{V}_m^\dagger \mathbf{e}_0$ and $\mathbf{b}_M = \begin{bmatrix} 0 & 1 & 2 & \dots & M-1 \end{bmatrix}^T$. Eqn. (5.11a) further simplifies to

$$\bar{\mathbf{E}}_0 \check{\mathbf{k}}_M = -c_0 M \sum_{m=1}^L \check{\mathbf{p}}_m \quad (5.11b)$$

where $\mathbf{p}_m \triangleq \begin{bmatrix} p_m^0 & \check{\mathbf{p}}_m^T \end{bmatrix}^T$, $\mathbf{k}_M \triangleq \mathbf{R}[\mathbf{1}_M] \mathbf{b}_M = \begin{bmatrix} k_M^0 & \check{\mathbf{k}}_M^T \end{bmatrix}^T$, and $\bar{\mathbf{E}}_0$ is as defined in Theorem 5.1.

Parameterization of Non-Singular Matrices With Constrained Rows

In the design process, given all the \mathbf{p}_m , one needs to parameterize $\bar{\mathbf{E}}_0$ so as to satisfy (5.11b). The parameterization technique for $(1, 1)$ -regular BOFBs can be modified for this purpose. Eqn. (5.11b) has the general form

$$\mathbf{A}\mathbf{b} = \mathbf{c} \quad (5.12)$$

where $\mathbf{b}, \mathbf{c} \in \mathbb{C}^n$ are given, and we are to parameterize the $n \times n$ non-singular matrix \mathbf{A} so as to satisfy $\mathbf{A}\mathbf{b} = \mathbf{c}$. We want to convert (5.12) to an equivalent one whose right-hand side is one of the unit vectors \mathbf{e}_i , so we can infer the constraint on the inverse of a suitable matrix. We choose \mathbf{e}_0 and pre-multiply (5.12) by the Householder matrix $\mathbf{R}[\mathbf{c}]$ to obtain

$$\mathbf{R}[\mathbf{c}]\mathbf{A}\mathbf{b} = \|\mathbf{c}\| \mathbf{e}_0$$

which implies that the 0th column of $(\mathbf{R}[\mathbf{c}]\mathbf{A})^{-1}$ is $\frac{\mathbf{b}}{\|\mathbf{c}\|}$, since $\mathbf{R}[\mathbf{c}]\mathbf{A}$ is non-singular. Therefore, the key to parameterizing \mathbf{A} is to start with its inverse: pre-multiplying $(\mathbf{R}[\mathbf{c}]\mathbf{A})^{-1}$ by $\mathbf{R}[\mathbf{b}]$ gives

$$\mathbf{R}[\mathbf{b}]\mathbf{A}^{-1}\mathbf{R}[\mathbf{c}] = \begin{bmatrix} \frac{\|\mathbf{b}\|}{\|\mathbf{c}\|} & \times & \dots & \times \\ 0 & \times & \dots & \times \\ \vdots & \vdots & \ddots & \vdots \\ 0 & \times & \dots & \times \end{bmatrix} \triangleq \begin{bmatrix} \frac{\|\mathbf{b}\|}{\|\mathbf{c}\|} & 0 & \dots & 0 \\ 0 & \ddots & & \\ \vdots & & \mathbf{A}_0^{-1} & \\ 0 & & & \end{bmatrix} \underbrace{\begin{bmatrix} 1 & \mu_1 & \dots & \mu_{n-1} \\ & 1 & & \\ & & \ddots & \\ & & & 1 \end{bmatrix}}_{\mathbf{U}^{-1}},$$

or equivalently,

$$\mathbf{A} = \mathbf{R}[\mathbf{c}]\mathbf{U} \begin{bmatrix} \frac{\|\mathbf{c}\|}{\|\mathbf{b}\|} & \mathbf{0}^T \\ \mathbf{0} & \mathbf{A}_0 \end{bmatrix} \mathbf{R}[\mathbf{b}] \quad (5.13)$$

where \mathbf{A}_0 is any $(n - 1) \times (n - 1)$ non-singular matrix.

Lemma 5.2 (Row-Constrained Parameterization). *Let $\mathbf{b}, \mathbf{c} \in \mathbb{C}^n$ be given. Any $n \times n$ non-singular matrix \mathbf{A} satisfying $\mathbf{Ab} = \mathbf{c}$ assumes the general form (5.13).*

Remarks: The free design parameters are embedded in \mathbf{A}_0 and the μ_i . \mathbf{A}_0 can be parameterized using the SVD- or QR-based approach as discussed in Chapter 2. An alternative method for parameterizing \mathbf{A} can be found in [93], which involves an unknown permutation matrix. As a comparison, our Householder-based approach is permutation-free¹.

5.2.3 (2, 1)-Regular BOFBs

Again, we assume the analysis and synthesis lowpass filters $H_0(z)$ and $F_0(z)$ are already one-regular. For (2, 1)-regularity, we need to impose the second degree of regularity onto the analysis lowpass filter $H_0(z)$, which is equivalent to the requirement that the bandpass

¹In the design process, finding the optimal permutation is a discrete optimization and is much more difficult compared to continuous optimizations. When combined with the remaining continuous problem, the undetermined permutation makes the filter bank design a mixed optimization problem, which is even harder.

and highpass synthesis filters $F_i(z)$ have a double zero at DC ($z = 1$), $i = 1, 2, \dots, M - 1$. Namely, we need to impose additionally

$$\frac{d}{dz} \mathbf{R}^T(z^M) \mathbf{J} \mathbf{e}_M(z) \Big|_{z=1} = \begin{bmatrix} d_1 \\ 0 \\ \vdots \\ 0 \end{bmatrix}, \quad \text{some } d_1 \neq 0$$

on top of the $(1, 1)$ -regularity. Substituting the anti-causal version² of (5.4) for $\mathbf{R}(z)$ gives

$$d_1 \mathbf{e}_0 = \frac{d}{dz} \mathbf{R}^T(z^M) \Big|_{z=1} \mathbf{J} \mathbf{1}_M + \mathbf{R}^T(1) \mathbf{J} \frac{d}{dz} \mathbf{e}_M(z) \Big|_{z=1} \quad (5.14)$$

$$= M \sum_{m=1}^L (\mathcal{U}_m \mathcal{V}_m^\dagger)^T \mathbf{E}_0^{-T} \mathbf{1}_M - \mathbf{E}_0^{-T} \mathbf{J} \mathbf{b}_M \quad (5.15)$$

where $\mathbf{b}_M = [0 \ 1 \ 2 \ \dots \ M-1]^T$ and we have used the identity³

$$\mathbf{W}_m^{-1}(z) = \mathbf{I} - \mathcal{U}_m \mathcal{V}_m^\dagger + z \mathcal{U}_m \mathcal{V}_m^\dagger = \mathbf{W}_m(z^{-1}).$$

We summarize the necessary and sufficient conditions for $(2, 1)$ -regularity by the following theorem.

Theorem 5.3 ((2, 1)-Regular BOFB). *An M -channel BOFB as in (5.1) and (5.4) is $(2, 1)$ -regular if and only if it is $(1, 1)$ -regular as in Theorem 5.1 and*

$$\frac{M^2}{c_0} \sum_{m=1}^L \mathbf{q}_m - \mathbf{E}_0^{-T} \mathbf{J} \mathbf{b}_M = d_1 \mathbf{e}_0, \quad d_1 \neq 0 \quad (5.16a)$$

where $\mathbf{q}_m = (\mathcal{U}_m \mathcal{V}_m^\dagger)^T \mathbf{e}_0$ and $\mathbf{b}_M = [0 \ 1 \ 2 \ \dots \ M-1]^T$. Eqn. (5.16a) further simplifies

²Namely, $\mathbf{R}(z)$ without the z^{-L} term. This simplifies calculation and is done without loss of generality, amounting to redefining the nonzero regularity constant d_1 .

³In this chapter, we assume $\Delta_m = \mathbf{I}$ for simplicity, resulting in equal-length analysis and synthesis banks. See (5.3) and the discussions following it.

to

$$\bar{\mathbf{E}}_0^{-T} \check{\mathbf{h}}_M = \frac{M^2}{c_0} \sum_{m=1}^L \check{\mathbf{q}}_m \quad (5.16b)$$

where $\mathbf{q}_m \triangleq \begin{bmatrix} q_m^0 & \check{\mathbf{q}}_m^T \end{bmatrix}^T$, $\mathbf{h}_M \triangleq \mathbf{R}[\mathbf{1}_M] \mathbf{J} \mathbf{b}_M = \begin{bmatrix} h_M^0 & \check{\mathbf{h}}_M^T \end{bmatrix}^T$, and $\bar{\mathbf{E}}_0$ is as defined in Theorem 5.1.

Remark: Again, $\bar{\mathbf{E}}_0^{-T}$ in (5.16b) can be parameterized as in Lemma 5.2. In the design process, one chooses the \mathbf{q}_m or $\mathbf{W}_m(z)$ first, $m = 1, 2, \dots, L$, and let $\bar{\mathbf{E}}_0$ be determined accordingly using Lemma 5.2. The result is (2, 1)-regular.

5.3 Linear-Phase Biorthogonal Filter Banks Revisited

Recall that an M -channel (M even) linear-phase biorthogonal filter bank (BOLP) of order L can be factored as follows [41, 119]

$$\mathbf{E}(z) = \mathbf{G}_L(z) \mathbf{G}_{L-1}(z) \dots \mathbf{G}_1(z) \mathbf{E}_0^{LP} \quad (5.17)$$

where $\mathbf{G}_m(z) = \Gamma_m \mathbf{W} \Lambda(z) \mathbf{W}$ is the BOLP building block, and the initial non-singular matrix $\mathbf{E}_0^{LP} = \Gamma_0 \tilde{\mathbf{I}} \mathbf{W} \tilde{\mathbf{I}}$, with

$$\begin{aligned} \Gamma_m &= \begin{bmatrix} \mathbf{U}_m & \mathbf{0}_{M/2} \\ \mathbf{0}_{M/2} & \mathbf{V}_m \end{bmatrix}, & \mathbf{W} &= \frac{1}{\sqrt{2}} \begin{bmatrix} \mathbf{I}_{M/2} & \mathbf{I}_{M/2} \\ \mathbf{I}_{M/2} & -\mathbf{I}_{M/2} \end{bmatrix}, \\ \Lambda(z) &= \begin{bmatrix} \mathbf{I}_{M/2} & \mathbf{0}_{M/2} \\ \mathbf{0}_{M/2} & z^{-1} \mathbf{I}_{M/2} \end{bmatrix}, & \text{and} \quad \tilde{\mathbf{I}} &= \begin{bmatrix} \mathbf{I}_{M/2} & \mathbf{0}_{M/2} \\ \mathbf{0}_{M/2} & \mathbf{J}_{M/2} \end{bmatrix}. \end{aligned}$$

The \mathbf{U}_m and \mathbf{V}_m are $M/2 \times M/2$ non-singular. Figure 5-2 shows the lattice structure of an eight-channel BOLP of order L .

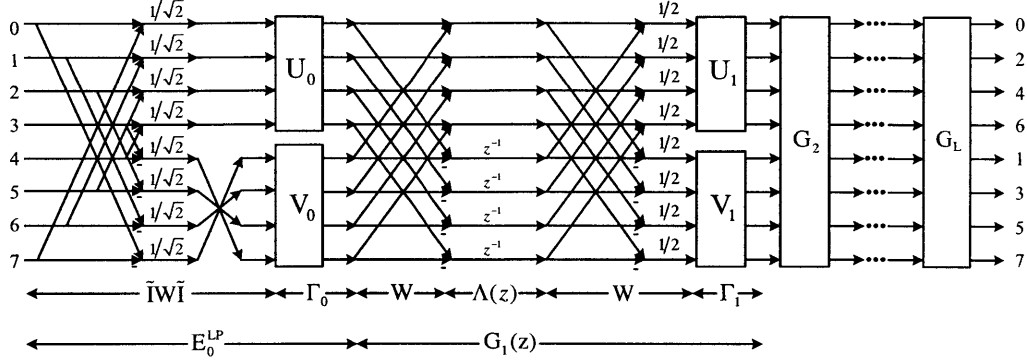


Figure 5-2: Lattice structure for biorthogonal LP lapped transform.

5.3.1 BOLP in Standard Dyadic Form (5.1)

By construction, each FIR LP building block $\mathbf{G}_m(z)$ is causal of order one and has an anti-causal inverse. Namely, it is a BOLT [132], and it follows that one can *always* express $\mathbf{G}_m(z)$ in terms of the first-order BO building block $\mathbf{W}_m(z)$, with a suitable choice of parameter matrices \mathcal{U}_m and \mathcal{V}_m (this is in fact a rather deep result [132]). In particular, one can show that (with subscripts $M/2$ dropped for simplicity)

$$\begin{aligned} \mathbf{G}_L(z) &= \Gamma_L \left\{ \mathbf{I} + \frac{(z^{-1}-1)}{2} \begin{bmatrix} \mathbf{I} & -\mathbf{I} \\ -\mathbf{I} & \mathbf{I} \end{bmatrix} \right\} = \left\{ \mathbf{I} + \frac{(z^{-1}-1)}{2} \Gamma_L \begin{bmatrix} \mathbf{I} & -\mathbf{I} \\ -\mathbf{I} & \mathbf{I} \end{bmatrix} \Gamma_L^{-1} \right\} \Gamma_L \\ &= \left\{ \mathbf{I} + \frac{(z^{-1}-1)}{2} \begin{bmatrix} \mathbf{I} & -\mathbf{U}_L \mathbf{V}_L^{-1} \\ -\mathbf{V}_L \mathbf{U}_L^{-1} & \mathbf{I} \end{bmatrix} \right\} \Gamma_L \triangleq \mathbf{W}_L(z) \Gamma_L, \end{aligned} \quad (5.18)$$

where the first-order BO building block $\mathbf{W}_L(z)$ is given by

$$\mathbf{W}_L(z) = \mathbf{I} + (z^{-1}-1) \frac{1}{2} \begin{bmatrix} \mathbf{I} & -\mathbf{U}_L \mathbf{V}_L^{-1} \\ -\mathbf{V}_L \mathbf{U}_L^{-1} & \mathbf{I} \end{bmatrix}.$$

The trailing factor $\mathbf{\Gamma}_L$ is absorbed by $\mathbf{G}_{L-1}(z)$ so that

$$\begin{aligned}\mathbf{G}_L(z)\mathbf{G}_{L-1}(z) &= \mathbf{W}_L(z) \begin{bmatrix} \mathbf{U}_L & \mathbf{0} \\ \mathbf{0} & \mathbf{V}_L \end{bmatrix} \mathbf{G}_{L-1}(z) = \mathbf{W}_L(z) \begin{bmatrix} \tilde{\mathbf{U}}_{L-1} & \mathbf{0} \\ \mathbf{0} & \tilde{\mathbf{V}}_{L-1} \end{bmatrix} \mathbf{W}\Lambda(z)\mathbf{W} \\ &= \mathbf{W}_L(z)\mathbf{W}_{L-1}(z) \begin{bmatrix} \tilde{\mathbf{U}}_{L-1} & \mathbf{0} \\ \mathbf{0} & \tilde{\mathbf{V}}_{L-1} \end{bmatrix},\end{aligned}$$

where the relation in (5.18) has been employed in the last equality with $\tilde{\mathbf{U}}_m \triangleq \mathbf{U}_L\mathbf{U}_{L-1}\dots\mathbf{U}_m$ and $\tilde{\mathbf{V}}_m \triangleq \mathbf{V}_L\mathbf{V}_{L-1}\dots\mathbf{V}_m$, and $\mathbf{W}_m(z)$ is given by

$$\mathbf{W}_m(z) = \mathbf{I} + (z^{-1}-1)\frac{1}{2} \begin{bmatrix} \mathbf{I} & -\tilde{\mathbf{U}}_m\tilde{\mathbf{V}}_m^{-1} \\ -\tilde{\mathbf{V}}_m\tilde{\mathbf{U}}_m^{-1} & \mathbf{I} \end{bmatrix}. \quad (5.19)$$

We can carry out the same procedure until arriving at

$$\mathbf{E}(z) = \underbrace{\mathbf{W}_L(z)\dots\mathbf{W}_1(z)}_{\mathbf{E}_0} \begin{bmatrix} \tilde{\mathbf{U}}_0 & \mathbf{0} \\ \mathbf{0} & \tilde{\mathbf{V}}_0 \end{bmatrix} \tilde{\mathbf{I}}\mathbf{W}\tilde{\mathbf{I}}, \quad (5.20)$$

which is in the standard dyadic form (5.1).

5.3.2 LP-Propagating Standard Dyadic Structure

Consider the first-order BO building block as in (5.19). The corresponding parameter matrices \mathcal{U}_m and \mathcal{V}_m can be chosen to be

$$\mathcal{U}_m = \frac{1}{\sqrt{2}} \begin{bmatrix} \mathbf{I} \\ -\tilde{\mathbf{V}}_m\tilde{\mathbf{U}}_m^{-1} \end{bmatrix} \mathbf{S}_m, \quad (5.21a)$$

$$\mathcal{V}_m^\dagger = \frac{\mathbf{S}_m^{-1}}{\sqrt{2}} \begin{bmatrix} \mathbf{I} & -(\tilde{\mathbf{V}}_m\tilde{\mathbf{U}}_m^{-1})^{-1} \end{bmatrix} \quad (5.21b)$$

for any $\gamma_m \times \gamma_m$ non-singular matrix \mathbf{S}_m . Note that for the LP case, $\gamma_m \equiv \frac{M}{2}$ and $\Delta_m \equiv \mathbf{I}$ for all m . Along with the initial non-singular matrix $\mathbf{E}_0 = \text{diag}\{\tilde{\mathbf{U}}_0, \tilde{\mathbf{V}}_0\} \tilde{\mathbf{I}} \mathbf{W} \tilde{\mathbf{I}}$, the choice in (5.21) guarantees that the standard dyadic form (5.1) preserves the linear phase property.

5.3.3 Degrees of Freedom

The standard dyadic form (5.1) provides a new parameterization of BOLP by defining

$$\begin{aligned}\hat{\mathbf{U}}_0 &= \tilde{\mathbf{U}}_0, \quad \hat{\mathbf{V}}_0 = \tilde{\mathbf{V}}_0, \quad \text{and} \\ \hat{\mathbf{V}}_m &= -\tilde{\mathbf{V}}_m \tilde{\mathbf{U}}_m^{-1}, \quad m = 1, 2, \dots, L,\end{aligned}$$

and forming the parameter matrices according to

$$\mathcal{U}_m = \frac{1}{\sqrt{2}} \begin{bmatrix} \mathbf{I} \\ \hat{\mathbf{V}}_m \end{bmatrix}, \quad \mathcal{V}_m^\dagger = \frac{1}{\sqrt{2}} \begin{bmatrix} \mathbf{I} & \hat{\mathbf{V}}_m^{-1} \end{bmatrix}. \quad (5.22)$$

Namely, there are in total $L + 2$ non-singular matrices $\hat{\mathbf{U}}_0$ and $\hat{\mathbf{V}}_i$ of size $M/2 \times M/2$, consisting of free parameter. This is less than $2L + 2$ as in (5.17) and is as efficient as the reduced-parameter structure for BOLPs established in [52, 94]. Note that starting with a set of (original) parameter matrices \mathbf{U}_m and \mathbf{V}_m as in (5.17), one can always obtain a corresponding *smaller* set of matrices $\hat{\mathbf{U}}_0$ and $\hat{\mathbf{V}}_m$. Hence, the completeness of the structure is not affected by the proposed parameterization.

Theorem 5.4. *The standard dyadic form (5.1) spans all M -band GLBTs (M even) if it is parameterized by non-singular matrices $\hat{\mathbf{U}}_0$ and $\hat{\mathbf{V}}_i$ of size $\frac{M}{2} \times \frac{M}{2}$ in such a way that*

$$\mathbf{E}_0 = \text{diag}\{\hat{\mathbf{U}}_0, \hat{\mathbf{V}}_0\} \tilde{\mathbf{I}} \mathbf{W} \tilde{\mathbf{I}} = \frac{1}{\sqrt{2}} \begin{bmatrix} \hat{\mathbf{U}}_0 & \hat{\mathbf{U}}_0 \mathbf{J} \\ \hat{\mathbf{V}}_0 \mathbf{J} & -\hat{\mathbf{V}}_0 \end{bmatrix} \quad (5.23)$$

and the parameter matrices \mathcal{U}_m and \mathcal{V}_m of $\mathbf{W}_m(z)$ are as given in (5.22) in terms of $\hat{\mathbf{V}}_m$.

5.4 Regular Linear-Phase Biorthogonal Filter Banks

As we can now parameterize any GLBT using the standard dyadic form (5.1), the regularity conditions on the general dyadic-based BO structure without the LP constraint can be applied. In particular, we will see how they simplify under the LP assumption.

Suppose the synthesis bank $\mathbf{R}(z)$ is at least one-regular. It follows that $\mathbf{E}_0 \mathbf{1}_M = c_0 \mathbf{e}_0$ for some $c_0 \neq 0$. Substituting (5.23) gives

$$c_0 \mathbf{e}_0 = \frac{1}{\sqrt{2}} \begin{bmatrix} \hat{\mathbf{U}}_0 & \hat{\mathbf{U}}_0 \mathbf{J} \\ \hat{\mathbf{V}}_0 \mathbf{J} & -\hat{\mathbf{V}}_0 \end{bmatrix} \begin{bmatrix} \mathbf{1} \\ \mathbf{1} \end{bmatrix} = \sqrt{2} \begin{bmatrix} \hat{\mathbf{U}}_0 \mathbf{1} \\ \mathbf{0} \end{bmatrix},$$

or $\frac{c_0}{\sqrt{2}} \mathbf{e}_0 = \hat{\mathbf{U}}_0 \mathbf{1}_{\frac{M}{2}}$, implying the 0th row of $\hat{\mathbf{U}}_0^{-T}$ has equal entries. See Lemma 5.1. Similarly, if the analysis bank $\mathbf{E}(z)$ is at least one-regular, one arrives at $\frac{d_0}{\sqrt{2}} \mathbf{e}_0 = \hat{\mathbf{U}}_0^{-T} \mathbf{1}_{\frac{M}{2}}$. The technique employed in Sec. 5.2 applies here.

Now, suppose the synthesis bank $\mathbf{R}(z)$ is at least two-regular. Plugging (5.22) into (5.11a) results in

$$-\frac{c_0 M}{2} \sum_{m=1}^L \begin{bmatrix} \mathbf{e}_0 \\ \hat{\mathbf{V}}_m \mathbf{e}_0 \end{bmatrix} - \mathbf{E}_0 \mathbf{b}_M = c_1 \begin{bmatrix} \mathbf{e}_0 \\ \mathbf{0} \end{bmatrix} \quad (5.24)$$

where $\mathbf{e}_0 \in \mathbb{R}^{M/2}$. Now using (5.23) and noting that $\mathbf{b}_M = \left[\mathbf{b}_{\frac{M}{2}}^T \ \mathbf{b}_{\frac{M}{2}}^T + \left(\frac{M}{2}\right) \mathbf{1}_{\frac{M}{2}}^T \right]^T$ and $\mathbf{b}_{\frac{M}{2}} + \mathbf{J} \mathbf{b}_{\frac{M}{2}} = \left(\frac{M}{2} - 1\right) \mathbf{1}_{\frac{M}{2}}$, we have

$$\mathbf{E}_0 \mathbf{b}_M = \frac{1}{\sqrt{2}} \begin{bmatrix} \hat{\mathbf{U}}_0 \left(\mathbf{b}_{\frac{M}{2}} + \mathbf{J} \mathbf{b}_{\frac{M}{2}} + \frac{M}{2} \mathbf{1}_{\frac{M}{2}} \right) \\ \hat{\mathbf{V}}_0 \left(\mathbf{J} \mathbf{b}_{\frac{M}{2}} - \mathbf{b}_{\frac{M}{2}} - \frac{M}{2} \mathbf{1}_{\frac{M}{2}} \right) \end{bmatrix} = \begin{bmatrix} \frac{M-1}{2} c_0 \mathbf{e}_0 \\ \times \end{bmatrix}$$

which indicates that the first $\frac{M}{2}$ equations in (5.24) are automatically satisfied, and (5.24)

reduces to

$$\sum_{m=1}^L \hat{\mathbf{V}}_m \mathbf{e}_0 = \frac{\sqrt{2}}{c_0 M} \begin{bmatrix} -\hat{\mathbf{V}}_0 \mathbf{J} & \hat{\mathbf{V}}_0 \end{bmatrix} \mathbf{b}_M, \quad (5.25)$$

which is a condition on the 0th columns of the $\hat{\mathbf{V}}_m$. In essence, we have obtained an alternative characterization of structurally regular synthesis bank using dyadic-based structures, with an equivalent but simpler condition (5.25) to impose (c.f. [93, Cond. A_{02}]). One can similarly derive structure conditions for the analysis bank which are simpler than those in [93].

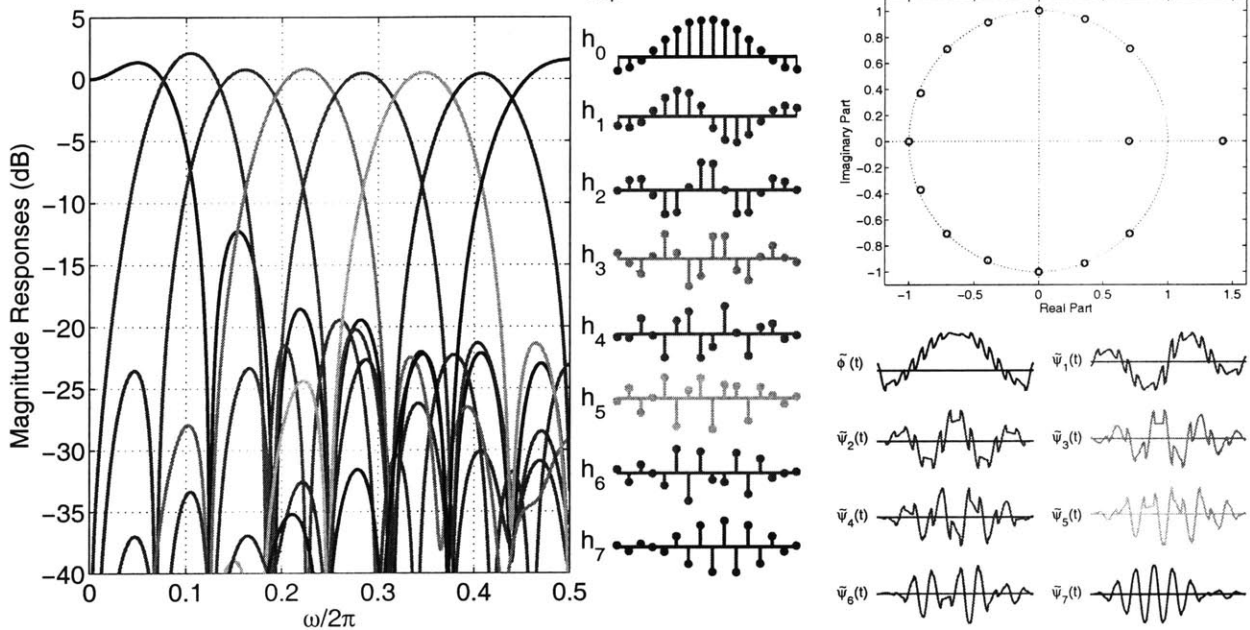
5.5 Examples of Regular Biorthogonal Filter Banks

In this section, the proposed theories are applied for regular BOFB designs. Based on the regular structures, the resulting filter banks are *structurally* guaranteed to be biorthogonal and regular, regardless of the choice of free parameters in the structures. Because regularity is structurally imposed, the optimal regular BOFB can be designed using unconstrained optimization [13], so as to minimize stopband energy C_{stop} and maximize coding gain CG, for which an AR(1) model with correlation coefficient 0.95 is assumed for the input.

5.5.1 Example 1: (1, 1)-Regular, 8×16 BOFB

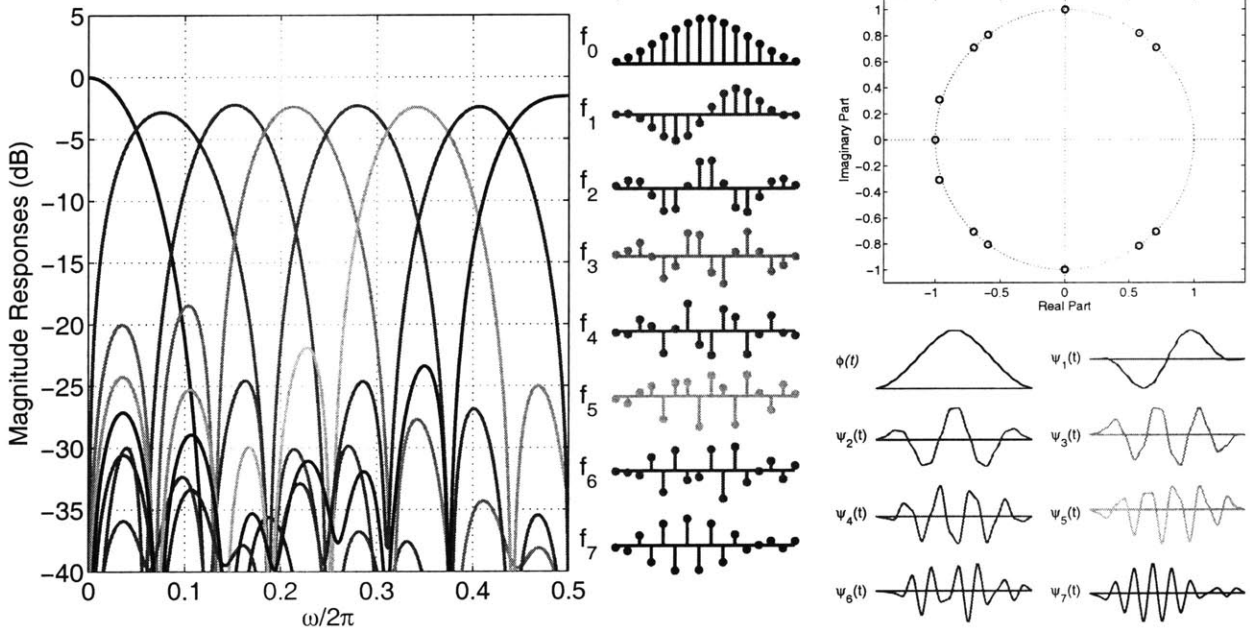
In this example, a (1, 1)-regular, 8-channel, 16-tap BOFB is designed according to Theorem 5.1. Related parameters are: $L = 1$, $\gamma_1 = 4$, and $\Delta_1 = \mathbf{I}$ for simplicity. Each non-singular matrix is parameterized using the *QR* factorization [107]. Figure 5-3 shows the resulting design with coding gain 9.62 dB. This is within 0.1% range of the theoretically *optimal* 9.63 dB for 8×16 BOFB as derived in [1], which is also very close to the optimal 9.69 dB obtained from (2.14) assuming ideal brick-wall filters.

(1,1)-Reg, analysis 8x16 BOFB, CG=9.6226dB, $C_{stop} = 0.2590$



(a) Analysis bank: $s_{max} = 0.3806$.

(1,1)-Reg, synthesis 8x16 BOFB, CG=9.6226dB, $C_{stop} = 0.2533$



(b) Synthesis bank: $s_{max} = 0.9891$.

Figure 5-3: (1,1)-regular 8×16 BOFB: impulse and frequency responses, along with zero plots of $H_0(z)$ and $F_0(z)$, and the wavelet bases.

5.5.2 Example 2: (1, 2)-Regular, 8×16 BOFB

Using Thoerem 5.2, we design a (1, 2)-regular BOFB of eight channels ($M = 8$) and length 16 ($L = 1$), with $\gamma_1 = 4$ and $\Delta_1 = \mathbf{I}$. Figure 5-4 shows the resulting design with coding gain 9.6031dB. Observe the double zeros of $F_0(z)$ at the aliasing frequencies, implying a two-regular synthesis bank. The synthesis basis is thus smoother than the analysis basis.

5.5.3 Example 3: (1, 2)-Regular, 4×8 BOFB

Using Thoerem 5.2, we design a (1, 2)-regular BOFB of four channels ($M = 4$) and length 8 ($L = 1$), with $\gamma_1 = 2$ and $\Delta_1 = \mathbf{I}$. Figure 5-5 shows the resulting design with coding gain 8.6371dB. Observe the double zeros of $F_0(z)$ at the aliasing frequencies, implying a two-regular synthesis bank. The synthesis basis is thus smoother than the analysis basis.

5.5.4 Example 4: (1, 1)-Regular, 8×24 BOFB

In this example, a (1, 1)-regular, 8-channel, 24-tap BOFB is designed according to Theorem 5.1. Related parameters are: $L = 2$, $\gamma_1 = \gamma_2 = 4$, and $\Delta_1 = \Delta_2 = \mathbf{I}$, with each non-singular matrix parameterized using the QR factorization. Figure 5-6 shows the resulting design with coding gain 9.6414dB.

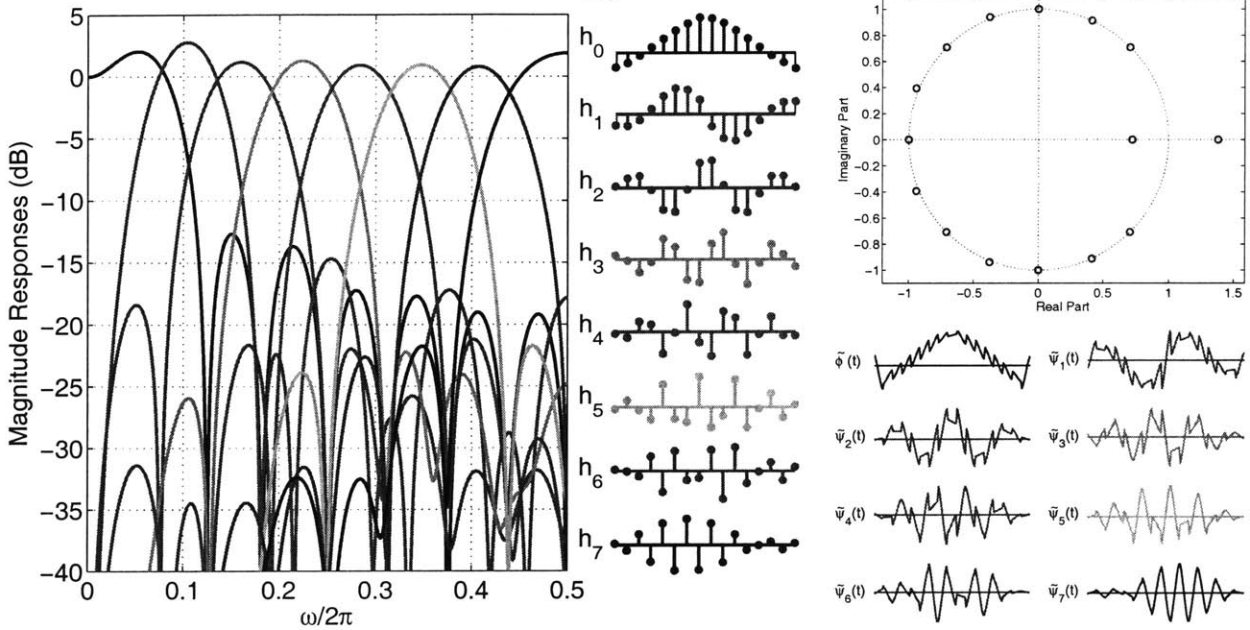
5.5.5 Example 5: (1, 2)-Regular, 8×24 BOFB

Using Thoerem 5.2, we design a (1, 2)-regular BOFB of eight channels ($M = 8$) and length 24 ($L = 2$), with $\gamma_1 = \gamma_2 = 4$ and $\Delta_1 = \Delta_2 = \mathbf{I}$. Figure 5-7 shows the resulting design with coding gain 9.6367dB. Observe the double zeros of $F_0(z)$ at the aliasing frequencies, implying a two-regular synthesis bank. The synthesis basis is thus smoother than the analysis basis.

5.5.6 Example 6: (1, 2)-Regular, 8×32 BOFB

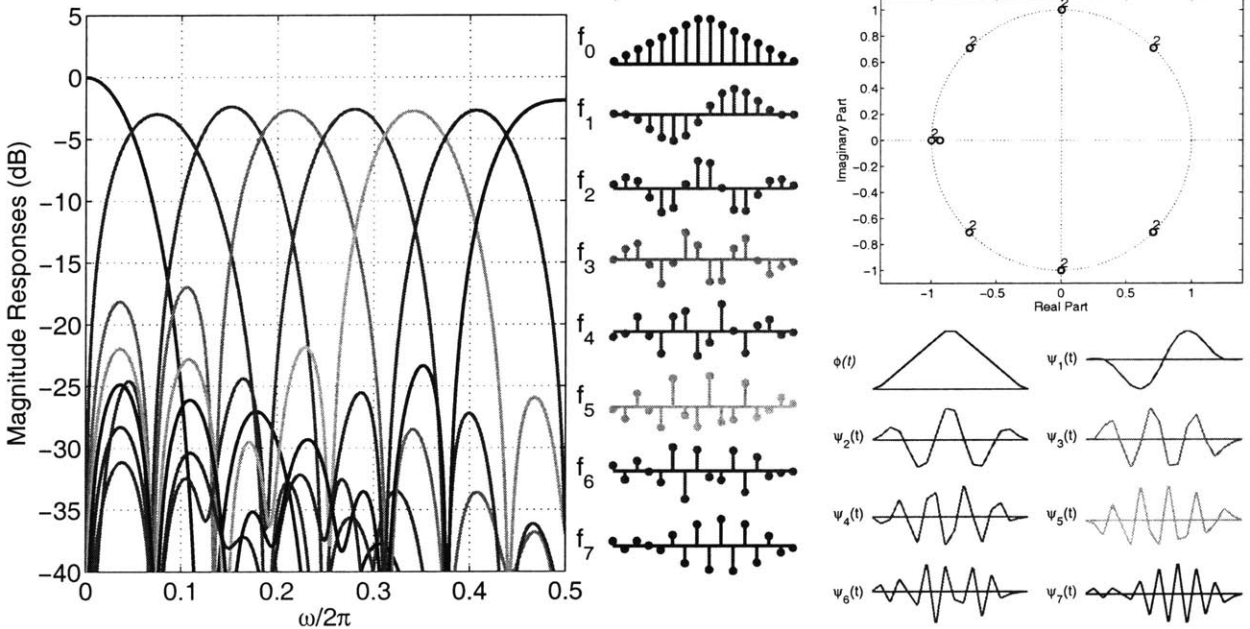
Using Thoerem 5.2, we design a (1, 2)-regular BOFB of eight channels ($M = 8$) and length 32 ($L = 3$), with $\gamma_m = 4$ and $\Delta_m = \mathbf{I}$, $m = 1, 2, 3$. Figure 5-8 shows the resulting design with

(1,2)-Reg, analysis 8x16 BOFB, CG=9.6031dB, $C_{stop}=0.3412$



(a) Analysis bank: $s_{max} = 0.2974$.

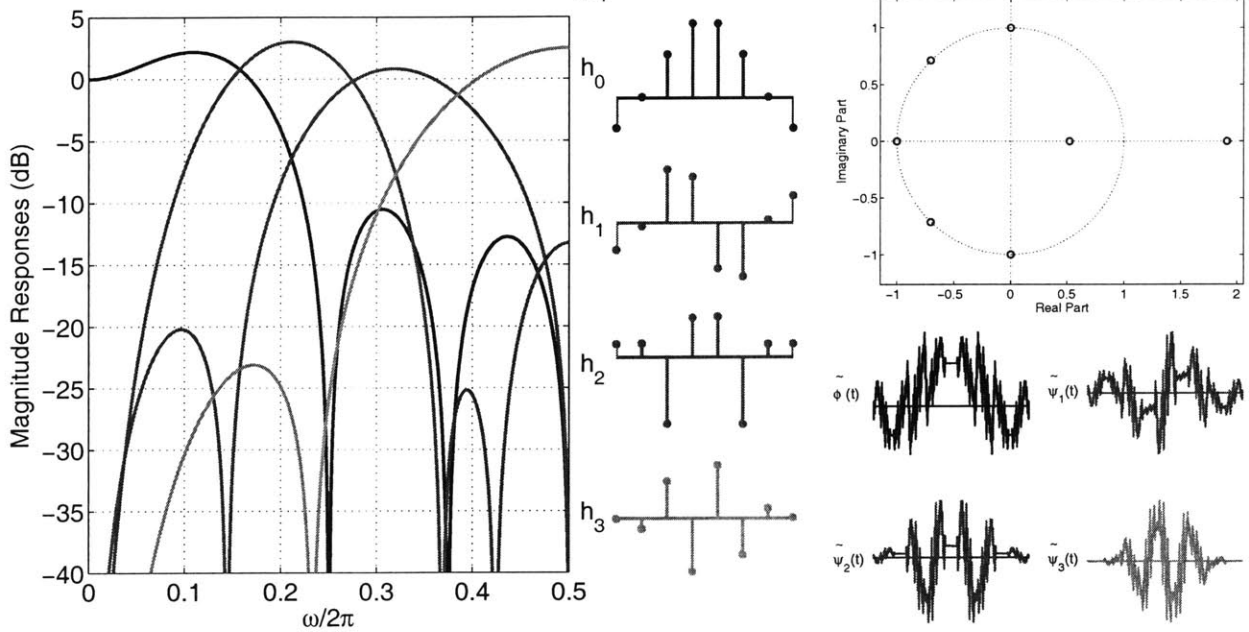
(1,2)-Reg, synthesis 8x16 BOFB, CG=9.6031dB, $C_{stop}=0.3378$



(b) Synthesis bank: $s_{max} = 1.6664$.

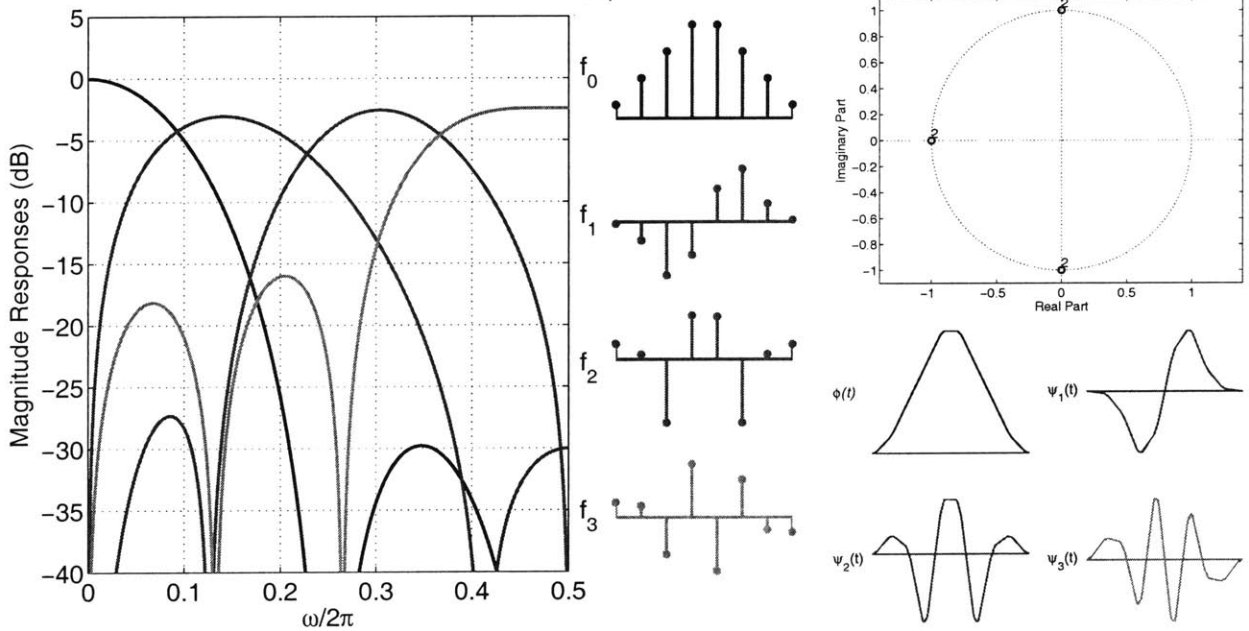
Figure 5-4: (1,2)-regular 8×16 BOFB: impulse and frequency responses, along with zero plots of $H_0(z)$ and $F_0(z)$, and the wavelet bases.

(1,2)-Reg, analysis 4x8 BOFB, CG=8.6370dB, $C_{stop} = 0.1877$



(a) Analysis bank: $s_{max} = 0.1179$.

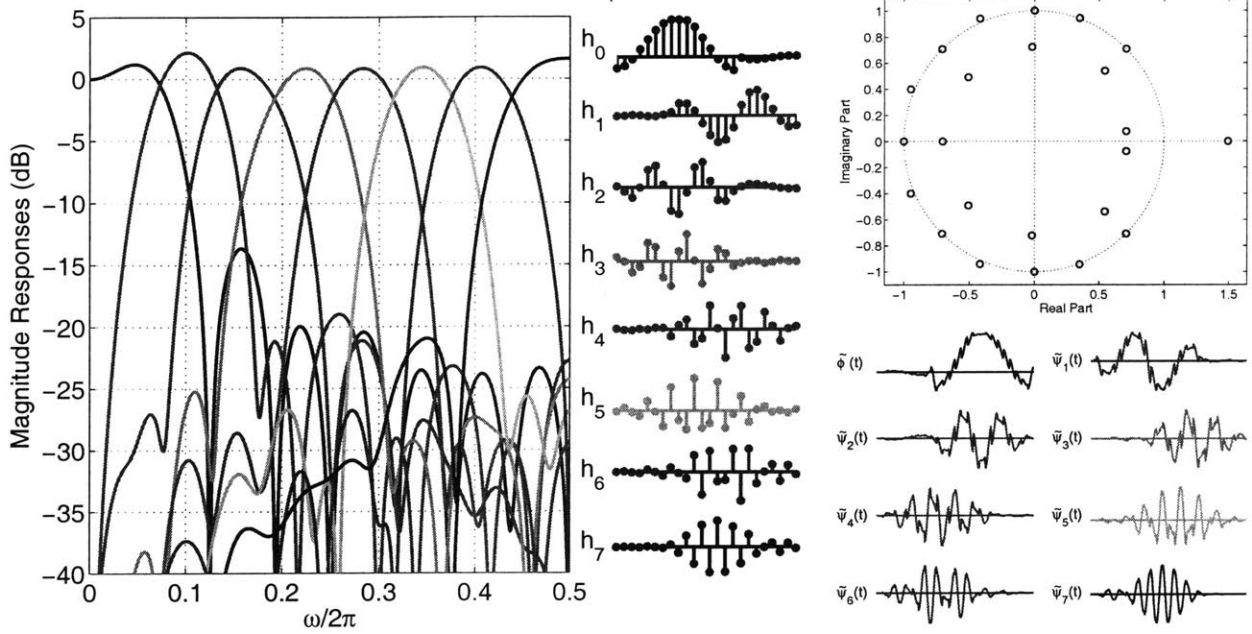
(1,2)-Reg, synthesis 4x8 BOFB, CG=8.6370dB, $C_{stop} = 0.1938$



(b) Synthesis bank: $s_{max} = 1.7500$.

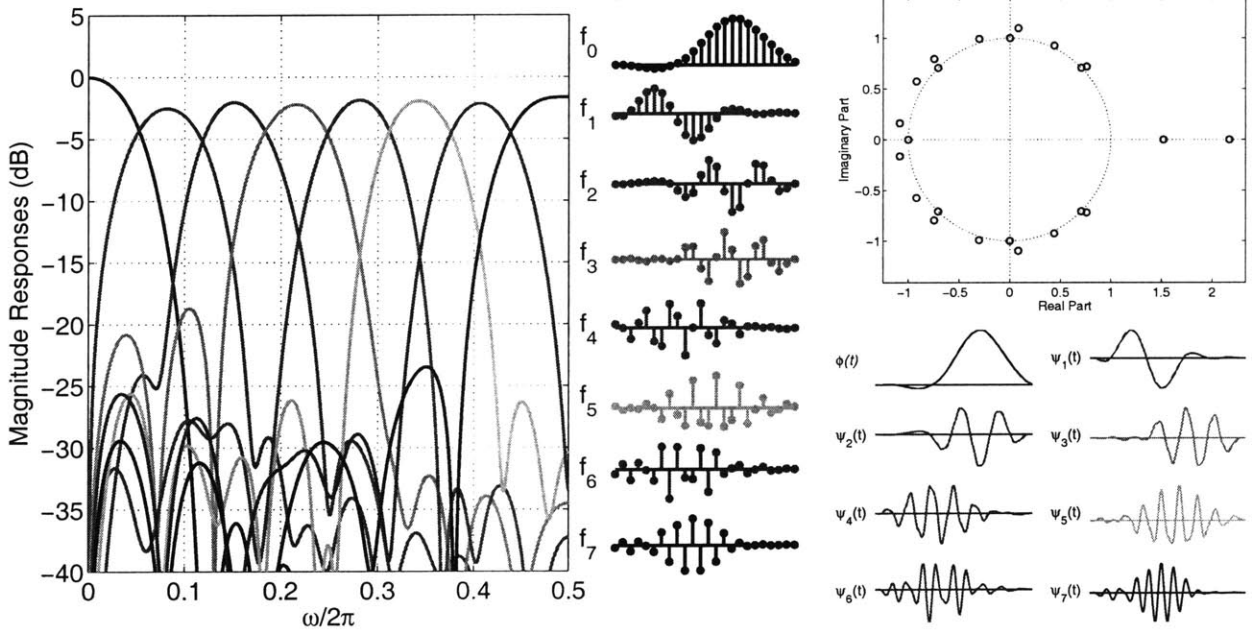
Figure 5-5: (1,2)-regular 4×8 BOFB: impulse and frequency responses, along with zero plots of $H_0(z)$ and $F_0(z)$, and the wavelet bases.

(1,1)-Reg, analysis 8x24 BOFB, CG=9.6414dB, $C_{stop} = 0.1976$



(a) Analysis bank: $s_{max} = 0.4732$.

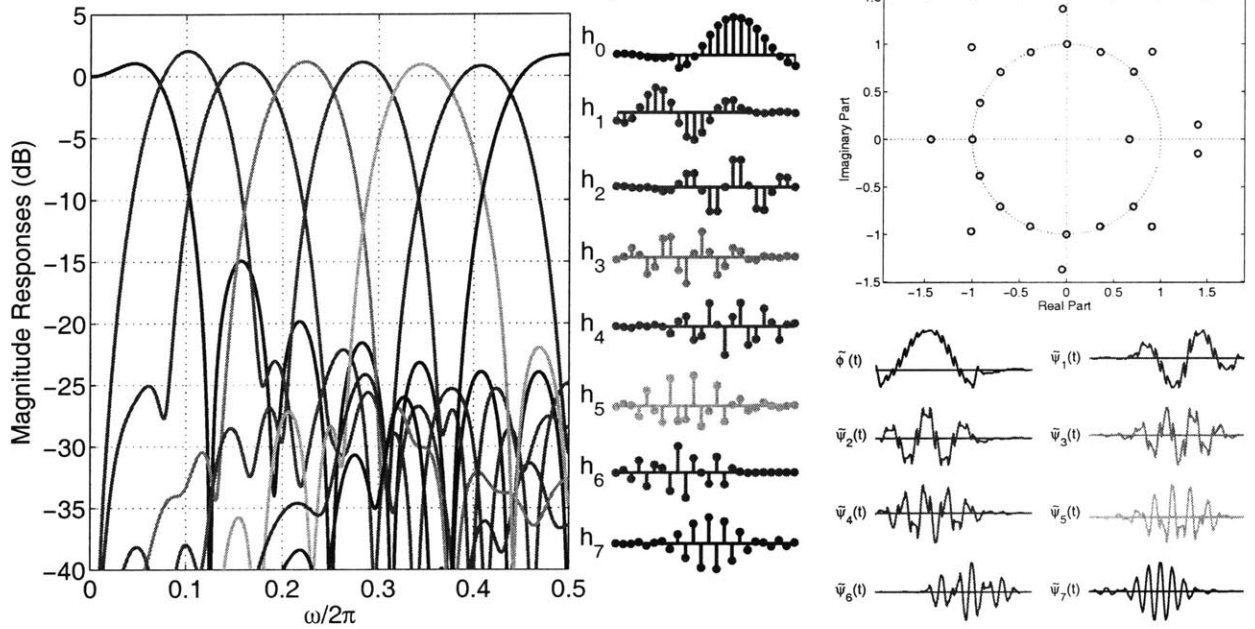
(1,1)-Reg, synthesis 8x24 BOFB, CG=9.6414dB, $C_{stop} = 0.1920$



(b) Synthesis bank: $s_{max} = 0.9974$.

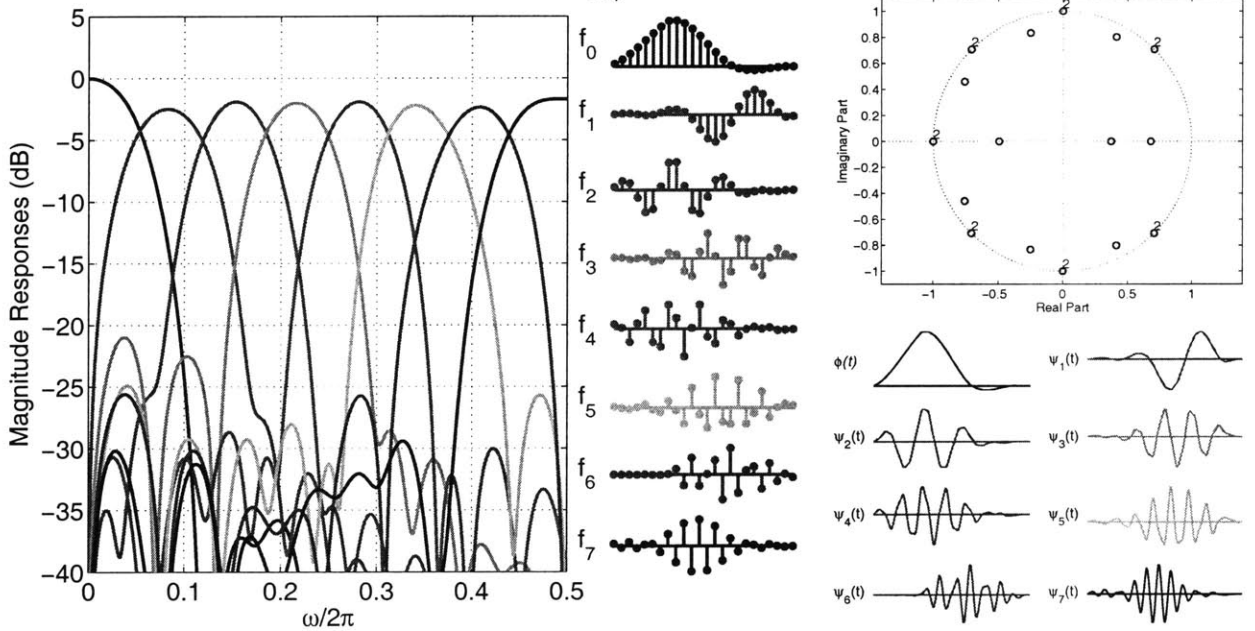
Figure 5-6: (1,1)-regular 8×24 BOFB: impulse and frequency responses, along with zero plots of $H_0(z)$ and $F_0(z)$, and the wavelet bases.

(1,2)-Reg, analysis 8x24 BOFB, CG=9.6367dB, $C_{\text{stop}} = 0.1538$



(a) Analysis bank: $s_{\max} = 0.5010$.

(1,2)-Reg, synthesis 8x24 BOFB, CG=9.6367dB, $C_{\text{stop}} = 0.1535$



(b) Synthesis bank: $s_{\max} = 1.7221$.

Figure 5-7: (1,2)-regular 8×24 BOFB: impulse and frequency responses, along with zero plots of $H_0(z)$ and $F_0(z)$, and the wavelet bases.

coding gain 9.6403dB. Observe the double zeros of $F_0(z)$ at the aliasing frequencies, implying a two-regular synthesis bank. The synthesis basis is thus smoother than the analysis basis.

5.6 Application to Data Compression

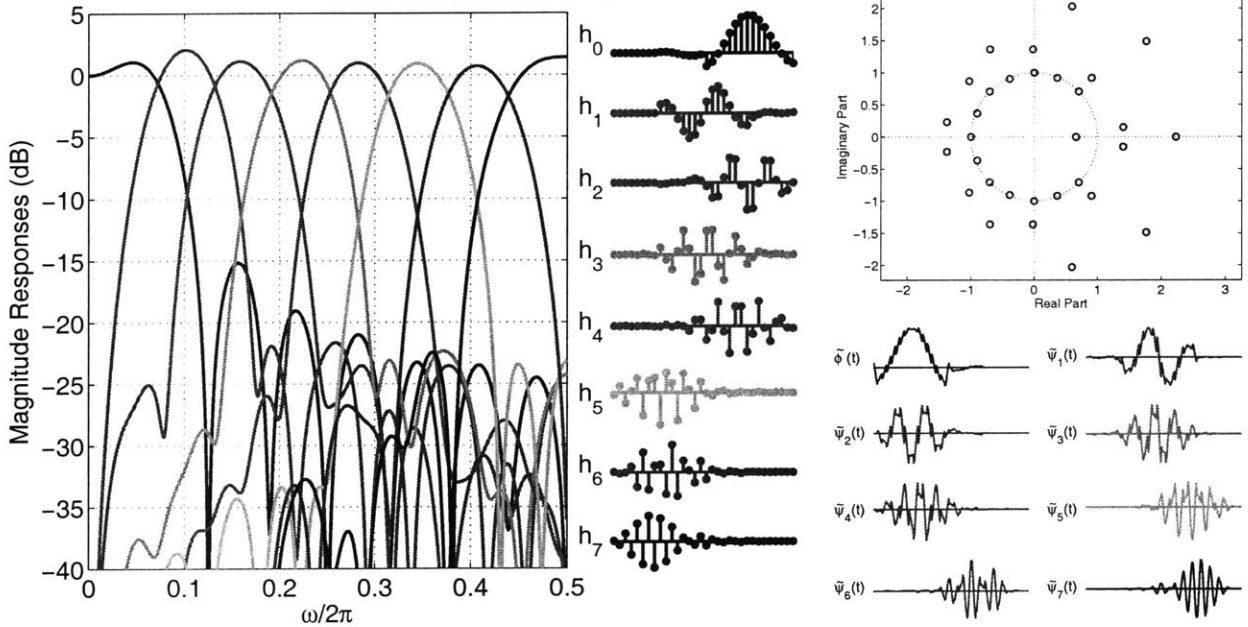
In this section, the regular BOFBs obtained in the previous section are evaluated by a transform-based image coder [40, 147] with its block diagram shown in Figure 5-9. The *transform coefficients* of the input signal are first computed, representing the *coordinate* of the signal with respect to the transform basis functions⁴. Examples of the transform stage include the discrete wavelet trasforms (DWT), Karhunen Loève Transform (KLT), the discrete cosine transform (DCT, used in JPEG/MPEG/H.263+, etc.), the Walsh Hadamard transform (WHT), M -channel PRFB, etc. A good transform is such that the signal energy is concentrated in a few transform coefficients, so-called *energy compaction*.

After the transform, the coefficients are subject to quantization, using the optimal bit allocation determined by the spectral estimator. This step achieves (lossy) compression by reducing the dynamic range of the transform coefficients. The quantized coefficients are then entropy-coded, e.g., Huffman and arithmetic coders, to achieve further (lossless) compression. The quantizer and spectral estimator are usually embedded in the particular choice of the coefficient encoding algorithm, including wavelet difference reduction (e.g. [148]), JPEG, and embedded zerotree coder (e.g. [104]).

In the following experiment, test images considered include 512×512 8-bit grayscale *Lena*, *Barbara*, *Goldhill*, and three fingerprints. To have a fair comparison of the various filter banks, we fix the encoding algorithm in the experiment. In particular, we choose the *set partitioning in hierarchical trees* (SPIHT) [104] algorithm for efficient encoding of the transform coefficients.

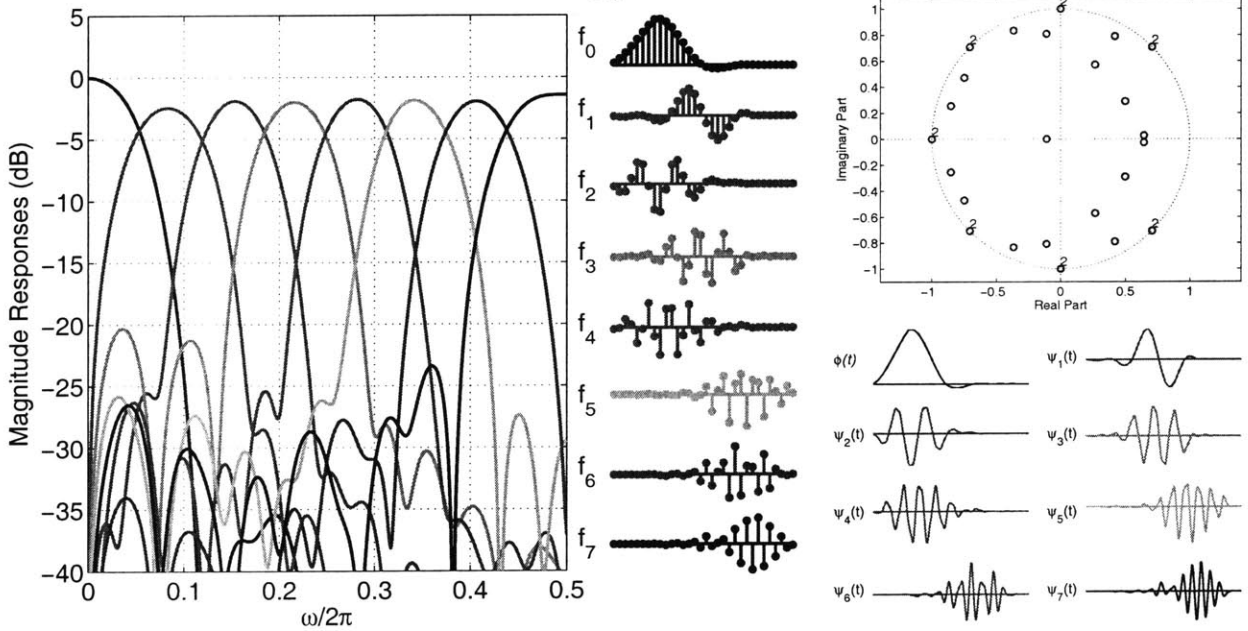
⁴Corresponding to the synthesis bank.

(1,2)-Reg, analysis 8x32 BOFB, CG=9.6403dB, $C_{\text{stop}}=0.1623$



(a) Analysis bank: $s_{\max} = 0.4957$.

(1,2)-Reg, synthesis 8x32 BOFB, CG=9.6403dB, $C_{\text{stop}}=0.1653$



(b) Synthesis bank: $s_{\max} = 1.7177$.

Figure 5-8: (1,2)-regular 8×32 BOFB: impulse and frequency responses, along with zero plots of $H_0(z)$ and $F_0(z)$, and the wavelet bases.

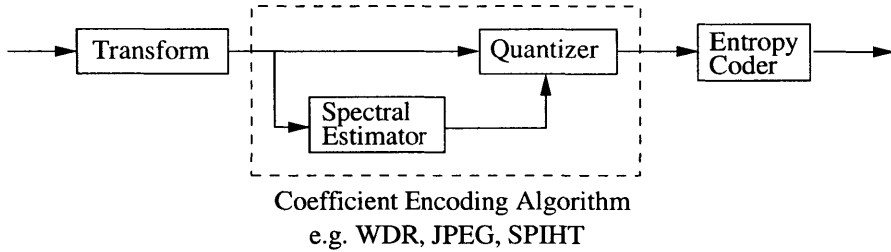


Figure 5-9: Transform-based image coder. Examples of the transform stage include DWT, DCT, M -channel PRFB, etc. Common encoding algorithms include wavelet difference reduction (e.g. [148]), JPEG, and embedded zerotree coder (e.g. [104]).

5.6.1 Performance Summary

The objective properties of the filter banks used in the image coding experiment are summarized in Table 5.1, including the degree of regularity, coding gain, stopband energy, and the Sobolev smoothness index, s_{max} , of the basis functions. Ideally, we wish to have smooth synthesis bases (large s_{max}), high coding gain, and small stopband energy. Except for coding gain, all the properties take the form of an ordered pair for biorthogonal filter banks, corresponding to the analysis and synthesis banks. As the analysis banks are designed to maximize energy compaction whereas the synthesis banks for smooth reconstruction, it should be noted that the Sobolev index for the synthesis banks is larger than that of the analysis banks, especially so when $K_s = 2$ as compared to $K_s = 1$. Furthermore, due to the increased design flexibility, the BOFBs can achieve comparable performance at fewer filter taps, and they have a smoother synthesis basis than their PU counterparts, which results in reconstructions of better visual quality as will be seen below.

The objective coding results (PSNR) are listed in Table 5.2 for *Barbara*, *Lena*, and *Goldhill*, whereas those for the fingerprints are listed in Table 5.3. The image *Barbara* is rich in textures, and the use of M -channel filter banks consistently outperforms the state-of-the-art 9/7-based SPIHT codec for which $M = 2$. This is because the conventional two-channel wavelet transforms fail to provide enough frequency resolution and hence over-smooth the details. In Figure 5-11, the strips of the tablecloth and the fine textures on the pants are smoothed out by Daubechies 9/7 wavelet, whereas they are much better preserved by

	8×8 DCT	8×16 LOT	8×24 LPv1	8×24 LPv2	8×24 PUv1	8×24 PUv2	8×16 BOv11	8×16 BOv12	8×24 BOv11	8×24 BOv12
Reg. K	1	1	1	2	1	2	(1,1)	(1,2)	(1,1)	(1,2)
G (dB)	8.83	9.22	9.36	9.33	9.49	9.43	9.62	9.60	9.64	9.64
C_{stop}	3.09	.211	.133	.374	.088	.078	.259	.341	.198	.154
s_{\max}	.500	.709	.866	1.33	.989	1.30	.381	.297	.473	.501
							.253	.338	.192	.154
							.989	1.67	.997	1.72

Table 5.1: Objective properties of the regular perfect reconstruction filter banks used in transform-based image coding experiments: G =coding gain, C_{stop} =stopband energy, s_{\max} =Sobolev smoothness. LPvn= n -Regular PULP in [92]; PUv1 and PUv2 are presented in Sec. 4.5.1 and Sec. 4.5.2, respectively. BOvn_{an_s}'s are the corresponding eight-channel designs presented in the previous section. For coding gain with $M = 8$, $G_{\text{KLT}} = 8.85$ dB, $G_{\text{brick-wall}} = 9.69$ dB.

the other transforms considered, except for DCT which exhibits highly blocking artifacts. Furthermore, the biorthogonal filter banks preserve the texture details even better than the PU counterparts.

For *Lena*, Daubechies 9/7 wavelet results in the highest PSNR, except at 16:1 compression for which 8×16 BOv11 is the best. This is because *Lena* contains a lot of low-frequency, smooth regions and the conventional Daubechies 9/7 wavelet already does a good job in term of objective coding performance. However, the designed regular biorthogonal filter banks are able to provide better visual quality.

Visual comparisons of *Goldhill* are shown in Figure 5-13. Though they have very similar PSNRs, again the designed regular biorthogonal filter banks preserve the textures much better than the Daubechies 9/7 wavelet. One can observe how the details of the roof are completed smoothed out by the Daubechies 9/7 wavelet, while they are better preserved by the designed regular filter banks.

We also apply the transforms to the three fingerprint images labeled *fp1*, *fp2*, and *fp3* as shown in Figure 5-10. From Table 5.3 and the rate-distortion curves shown in Figure 5-14, we observe that the designed (1,1)- and (1,2)-regular biorthogonal filter banks consistently

Barb	PSNR(dB) for encoding scheme: SPIHT											
Comp. ratio	SPIHT Db9/7	8×8 DCT	8×16 LOT	8×24 LPv1	8×24 LPv2	8×24 PUv1	8×24 PUv2	8×16 BOv11	8×16 BOv12	8×24 BOv11	8×24 BOv12	
8:1	36.44	36.25	37.40	37.89	37.43	38.02	38.01	37.82	37.59	37.79	37.84	
16:1	31.44	31.08	32.73	33.09	32.62	33.37	33.33	33.00	32.74	33.03	33.11	
32:1	27.63	27.27	28.80	29.06	28.71	29.42	29.32	28.96	28.79	29.11	29.15	
64:1	24.90	24.57	25.68	25.92	25.75	26.25	26.15	25.81	25.67	25.94	25.98	
100:1	23.81	23.41	24.32	24.59	24.49	24.86	24.80	24.45	24.32	24.58	24.63	
128:1	23.42	22.61	23.32	23.67	23.67	23.87	23.84	23.74	23.65	23.87	23.86	

Lena	PSNR(dB) for encoding scheme: SPIHT											
Comp. ratio	SPIHT Db9/7	8×8 DCT	8×16 LOT	8×24 LPv1	8×24 LPv2	8×24 PUv1	8×24 PUv2	8×16 BOv11	8×16 BOv12	8×24 BOv11	8×24 BOv12	
8:1	40.26	39.73	39.89	40.17	40.02	40.20	40.20	40.22	40.06	40.18	40.16	
16:1	37.17	36.28	36.63	37.04	36.79	37.14	37.11	37.18	36.99	37.13	37.10	
32:1	34.15	32.80	33.46	33.84	33.48	34.00	33.98	34.02	33.81	33.98	33.93	
64:1	31.20	29.53	30.31	30.63	30.28	30.81	30.79	30.80	30.58	30.80	30.73	
100:1	29.47	27.57	28.35	28.68	28.42	28.87	28.85	28.86	28.69	28.88	28.88	
128:1	28.51	26.71	27.44	27.74	27.53	27.90	27.85	27.84	27.63	27.89	27.82	

Gold	PSNR(dB) for encoding scheme: SPIHT											
Comp. ratio	SPIHT Db9/7	8×8 DCT	8×16 LOT	8×24 LPv1	8×24 LPv2	8×24 PUv1	8×24 PUv2	8×16 BOv11	8×16 BOv12	8×24 BOv11	8×24 BOv12	
8:1	36.52	36.23	36.60	36.71	36.57	36.63	36.64	36.66	36.54	36.60	36.58	
16:1	33.11	32.74	33.17	33.27	33.13	33.25	33.23	33.33	33.19	33.27	33.26	
32:1	30.53	30.06	30.56	30.64	30.49	30.69	30.65	30.66	30.53	30.65	30.63	
64:1	28.43	27.85	28.30	28.40	28.27	28.46	28.43	28.42	28.27	28.41	28.37	
100:1	27.38	26.54	27.02	27.10	27.00	27.22	27.14	27.34	27.21	27.32	27.29	
128:1	26.76	25.90	26.40	26.47	26.38	26.60	26.53	26.57	26.42	26.57	26.52	

Table 5.2: Objective coding performance using the various transforms with two levels of decomposition in the lowpass band.

outperform the FBI/WSQ fingerprint compression specification [48] by 2-6 dB in PSNR and the latest still image compression standard, JPEG2000, by a significant margin.

5.7 Conclusion

Using a dyadic-based structure which is minimal, we have established the framework for *structurally* regular BOFBs with length constraint. By specializing this to filters with linear phase (LP), we have identified the connection between the dyadic-based structure and the

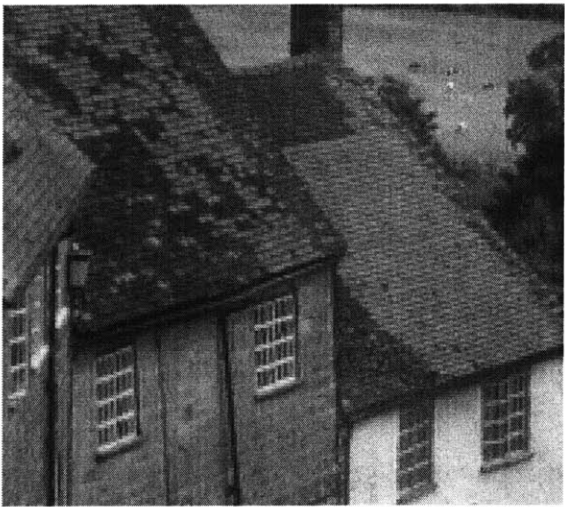
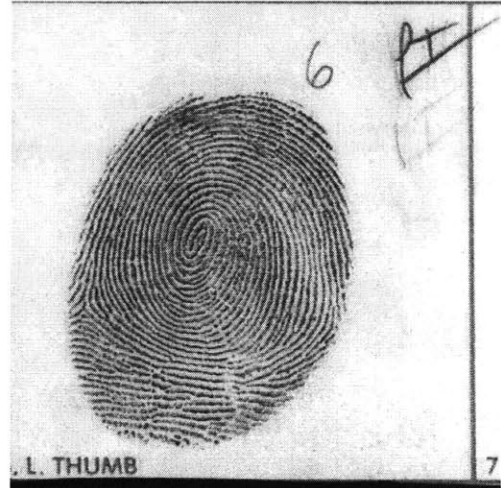


Figure 5-10: Enlarged portions of original *Barbara*, *Lena*, *Goldhill* (Left column), and three fingerprints *fp1*, *fp2*, and *fp3* (Right column).

BO8x16v12 @ 32:1



PUv1 @ 32:1



db97 @ 32:1



BO8x24v12 @ 32:1



PUv2 @ 32:1



DCT @ 32:1



Figure 5-11: Enlarged portions of *Barbara* at 32:1 compression using Daubechies 9/7 wavelet, 8 × 8 DCT, 8 × 24 PUv1 and PUv2, 8 × 16 and 8 × 24 BOFBv12.



Figure 5-12: Enlarged portions of *Lena* at 64:1 compression using Daubechies 9/7 wavelet, 8×8 DCT, 8×24 PUv1 and PUv2, 8×16 and 8×24 BOFBv12.

BO8x16v12 @ 32:1



PUv1 @ 32:1



db97 @ 32:1



BO8x24v12 @ 32:1



PUv2 @ 32:1



DCT @ 32:1



Figure 5-13: Enlarged portions of *Goldhill* at 32:1 compression using Daubechies 9/7 wavelet, 8 × 8 DCT, 8 × 24 PUv1 and PUv2, 8 × 16 and 8 × 24 BOFBv12.

Fp1	PSNR(dB) for encoding scheme: SPIHT											
Comp. ratio	Daub 9/7	8×8 DCT	8×16 LOT	8×24 LPv1	8×24 LPv2	8×24 PUv1	8×24 PUv2	8×16 BOv11	8×16 BOv12	8×24 BOv11	8×24 BOv12	
8:1	39.83	39.85	40.44	40.71	40.57	40.80	40.74	40.74	40.58	40.75	40.76	
9:1	39.19	39.08	39.75	40.01	39.88	40.11	40.04	40.04	39.89	40.05	40.06	
10:1	38.51	38.23	38.89	39.18	39.04	39.29	39.22	39.30	39.14	39.31	39.33	
11:1	37.77	37.38	38.02	38.29	38.15	38.40	38.33	38.27	38.15	38.26	38.29	
13:1	36.90	36.52	37.10	37.38	37.23	37.50	37.42	37.37	37.24	37.41	37.41	
16:1	35.96	35.47	36.14	36.41	36.25	36.53	36.46	36.41	36.29	36.44	36.46	
20:1	34.92	34.18	34.90	35.11	34.95	35.21	35.15	35.25	35.11	35.27	35.29	

Fp2	PSNR(dB) for encoding scheme: SPIHT											
Comp. ratio	Daub 9/7	8×8 DCT	8×16 LOT	8×24 LPv1	8×24 LPv2	8×24 PUv1	8×24 PUv2	8×16 BOv11	8×16 BOv12	8×24 BOv11	8×24 BOv12	
8:1	35.14	34.67	35.76	36.10	35.91	36.32	36.19	36.21	36.04	36.21	36.26	
9:1	34.42	33.89	35.04	35.38	35.16	35.60	35.49	35.42	35.25	35.42	35.47	
10:1	33.66	32.98	34.23	34.54	34.34	34.77	34.65	34.62	34.46	34.63	34.69	
11:1	32.89	31.98	33.30	33.55	33.39	33.80	33.67	33.72	33.53	33.73	33.80	
13:1	31.95	31.03	32.29	32.52	32.30	32.81	32.68	32.65	32.46	32.68	32.74	
16:1	30.89	29.88	31.25	31.45	31.20	31.69	31.58	31.50	31.34	31.57	31.59	
20:1	29.79	28.51	29.94	30.12	29.85	30.43	30.28	30.21	30.03	30.29	30.34	

Fp3	PSNR(dB) for encoding scheme: SPIHT											
Comp. ratio	Daub 9/7	8×8 DCT	8×16 LOT	8×24 LPv1	8×24 LPv2	8×24 PUv1	8×24 PUv2	8×16 BOv11	8×16 BOv12	8×24 BOv11	8×24 BOv12	
8:1	38.00	37.44	38.38	38.78	38.65	38.93	38.81	39.01	38.84	38.99	39.01	
9:1	37.34	36.66	37.53	37.83	37.70	37.98	37.86	38.14	37.96	38.09	38.11	
10:1	36.53	35.88	36.74	37.03	36.89	37.17	37.05	37.17	36.97	37.12	37.12	
11:1	35.70	34.98	35.93	36.22	36.08	36.35	36.23	36.34	36.15	36.30	36.32	
13:1	34.83	33.92	34.98	35.27	35.11	35.42	35.30	35.43	35.25	35.40	35.43	
16:1	33.85	32.77	33.88	34.15	33.94	34.28	34.18	34.28	34.11	34.27	34.30	
20:1	32.72	31.46	32.61	32.84	32.62	33.01	32.86	32.98	32.79	32.98	32.98	

Table 5.3: Objective coding performance using the various transforms with two levels of decomposition in the lowpass band.

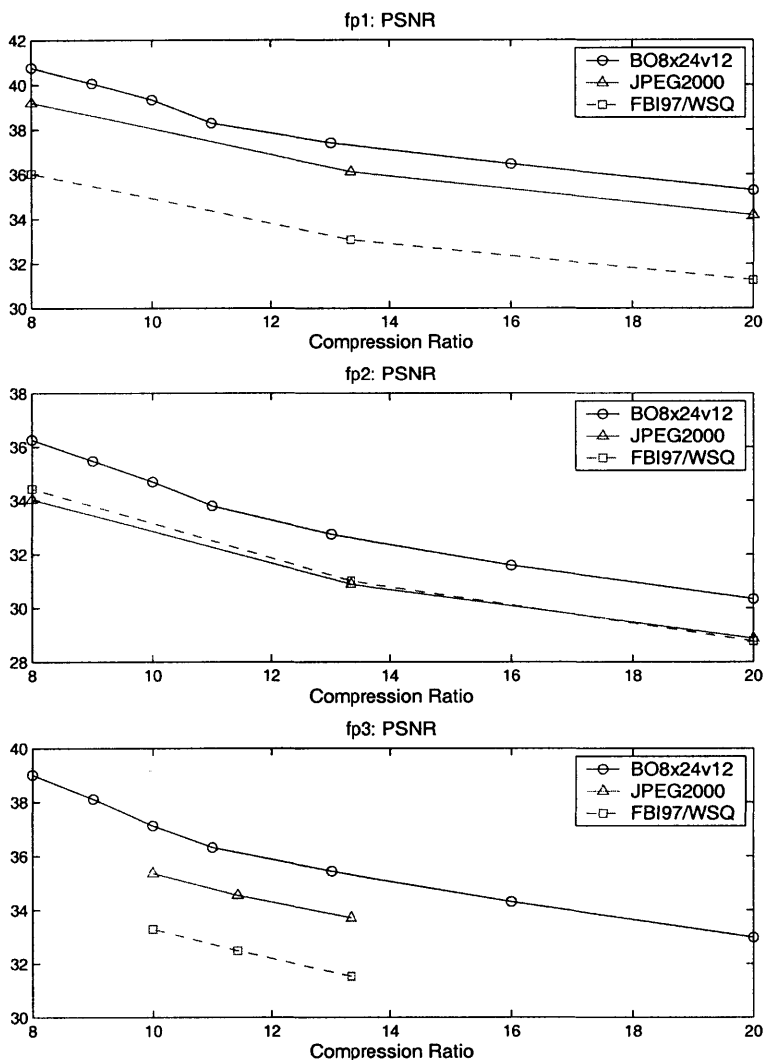


Figure 5-14: Fingerprint compression performance.

LP-propagating lattice structure commonly used for designing the GLBT, and regularity conditions on the LP-propagating dyadic-based structure are presented. As a by-product, we obtain a simplified representation of the GLBT with fewer parameters. A few regular biorthogonal filter banks are designed using the proposed theories, and are evaluated in a transform-based image codec. As their smooth basis functions achieve a finer frequency resolution than two-channel wavelets, these regular M -channel filter banks have been found to result in superior compression performance, both objectively (higher PSNR) and subjectively (better visual quality). Our experiments show that both JPEG2000 and FBI/WSQ standards are outperformed.

Chapter 6

Paraunitary Filter Bank Completion

This chapter presents the complete parameterizations of the class of M -channel paraunitary filter banks (PUFBs) having a prescribed admissible scaling filter $H_0(z)$. We propose a novel *order-one factorization* of the $M \times 1$ lossless *polyphase vector* of $H_0(z)$ to facilitate the completion of PUFBs with a certain *length*, and consequently to relax the constraint on McMillan degree of the completed PUFBs inherent in the literature, which has impaired the performance of the completed filter banks. The relaxation of the constraint on McMillan degree lends itself well to completion of linear-phase PUFBs: If additionally the PUFB-admissible scaling filter $H_0(z)$ has linear phase *and* a LPPUFB is sought, the proposed approach can be specialized to obtain a complete parameterization such that the resulting $M - 1$ bandpass/highpass filters $H_i(z)$ and $H_0(z)$ form a LPPUFB. Furthermore, the proposed completion technique can serve as a tool for improved filter bank design. PUFBs with better performance are obtained.

6.1 Introduction

Recently, M -channel maximally decimated filter banks have found several applications in signal processing, data compression, and smooth approximation, etc. [19, 72, 108, 113, 139]. As shown in Figure 6-1, for $i = 0, \dots, M - 1$, $H_i(z)$ and $F_i(z)$ denote the analysis and

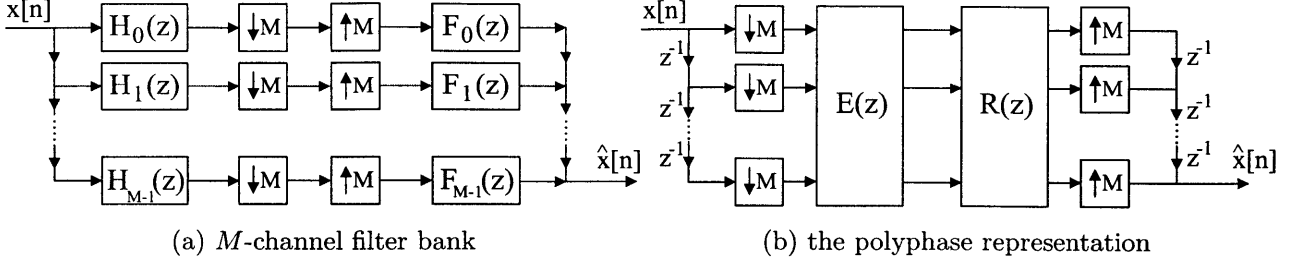


Figure 6-1: M -channel perfect reconstruction filter bank.

synthesis filters, respectively, where the low-pass filters $H_0(z)$ and $F_0(z)$ are also referred to as the *scaling filters*, as they govern the M -band dilation equations for the underlying multiresolution analysis (MRA) of the Hilbert space. These filters are related to the *polyphase* representation through

$$\begin{bmatrix} H_0(z) & \dots & H_{M-1}(z) \end{bmatrix} = \begin{bmatrix} 1 & z^{-1} & \dots & z^{1-M} \end{bmatrix} \mathbf{E}^T(z^M)$$

$$\begin{bmatrix} F_0(z) & \dots & F_{M-1}(z) \end{bmatrix} = \begin{bmatrix} z^{1-M} & \dots & z^{-1} & 1 \end{bmatrix} \mathbf{R}(z^M)$$

where $\mathbf{E}(z)$ and $\mathbf{R}(z)$ are the type-I and type-II polyphase matrices, respectively. Perfect reconstruction (PR) requires that $\mathbf{E}(z)$ be non-singular for all z , so that the analysis filters $H_i(z)$ can be jointly inverted by the synthesis filters $F_i(z)$. Paraunitary filter banks (PUFB) are an important class for which $\mathbf{E}(z)$ is unitary on the unit circle; as a result, signal energy is preserved, and $F_i(z)$ can be found from $H_i(z)$ by inspection [129]. If all the filters $H_i(z)$ have symmetry/antisymmetry in their impulse responses, the resulting filter bank is termed *linear-phase* [41, 119].

Recall that for an M -channel filter bank $\mathbf{E}(z)$ of order L , the filters $H_i(z)$ in general have lengths $M(L + 1)$. However, a PUFB of length $M(L + 1)$ can have degree ranging from L to ML . Gao *et al.* have recently proposed *order-one* factorization for designing PUFBs with length constraint [52] as summarized in Lemma 2.2, where order-one PU building block $\mathbf{W}_m(z)$ is involved.

Filter bank completion is to address the following issue: given partial information in

terms of the (admissible) scaling filter $H_0(z)$ of a perfect reconstruction filter bank, how do we come up with a representation that characterizes *all* possible solutions? Note that this is not an issue for $M = 2$, as one filter determines the remaining three (assume paraunitarity) [108]. However, for $M > 2$, there are much more degrees of freedom, and the choice of one filter does not determine the other choices. Therefore, filter bank completion is significant in that it ensures the best possible solution is obtainable out of the structure used.

To complete a PUFB from its scaling filter $H_0(z)$, two methods based on *degree-one factorization* (Lemma 2.1) were proposed: the one in [134] serves as a way to initialize the parameters in designing a PUFB; while the one in [58, 59, 105] requires further specification of an initial unitary matrix \mathbf{E}_0 for the method to work; however, how to choose \mathbf{E}_0 was not fully addressed. *In both cases, the McMillan degree of the completed PUFB is limited by that of the polyphase vector of $H_0(z)$, and thus the optimal performance of the PUFB given the filter $H_0(z)$ may not be obtained.* In fact, our work was partly motivated by this difficulty. One might attempt the M -channel lifting-based completion technique proposed in Chapter 3 to resolve this degree constraint; however, since lifting steps are biorthogonal in nature, the method may not directly carry through to the paraunitary case. Our work resulted partly from our attempt to specialize the lifting-based biorthogonal completion.

In this chapter, we propose a novel *order-one factorization* of a causal lossless polyphase *vector* to address the above issues. We will demonstrate how to factor a polyphase *vector* into a product of order-one PU building blocks $\mathbf{W}_m(z)$ so as to complete PUFBs without the conventional constraint on McMillan degree. At the same time, we have the option of completing linear-phase PUFBs (LPPUFB) if so desired. Furthermore, the proposed framework complements the filter design method in [58]. PUFB design based on order-one completion is also discussed and design examples are presented.

In the following, the McMillan degree and the order of $\mathbf{E}(z)$ are denoted by $\deg(\mathbf{E}(z))$ and $\text{ord}(\mathbf{E}(z))$, respectively.

6.2 Prior Arts on PUFB Completion

6.2.1 PUFB Admissibility

Let $H_0(z)$ be the scaling filter of some M -channel PUFB. It is necessary and sufficient that the vector of its M polyphase components

$$\mathbf{p}(z) = \begin{bmatrix} H_{0,0}(z) & H_{0,1}(z) & \dots & H_{0,M-1}(z) \end{bmatrix}^T \quad (6.1)$$

be paraunitary (See Chapter 2 for the tilde notation used below):

$$\tilde{\mathbf{p}}(z)\mathbf{p}(z) = \sum_{i=0}^{M-1} \tilde{H}_{0,i}(z)H_{0,i}(z) = c^2, \quad \text{some } c > 0.$$

Therefore, a filter $H_0(z)$ is PUFB-admissible if and only if the vector of its polyphase components (6.1) is paraunitary. Without loss of generality, we will consider *normalized* PUFBs for which $c = 1$.

6.2.2 Degree-One Factorization of $M \times 1$ Lossless FIR Systems

Recall that an M -channel *degree-one* paraunitary building block $\mathbf{V}_m(z) \triangleq \mathbf{I} - \mathbf{v}_m\mathbf{v}_m^\dagger + z^{-1}\mathbf{v}_m\mathbf{v}_m^\dagger$ is parameterized by a unit-norm M -vector $\mathbf{v}_m \in \mathbb{C}^M$. This is an FIR system with an FIR inverse given by $\tilde{\mathbf{V}}_m(z) = \mathbf{I} - \mathbf{v}_m\mathbf{v}_m^\dagger + z\mathbf{v}_m\mathbf{v}_m^\dagger$. With $\mathbf{V}_m(z)$, any degree- N FIR $M \times 1$ causal lossless transfer function $\mathbf{p}(z)$ can be *uniquely* factorized as [129, 134]

$$\mathbf{p}(z) = \mathbf{V}_N(z) \dots \mathbf{V}_1(z) \mathbf{p}_0 \quad (6.2)$$

for some PU building blocks $\mathbf{V}_m(z)$ and $M \times 1$ unitary $\mathbf{p}_0 = \mathbf{p}(1)$.

6.2.3 Degree-One Completion of PUFBs

Below, the special Householder matrix $\mathbf{R}[\cdot]$ defined in Definition 2.3 will be very useful.

Given $\mathbf{p}(z)$ as in (6.1) and (6.2), we have

$$\mathbf{p}(z) = e^{j\theta_0} \mathbf{V}_N(z) \dots \mathbf{V}_1(z) \mathbf{R}[\mathbf{p}_0] \mathbf{e}_0 \quad (6.3)$$

using the Householder matrix $\mathbf{R}[\mathbf{p}_0]$. By augmenting the column vector \mathbf{e}_0 as follows, we can now *complete* the degree- N PUFB $\mathbf{E}(z)$ having $\mathbf{p}(z)$ as the polyphase vector of the prescribed scaling filter $H_0(z)$:

$$\mathbf{E}^T(z) = e^{j\theta_0} \mathbf{V}_N(z) \dots \mathbf{V}_1(z) \mathbf{R}[\mathbf{p}_0] \begin{bmatrix} 1 & \mathbf{0}^T \\ \mathbf{0} & \Theta \end{bmatrix}. \quad (6.4)$$

We refer to (6.4) as *degree-one completion* of $\mathbf{E}(z)$ as degree-one PU building blocks are involved. The $(M - 1) \times (M - 1)$ unitary matrix Θ contains all the degrees of freedom, and can be parameterized by Householder matrices or by planar rotations [85, 129]. The paraunitarity of $\mathbf{E}(z)$ is guaranteed since all the components involved are unitary/paraunitary.

Limitation Imposed by (6.4)

However, the degree-one completion of $\mathbf{E}(z)$ in (6.4) is *degree-constrained* in that it spans *only* the set of PUFBs *of the same degree as* $\mathbf{p}(z)$, with $\mathbf{p}^T(z)$ being the 0th row of $\mathbf{E}(z)$. Namely, the completed $\mathbf{E}(z)$ is constrained in such a way that

$$\deg(\mathbf{E}(z)) = \text{ord}(\mathbf{E}(z)) \equiv \deg(\mathbf{p}(z)).$$

In general, $\deg(\mathbf{E}(z))$ should be no less and can be greater than $\text{ord}(\mathbf{E}(z))$, and oftentimes it is desirable to allow for such a possibility. For example, suppose that $\mathbf{p}(z)$ of order L

$$\mathbf{p}(z) = \mathbf{a}_0 + \mathbf{a}_1 z^{-1} + \dots + \mathbf{a}_L z^{-L}$$

is causal and is the vector of the M polyphase components of a PUFB-admissible linear-phase filter $H_0(z)$. If $\mathbf{E}(z)$ of order L corresponds to a linear-phase PUFB, its degree must

be $\frac{ML}{2}$ [41, 129], which is greater than L ; however, this is not possible under (6.4). Furthermore, experiments indicate that, given the order of $\mathbf{E}(z)$, PUFBs with better performance are usually obtained by allowing $\deg(\mathbf{E}(z)) > \text{ord}(\mathbf{E}(z))$, as evidenced in Figure 2-18, for example.

6.3 Improved Technique For Completing General Parauitary Filter Banks

To relax the degree constraint on $\mathbf{E}(z)$ intrinsic in the degree-one completion (6.4), we propose below an improved technique by which the designer has control over the resulting McMillan degree of the completed PUFB, with (6.4) as a special case.

This improved technique relies on a more general factorization of an $M \times 1$ lossless FIR system. In particular, the factorization will use *order-one* PU building blocks

$$\mathbf{W}_m(z) = \mathbf{I} - \mathbf{w}_m \mathbf{w}_m^\dagger + z^{-1} \mathbf{w}_m \mathbf{w}_m^\dagger$$

parameterized by some $M \times \gamma_m$ unitary parameter matrices \mathbf{w}_m (satisfying $\mathbf{w}_m^\dagger \mathbf{w}_m = \mathbf{I}_{\gamma_m}$), where $1 \leq \gamma_m \triangleq \rho(\mathbf{w}_m) \leq M$. Using order-one PU building blocks to decompose $M \times M$ FIR lossless systems has been reported in [52]. Here, our focus is to derive an *order-one factorization* of an $M \times 1$ FIR causal lossless system $\mathbf{p}(z)$. As one shall see, the proposed order-one factorization of $\mathbf{p}(z)$ results in “degree elevation:” the nominal degree of $\mathbf{p}(z)$ is pre-elevated so as to accommodate the degree requirement of the resulting $\mathbf{E}(z)$.

6.3.1 Order-One Factorization of $M \times 1$ Lossless FIR Systems

Theorem 6.1 (Order-One Factorization of $M \times 1$ Lossless FIR Systems). *Given an $M \times 1$ FIR lossless causal transfer function $\mathbf{p}_L(z)$ of order¹ L , it can be decomposed into the*

¹For an $M \times 1$ FIR causal $\mathbf{p}(z)$, $\deg(\mathbf{p}(z)) = \text{ord}(\mathbf{p}(z))$.

following order-one factorization

$$\mathbf{p}_L(z) = \widehat{\mathbf{W}}_L(z) \dots \widehat{\mathbf{W}}_1(z) \mathbf{p}_0 \quad (6.5)$$

for some (non-unique) order-one PU building blocks²

$$\widehat{\mathbf{W}}_m(z) = \mathbf{I} - \widehat{\mathbf{w}}_m \widehat{\mathbf{w}}_m^\dagger + z^{-1} \widehat{\mathbf{w}}_m \widehat{\mathbf{w}}_m^\dagger, \quad \rho(\widehat{\mathbf{w}}_m) = \widehat{\gamma}_m$$

and $\mathbf{p}_0 = \mathbf{p}_L(1)$.

Proof: By assumption, we can write

$$\mathbf{p}_L(z) = \mathbf{a}_0 + \mathbf{a}_1 z^{-1} + \dots + \mathbf{a}_L z^{-L}$$

for some $M \times 1$ coefficient vectors \mathbf{a}_k with $\mathbf{a}_L \neq \mathbf{0}$. By losslessness of $\mathbf{p}_L(z)$, we have $\mathbf{a}_L^\dagger \mathbf{a}_0 = 0$, implying that \mathbf{a}_0 and \mathbf{a}_L are perpendicular to each other [129]. The goal is to construct an order-one building block $\widehat{\mathbf{W}}_L(z)$ based on this property so that the product of $[\widehat{\mathbf{W}}_L(z)]^{-1}$ and $\mathbf{p}_L(z)$

$$\mathbf{p}_{L-1}(z) \triangleq [\widehat{\mathbf{W}}_L(z)]^{-1} \mathbf{p}_L(z) = \left(\mathbf{I} - \widehat{\mathbf{w}}_L \widehat{\mathbf{w}}_L^\dagger + z \widehat{\mathbf{w}}_L \widehat{\mathbf{w}}_L^\dagger \right) \sum_{k=0}^L \mathbf{a}_k z^{-k} \quad (6.6)$$

is causal FIR and lossless with order $L - 1$, thus achieving order reduction. The trick is to define the $M \times \widehat{\gamma}_L$ unitary parameter matrix $\widehat{\mathbf{w}}_L$ of $\widehat{\mathbf{W}}_L(z)$ to take the form

$$\widehat{\mathbf{w}}_L \triangleq \left[\begin{array}{c|c} & \mathbf{B}_L \\ \frac{\mathbf{a}_L}{\|\mathbf{a}_L\|} & \\ \hline & \end{array} \right]_{M \times \widehat{\gamma}_L} \quad (6.7)$$

where \mathbf{B}_L consists of $\widehat{\gamma}_L - 1$ orthonormal columns that are orthogonal to both \mathbf{a}_0 and \mathbf{a}_L . It then follows that $\widehat{\mathbf{w}}_L^\dagger \mathbf{a}_0 = \mathbf{0}$ and that $\widehat{\mathbf{w}}_L^\dagger \mathbf{a}_L = \left[\|\mathbf{a}_L\| \ 0^T \right]^T$, and thus we have for $\mathbf{p}_{L-1}(z)$

²We reserve the notation $\mathbf{W}_m(z)$ for order-one completion of PUFBs to avoid possible confusion.

that

$$z^1 \text{ term: } \widehat{\mathbf{w}}_L \widehat{\mathbf{w}}_L^\dagger \mathbf{a}_0 = \widehat{\mathbf{w}}_L \mathbf{0} = \mathbf{0}, \quad (6.8)$$

and that

$$z^{-L} \text{ term: } (\mathbf{I} - \widehat{\mathbf{w}}_L \widehat{\mathbf{w}}_L^\dagger) \mathbf{a}_L = \mathbf{a}_L - \mathbf{a}_L = \mathbf{0}. \quad (6.9)$$

Hence, $\mathbf{p}_{L-1}(z)$ defined by (6.6) is indeed causal FIR and lossless with order $L - 1$, and we can write $\mathbf{p}_L(z) = \widehat{\mathbf{W}}_L(z) \mathbf{p}_{L-1}(z)$. The above order reduction procedure is then repeated on $\mathbf{p}_{L-1}(z)$ to obtain $\widehat{\mathbf{W}}_{L-1}(z), \dots$, and so on, until we arrive at (6.5).

As the choice of unitary matrix \mathbf{B}_m in the m th step of order reduction is not unique (depending on Θ_m) unless $\widehat{\gamma}_m = 1$, so is the order-one factorization (6.5) of $\mathbf{p}_L(z)$. ■

Remarks:

1. The matrix \mathbf{B}_L in (6.7) can be parameterized as follows:

$$\mathbf{B}_L = \mathbf{R}_{0L} \begin{bmatrix} -\mathbf{0}^T - \\ -\mathbf{0}^T - \\ \hline \Theta_L \end{bmatrix}, \quad (6.10)$$

where Θ_L is $(M - 2) \times (\widehat{\gamma}_L - 1)$ unitary and \mathbf{R}_{0L} is such that

$$\begin{bmatrix} | & | \\ \frac{\mathbf{a}_0}{\|\mathbf{a}_0\|} & \frac{\mathbf{a}_L}{\|\mathbf{a}_L\|} \\ | & | \end{bmatrix} = \mathbf{R}_{0L} \begin{bmatrix} | & | \\ \mathbf{e}_0 & \mathbf{e}_1 \\ | & | \end{bmatrix}.$$

In particular, one may choose \mathbf{R}_{0L} as follows:

$$\mathbf{R}_{0L} = \mathbf{R}[\mathbf{a}_0] \begin{bmatrix} 1 & \mathbf{0}^T \\ \mathbf{0} & \mathbf{R}[\mathbf{y}] \end{bmatrix} \quad (6.11)$$

where $\mathbf{y} \in \mathbb{C}^{M-1}$ is such that

$$\mathbf{R}[\mathbf{a}_0] \mathbf{a}_L = \|\mathbf{a}_L\| \begin{bmatrix} 0 \\ \mathbf{y} \end{bmatrix}.$$

2. Compared to the *unique* degree-one factorization of $\mathbf{p}_L(z)$, the extra degrees of freedom due to the non-uniqueness of (6.5) are captured by the Θ_m . Any choice of Θ_m results in the same $\mathbf{p}_L(z)$ — The difference will be at the later stage of PUFB completion, where the extra degrees of freedom will be exploited for the benefit of the completed $\mathbf{E}(z)$. This is to be discussed next.
3. As $\mathbf{W}_m(1) = \mathbf{I}$, the initial unitary vectors \mathbf{p}_0 are identical for both degree-one and order-one factorizations of $\mathbf{p}(z)$. However, the intermediate polyphase vectors $\mathbf{p}_\ell(z)$ are not unique, depending on the choice of \mathbf{B}_ℓ or Θ_ℓ . In particular, during the course of order-one factorization, the coefficient of $z^{-(L-1)}$ of $\mathbf{p}_{L-1}(z)$ depends on \mathbf{B}_L in the following fashion:

$$\left(1 - \frac{\mathbf{a}_L^\dagger \mathbf{a}_{L-1}}{\|\mathbf{a}_L\|^2}\right) \mathbf{a}_L + \left(\mathbf{I} - \mathbf{B}_L \mathbf{B}_L^\dagger\right) \mathbf{a}_{L-1}.$$

6.3.2 Order-One Completion of PUFBs

Based on the above order-one factorization of $\mathbf{p}(z)$ of degree or order L , one can again express $\mathbf{p}_0 = \mathbf{p}(z)|_{z=1}$ in terms of the Householder matrix $\mathbf{R}[\mathbf{p}_0]$ and the unit vector \mathbf{e}_0 to have

$$\mathbf{p}(z) = e^{j\theta_0} \widehat{\mathbf{W}}_L(z) \dots \widehat{\mathbf{W}}_1(z) \mathbf{R}[\mathbf{p}_0] \mathbf{e}_0. \quad (6.12)$$

Then the PUFB $\mathbf{E}(z)$ having $\mathbf{p}(z)$ as the polyphase vector of the scaling filter $H_0(z)$ can be completed by augmenting the vector \mathbf{e}_0 in (6.12) as follows:

$$\mathbf{E}^T(z) = e^{j\theta_0} \widehat{\mathbf{W}}_L(z) \dots \widehat{\mathbf{W}}_1(z) \mathbf{R}[\mathbf{p}_0] \begin{bmatrix} 1 & \mathbf{0}^T \\ \mathbf{0} & \Theta \end{bmatrix} \quad (6.13)$$

where Θ is $(M - 1) \times (M - 1)$ unitary consisting of free parameters. We refer to (6.13) as *order-one completion* of $\mathbf{E}(z)$ as order-one PU building blocks are involved.

Canonical Representation

Worth noting is the identification

$$\mathbf{R}[\mathbf{p}_0] \begin{bmatrix} 1 & \mathbf{0}^T \\ \mathbf{0} & \Theta \end{bmatrix} \equiv \mathbf{E}_0^T \quad (6.14)$$

between (6.13) and (2.53), which results if we set $z = 1$ in both (6.13) and (2.53). Notice that (6.13) is transposed, not in the standard form given by (2.53). Plugging (6.14) in and transposing (6.13), we have

$$\begin{aligned} \mathbf{E}(z) &= \mathbf{E}_0 \widehat{\mathbf{W}}_1^T(z) \dots \widehat{\mathbf{W}}_L^T(z) \\ &= \mathbf{W}_L(z) \dots \mathbf{W}_1(z) \mathbf{E}_0 \end{aligned}$$

where the mappings are

$$\mathbf{W}_m(z) \triangleq \mathbf{E}_0 \widehat{\mathbf{W}}_{L-m+1}^T(z) \mathbf{E}_0^\dagger \quad (6.15)$$

$$\mathbf{w}_m \triangleq \mathbf{E}_0 \widehat{\mathbf{w}}_{L-m+1}^* \quad (6.16)$$

$$\gamma_m \triangleq \rho(\mathbf{w}_m) = \widehat{\gamma}_{L-m+1}. \quad (6.17)$$

We refer to (6.15) as the (canonical) *order-one completion* of (causal) $\mathbf{E}(z)$ of order L , of which the free parameters are embedded in each Θ_m of \mathbf{B}_m as well as in Θ . This is a *complete* parameterization of $\mathbf{E}(z)$ having $\mathbf{p}^T(z)$ as its top row.

Remark: The exact choices of the \mathbf{w}_m are to be dictated by some performance criterion or optimization objective associated with $\mathbf{E}(z)$.

6.4 Completing Linear-Phase Paraunitary Filter Banks

It is shown in Chapter 4 (and also in [6]) that the following specialization of the order-one factorization (2.53) corresponds to M -channel real-coefficient LPPUFBs with M even: for $m = 1, 2, \dots, L$, parameterize the $M \times \frac{M}{2}$ unitary matrix \mathbf{w}_m as

$$\mathbf{w}_m = \frac{1}{\sqrt{2}} \begin{bmatrix} \mathbf{U}_m \\ \mathbf{V}_m \end{bmatrix} \quad (6.18a)$$

and the initial unitary matrix \mathbf{E}_0 as

$$\mathbf{E}_0 = \frac{1}{\sqrt{2}} \begin{bmatrix} \mathbf{U}_0 & \mathbf{U}_0 \mathbf{J} \\ \mathbf{V}_0 & -\mathbf{V}_0 \mathbf{J} \end{bmatrix}, \quad (6.18b)$$

where \mathbf{U}_i and \mathbf{V}_i are $\frac{M}{2} \times \frac{M}{2}$ orthonormal.

To ensure linear phase property of the completed PUFB, both (6.18a) and (6.18b) must be satisfied on top of the order-one completion (6.15). As $\mathbf{p}(z)$ is the polyphase vector of a LPPUFB-admissible scaling filter $H_0(z)$, one can easily show that $\mathbf{p}_0 \triangleq \mathbf{p}(z)|_{z=1}$ always takes the following symmetric form:

$$\|\mathbf{p}_0\|^{-1} \mathbf{p}_0^T = \begin{bmatrix} \hat{\mathbf{u}}_0^T & \hat{\mathbf{u}}_0^T \mathbf{J} \end{bmatrix}, \quad \text{some } \hat{\mathbf{u}}_0 \text{ with } \|\hat{\mathbf{u}}_0\| = \frac{1}{\sqrt{2}},$$

which should be the 0th row of \mathbf{E}_0 in (6.18b). Therefore, it is necessary and sufficient that the unitary sub-matrix \mathbf{U}_0 of \mathbf{E}_0 satisfy

$$\mathbf{e}_0^T \mathbf{U}_0 = \sqrt{2} \hat{\mathbf{u}}_0^T \quad (6.19)$$

in order for the scaling filter of the resulting PUFB to be as prescribed.

Having constrained \mathbf{E}_0 by (6.19), we now proceed to parameterize \mathbf{w}_m in such a way that the condition of order-one completion on $\hat{\mathbf{w}}_{L-m+1}$ in (6.7) holds. As the procedure of

order-one completion calculates $\widehat{\mathbf{w}}_L$ before the others, \mathbf{w}_1 is determined first by (6.16). In particular, assuming \mathbf{E}_0 (or \mathbf{U}_0 and \mathbf{V}_0) has been chosen, it must be true from (6.16) that

$$\begin{bmatrix} \mathbf{U}_1 \\ \mathbf{V}_1 \end{bmatrix} = \begin{bmatrix} \mathbf{U}_0 & \mathbf{U}_0\mathbf{J} \\ \mathbf{V}_0 & -\mathbf{V}_0\mathbf{J} \end{bmatrix} \underbrace{\left[\begin{array}{c|c} \frac{\mathbf{a}_L^0}{\|\mathbf{a}_L\|} & \mathbf{B}_L^0 \\ \hline \frac{\mathbf{a}_L^1}{\|\mathbf{a}_L\|} & \mathbf{B}_L^1 \end{array} \right]}_{\widehat{\mathbf{w}}_L} \quad (6.20)$$

where $\widehat{\mathbf{w}}_L$ has been partitioned into upper and lower $\frac{M}{2}$ rows as shown. As \mathbf{a}_L in $\widehat{\mathbf{w}}_L$ is given, the 0th columns of \mathbf{U}_1 and \mathbf{V}_1 are fixed:

$$\mathbf{U}_1\mathbf{e}_0 = \mathbf{U}_0 \left(\frac{\mathbf{a}_L^0}{\|\mathbf{a}_L\|} + \frac{\mathbf{J}\mathbf{a}_L^1}{\|\mathbf{a}_L\|} \right) \quad (6.21a)$$

$$\mathbf{V}_1\mathbf{e}_0 = \mathbf{V}_0 \left(\frac{\mathbf{a}_L^0}{\|\mathbf{a}_L\|} - \frac{\mathbf{J}\mathbf{a}_L^1}{\|\mathbf{a}_L\|} \right). \quad (6.21b)$$

It remains to ensure that columns of \mathbf{B}_L are orthogonal to both \mathbf{a}_L and \mathbf{a}_0 , as is required by order-one completion of $\mathbf{E}(z)$ given $\mathbf{p}^T(z)$ as the 0th row. The key is to parameterize \mathbf{U}_1 and \mathbf{V}_1 appropriately. Observe that any unitary \mathbf{U}_1 and \mathbf{V}_1 satisfying (6.21) will guarantee $\mathbf{B}_L^T\mathbf{a}_L = \mathbf{0}$ as a result of (6.20). To ensure $\mathbf{B}_L^T\mathbf{a}_0 = \mathbf{0}$, consider augmenting $\widehat{\mathbf{w}}_L$ with $\frac{\mathbf{a}_0}{\|\mathbf{a}_0\|}$ and pre-multiplying by \mathbf{E}_0 :

$$\mathbf{E}_0 \begin{bmatrix} \widehat{\mathbf{w}}_L \\ \frac{\mathbf{a}_0}{\|\mathbf{a}_0\|} \end{bmatrix} = \frac{1}{\sqrt{2}} \begin{bmatrix} \mathbf{U}_1 & \mathbf{u}_1 \\ \mathbf{V}_1 & \mathbf{v}_1 \end{bmatrix} \quad (6.22)$$

where the column vectors \mathbf{u}_1 and \mathbf{v}_1 are given by

$$\mathbf{u}_1 = \mathbf{U}_0 \left(\frac{\mathbf{a}_0^0}{\|\mathbf{a}_0\|} + \frac{\mathbf{J}\mathbf{a}_0^1}{\|\mathbf{a}_0\|} \right) \quad (6.23a)$$

$$\mathbf{v}_1 = \mathbf{V}_0 \left(\frac{\mathbf{a}_0^0}{\|\mathbf{a}_0\|} - \frac{\mathbf{J}\mathbf{a}_0^1}{\|\mathbf{a}_0\|} \right). \quad (6.23b)$$

As the LHS of (6.22) is unitary by construction, so is the RHS. Therefore,

$$\begin{bmatrix} \mathbf{I} & \mathbf{0} \\ \mathbf{0}^T & 1 \end{bmatrix} = \frac{1}{2} \begin{bmatrix} \mathbf{U}_1 & \mathbf{u}_1 \\ \mathbf{V}_1 & \mathbf{v}_1 \end{bmatrix}^T \begin{bmatrix} \mathbf{U}_1 & \mathbf{u}_1 \\ \mathbf{V}_1 & \mathbf{v}_1 \end{bmatrix} \quad (6.24)$$

from which we have

$$\mathbf{U}_1^T \mathbf{u}_1 = -\mathbf{V}_1^T \mathbf{v}_1 \quad (6.25)$$

$$\|\mathbf{u}_1\|^2 + \|\mathbf{v}_1\|^2 = 2. \quad (6.26)$$

Since \mathbf{U}_1 and \mathbf{V}_1 are unitary, we conclude that \mathbf{u}_1 and \mathbf{v}_1 are unit-norm.

As the 0th columns of \mathbf{U}_1 and \mathbf{V}_1 are fixed as in (6.21), one can show that the top-most equation in (6.25) is automatically satisfied as a result of (6.21). In particular, it can be shown that

$$\mathbf{e}_0^T \mathbf{U}_1^T \mathbf{u}_1 = \frac{\mathbf{a}_L^T \mathbf{J} \mathbf{a}_0}{\|\mathbf{a}_L\| \|\mathbf{a}_0\|} = -\mathbf{e}_0^T \mathbf{V}_1^T \mathbf{v}_1.$$

Therefore, it remains to jointly parameterize \mathbf{U}_1 and \mathbf{V}_1 in such a way that $\mathbf{e}_k^T \mathbf{U}_1^T \mathbf{u}_1 = -\mathbf{e}_k^T \mathbf{V}_1^T \mathbf{v}_1$ for $k = 1, 2, \dots, \frac{M}{2} - 1$. This can be achieved by first choosing \mathbf{V}_1 subject to (6.21), and then letting \mathbf{U}_1 depend on it (or vice versa).

Joint Parameterization of \mathbf{U}_1 and \mathbf{V}_1

Suppose \mathbf{V}_1 has been chosen subject to (6.21). Then the RHS of (6.25) is a fixed vector with unit norm. This takes away a few degrees of freedom from \mathbf{U}_1 , and we are interested in identifying the remaining degrees of freedom in \mathbf{U}_1 , for which the Householder matrix is found to be useful. According to (6.25), one can write

$$\mathbf{u}_1 = \mathbf{U}_1(-\mathbf{V}_1^T \mathbf{v}_1) \triangleq \mathbf{U}_1 \mathbf{b}_1.$$

By assumption, \mathbf{b}_1 is known and unit-norm, and can be written as $\mathbf{b}_1 = \mathbf{R}[\mathbf{b}_1] \mathbf{e}_0$. Hence,

$$\mathbf{u}_1 = \mathbf{U}_1 \mathbf{R}[\mathbf{b}_1] \mathbf{e}_0,$$

which implies that the 0th column of $\mathbf{U}_1 \mathbf{R}[\mathbf{b}_1]$ is \mathbf{u}_1 . Applying $\mathbf{R}[\mathbf{u}_1]$ to $\mathbf{U}_1 \mathbf{R}[\mathbf{b}_1]$, we arrive at

$$\mathbf{R}[\mathbf{u}_1] \mathbf{U}_1 \mathbf{R}[\mathbf{b}_1] = \left[\begin{array}{c|c} 1 & \\ \hline & \Phi_1 \end{array} \right]$$

for some $(\frac{M}{2} - 1) \times (\frac{M}{2} - 1)$ unitary matrix Φ_1 which consists of all the remaining degrees of freedom for \mathbf{U}_1 given \mathbf{V}_1 . Therefore, we have shown that \mathbf{U}_1 can be parameterized as

$$\mathbf{U}_1 = \mathbf{R}[\mathbf{u}_1] \cdot \text{diag}(1, \Phi_1) \cdot \mathbf{R}[\mathbf{b}_1] \quad (6.27)$$

once \mathbf{V}_1 has been chosen subject to (6.21). Note that \mathbf{U}_1 and \mathbf{V}_1 so obtained guarantee that $\widehat{\mathbf{w}}_L$ given by

$$\widehat{\mathbf{w}}_L = \frac{1}{2} \begin{bmatrix} \mathbf{U}_0 & \mathbf{U}_0 \mathbf{J} \\ \mathbf{V}_0 & -\mathbf{V}_0 \mathbf{J} \end{bmatrix}^T \begin{bmatrix} \mathbf{U}_1 \\ \mathbf{V}_1 \end{bmatrix} \quad (6.28)$$

is orthonormal and orthogonal to \mathbf{a}_0 as required, with the 0th column being exactly $\frac{\mathbf{a}_L}{\|\mathbf{a}_L\|}$.

Order Reduction

So far, we have parameterized the initial unitary matrix \mathbf{E}_0 and the building block $\mathbf{W}_1(z)$ or $\widehat{\mathbf{W}}_L(z)$ of the order-one completion of $\mathbf{E}(z)$ as in (6.15), while simultaneously imposing the linear phase property. The obtained $\widehat{\mathbf{W}}_L(z)$ is then used to reduce the order of $\mathbf{p}(z)$ by one as described in Theorem 6.1 and [26]. In particular, $\mathbf{p}'(z) \triangleq \widehat{\mathbf{W}}_L(z^{-1}) \mathbf{p}(z)$ will be LPPUFB-admissible with order $L - 1$, and the above procedure is repeated on

$$\mathbf{p}'(z) = \mathbf{a}'_0 + \mathbf{a}'_1 z^{-1} + \dots + \mathbf{a}'_{L-1} z^{-(L-1)}$$

to obtain \mathbf{U}_2 and \mathbf{V}_2 , and so on. Note that once determined in the initial iteration, \mathbf{E}_0 will be used throughout the completion of $\mathbf{E}(z)$. The result is a *complete* parameterization of all LPPUFBs $\mathbf{E}(z)$ having $\mathbf{p}^T(z)$ as its 0th row.

6.5 Completion Examples

6.5.1 General PUFBs

Figure 6-2 shows two completions of PUFBs with an admissible scaling filter $H_0(z)$ taken from some 8×24 GenLOT [41]. Thus, $M = 8$ and $L = 2$. The frequency response magnitude of the PUFB obtained from degree-one completion is shown in Figure 6-2(a) with coding gain 9.17dB and stopband energy 1.16. Note that the impulse response coefficients of $H_i(z)$, $i > 0$, are “concentrated” up front or “minimum-phase,” characteristic of the case when $\text{ord}(\mathbf{E}(z)) = \deg(\mathbf{E}(z))$. On the other hand, the design using the proposed order-one completion with $\gamma_1 = \gamma_2 = 4$ allows for more flexibility and the result is shown in Figure 6-2(b) with coding gain 9.32dB and stopband energy 0.14 — the resulting filter coefficients are more evenly distributed. Obviously, the proposed order-one completion outperforms conventional degree-one completion.

6.5.2 Linear-Phase PUFBs

We demonstrate the proposed theory of LPPUFB completion by considering an eight-channel, length-40 LPPUFB-admissible scaling filter $H_0(z)$ which is shown in Figure 6-3(a) along with the resulting completion. As a comparison, using the same admissible $H_0(z)$, the completion of a general PUFB is shown in Figure 6-3(b) based on the order-one completion introduced in Sec. 6.3, with parameters $M = 8$, $L = 4$, and $\gamma_m = M/2 = 4$, $m = 1, 2, 3, 4$. It is obvious that the proposed PUFB completion does ensure linear phase while guaranteeing $H_0(z)$ as prescribed.

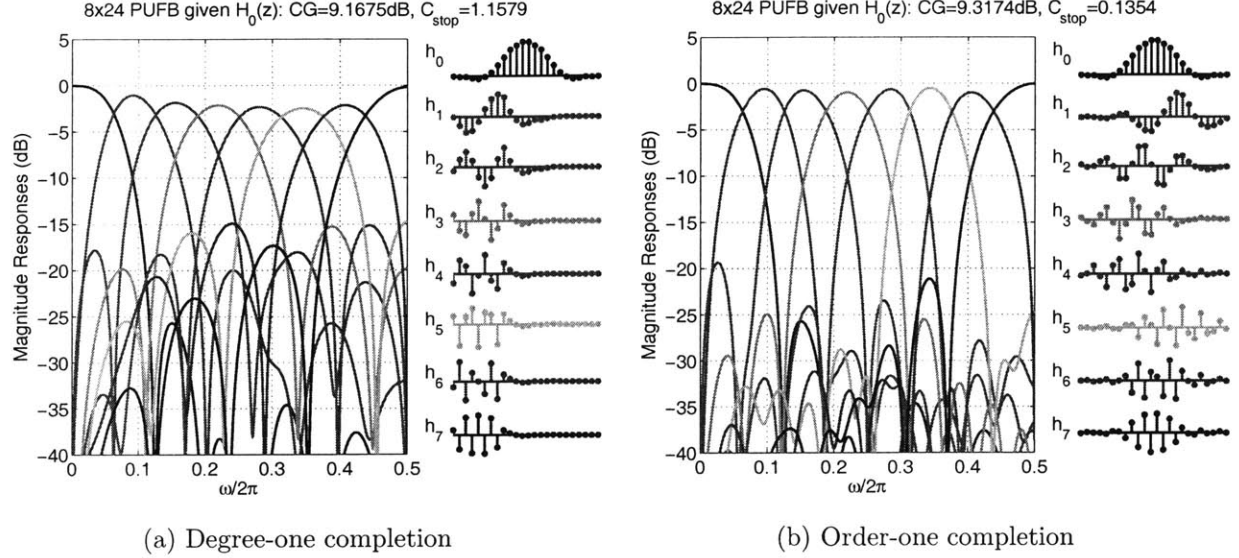


Figure 6-2: Completions of general PUFBs: (a) Coding gain 9.17dB, stopband energy 1.16. (b) Coding gain 9.32dB, stopband energy 0.14.

6.6 Completion As Filter Bank Design Technique

As pointed out by Vaidyanathan *et al.* in [134], filter bank completion can serve to better initialize part of the design parameters. However, as *degree-one* completion was used, the PUFBs that could be completed had the same degree as $H_0(z)$. We demonstrate below how the proposed *order-one* completion helps improve PUFB design.

6.6.1 PUFB Design Based On Order-One Completion

The idea behind *completion-based design approach* is the simplicity of designing a *single* filter, say $H_0(z)$, versus a *bank of them at a time*. The filter $H_0(z)$ so obtained will determine part of the design variables (through its order-one factorization), which provides a good initialization for the entire filter bank as $H_0(z)$ is designed to be a good filter.

The approach begins with designing a good $H_0(z)$ using order-one factorization (6.12). Once a good $H_0(z)$ is obtained, the PUFB can be completed as in (6.13). At this stage, we allow the parameters related to $H_0(z)$ to be re-optimized, and iterate the above completion procedure until a good design is obtained.

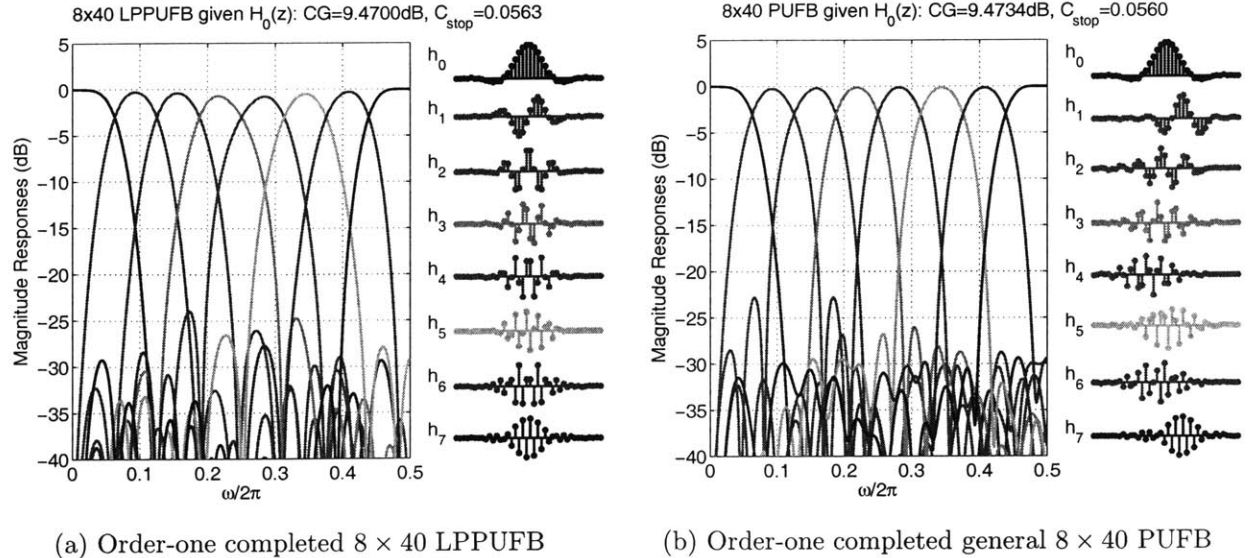


Figure 6-3: Order-one completion of general 8×40 PUFB.

In fact, the completion step (6.13) can be decomposed into $M - 1$ steps corresponding to completing one filter at a time. Again, the idea is that few filters are easier to design than the entire filter bank. This procedure is illustrated below by way of an example.

6.6.2 Examples of Completion-Based Design

Four-channel Design

We consider the design of 4×32 PUFBs with McMillan degree 14, i.e. $\gamma_1 = \dots = \gamma_7 = 2$. This is so chosen because we wish to compare with the cosine-modulated filter banks (CMFB) [108, 129]. Figure 6-4 shows how this completion-based design approach works, starting from one single filter all the way to completion. Notice that the resulting design can serve to initialize other (more difficult) designs, for example, PUFBs with equi-ripple responses, as shown in Figure 6-4(h).

Figure 6-5 compares four design approaches to four-channel PUFBs with length 32 or order 7: (a) order-one completion, (b) degree-one completion, (c) CMFB, and (d) direct approach. Note that (a), (c), and (d) are all degree-14 while (b) is only degree-7 (thus the limited performance of (b)). The proposed completion-based design approach results in the

best design in terms of stopband energy C_{stop} , stopband attenuation C_{att} and coding gain. In particular, it outperforms the CMFB by a significant margin in terms of C_{stop} and C_{att} .

4 × 32 PUFBs: Performance Comparison			
Approach \ Criteria	stopband energy	stopband attenuation	coding gain
Order-one completion-based	4.7e-5	43.7 dB	8.54 dB
Degree-one completion-based	1.5e-3	28.2 dB	8.49 dB
CMFB	6.8e-4	33.3 dB	8.52 dB
Direct	2.4e-3	27.1 dB	8.49 dB

Eight-channel Design

We apply the order-one completion-based approach with $\gamma_1 = \dots = \gamma_5 = 4$ to design an 8×48 PUFB with McMillan degree 20, which is also the degree of an 8×48 CMFB. The results are shown in Figure 6-6.

8 × 48 PUFBs: Performance Comparison			
Approach \ Criteria	stopband energy	stopband attenuation	coding gain
Order-one completion-based	2.1e-3	31.0 dB	9.57 dB
CMFB	6.3e-3	27.8 dB	9.56 dB
Direct	3.5e-2	19.0 dB	9.48 dB

Remark

The completion-based design approach can incorporate filter bank regularity. For example, one degree of regularity can be imposed onto the constant matrix \mathbf{E}_0 , by designing one-regular $H_0(z)$ to begin with. Figures 6-7 and 6-8 show such one-regular designs.

6.7 Concluding Remarks

Complete parameterizations of M -channel PUFBs with a prescribed admissible FIR scaling filter have been proposed based on a novel order-one factorization of the $M \times 1$ polyphase

vector of the scaling filter. In particular, the novel order-one factorization has made possible the completion of PUFBs without degree constraint, resulting in PUFBs with better performance. An important example is the completion of linear-phase PUFBs – impossible under conventional degree-one completion. Furthermore, the proposed order-one completion has been shown to facilitate PUFB design. Examples have been given to demonstrate the proposed theories.

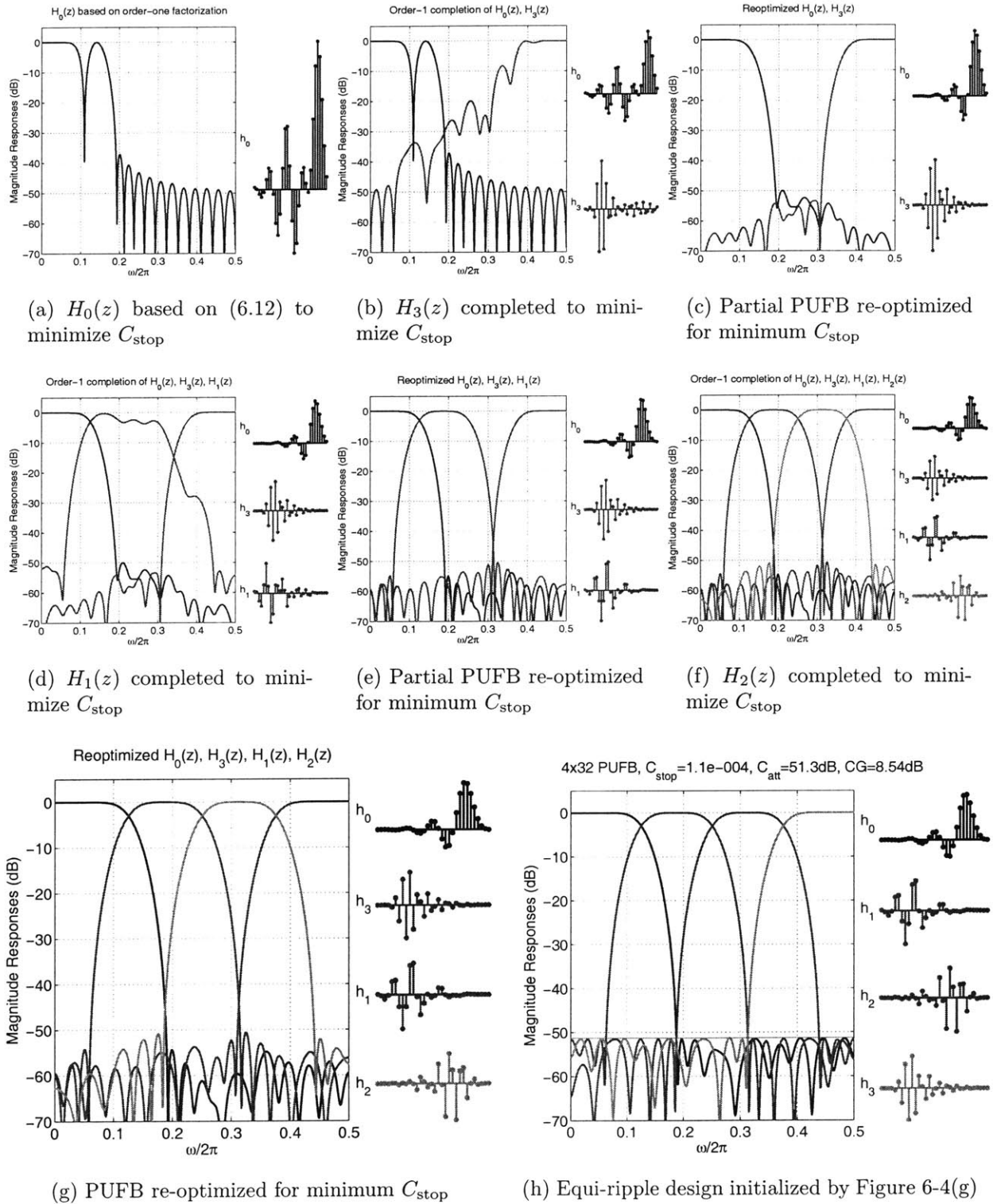


Figure 6-4: Example of PUFB design based on order-one completion

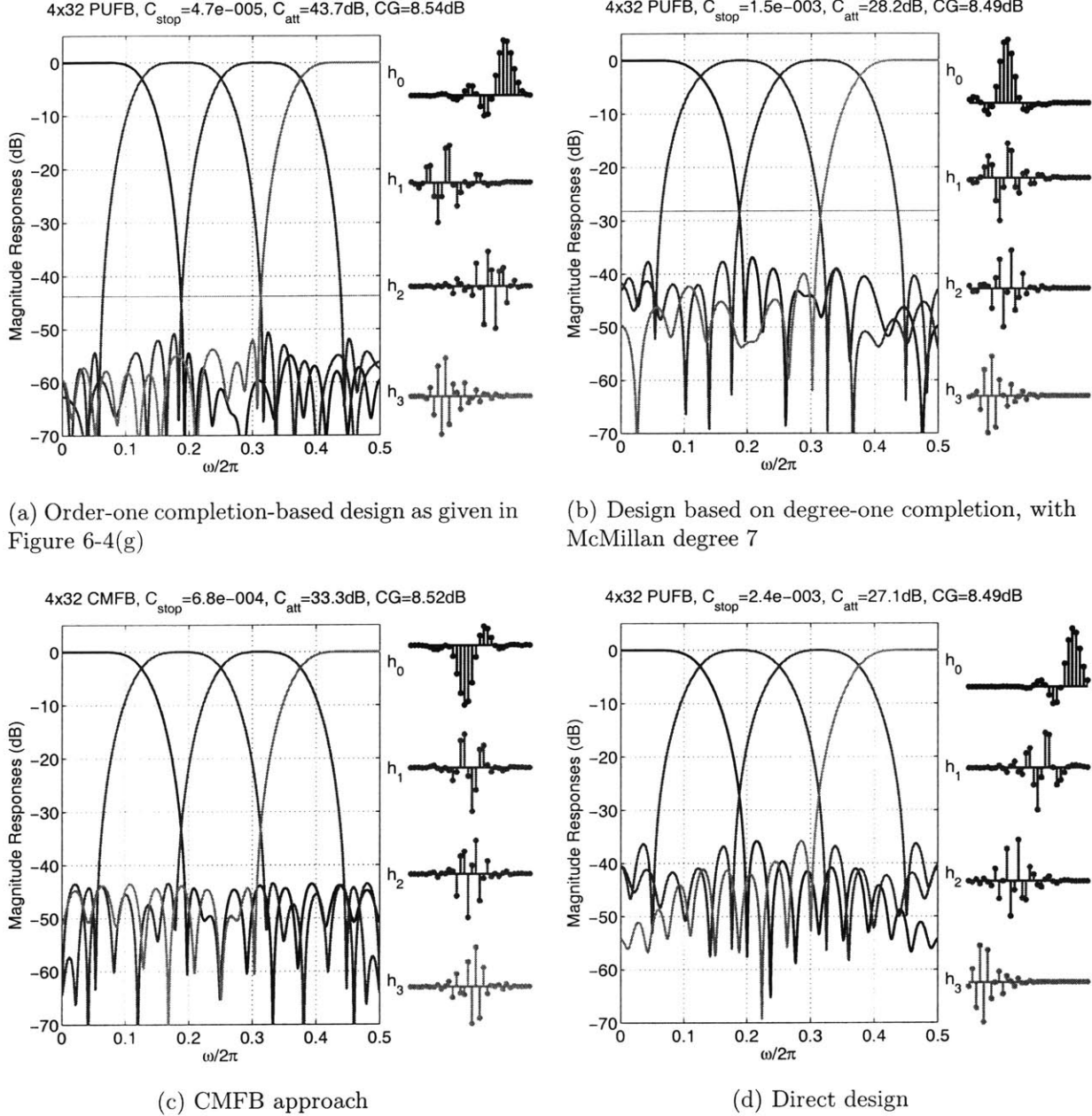
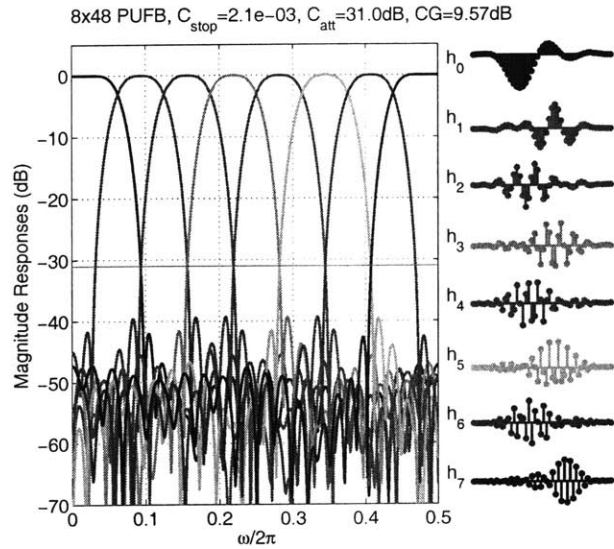
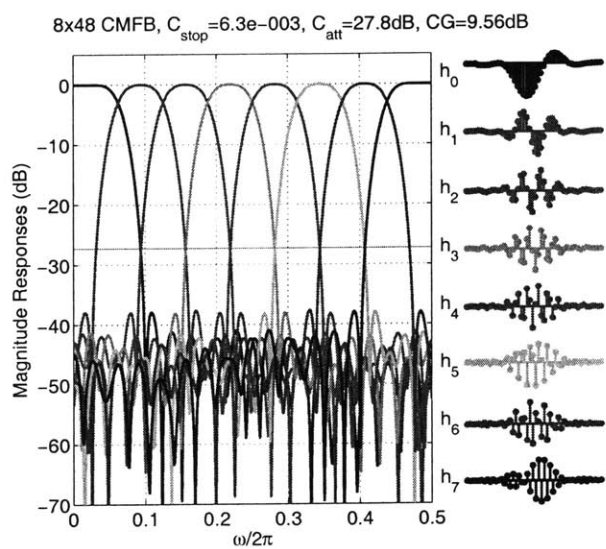


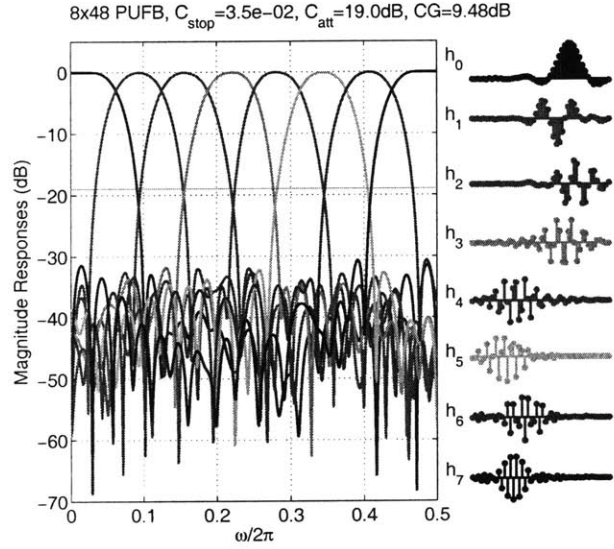
Figure 6-5: Three design approaches to 4×32 PUFBs with McMillan degree 14, along with one which is based on degree-one completion and renders only degree 7. Design objective is to minimize stopband energy C_{stop} . In the figures, C_{att} and CG denote stopband attenuation and coding gain, respectively.



(a) Order-one completion-based design

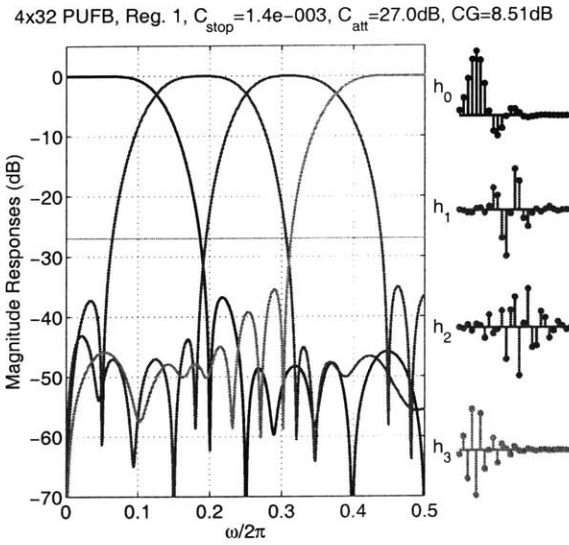


(b) CMFB approach

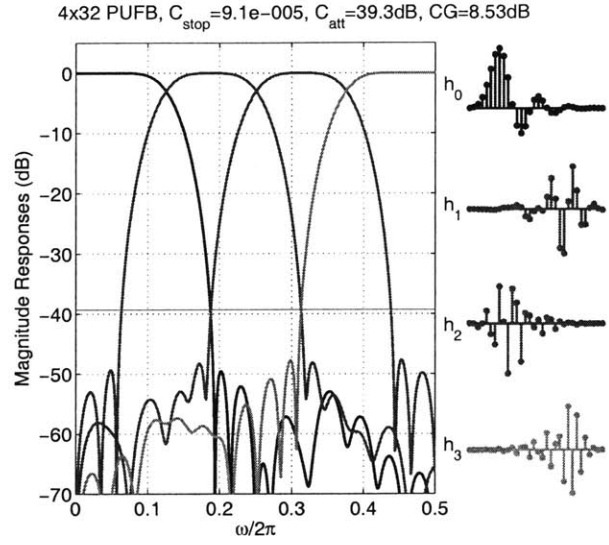


(c) Direct design

Figure 6-6: Comparison of the proposed completion-based approach, the CMFB and the direct approach for designing 8×48 PUFBs, where the design objective is to minimize stopband energy.

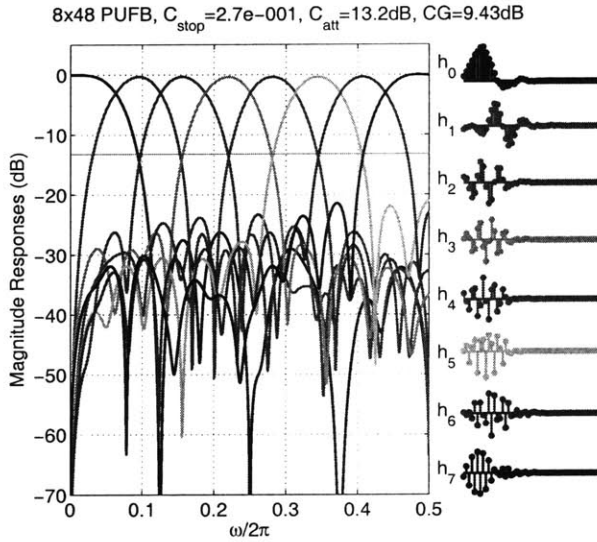


(a) Degree-1 ($\gamma_m = 1$) completion with McMillan degree 7.

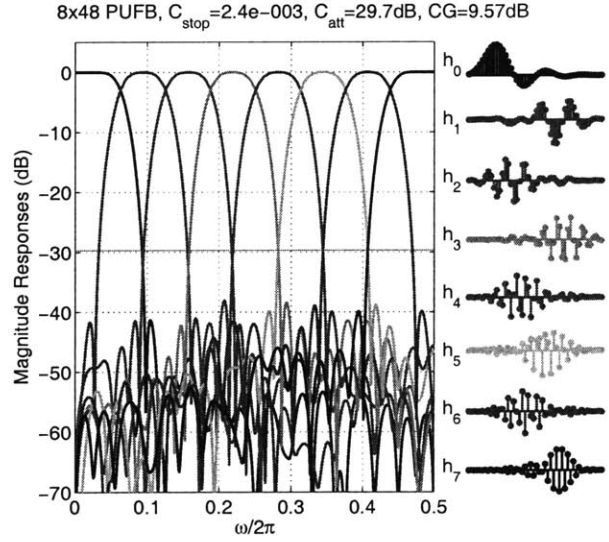


(b) Order-1 ($\gamma_m = 2$) completion with McMillan degree 14.

Figure 6-7: One-regular 4×32 PUFB design based on completion.



(a) Degree-1 ($\gamma_m = 1$) completion with McMillan degree 5.



(b) Order-1 ($\gamma_m = 4$) completion with McMillan degree 20.

Figure 6-8: One-regular 8×48 PUFB design based on completion.

Chapter 7

Low-Power Integer Tranforms via Multiplierless Approximation with Adder Constraint

This chapter describes an algorithm for systematically finding a multiplierless approximation of transforms by replacing floating-point multipliers with VLSI-friendly binary coefficients of the form $k/2^n$. Assuming the cost of hardware binary shifters is negligible, the total number of binary adders employed to approximate the transform can be regarded as an index of complexity. Because the new algorithm is more systematic and faster than trial-and-error binary approximations with adder constraint, it is a much more efficient design tool. Furthermore, the algorithm is not limited to a specific transform; various approximations of the discrete cosine transform (DCT) are presented as examples of its versatility.

7.1 Introduction

Recently there has been increasing interest in approximating a given floating-point transform using only VLSI-friendly binary, multiplierless coefficients of the form $k/2^n$ [2, 18, 22, 30, 66, 91, 118, 152, 154]. Because only binary coefficients are needed, the resulting transform

approximation is multiplierless, and the overall complexity of hardware implementation can be measured in terms of the total number of adders and/or shifters required in the implementation.

Usually, a higher complexity can achieve a higher accuracy. Since the cost of a hardware bit shifter is negligible as compared with that of an adder, the overall complexity can safely be measured by the total number of adders only. Thus, given a total number of adders as the design constraint, it is desirable to come up with a good adder allocation among the various multipliers so that the highest possible accuracy can be achieved. However, little attention has been paid to this issue.

We propose a new algorithm based on quasi-coordinate descent for systematically finding the multiplierless approximation of a given transform. Specifically, the discrete cosine transform (DCT) [100] will be used as an example to illustrate how the algorithm works. Extending this to other transforms is straightforward. Furthermore, the proposed algorithm will be applied on an efficient, sparse representation of the given transform, in order to minimize the number of floating-point multipliers. In particular, the lifting factorization [39, 106, 117] will be the efficient representation of choice. [106] details how to obtain such a lifting-like factorization for an $N \times N$ non-singular constant matrix.

The chapter is organized as follows: Section 7.2 discusses the minimum-adder representation of an integer and the corresponding reducibility issue in terms of adders. These properties are used in Section 7.3 to derive the proposed algorithm for finding the multiplierless approximation of a transform with adder constraint. Two DCT approximation examples are presented in Section 7.4. Section 7.5 concludes the chapter.

7.2 Minimum-Adder Multiplications

7.2.1 Integers

An integer multiplication is equivalent to bit-shifting the multiplicand to the left by different numbers of bits and summing up these bit-shifted versions. The total number of shifts and

adds required can be counted from the binary representation of the integer multiplier. For example, multiplication by $5 = (101)_2$ can be implemented by 1 adder and 1 shift. Similarly, multiplication by $7 = (111)_2$ can be done using 2 adders and 2 shifts. However, this is not the minimum number of adders needed to multiply a number by 7, because if we express

$$7 = 8 - 1 = (1000)_2 - (1)_2$$

it is immediately clear that only 1 adder and 1 shift are required. In essence, this involves the following signed digit representation of numbers [11, 54, 102].

To begin with, let's first introduce the concept of multiplicative irreducibility in terms of adders.

Definition 7.1 (Multiplicative Irreducibility). *A positive integer multiplier X is said to be multiplicatively irreducible in terms of adders if the minimum number of adders required to implement its multiplication is equal to $N_X - 1$ where N_X is the number of 1's in the binary representation of X .*

As a consequence, the following condition on the binary patterns results.

Fact 7.1. A positive integer X is multiplicatively irreducible if and only if its binary representation contains not more than two consecutive 1's, and any pairs of two consecutive 1's are separated by at least two 0's.

The multiplicative irreducibility is important in determining the minimum-adder representation of an integer multiplier, as follows.

Fact 7.2 (Minimum-Adder Representation). An integer X can be decomposed into the following form:

$$X = A - B,$$

where $A, B \in \mathbb{N}$ are multiplicatively irreducible containing N_A and N_B binary 1's, respectively. Furthermore, the minimum number of adders required to implement the multiplication by X is $N_A + N_B - 1$.

Definition 7.2 (Irreducible Form). Given an integer X , the above minimum-adder representation is said to be the irreducible form of X .

Now, to find out the minimum-adder representation of a given integer X , the idea is to look for both

- n consecutive 1's, $n \geq 3$, in the binary representation and
- two groups of n consecutive 1's, $n \geq 2$, separated by only one 0.

For instance, the following number has a group of 3 consecutive 1's and two groups of 4-consecutive 1's:

$$\begin{array}{rcl} X = & \overbrace{1111}^4 00 \overbrace{111}^3 00 \overbrace{1111}^4 & \Rightarrow 10 \text{ adders, } 10 \text{ shifts} \\ & \left. \begin{array}{l} = 10000\ 01000\ 010000 \\ - \quad 100001\ 000001 \end{array} \right\} & \Rightarrow 5 \text{ adders, } 5 \text{ shifts} \end{array}$$

Here is another example:

$$\begin{array}{rcl} X = & \overbrace{1111}^4 0 \overbrace{111}^3 & \Rightarrow 6 \text{ adders, } 6 \text{ shifts} \\ & \left. \begin{array}{l} = 11111\ 000 \\ - \quad 1 \\ = 10000\ 0\ 000 \\ - 1001 \end{array} \right\} & \begin{array}{l} \Rightarrow 5 \text{ adders, } 5 \text{ shifts} \\ \Rightarrow 2 \text{ adders, } 2 \text{ shifts} \end{array} \end{array}$$

7.2.2 Binary Fractions

A binary fractional multiplier of the form $\pm k/2^b$, $k, b \in \mathbb{N}$, k odd, can also be implemented using only integer arithmetic. The multiplicand is first multiplied by $\pm k$ and the result is right-shifted by b bits. Therefore, in our set-up, the minimum number of adders required for implementing a given binary fraction is equal to that for implementing its numerator.

7.3 Adder-Constrained Multiplierless Approximation Algorithm

Let T denote the given transform of interest whose sparse matrix factorization consists of M (usually floating-point) multipliers λ_i , $i = 1, 2, \dots, M$. Equivalently, T can be thought of as being parameterized by these λ_i :

$$T = T(\lambda_1, \lambda_2, \dots, \lambda_M). \quad (7.1)$$

Usually, such sparse factorizations of T are not unique, and one is preferred whenever all the λ_i satisfy $|\lambda_i| \leq 1$. These multipliers are usually floating-point numbers. Let $[\lambda]_p$ denote the best achievable binary (fractional) approximation of λ with only p adders. Specifically, if

$$[\lambda_i]_{n_i} = \pm \frac{k_i}{2^{b_i}}, \quad i = 1, 2, \dots, M,$$

where $b_i \in \mathbb{N}$ and k_i is odd, then the irreducible form of k_i contains a total of $(n_i + 1)$ binary 1's. Call $[\lambda]_n$ the n -adder binary approximation, or n -ABA, of λ .

7.3.1 Finding the n -ABA

To compute the n -ABA, $[\lambda]_n$, of some floating-point number λ , its binary representation

$$k_b/2^b, \quad k_b \in \mathbb{Z}, \quad b \in \mathbb{N},$$

is first calculated with a sufficient precision, namely, with b large enough, depending on the dynamic range of n . Then based on the irreducible form of $|k_b|$,

$$|k_b| = A_{k_b} - B_{k_b},$$

a positive integer m is determined such that the total number of 1's in the binary representations of integers

$$\left\lfloor \frac{A_{k_b}}{2^m} \right\rfloor \text{ and } \left\lfloor \frac{B_{k_b}}{2^m} \right\rfloor$$

is equal to $n + 1$. Then the n -ABA of λ is given by

$$[\lambda]_n = \text{sgn}(\lambda) \left(\left\lfloor \frac{A_{k_b}}{2^m} \right\rfloor - \left\lfloor \frac{B_{k_b}}{2^m} \right\rfloor \right) 2^{m-b}. \quad (7.2)$$

7.3.2 Quasi-Coordinate Descent

In (7.1), if all the λ_i are replaced by the respective n_i -ABA's, $[\lambda_i]_{n_i}$, the resulting transform

$$\widehat{T} = T([\lambda_1]_{n_1}, [\lambda_2]_{n_2}, \dots, [\lambda_M]_{n_M})$$

becomes a multiplierless approximation of the original T . In this case, the minimum number of adders required to implement \widehat{T} , $N_{\widehat{T}}$, is given by

$$N_{\widehat{T}} = N_0 + \sum_{i=1}^M n_i,$$

where N_0 is the number of “basic” adders associated with the particular sparse matrix factorization structure used to parameterize T . In other words, N_0 is the number of the adders that remain when all the λ_i in T are set to zero, which corresponds to configurations C9 in Tables 7.1 & 7.2. The significance of N_0 should become clear in Section 7.4 where sparse factorizations of the DCT are presented.

Now, the goal is to find a good adder allocation, subject to the given signal statistics and a given value of $N_{\widehat{T}}$. Two common performance measures defining a good adder allocation are: (a) the transform coding gain of \widehat{T} and (b) the MSE between the outputs of T and \widehat{T} .

Let Φ denote the performance measure, defined over the same parameter space as \widehat{T} . Then, based on the chosen Φ , the proposed algorithm to find the optimal adder allocation (assuming $N_{\widehat{T}} \geq N_0$) is given as follows:

```

1: Initialize all  $n_i = 0$ 
2: for  $j = 1, 2, \dots, (N_{\widehat{T}} - N_0)$ 
3:   for  $i = 1, 2, \dots, M$ 
4:      $\rho_i = \Phi([\lambda_1]_{n_1}, [\lambda_2]_{n_2}, \dots, [\lambda_i]_{n_i+1}, \dots, [\lambda_M]_{n_M})$ 
5:   end
6:    $i^* = \arg \min_{i=1}^M \{\rho_i\}$  or  $i^* = \arg \max_{i=1}^M \{\rho_i\}$ 
7:    $n_{i^*} := n_{i^*} + 1$ 
8: end

```

The algorithm begins with a given value of $N_{\widehat{T}}$, which serves as the adder constraint, with all the multipliers initialized to zero ($n_i = 0$). Then, in each iteration (indexed by j), the most “effective” multiplier (λ_{i^*}) is identified and is assigned one more adder ($n_{i^*} := n_{i^*} + 1$) to increase its accuracy. This is repeated until all the $N_{\widehat{T}}$ adders are exhausted.

Upon termination of the algorithm, the final n_i represent the desired adder allocation. Note that the proposed algorithm completes in a finite number of steps equal to the number of the excess adders ($N_{\widehat{T}} - N_0$). Also, the choice in Step 6 depends on the performance measure Φ . For example, we wish to minimize the MSE, while maximizing the coding gain. In essence, given one more adder to the intermediate system at stage j , the deepest coordinate descent direction is found and the added adder is allocated to the corresponding multiplier.

7.3.3 Adaptation to Lifting Structures

The lifting structure [39], as shown in Figure 7-1, will be used exclusively in this chapter for the factorization of the DCT kernel. Now, all the λ_i in (7.1) are the lifting multipliers, and it is immediately clear that if some λ_i is zero, the corresponding lifting step and hence the associated adder will vanish.

To take this into account, the proposed algorithm is modified by initializing all the n_i to -1 and defining $[\lambda_i]_{-1} \equiv 0$. With these modifications, the lifting-adapted algorithm is then given below:

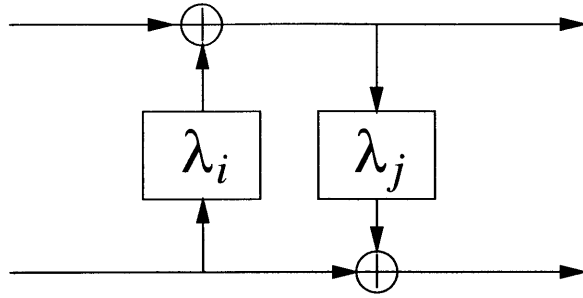


Figure 7-1: The lifting structure, used exclusively in the design examples of the proposed algorithm, consists of several one-wing butterflies with multipliers λ . The adder \oplus will effectively vanish if the corresponding λ_i or λ_j is zero.

```

1: Initialize all  $n_i = -1$ 
2: for  $j = -(M - 1), \dots, -1, 0, 1, 2, \dots, (N_{\widehat{T}} - N_0)$ 
3:   for  $i = 1, 2, \dots, M$ 
4:      $\rho_i = \Phi([\lambda_1]_{n_1}, [\lambda_2]_{n_2}, \dots, [\lambda_i]_{n_{i+1}}, \dots, [\lambda_M]_{n_M})$ 
5:   end
6:    $i^* = \arg \min_{i=1}^M \{\rho_i\}$  or  $i^* = \arg \max_{i=1}^M \{\rho_i\}$ 
7:    $n_{i^*} := n_{i^*} + 1$ 
8: end

```

7.4 Design Examples

In this section, the discrete cosine transform (DCT) is selected to demonstrate how the proposed algorithm works. A lifting-like factorization of the DCT is considered. Throughout this section, it is assumed that the input signal to the DCT is an AR(1) process with $\rho = 0.95$ and unit variance.

7.4.1 IntDCT

In [30], a Walsh-Hadamard-based factorization of the DCT was used and each of the resulting rotation angles was lifted. Figure 7-2 illustrates how the DCT kernel is factored in this case: there are $M = 15$ multipliers, p_i and u_j , for $1 \leq i \leq 10$ and $1 \leq j \leq 5$. The minimum number

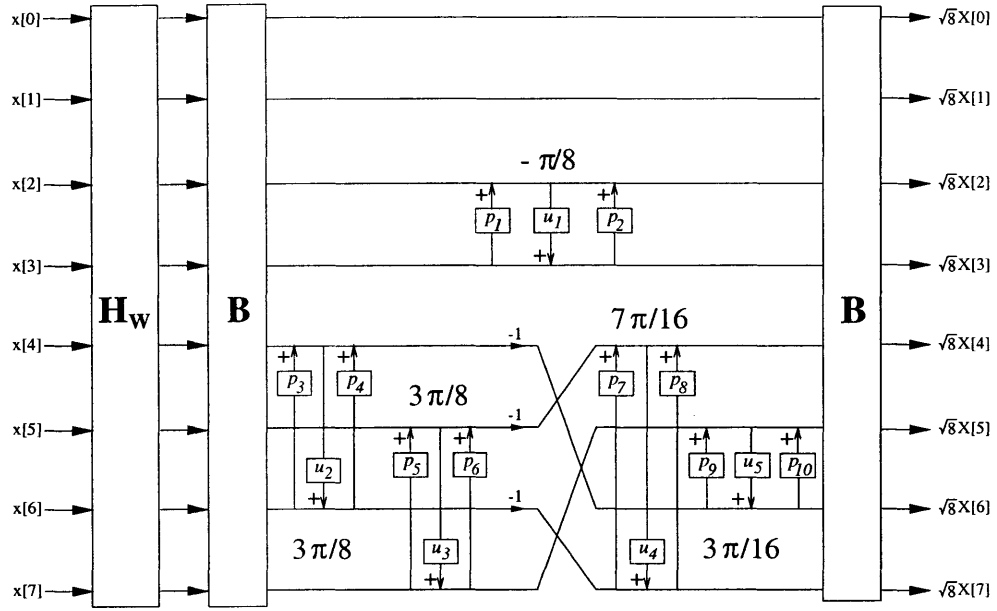


Figure 7-2: The IntDCT parameterized by p_i and u_j . \mathbf{H}_w is the Walsh-Hadamard transform and \mathbf{B} is bit-reversal. $N_0 = 24$ is the number of the adders that remain when all the p_i and u_j are set to zero. Actually, these are the adders internal to \mathbf{H}_w .

of adders $N_0 = 24$, which is the number of the remaining adders when all the p_i and u_j are set to zero. Table 7.1 shows the results of the IntDCT-based multiplierless approximations of the DCT with various adder constraints. The MSE was chosen as the performance measure. As a comparison, the configuration reported in [30, 152] requires 45 adds and 18 shifts with $MSE=1.2e-3$, while the MSE of configuration C1 in Table 7.1 is only $8.6e-4$. C2 – C8 are our new designs. Note that configuration C9 is nothing but the Walsh-Hadamard Transform. The IntDCT has uniform scaling of each subband, which is helpful in applications such as embedded coding, because no coefficient re-alignment is required.

7.4.2 BinDCT

Figure 7-3 shows the structure of the BinDCT proposed in [66, 118], with $N_0 = 18$. The proposed algorithm is also applied to this factorization structure of the DCT, and these BinDCT-based multiplierless approximations are shown in Table 7.2 with various adder

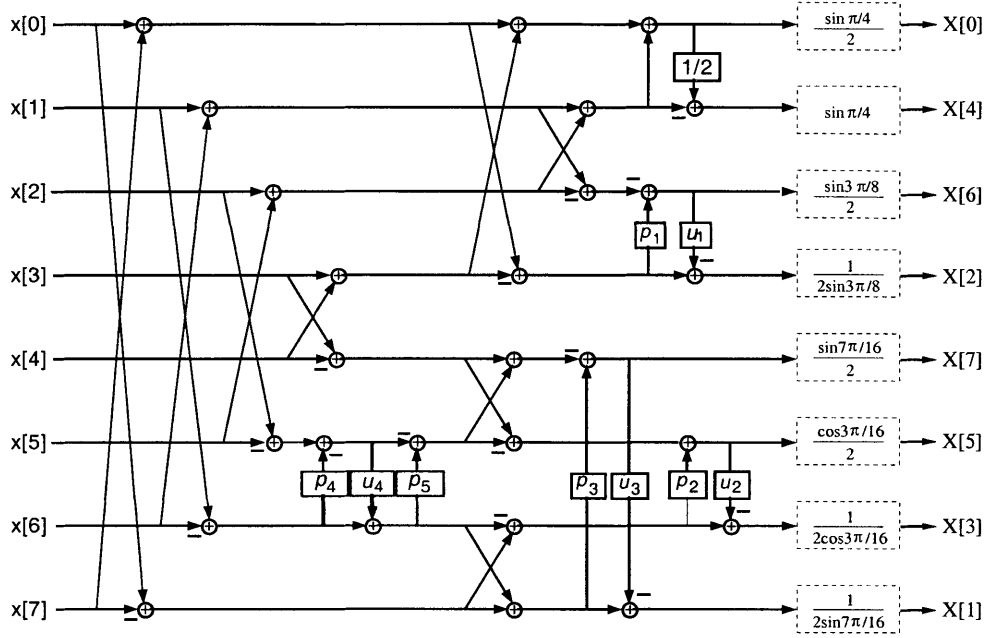


Figure 7-3: The BinDCT parameterized by p_i and u_j . $N_0 = 18$ is the number of the adders that remain when all the p_i and u_j are set to zero.

constraints. The MSE was used as the performance measure. Our algorithm results in a better MSE performance (C2 – C8) than was reported in [66, Table II] at the same adder constraints (except C1 for which the MSE was $1.1e-5$ as reported in [66, Table II]), which confirms the effectiveness of our algorithm.

In both examples, one can observe that the MSE decreases monotonically with the increased number of adders. Our new designs in Tables 7.1 and 7.2 yield lower MSE as compared with previous solutions presented in [30, 66].

7.5 Conclusions

A quasi-coordinate descent algorithm has been presented for systematically finding, with adder constraint, a multiplierless approximation of transforms. Based on a particular sparse matrix factorization used, the given transform is parameterized by a few (floating-point) multipliers in terms of which a performance measure is formed, and the proposed algorithm

finds the binary approximations of the (floating-point) multipliers using only a finite number of evaluations and comparisons of the performance measure, and therefore good approximations are readily available even in the case where exhaustive search becomes intractible. When necessary, the resulting binary approximations may serve as the initial conditions for other more sophisticated approximation algorithms. Because the new algorithm is more systematic and faster than trial-and-error adder-constrained binary approximations, it manifests itself as a more efficient design tool. Furthermore, the algorithm is not limited to a specific transform; various multiplierless approximations of the DCT have been presented to demonstrate its versatility.

Table 7.1: Proposed multiplierless approximations of the DCT based on the IntDCT structure, with various adder constraints. C1 has better MSE performance than was previously published at the same adder constraint. C2 – C8 are our new designs.

	Floating-pt	C1	C2	C3	C4	C5	C6	C7	C8	C9
p_1	.1989123	1/8	1/8	1/8	0	0	0	0	0	0
u_1	-.3826834	-3/8	-1/4	-1/4	-1/4	-1/4	-1/4	0	0	0
p_2	.1989123	1/8	0	0	0	0	0	0	0	0
p_3	-.6681786	-5/8	-5/8	-1/2	-1/2	-1/2	-1/2	-1/2	-1/2	0
u_2	.9238795	1	1	1	1	1	1	1	0	0
p_4	-.6681786	-5/8	-5/8	-5/8	-5/8	-1/2	-1/2	-1/2	-1/2	0
p_5	-.6681786	-1/2	-1/2	-1/2	-1/2	-1/2	-1/2	-1/2	0	0
u_3	.9238795	1	1	1	1	1	1	0	0	0
p_6	-.6681786	-5/8	-1/2	-1/2	-1/2	-1/2	-1/2	0	0	0
p_7	-.8206787	-13/16	-13/16	-3/4	-3/4	-3/4	-3/4	-3/4	-1/2	0
u_4	.9807852	1	1	1	1	1	1	1	0	0
p_8	-.8206787	-1/2	-1/2	-1/2	-1/2	-1/2	-1/2	-1/2	-1/2	0
p_9	-.3033466	-1/4	-1/4	-1/4	-1/4	0	0	0	0	0
u_5	.5555702	1/2	1/2	1/2	1/2	1/2	1/2	1/2	0	0
p_{10}	-.3033466	-1/4	-1/4	-1/4	-1/4	-1/4	0	0	0	0
Shifts	-	9	6	4	3	2	2	2	0	0
Adds	-	45	42	40	39	37	36	33	28	24
MSE	-	8.6e-4	1.7e-3	2.5e-3	3.0e-3	6.0e-3	8.5e-3	1.9e-2	8.4e-2	1.6e-1
CG	-	8.735	8.680	8.586	8.571	8.334	8.021	7.829	6.936	7.946

Table 7.2: Proposed multiplierless approximations of the DCT based on the BinDCT structure, with various adder constraints. The MSE performance (C2 – C8) is better than that previously published at the same adder constraints, except for C1.

	Floating-pt	C1	C2	C3	C4	C5	C6	C7	C8	C9
p_1	.4142135	13/32	13/32	13/32	3/8	3/8	3/8	1/4	1/4	0
u_1	.3535533	11/32	5/16	5/16	5/16	5/16	1/4	1/4	0	0
p_2	.6681786	21/32	21/32	21/32	5/8	5/8	5/8	1/2	1/2	0
u_2	.4619397	15/32	1/2	1/2	1/2	1/2	1/2	1/2	1/2	0
p_3	.1989123	3/16	3/16	3/16	3/16	3/16	3/16	1/8	0	0
u_3	.1913417	3/16	3/16	1/8	1/8	1/8	1/8	0	0	0
p_4	.4142135	13/32	13/32	13/32	13/32	3/8	3/8	3/8	1/4	0
u_4	.7071067	11/16	11/16	11/16	11/16	11/16	5/8	1/2	1/2	0
p_5	.4142135	13/32	13/32	13/32	13/32	13/32	3/8	3/8	1/4	0
Shifts	-	25	23	22	20	19	16	11	7	1
Adds	-	42	40	39	37	36	33	28	24	18
MSE	-	1.3e-5	3.0e-5	4.0e-5	8.4e-5	1.2e-4	3.3e-4	1.4e-3	4.2e-3	2.9e-2
CG	-	8.824	8.820	8.819	8.815	8.813	8.795	8.701	8.556	7.920

Chapter 8

Conclusion and Future Work

8.1 Summary

In this thesis, we have focused on the factorization aspects of a perfect reconstruction filter bank, including M -channel lifting factorization and the factorizations using dyadic-based structures. Completing the factorization given the scaling filter $H_0(z)$ is also studied and is shown to improve on the frequency selectivity and energy compaction of the filter bank.

The M -channel lifting factorization allows for fast, in-place, reversible, and possibly integer implementations of any perfect reconstruction filter bank. A systematic approach to computing the lifting factors was described. The algorithm is complete in the sense that every perfect reconstruction filter bank can be so decomposed, and that any lifting factorization corresponds to a perfect reconstruction filter bank. It is found that the lifting structures can be used for the benefit of imposing regularity, which is an important property and relates to the smoothness of the wavelet basis and its approximation accuracy. Lifting solutions of special filter banks are obtained, including paraunitary, unimodular, a class of biorthogonal filter banks, the DCT, etc., providing a robust, possibly multiplierless, implementation option that enforces perfect reconstruction even under finite precision. For this purpose, the proposed Monic Euclidean algorithm always ensures unity diagonal scaling of all the lifting factors, which allows reversibility under finite precision. For optimal integer

implementation under the lifting context, an algorithm for optimally approximating the filter bank using only integer arithmetic is proposed. This algorithm complements the M -channel lifting factorization for multiplierless implementations and approximations.

Of particular interest is the structural imposition of regularity onto factorizations based on the dyadic form \mathbf{uv}^\dagger . Theories of structural regularity were developed that guarantee the resulting filter banks possess the desired degree of regularity, regardless of the choice of free parameters in the filter bank structure. As regularity is robustly enforced, we can use *unconstrained* optimizations to efficiently design regular filter banks subject to desired performance criteria such as stopband energy and coding gain. High-performance regular filter banks were obtained with improved frequency selectivity and superior coding gain within 0.1% of the optimum. As our designs focus on greater energy compaction, smoother reconstructions and the ability to preserve texture details, the benchmarks conducted on image compression applications show clear improvements in perceptual and objective performance, while existing designs in the literature either over-smooth the texture regions of the image or exhibit blocking artifacts to some extent. Remarkably, our regular filter banks outperform JPEG2000 and the FBI/WSQ standard for fingerprint compression.

The linear phase aspect of dyadic-based structures was studied as well. We showed how they can be specialized to ensure phase linearity of the system. This also leads naturally to a simplified parameterization of the resulting linear-phase filter banks, using only approximately 50% of the original parameters while spanning the same design space. The result is efficiency in design and implementation of linear-phase filter banks using dyadic-based structures.

We have also considered the problem of multi-channel filter bank completion given only the scaling filter. M -channel lifting factorization is effective in completing M -channel biorthogonal filter banks; a B-spline example was given. On the other hand, we proposed a novel order-one factorization which allows greater design flexibility, resulting in an improved completion scheme for paraunitary filter banks. It enables the designer to allocate more degrees of freedom for expressing the scaling filter, and thus improves upon the conventional

degree-constrained counterpart. A special version of the proposed order-one factorization guarantees PUFB completion with linear phase, which is not possible for the conventional approach. Improved frequency selectivity and energy compaction over existing state of the art methods are demonstrated. Note that the technique can be applied in a dual setting to transmultiplexer design to achieve higher-rate data transmission subject to a fixed error rate and transmission power.

8.2 Future Directions

We note below some possible future directions:

Complex-valued wavelets and filter banks By allowing the filters to be complex-valued, one can obtain more design flexibility. For example, a study by Gao *et al.* [53] shows that orthogonality and filter symmetry can be simultaneously achieved for two-channel complex-valued filter banks, which is known to be impossible for two-channel real-valued filter banks except trivial cases. Complex-valued filter banks can benefit applications such as synthetic aperture radar (SAR), communications, medical imaging, etc. where the signals are complex-valued in nature.

Improved lifting scheme with reduced approximation error In [55], a “vectorized” version of lifting is proposed for a special class of filter banks whose polyphase matrices are constant and block-diagonal of the form $\mathbf{E}(z) = \text{diag}\{\mathbf{T}, \mathbf{T}^{-1}\}$ where \mathbf{T} is non-singular. The conventional two-channel lifting result is then generalized to this case to obtain

$$\mathbf{E}(z) = \begin{bmatrix} \mathbf{T} & \\ & \mathbf{T}^{-1} \end{bmatrix} = \begin{bmatrix} -\mathbf{I} & \mathbf{0} \\ \mathbf{T}^{-1} & \mathbf{I} \end{bmatrix} \begin{bmatrix} \mathbf{I} & -\mathbf{T} \\ \mathbf{0} & \mathbf{I} \end{bmatrix} \begin{bmatrix} \mathbf{0} & \mathbf{I} \\ \mathbf{I} & \mathbf{T}^{-1} \end{bmatrix}.$$

For integer approximations with reduced error, the innovation here is to round to integers the matrix multiplication results of \mathbf{T}^{-1} , $-\mathbf{T}$ and \mathbf{T}^{-1} coming from the three “vectorized” lifting steps. Namely, we do not lift each individual \mathbf{T}^{-1} and $-\mathbf{T}$. In this way, the number of rounding operations is reduced, and so is the integer approximation

error (due to rounding). The Modified DCT (MDCT) is such an example which is discussed in detail in [55]. It would be interesting to develop similar techniques for arbitrary filter banks to improve the accuracy of their integer approximations.

Characterization of unimodular filter banks Recall that a unimodular filter bank is one whose polyphase matrix has a constant determinant, having no z dependency. The theoretical minimum system delay, $M - 1$, of an M -channel filter banks is achieved by unimodular filter banks, irrespective of the filter lengths. This is essential for real-time applications which require low latency of signal processing. Furthermore, another (theoretical) significance of unimodular matrices is that the *entire* space of biorthogonal filter banks can be *completely* parameterized as a cascade of paraunitary and unimodular systems [128, 132], although it is nontrivial to characterize all unimodular matrices [128, 132].

Note that the lifting steps are unimodular in nature, with determinants ± 1 . Therefore, it would be interesting to construct a class of useful unimodular filter banks using the lifting structures.

Numerical applications Two-channel wavelet-based hierarchical approaches have been successfully applied to numerical solutions of PDE, by providing an efficient scheme for incremental solution refinement. Extending this idea, M -band wavelets would provide a more flexible refinement scheme. However, the scaling functions may not have a closed-form expression for the benefit of numerical solutions of PDE. The M -band B-spline filter banks based on the proposed filter bank completion technique feature *closed-form* expressions of the resulting M -band wavelet basis. It would be of practical interest and importance to study how a suitably constructed M -band B-spline filter bank influences the numerical solution of PDE, exploiting the greater flexibility in solution refinement.

Bibliography

- [1] S. Aase and T. Ramstad, “On the optimality of nonunitary filter banks in subband coders,” *IEEE Trans. Image Processing*, vol. 4, no. 12, pp. 1585–1591, Dec. 1995.
- [2] M. Adam and F. Kossentni, “Reversible integer-to-integer wavelet transforms for image compression: performance evaluation and analysis,” *IEEE Trans. Image Processing*, vol. 9, pp. 1010–1024, Jun. 2000.
- [3] A. Akansu and R. Haddad, *Multiresolution Signal Decomposition: Transforms, Subbands and Wavelets*. Academic Press, 2001.
- [4] K. Amaratunga, “A wavelet-based approach for compressing kernel data in large-scale simulations of 3D integral problems,” *IEEE Computing in Science and Engineering*, vol. 2, no. 4, pp. 34–45, 2000.
- [5] K. Amaratunga and J. Castrillón-Candás, “Surface wavelets: A multiresolution tool for 3D computational modelling,” *Int'l J. Numer. Meth. Eng.*, vol. 52, no. 3, pp. 239–271, 2001.
- [6] K. Amaratunga, Y.-J. Chen, and S. Oraintara, “Characterization of regular linear-phase paraunitary filter banks using dyadic-based structures,” in *Proc. IEEE Int'l Symp. Circuits Syst.*, May 2004.
- [7] K. Amaratunga, R. Sudarshan, and S. D'Heedene, “Multiresolution finite element methods based on wavelet and subdivision theory,” in *Proceedings of the VII U.S National Congress on Computational Mechanics*, Jul. 2003.
- [8] K. Amaratunga and J. Williams, “Wavelet-galerkin solution of boundary value problems,” *Archives of Computational Methods in Engineering*, vol. 4, no. 3, pp. 243–285, 1997.
- [9] K. Amaratunga, “MIT 1.130/18.327 lecture notes—Wavelets and Multiscale Methods in Engineering Computation and Information Processing.” [Online]. Available: <http://web.mit.edu/1.130>
- [10] AD12400, a 12-bit, 400 MSPS, analog-to-digital converter. [Online]. Available: <http://products.analog.com/products/info.asp?product=AD12400>

- [11] A. Avizienis, “Signed-digit number representations for fast parallel arithmetic,” *IRE Trans. Electronic Computers*, vol. 10, pp. 389–400, 1961.
- [12] S. Beheshti and M. A. Dahleh, “New information theoretic approach to signal denoising and best basis selection,” *IEEE Trans. Signal Processing*, submitted.
- [13] D. P. Bertsekas, *Nonlinear Programming*, 2nd ed. Belmont, MA: Athena Scientific, 1999.
- [14] G. Beylkin, “On the representation of operators in bases of compactly supported wavelets,” *SIAM J. Numer. Anal.*, vol. 6, no. 6, pp. 1716–1740, Dec. 1992.
- [15] G. Beylkin, R. Coifman, and V. Rokhlin, “Fast wavelet transforms and numerical algorithms I,” *Comm. Pure Appl. Math.*, vol. 44, pp. 141–183, 1991.
- [16] M. Bhatia, W. Karl, and A. Willsky, “Tomographic reconstruction and estimation based on multiscale natural-pixel bases,” *IEEE Trans. Image Processing*, vol. 6, no. 3, pp. 463–478, Mar. 1997.
- [17] S. Bhunia and K. Roy, “Fault detection and diagnosis using wavelet based transient current analysis,” in *ACM Design, Automation, and Test in Europe*, 2002, p. 1118. [Online]. Available: http://www.sigda.org/Archives/ProceedingArchives/Date/papers/2002/date0%2/pdffiles/p1d_3.pdf
- [18] F. A. M. L. Bruekers and A. W. M. van den Enden, “New networks for perfect inversion and perfect reconstruction,” *IEEE J. Select. Areas Commun.*, vol. 10, no. 1, Jan. 1992.
- [19] C. Burrus, R. Gopinath, and H. Guo, *Introduction to Wavelets and Wavelet Transforms: A Primer*. Prentice Hall, 1998.
- [20] R. Calderbank, I. Daubechies, W. Sweldens, and B.-L. Yeo, “Wavelet transforms that map integers to integers,” *Appl. Comput. Harmon. Anal.*, vol. 5, no. 3, pp. 332–369, 1998.
- [21] J. Castrillón-Candás and K. Amaratunga, “Spatially adapted multiwavelets and sparse representation of integral operators on general geometries,” *SIAM Journal on Scientific Computing*, vol. 24, no. 5, pp. 1530–1566, 2003.
- [22] S. C. Chan, W. Liu, and K. L. Ho, “Multiplierless perfect reconstruction modulated filter banks with sum-of-powers-of-two coefficients,” *IEEE Signal Processing Lett.*, vol. 8, no. 6, pp. 163–166, Jun. 2001.
- [23] T. Chang and C.-C. Kuo, “Texture analysis and classification with tree-structured wavelet transform,” *IEEE Trans. Image Processing*, vol. 2, no. 4, pp. 429–441, Oct. 1993.

- [24] C.-H. Chen, J.-S. Lee, and Y.-N. Sun, “Wavelet transformation for gray-level corner detection,” *Patt. Recog.*, vol. 28, no. 6, pp. 853–861, 1995.
- [25] Y.-J. Chen and K. Amaratunga, “ M -channel lifting factorization of perfect reconstruction filter banks and reversible M -band wavelet transforms,” *IEEE Trans. Circuits Syst. II*, Dec. 2003.
- [26] ——, “On completion of M -channel perfect reconstruction filter banks with prescribed admissible FIR scaling filter,” in *Proc. IEEE Int'l Symp. Circuits Syst.*, May 2004.
- [27] Y.-J. Chen, S. Oraintara, and K. Amaratunga, “ M -channel lifting-based design of paraunitary and biorthogonal filter banks with structural regularity,” in *Proc. IEEE Int'l Symp. Circuits Syst.*, May 2003.
- [28] ——, “Dyadic-based structure for regular biorthogonal filter banks with linear phase,” in *Proc. IEEE Int'l Conf. Acoust., Speech, Signal Processing*, May 2004.
- [29] Y.-J. Chen, S. Oraintara, and T. Nguyen, “Integer discrete cosine transform (Int-DCT),” in *the 2nd Int'l Conf. Info. Comm. Signal Processing*. Singapore: Invited paper, Dec. 1999.
- [30] Y.-J. Chen, S. Oraintara, and T. Q. Nguyen, “Video compression using integer DCT,” in *IEEE Int'l Conf. Image Processing*, vol. 2, Vancouver, Canada, Sep. 2000, pp. 844–847.
- [31] Y.-J. Chen, S. Oraintara, T. Tran, K. Amaratunga, and T. Q. Nguyen, “Multiplierless approximation of transforms with adder constraint,” *IEEE Signal Processing Lett.*, vol. 9, no. 11, Nov. 2002.
- [32] G. Cherubini, E. Eleftheriou, S. Oker, and J. Cioffi, “Filter bank modulation techniques for very high speed digital subscriber lines,” *IEEE Commun. Mag.*, vol. 38, no. 5, pp. 98–104, May 2000.
- [33] G. C.-H. Chuang and C.-C. J. Kuo, “Wavelet descriptor of planar curves: Theory and applications,” *IEEE Trans. Image Processing*, vol. 5, no. 1, Jan. 1996.
- [34] A. Cohen, I. Daubechies, and J. Feauveau, “Biorthogonal bases of compactly supported wavelets,” *Comm. Pur. Appl. Math.*, vol. 45, pp. 485–560, 1992.
- [35] R. E. Crochiere and L. R. Rabiner, *Multirate Digital Signal Processing*. Englewood Cliffs, NJ: Prentice-Hall, 1983.
- [36] A. Croisier, D. Esteban, and C. Galand, “Perfect channel splitting by use of interpolation, decimation, tree decomposition techniques,” in *Proc. Int. Conf. Inform. Sci. Syst*, Patras, Greece, Aug. 1976, pp. 443–446.

- [37] I. Daubechies, “Orthogonal bases of compactly supported wavelets,” *Comm. Pur. Appl. Math.*, vol. 41, pp. 909–996, 1988.
- [38] ——, *Ten Lectures on Wavelets*. Philedelphia, PA: SIAM, 1993.
- [39] I. Daubechies and W. Sweldens, “Factoring wavelet transforms into lifting steps,” *J. Fourier Anal. Appl.*, vol. 4, no. 3, pp. 245–267, 1998.
- [40] R. L. de Queiroz and T. D. Tran, “Lapped transforms for image compression,” in *The Handbook on Transforms and Data Compression*, K. R. Rao and P. Yip, Eds. CRC Press, Oct. 2000, pp. 197–265.
- [41] R. de Queiroz, T. Nguyen, and K. Rao, “The GenLOT: Generalized linear-phase lapped orthogonal transform,” *IEEE Trans. Signal Processing*, vol. 44, no. 3, pp. 497–507, 1996.
- [42] Y. Dehery, M. Lever, and P. Urcun, “A MUSICAM source codec for digital audio broadcasting and storage,” in *Proc. IEEE Int'l Conf. Acoust., Speech, Signal Processing*, vol. 5, 1991, pp. 3605–3608.
- [43] A. Djohan, T. Q. Nguyen, and W. Tompkins, “ECG compression using discrete symmetric wavelet transform,” in *International Conf. EMBS*, Sept. 1995.
- [44] D. L. Donoho and I. M. Johnstone, “Adapting to unknown smoothness via wavelet shrinkage,” *Journal of the American Statistical Association*, vol. 90, no. 432, pp. 1200–1224, Dec. 1995. [Online]. Available: <http://citeseer.nj.nec.com/donoho95adapting.html>
- [45] L. Duval, V. Bui-Tran, T. Nguyen, and T. Tran, “GenLOT optimization techniques for seismic data compression,” in *Proc. IEEE Int'l Conf. Acoust., Speech, Signal Processing*, vol. 6, 2000, pp. 2111–2114.
- [46] L. Duval and T. Nagai, “Seismic data compression using GULLOTS,” in *Proc. IEEE Int'l Conf. Acoust., Speech, Signal Processing*, vol. 3, May 2001, pp. 1765–1768.
- [47] D. Esteban and C. Galand, “Application of quadrature mirror filters to split band voice coding schemes,” in *Proc. IEEE Int'l Conf. Acoust., Speech, Signal Processing*, Hartford, CT, May 1977, pp. 191–195.
- [48] FBI Criminal Justice Information Services, “Wavelet scalar quantization gray-scale fingerprint image compression specification,” Washington, DC, 1993.
- [49] L. Gan and K.-K. Ma, “Oversampled linear-phase perfect reconstruction filterbanks: theory, lattice structure and parameterization,” *IEEE Trans. Signal Processing*, vol. 51, pp. 744–759, Mar. 2003.

- [50] ——, “On simplified order-one factorizations of paraunitary filterbanks,” *IEEE Trans. Signal Processing*, Mar. 2004.
- [51] ——, “Time-domain oversampled lapped transforms: theory, structure and application in image coding,” *IEEE Trans. Signal Processing*, to appear.
- [52] X. Gao, T. Q. Nguyen, and G. Strang, “On factorization of M -channel paraunitary filterbanks,” *IEEE Trans. Signal Processing*, vol. 49, no. 7, pp. 1433–1446, Jul. 2001.
- [53] ——, “A study of two-channel complex-valued filterbanks and wavelets with orthogonality and symmetry properties,” *IEEE Trans. Signal Processing*, vol. 50, no. 4, pp. 824–833, Apr. 2002.
- [54] H. L. Garner, “Number systems and arithmetic,” *Adv. Computers*, vol. 6, pp. 131–194, 1965.
- [55] R. Geiger, Y. Yokotani, G. Schuller, and J. Herre, “Improved integer transforms using multi-dimensional lifting,” in *Proc. IEEE Int'l Conf. Acoust., Speech, Signal Processing*, Montreal, Canada, May 2004.
- [56] A. Grossmann and J. Morlet, “Decomposition of Hardy functions into square-integrable wavelets of constant shape,” *SIAM J. Math. Anal.*, vol. 15, pp. 723–736, 1984.
- [57] P. N. Heller and R. O. Wells, Jr., “Sobolev regularity for rank M wavelets,” Computational Math. Laboratory, Rice University, Tech. Rep. TR 96-08, 1996.
- [58] P. N. Heller, “Rank M wavelets with N vanishing moments,” *J. Matrix Anal. Appl.*, vol. 16, no. 2, pp. 502–519, Apr. 1995.
- [59] P. N. Heller and H. L. Resnikoff, “Regular M -band wavelets and applications,” in *Proc. IEEE Int'l Conf. Acoust., Speech, Signal Processing*, vol. 3, Apr. 1993, pp. 229–232.
- [60] JPEG2000 Standard. [Online]. Available: <http://www.jpeg.org/CDs15444.html>
- [61] J. Kominek, “The Waterloo BragZone.” [Online]. Available: <http://links.uwaterloo.ca/bragzone.base.html>
- [62] B. K. Krishnan, “Feature selection in the wavelet domain through regularization,” MIT, Tech. Rep., 2003.
- [63] R. Kumar, Y.-J. Chen, S. Oraintara, and K. Amarasinghe, “ M -channel lifting structure for unimodular filter bank,” in *Proc. IEEE Int'l Symp. Circuits Syst.*, May 2004.
- [64] J.-S. Lee, Y.-N. Sun, and C.-H. Chen, “Multiscale corner detection by using wavelet transform,” *IEEE Trans. Image Processing*, vol. 4, no. 1, pp. 100–104, Jan. 1995.

- [65] H. Li, B. S. Manjunath, and S. K. Mitra, “Multisensor image fusion using the wavelet transform,” *Graphical Models And Image Processing*, vol. 57, no. 3, pp. 235–245, May 1995.
- [66] J. Liang and T. D. Tran, “Fast multiplierless approximations of the DCT with the lifting scheme,” *IEEE Trans. Signal Processing*, Dec. 2001.
- [67] F.-H. Lin, Y.-J. Chen, J. W. Belliveau, and L. L. Wald, “A wavelet-based approximation of surface coil sensitivity profiles for correction of image intensity inhomogeneity and parallel imaging reconstruction,” *Human Brain Mapping*, vol. 19, no. 2, pp. 96–111, Jun. 2003.
- [68] C. Loeffler, A. Ligtenberg, and G. S. Moschytz, “Practical fast 1-D DCT algorithms with 11 multiplications,” in *Proc. IEEE Int'l Conf. Acoust., Speech, Signal Processing*, vol. 2, May 1989, pp. 988–991.
- [69] S. Mallat and S. Zhong, “Characterization of signals from multiscale edges,” *IEEE Trans. Pattern Anal. Machine Intell.*, vol. 14, no. 7, pp. 710–732, Jul. 1992.
- [70] S. G. Mallat, “Multiresolution approximation and wavelet orthonormal bases of $L^2(R)$,” *Trans. Amer. Math. Soc.*, vol. 315, no. 1, pp. 69–87, Sep. 1989.
- [71] ——, “A theory for multiresolution signal decomposition: the wavelet representation,” *IEEE Trans. Pattern Anal. Machine Intell.*, vol. 11, no. 7, pp. 674–693, Jul. 1989.
- [72] ——, *A Wavelet Tour of Signal Processing*. Academic Press, 1999.
- [73] S. G. Mallat and W. L. Huang, “Singularity detection and processing with wavelets,” *IEEE Trans. Inform. Theory*, vol. 38, no. 2, pp. 617–643, Mar. 1992.
- [74] H. S. Malvar, *Signal Processing with Lapped Transforms*. Norwood, MA: Artech House, 1992.
- [75] ——, “Enhancing the performance of subband audio coders for speech signals,” in *Proc. IEEE Int'l Symp. Circuits Syst.*, vol. 5, 1998, pp. 98–101.
- [76] ——, “A modulated complex lapped transform and its applications to audio processing,” in *Proc. IEEE Int'l Conf. Acoust., Speech, Signal Processing*, Phoenix, AZ, Mar. 1999, pp. 1421–1424.
- [77] ——, “Fast progressive image coding without wavelets,” in *IEEE Data Compression Conference*, Snowbird, UT, Mar. 2000.
- [78] H. S. Malvar, A. Hallapuro, M. Karczewicz, and L. Kerofsky, “Low-complexity transform and quantization in H.264/AVC,” *IEEE Trans. Circuits Syst. Video Technol.*, vol. 13, no. 7, pp. 598–603, July 2003.

- [79] M. Maslen and P. Abbott, “Automation of the lifting factorisation of wavelet transforms,” *Computer Physics Communications*, vol. 127, pp. 309–326, 2000.
- [80] Y. Meyer, “Ondelettes,” in *Ondelettes et Opérateurs*. Paris: Hermann, 1990, vol. 1.
- [81] J. Morlet, “Sampling theory and wave propagation,” in *NATO ASI Series, Issues in Acoustic Signal/Image Processing and Recognition*, C. H. Chen, Ed. Berlin: Springer-Verlag, 1983, vol. 1, pp. 233–261.
- [82] J. Morlet, G. Arens, I. Fourgeau, and D. Giard, “Wave propagation and sampling theory — Part I: Complex signal and scattering in multilayered media,” *Geophysics*, vol. 47, pp. 203–221, 1982.
- [83] ——, “Wave propagation and sampling theory — Part II: Sampling theory and complex waves,” *Geophysics*, vol. 47, pp. 222–236, 1982.
- [84] MPEG4, ISO/IEC 14496: Information technology – Coding of audio-visual objects.
- [85] F. D. Murnaghan, *The Unitary and Rotation Groups*. Washington, D.C.: Spartan Books, 1962.
- [86] T. Q. Nguyen, T. Saramäki, and P. P. Vaidyanathan, “Eigenfilters for the design of special transfer functions with applications in multirate signal processing,” in *Proc. IEEE Int'l Conf. Acoust., Speech, Signal Processing*, New York, NY, Apr. 1988, pp. 1467–1470.
- [87] T. Q. Nguyen, “A tutorial on filter banks and wavelets.” [Online]. Available: <ftp://ftp.ece.wisc.edu/pub/nguyen/LECTURE/paper1.ps.gz>
- [88] J. Nohrden and T. Q. Nguyen, “Constraints on the cutoff frequencies of m th band linear-phase fir filters,” *IEEE Trans. Signal Processing*, vol. 43, no. 10, pp. 2401–2405, Oct. 1995.
- [89] A. Nosratinia, G. Davis, Z. Xiong, and R. Rajagopalan, “Subband image compression,” in *Wavelets, Subband, and Block Transforms in Communications and Multimedia*, A. Akansu, Ed. Kluwer Academic, Jan. 1999.
- [90] A. V. Oppenheim and R. W. Schafer, *Discrete-Time Signal Processing*, 2nd ed. Prentice Hall, 1999.
- [91] S. Oraintara, Y.-J. Chen, and T. Q. Nguyen, “Integer fast Fourier transform,” *IEEE Trans. Signal Processing*, Mar. 2002.
- [92] S. Oraintara, T. Tran, P. Heller, and T. Nguyen, “Lattice structure for regular paraunitary linear-phase filterbanks and M -band orthogonal symmetric wavelets,” *IEEE Trans. Signal Processing*, vol. 49, pp. 2659–2672, Nov. 2001.

- [93] S. Oraintara, T. Tran, and T. Q. Nguyen, “A class of regular biorthogonal linear-phase filterbanks: Theory, structure, and application in image coding,” *IEEE Trans. Signal Processing*, vol. 51, no. 12, Dec. 2003.
- [94] S. Oraintara, “Regular linear phase perfect reconstruction filter banks for image compression,” Ph.D. dissertation, Boston University, Jun. 2000.
- [95] S. Oraintara and T. Nguyen, “A simple mapping between M th-band FIR filters using cosine modulation,” *IEEE Signal Processing Lett.*, vol. 10, no. 5, pp. 125–128, May 2003.
- [96] A. H. Osman and O. P. Malik, “Protection of parallel transmission lines using wavelet transform,” *IEEE Trans. Power Delivery*, vol. 19, no. 1, pp. 49–55, Jan. 2004.
- [97] W. B. Pennebaker and J. L. Mitchell, *JPEG Still Image Compression Standard*. Chapman & Hall, 1992.
- [98] S.-M. Phoong and Y.-P. Lin, “Lapped unimodular transform and its factorization,” *IEEE Trans. Signal Processing*, vol. 50, no. 11, pp. 2695–2701, Nov. 2002.
- [99] G. Plonka and M. Tasche, “Invertible integer DCT algorithms,” *Appl. Comput. Harmon. Anal.*, vol. 15, no. 1, pp. 70–88, Jul. 2003.
- [100] K. R. Rao and P. Yip, *Discrete Cosine Transform, Algorithms, Advantages, Applications*. Academic Press, 1990.
- [101] P. Rault and C. Guillemot, “Symmetric delay factorization: generalized framework for paraunitary filter banks,” *IEEE Trans. Signal Processing*, vol. 47, no. 12, pp. 3315–3325, Dec. 1999.
- [102] G. W. Reitwiesner, “Binary arithmetic,” *Adv. Computers*, vol. 1, pp. 232–308, 1960.
- [103] O. Rioul and M. Vetterli, “Wavelets and signal processing,” *IEEE Signal Processing Mag.*, vol. 8, no. 4, pp. 14–38, Oct. 1991.
- [104] A. Said and W. Pearlman, “A new, fast, and efficient image codec based on set partitioning in hierarchical trees,” *IEEE Trans. Circuits Syst. Video Technol.*, vol. 6, no. 3, pp. 243–250, Jun. 1996.
- [105] P. Steffen, P. N. Heller, R. A. Gopinath, and C. S. Burrus, “Theory of regular M -band wavelet bases,” *IEEE Trans. Signal Processing*, vol. 41, no. 12, pp. 3497–3510, Dec. 1993.
- [106] G. Strang, “Every unit matrix is a *LULU*,” *Linear Algebra and Its Applications*, vol. 265, pp. 165–172, Nov. 1997.
- [107] ——, *Introduction to Linear Algebra*, 3rd ed. Wellesley, MA: Wellesley-Cambridge Press, 2003.

- [108] G. Strang and T. Nguyen, *Wavelets and Filter Banks*, 2nd ed. Wellesley, MA: Wellesley-Cambridge Press, 1997.
- [109] G. Strang and V. Strela, “Short wavelets and matrix dilation equations,” *IEEE Trans. Signal Processing*, vol. 43, no. 1, pp. 108–115, Jan. 1995.
- [110] G. Strang, “Wavelets and dilation equations,” *SIAM Review*, vol. 31, pp. 613–627, 1989.
- [111] ——, “Wavelets,” *American Scientist*, vol. 82, pp. 250–255, Apr. 1994.
- [112] R. Sudarshan, S. D’Heedene, and K. Amarasinghe, “A multiresolution finite element method using second generation hermite multiwavelets,” in *Proceedings of the Second MIT Conference on Computational Fluid and Solid Mechanics*, K.J.Bathe, Ed., Jun. 2003.
- [113] B. W. Suter, *Multirate and Wavelet Signal Processing*, 1st ed. San Diego: Academic Press, Jan. 1998.
- [114] W. Sweldens, “The lifting scheme: A custom-design construction of biorthogonal wavelets,” *Appl. Comput. Harmon. Anal.*, vol. 3, no. 2, pp. 186–200, 1996.
- [115] ——, “The Lifting Scheme: A construction of second generation wavelets,” *SIAM Journal on Mathematical Analysis*, vol. 29, no. 2, pp. 511–546, 1998.
- [116] D. S. Taubman and M. W. Marcellin, *JPEG2000: image compression fundamentals, standards, and practice*. Boston: Kluwer Academic Publishers, 2002.
- [117] T. Toffoli, “Almost every unit matrix is a *ULU*,” *Linear Algebra and Its Applications*, vol. 259, pp. 31–38, Jul. 1997.
- [118] T. D. Tran, “The BinDCT: fast multiplierless approximation of the DCT,” *IEEE Signal Processing Lett.*, vol. 7, pp. 141–145, Jun. 2000.
- [119] T. Tran, R. de Queiroz, and T. Nguyen, “Linear-phase perfect reconstruction filter bank: lattice structure, design, and application in image coding,” *IEEE Trans. Signal Processing*, vol. 48, no. 1, pp. 133–147, Jan. 2000.
- [120] T. D. Tran, “ M -channel linear phase perfect reconstruction filter bank with rational coefficients,” *IEEE Trans. Circuits Syst. I*, vol. 49, no. 7, Jul. 2002.
- [121] T. D. Tran and T. Q. Nguyen, “On M -channel linear-phase FIR filter banks and application in image compression,” *IEEE Trans. Signal Processing*, vol. 45, pp. 2175–2187, Sep. 1997.
- [122] ——, “A progressive transmission image coder using linear phase uniform filter banks as block transforms,” *IEEE Trans. Image Processing*, vol. 48, pp. 1493–1507, Nov. 1999.

- [123] S. Trautmann and T. Nguyen, "UICODER: a MATLAB graphical user interface for a transform-based image coder." [Online]. Available: <http://videoprocessing.ucsd.edu>
- [124] M. Unser, "Approximation power of biorthogonal wavelet expansions," *IEEE Trans. Signal Processing*, vol. 44, no. 3, pp. 519–527, Mar. 1996.
- [125] M. Unser, A. Aldroubi, and M. Eden, "B-spline signal processing: Part I—Theory," *IEEE Trans. Signal Processing*, vol. 41, no. 2, pp. 821–833, Feb. 1993.
- [126] V Corp Technologies Inc. [Online]. Available: <http://www.v-corp.com/>
- [127] P. Vaidyanathan, "Theory and design of M -channel maximally decimated quadrature mirror filters with arbitrary M , having the perfect-reconstruction property," *IEEE Trans. Acoust., Speech, Signal Processing*, vol. 35, no. 4, pp. 476–492, Apr. 1987.
- [128] P. P. Vaidyanathan, "How to capture all FIR perfect reconstruction QMF banks with unimodular matrices?" in *Proc. IEEE Int'l Symp. Circuits Syst.*, vol. 3, 1990, pp. 2030–2033.
- [129] ———, *Multirate Systems and Filter Banks*. Prentice Hall, 1992.
- [130] ———, "Theory of optimal orthonormal subband coders," *IEEE Trans. Signal Processing*, vol. 46, no. 6, pp. 1528–1543, Jun. 1998.
- [131] ———, "Filter banks in digital communications," *IEEE Circuits Syst. Mag.*, vol. 1, no. 2, pp. 4–25, 2001.
- [132] P. P. Vaidyanathan and T. Chen, "Role of anticausal inverses in multirate filter-banks—Part II: The FIR case, factorizations, and biorthogonal lapped transforms," *IEEE Trans. Signal Processing*, vol. 43, no. 5, pp. 1103–1115, May 1995.
- [133] P. Vaidyanathan and A. Kirac, "Results on optimal biorthogonal filter banks," *IEEE Trans. Circuits Syst. II*, vol. 45, no. 8, pp. 932–947, Aug. 1998.
- [134] P. Vaidyanathan, T. Nguyen, Z. Doğanata, and T. Saramäki, "Improved technique for design of perfect reconstruction FIR QMF banks with lossless polyphase matrices," *IEEE Trans. Signal Processing*, vol. 37, no. 7, pp. 1042–1056, Jul. 1989.
- [135] S. R. Velazquez, T. Q. Nguyen, and S. R. Broadstone, "Design of hybrid filter banks for analog/digital conversion," *IEEE Trans. Signal Processing*, vol. 46, no. 4, pp. 956–967, Apr. 1998.
- [136] S. R. Velazquez, T. Q. Nguyen, S. R. Broadstone, and J. K. Roberge, "A hybrid filter bank approach to analog-to-digital conversion," in *Proceedings of the IEEE-SP International Symposium on Time-Frequency and Time-Scale Analysis*, Oct. 1994, pp. 116–119.

- [137] M. Vetterli, “A theory of multirate filter banks,” *IEEE Trans. Acoust., Speech, Signal Processing*, vol. 35, no. 3, pp. 356–372, Mar. 1987.
- [138] M. Vetterli and C. Herley, “Wavelets and filter banks: theory and design,” *IEEE Trans. Signal Processing*, vol. 40, no. 9, pp. 2207–2232, Sep. 1992.
- [139] M. Vetterli and J. Kovačević, *Wavelets and Subband Coding*. Prentice Hall, 1995.
- [140] M. Vetterli, “Wavelets, approximation, and compression,” *IEEE Signal Processing Mag.*, vol. 18, no. 5, pp. 59–73, Sep. 2001.
- [141] J. Villasenor, R. Ergas, and P. Donoho, “Seismic data compression using high-dimensional wavelet transforms,” in *Data Compression Conference*, 1996, pp. 396–405.
- [142] J. S. Walker and Y.-J. Chen, “Image denoising using tree-based wavelet subband correlations and shrinkage,” *Optical Engineering*, vol. 39, no. 11, pp. 2900–2908, Nov. 2000.
- [143] J. S. Walker, T. Q. Nguyen, and Y.-J. Chen, “A low-power, low-memory system for wavelet-based image compression,” in *Recent Research Developments in Optical Engineering*. Kerala, India: Research Signpost, 2003, vol. 5, pp. 111–125.
- [144] J. S. Walker, *A Primer on Wavelets and Their Scientific Applications*. Boca Raton: CRC Press, 1999.
- [145] ——, “Tree-adapted wavelet shrinkage,” in *Advances in Imaging and Electron Physics*. New York: Elsevier Science (USA), 2002, pp. 343–394.
- [146] ——, “Wavelet-based image processing,” in *Proceedings of 4th International Congress of ISAAC (International Society for Analysis, its Applications and Computation)*. Norwell, MA: Kluwer, to appear. [Online]. Available: <http://www.uwec.edu/walkerjs/media/WBIP.pdf>
- [147] J. S. Walker and T. Q. Nguyen, “Wavelet-based image compression,” in *The Transform and Data Compression Handbook*, P. C. Yip and K. R. Rao, Eds. Boca Raton: CRC Press, 2000, vol. 1, ch. 6, pp. 267–312.
- [148] ——, “Adaptive scanning methods for wavelet difference reduction in lossy image compression,” in *IEEE Int'l Conf. Image Processing*, vol. 3, Vancouver, Canada, Sep. 2000.
- [149] Y. Wisutmethangoon and T. Nguyen, “A method for design of M th-band filters,” *IEEE Trans. Signal Processing*, vol. 47, no. 6, pp. 1669–1678, Jun. 1999.
- [150] G. Wornell, “Emerging applications of multirate signal processing and wavelets in digital communications,” *Proceedings of the IEEE*, vol. 84, no. 4, pp. 586–603, Apr. 1996.

- [151] Y. Xu, J. B. Weaver, D. M. Healy, Jr., and J. Lu, "Wavelet transform domain filters: a spatially selective noise filtration technique," *IEEE Trans. Image Processing*, vol. 3, no. 6, pp. 747–758, Nov. 1994.
- [152] K. Yu, J. Lv, J. Li, and S. Li, "Practical real-time video codec for mobile devices," in *Proc. Int'l Conf. Multimedia Expo*, vol. 3, Jul. 2003, pp. 509–512.
- [153] W. R. Zettler, J. Huffman, and D. C. Linden, "Application of compactly supported wavelets to image compression," in *Proc. SPIE Image Processing Algorithms and Techniques*, vol. 1244, 1990, pp. 150–160.
- [154] Y. Zheng, G. Bi, and Z. Lin, "Integer sinusoidal transforms based on lifting factorization," in *Proc. IEEE Int'l Conf. Acoust., Speech, Signal Processing*, May 2002.
- [155] H. Zou and A. H. Tewfik, "Discrete orthogonal M -band wavelet decompositions," in *Proc. IEEE Int'l Conf. Acoust., Speech, Signal Processing*, vol. 4, 1992, pp. IV–605–IV–608.

Index

- M -channel lifting factorization, 75
 n -adder binary approximation, 207
HOUSE, 68
TRANS_MATRIX, 55
- ABA, 207
- B-spline filter bank completion, 99
- cascade algorithm, 52
causal filter, 33
CMFB, 97
coding gain, 44
- DC leakage, 61
DCT, 96
 BinDCT, 211
 IntDCT, 210
- degree-one building block
 biorthogonal, 93
 lifting factorization (PU), 90
 lifting factorization (unimodular), 94, 95
 paraunitary, 70
 unimodular, 93
- degree-one completion
 PUFBs, 182
- degree-one factorization
 polyphase matrix, 71
 polyphase vector, 182
- degree-one PU building block
 lifting factorization, 125
- dilation equation, 49
- dyadic-based structure, 69
- Euclidean algorithm, 81
- Monic, 82
- fast wavelet transform, 50
FIR filter, 33
- Givens rotation, 64
- Householder matrix, 64
 lifting factorization, 92
- IIR filter, 33
- infinite product formula, 55
inner product formula, 52
- lifting factorization
 M -channel, 83
 lossless systems, 33
- maximally-decimated uniform filter banks, 35
- McMillan degree, 45
- modulation matrix, 37
 PR condition, 38
- MRA, 47
- multiplierless approximation
 algorithm, 210
 BinDCT, 211
 IntDCT, 210
- multiresolution analysis, 47
- order of filter banks, 46
- order-one building block
 biorthogonal, 74
 paraunitary, 71
- order-one completion
 LPPUFB, 189
 PUFB, 187
 PUFB design technique, 194

order-one factorization
 polyphase matrix, 71
 polyphase vector, 184
order-one PU building block
 lifting factorization, 126

perfect reconstruction, 34
polynomial cancellation, 59
polyphase matrix, 38
 PR condition, 40
PR, 34

QR, 69

regular PRFB, 58
 polyphase matrices, 60

scaling function, 47
 filter bank approach, 55

Sobolev smoothness, 62

stopband energy, 43

SVD, 68

transition matrix, 53

unimodular filter bank, 43, 74
 lifting, 94
 lifting factorization, 94

unitary matrix, 63

vanishing moment, 59

wavelet equation, 49
wavelet series expansion, 49